

Systems biology of the central
metabolism of
Streptococcus pyogenes

Jennifer Levering

Dissertation
submitted to the
Combined Faculties for the Natural Sciences and for Mathematics
of the Ruperto-Carlo University of Heidelberg, Germany
for the degree of
Doctor of Natural Science

presented by
MSc Jennifer Levering
born in Wesel
Oral-examination: 2011/09/06

Systems biology of the central
metabolism of
Streptococcus pyogenes

Referees: Prof. Dr. Ursula Kummer
Prof. Dr. Thomas Höfer

So eine Arbeit wird eigentlich nie fertig,
man muss sie für fertig erklären,
wenn man nach Zeit und Umständen
das Möglichste getan hat.

Johann Wolfgang von Goethe

Contents

List of Figures	v
List of Tables	viii
List of Abbreviations	xii
Summary	xiii
1 Introduction	1
1.1 <i>Streptococcus pyogenes</i>	2
1.1.1 Interactions between pathogen and host	3
1.1.2 Metabolic capabilities	7
1.1.3 Studied kinetics and primary metabolism	9
1.2 Modelling strategies and existing glycolytic models	12
1.3 Project and cooperation partners	14
1.4 Goals of the thesis	17
2 Materials and Methods	19
2.1 Experimental data	20
2.1.1 Bacterial strains	20
2.1.2 Construction of recombinant vectors and mutant strains	20
2.1.3 CDM-LAB medium	21
2.1.4 Fermentation experiments	21
2.1.5 Glucose-pulse experiments	22
2.1.6 Kinetic measurements of individual enzymes	23
2.1.7 Substrate utilisation assays	24
2.1.8 Calculation of specific ATP synthesis rates	25
2.1.9 Amino acid leave-out experiments	25

2.2	Dynamic modelling	26
2.2.1	COPASI	26
2.2.2	Ordinary differential equations	27
2.2.3	Kinetics	28
2.2.4	Simulation	30
2.2.5	Parameter estimation	30
2.2.6	Local sensitivity analysis	31
2.2.7	Global sensitivity analysis	32
2.2.8	Steady state analysis	33
2.2.9	Metabolic control analysis	33
2.3	Genome-scale modelling	35
2.3.1	AUTOGRAPH and INPARANOID	35
2.3.2	Manual curation	36
2.3.3	Flux balance analysis	37
3	Results	39
3.1	Experimental results	40
3.1.1	Construction of recombinant vectors and mutant strains	40
3.1.2	Fermentation experiments	41
3.1.3	Glucose-pulse experiments	46
3.1.4	Kinetic parameters of individual enzymes	48
3.1.5	Substrate utilisation assays	49
3.1.6	Calculation of specific ATP synthesis rates	49
3.1.7	Amino acid leave-out experiments	49
3.2	Kinetic model of <i>S. pyogenes</i>	55
3.2.1	Setting up the model	55
3.2.2	The role of phosphate	62
3.2.3	Resulting fit	64
3.2.4	Sensitivity analysis	71
3.3	Comparison between <i>S. pyogenes</i> and <i>L. lactis</i>	76
3.3.1	Kinetic model of <i>L. lactis</i>	76
3.3.2	Topological and regulatory differences	79
3.3.3	Comparative systems biology of <i>L. lactis</i> and <i>S. pyogenes</i> glycolysis	82
3.4	Oscillations caused by the stoichiometry	85

3.4.1	Finding oscillations in the model	85
3.4.2	Results	86
3.5	Reconstructing the metabolic network of <i>S. pyogenes</i>	88
3.5.1	Metabolic pathways incorporated in the model	89
3.5.2	Orthology detection	89
3.5.3	Manual curation	90
3.5.4	Filling gaps	92
3.5.5	Characteristics of <i>S. pyogenes</i>	92
3.5.6	Results from flux balance analysis	100
3.5.7	Topological comparison with <i>L. lactis</i> and <i>L. plantarum</i>	109
4	Discussion	111
4.1	Kinetic model	112
4.1.1	Model set-up, topology and regulation	112
4.1.2	The role of phosphate	117
4.1.3	Parameter estimation and resulting fit	117
4.1.4	Sensitivity analysis	119
4.2	Comparison to <i>L. lactis</i>	121
4.2.1	Kinetic model of <i>L. lactis</i>	121
4.2.2	Role of phosphate in <i>L. lactis</i> and <i>S. pyogenes</i>	122
4.3	Genome-scale model	124
4.3.1	Orthology detection	124
4.3.2	Network composition	125
4.3.3	Simulation of experimental data	126
4.3.4	Predictions from the model	129
4.3.5	Differences and similarities between <i>S. pyogenes</i> and related bacteria	130
4.4	Discussion of thesis goals	132
5	Outlook	135
	Bibliography	137
	Acknowledgements	152

A	Glycolytic model of <i>S. pyogenes</i>	155
A.1	Kinetic parameters and initial concentrations	156
A.2	Rate laws, differential equations and moiety conservation	162
A.2.1	Rate laws	162
A.2.2	Differential equations and moiety conservation	166
A.3	Results from sensitivity analysis	168
B	Genome-scale model of <i>S. pyogenes</i>	179
B.1	Compounds	180
B.2	Reactions	188
B.3	Constraints	198
B.4	Simulation results	203

List of Figures

3.1	Overview of molecular interactions of <i>S. pyogenes</i> glycolysis	60
3.2	Metabolic profiles and model simulations of glucose-pulse experiments in <i>S. pyogenes</i>	66
3.3	Model simulations and experimental data of glucose-pulse experiments in <i>S. pyogenes</i>	68
3.4	Global sensitivity analysis results for the V_{\max} of the P_i transporter on FBP	72
3.5	Maximal global parameter sensitivities on FBP and P_i	73
3.6	Overview of molecular interactions of <i>L. lactis</i> glycolysis	78
3.7	Metabolic profiles and model simulations of glucose-pulse experiments in <i>L. lactis</i>	80
3.8	^{13}C - and ^{31}P -NMR time-series profiles and model simulations of glucose-pulse experiments in <i>L. lactis</i>	81
3.9	Model simulations of intracellular phosphate levels after a 20 mM glucose-pulse in <i>L. lactis</i>	83
3.10	Model simulations of glycolytic oscillations	87

List of Tables

1.1	Overview of all participating institutions and their roles within the SysMO-LAB project	16
3.1	Maximal specific growth rates of <i>S. pyogenes</i> wild-type and <i>ldh</i> -knock-out	40
3.2	Measured OD and dry weight of <i>S. pyogenes</i> wild-type and <i>ldh</i> -knock-out	41
3.3	Relative flux distribution in <i>S. pyogenes</i>	42
3.4	Product concentrations in <i>S. pyogenes</i> wild-type strain	43
3.5	Product concentrations in <i>S. pyogenes</i> <i>ldh</i> -negative mutant	43
3.6	Amino acid concentrations in <i>S. pyogenes</i> wild-type strain	44
3.7	Amino acid concentrations in <i>S. pyogenes</i> <i>ldh</i> -negative mutant	45
3.8	Metabolite concentration time-series in <i>S. pyogenes</i> for 0 mM P_i^{ex}	47
3.9	Metabolite concentration time-series in <i>S. pyogenes</i> for 10 mM P_i^{ex}	47
3.10	Metabolite concentration time-series in <i>S. pyogenes</i> for 50 mM P_i^{ex}	48
3.11	Substrate utilisation of <i>S. pyogenes</i> wild-type and its <i>ldh</i> -knock-out mutant on different carbon sources	50
3.12	Specific ATP synthesis rates of <i>S. pyogenes</i>	51
3.13	Final OD after 12 h growth of <i>S. pyogenes</i> in full CDM-LAB medium and medium with amino acid leave-outs	51
3.14	Essential amino acids for growth of <i>S. pyogenes</i> in CDM-LAB medium based on our experimental data	54
3.15	Rate of medium supply and influx of glucose, acetate and phosphate during continuous cultivation	61
3.16	Velocity constants (in $\frac{\text{mM}}{\text{s}}$) of the steady state model	69
3.17	Initial metabolite as well as simulated and measured steady state end-product concentrations (mM) of the steady state model	70

3.18	Predicted growth rates (h^{-1}) of <i>S. pyogenes</i>	103
3.19	Simulated growth rates of <i>S. pyogenes</i> wild-type strain grown in full CDM-LAB medium and medium with amino acid leave-outs	105
3.20	Essential amino acids for growth of <i>S. pyogenes</i> in CDM-LAB medium compared to literature data	108
A.1	Velocity constants (in $\frac{\text{mM}}{\text{s}}$)	156
A.2	Reversible processes: K_{eq}	157
A.3	Michaelis constants: K_{m} (mM)	157
A.4	Allosteric regulation binding constants (mM)	160
A.5	Hill coefficients	161
A.6	Initial concentrations (mM)	161
A.7	Parameter sensitivities on FBP	168
A.8	Parameter sensitivities on P_i	171
A.9	Parameter sensitivities on the PFK flux	173
A.10	Parameter sensitivities on the PTS flux	176
B.1	Compounds included in the genome-scale model	180
B.2	Reactions included in the genome-scale model	188
B.3	Assumed constraints on reaction fluxes	198
B.4	Calculated constraints for <i>S. pyogenes</i> wild-type strain at pH 6.5 . . .	199
B.5	Calculated constraints for <i>S. pyogenes</i> wild-type strain at pH 7.5 . . .	200
B.6	Calculated constraints for <i>S. pyogenes</i> <i>ldh</i> -deletion strain at pH 6.5 .	201
B.7	Calculated constraints for <i>S. pyogenes</i> <i>ldh</i> -deletion strain at pH 7.5 .	202
B.8	Optimal solution from FBA for <i>S. pyogenes</i> wild-type and its <i>ldh</i> - deletion at pH 6.5	203
B.9	Optimal solution from FBA for <i>S. pyogenes</i> wild-type and its <i>ldh</i> - deletion at pH 7.5	206

List of Abbreviations

μ_{\max}	Maximal specific growth rate
$q_{\text{ATP maintenance}}$	Rate of energy required for maintenance
$q_{\text{ATP } \mu_{\max}}$	ATP production rate at the maximal specific growth rate
2PG	2-phosphoglycerate
3PG	3-phosphoglycerate
<i>ldh</i>	L-lactate dehydrogenase gene
ADP	Adenosine diphosphate
Ala	Alanine
ALDO	Fructose-bisphosphate aldolase
Arg	Arginine
Asn	Asparagine
Asp	Aspartate
ATP	Adenosine triphosphate
AU	Arbitrary unit
BPG	1,3-bisphosphoglycerate
CDM-LAB	Chemically defined medium designed for culturing <i>S. pyogenes</i> , <i>L. lactis</i> and <i>E. faecalis</i>
CoA	Coenzyme A
Cyn	Cystine
Cys	Cysteine
D	Dilution rate (h^{-1})
DAP	Dihydroxyacetone phosphate
DW	Dry weight (g/l)
EC number	Enzyme Commission number, numerical classification scheme for enzymes, based on the chemical reactions they catalyse

EI	Enzyme I, unspecific cytoplasmic component of the PTS
EII	Enzyme II, specific component of the PTS
ENO	Enolase
F6P	Fructose-6-phosphate
FBA	Flux balance analysis
FBP	Fructose-1,6-bisphosphate
G6P	Glucose-6-phosphate
GAP	Glyceraldehyde-3-phosphate
GAPDH	Glyceraldehyde-3-phosphate dehydrogenase
GAPN	Non-phosphorylating NADP ⁺ -dependent glyceraldehyde-3-phosphate dehydrogenase
GAS	Group A streptococcus
Glc ^{ex}	Extracellular glucose
GlcP	Glucose permease
Gln	Glutamine
Glu	Glutamate
Gly	Glycine
His	Histidine
HPLC	High-pressure liquid chromatography
HPr	Heat-stable phosphocarrier histidine protein, part of the PTS
HPr-His-P	HPr phosphorylated at His-15
HPr-Ser-P	HPr phosphorylated at Ser-46
HPrK/P	HPr kinase/phosphatase, bifunctional enzyme
Ile	Isoleucine
K _A	Activator binding constant (mM)
K _{eq}	Equilibrium constant (dimensionless)
K _I	Inhibitor binding constant (mM)
K _m	Michaelis constant (mM), substrate concentration for that the reaction rate reaches half of its maximal velocity
LAB	Lactic acid bacteria
LDH	Lactate dehydrogenase
Leu	Leucine
LTA	Lipoteichoic acid

Lys	Lysine
MCA	Metabolic control analysis
Met	Methionine
MurNAc-GlcNAc	..	N-acetylmuramic acid-(β 1-4)-N-acetylglucosamine
NAD ⁺	Nicotinamide adenine dinucleotide, oxidized form
NADH	Nicotinamide adenine dinucleotide, reduced form
NADP ⁺	Nicotinamide adenine dinucleotide phosphate, oxidized form
NADPH	Nicotinamide adenine dinucleotide phosphate, reduced form
NPOX	NADP ⁺ regenerating reaction
OD	Optical density (arbitrary units)
ODE	Ordinary differential equation
P _i	Free inorganic phosphate
P _i ^{ex}	Extracellular phosphate
PaseII	Sugar-phosphate phosphatase II
PEP	Phosphoenolpyruvate
PFK	Phosphofructokinase
PFL	Pyruvate formate lyase
PG	Phosphoglycerate kinase
PGI	Phosphoglucose isomerase
PGM	Phosphoglycerate mutase
Phe	Phenylalanine
PP _i	Pyrophosphate
PPP	Pentose phosphate pathway
Pro	Proline
PTS	Phosphoenolpyruvate:carbohydrate phosphotransferase system
PYK	Pyruvate kinase
Ser	Serine
TCA cycle	Tricarboxylic acid cycle
Thr	Threonine
THY	Medium composed of 36.4 g/l Todd-Hewitt Broth and 5 g/l yeast extract
TMG	Thiomethyl- β -galactoside, a non-metabolisable lactose analogue

TPI	Triosephosphate isomerase
Triose-P	DAP and GAP
tRNA	Transfer RNA
Trp	Tryptophan
Tyr	Tyrosine
U	Enzyme activity, $U = \mu\text{mol}/\text{min}$, often given as specific activity in U per mg
V_{max}	Maximal reaction rate (mM/s), $V_{\text{max}} = [E] \cdot k_{\text{cat}}$
Val	Valine
Y_{atp}	Cell mass in g produced per mol of ATP generated by substrate catabolism

Summary

Streptococcus pyogenes is a lactic acid bacteria that colonises the skin or throat and causes many human diseases ranging from mild skin infections to serious systemic diseases like rheumatic fever. As a lactic acid bacteria it relies on substrate-level phosphorylation for its energy synthesis and ferments sugars primarily to lactate via the glycolytic pathway followed by pyruvate degradation. So far, some *S. pyogenes*-specific allosteric regulations of glycolytic processes have been identified, but no kinetic model of its glycolysis exists to study the dynamic interactions and understand their regulations. In order to explore the glycolytic pathway of *S. pyogenes* and to be able to compare it to other lactic acid bacteria, we set up a quantitative model of the central metabolism.

This first glycolytic model for the poorly-studied *S. pyogenes* is set up in close collaboration with experimental and theoretical groups within a SysMO consortium. Unknown parameters and allosteric regulation are adopted from related organisms, especially from the well-studied *Lactococcus lactis*. Due to unknown enzyme mechanisms convenience kinetics are exploited. To gain a satisfactory fit between the experimental data delivered from partners and the model, parameter estimation is applied.

Our glucose-pulse experiments show that an increase in the extracellular phosphate concentration induces a rise in the FBP level and in the glucose uptake rate. Both effects can be simulated with the developed model by integrating phosphate uptake. *S. pyogenes* possesses an ATP-dependent transport system but also genes predicted to encode a sodium phosphate symporter. Interestingly, so far, phosphate usually has not been considered as a free variable in glycolytic models and therefore its role has been underestimated.

Furthermore, a genome-scale model including all reactions required for growth is constructed. The reconstruction is based on the genome sequence and takes

advantage of already existing and curated metabolic networks of *Escherichia coli*, *Bacillus subtilis*, *Lactobacillus plantarum* and *Lactococcus lactis*.

Metabolic network analysis and simulation is carried out using flux balance analysis. Measured amino acid and product fluxes are used to constraint the genome-scale model. Since the network is constructed to simulate growth and reproduction the biomass function is chosen as objective function. To validate the reconstructed network, additional experiments are performed. We study growth on chemically defined medium with amino acid leave-outs. Furthermore, we investigate growth on different carbon sources. In accordance to our experimental data the *in silico* model is able to utilise trehalose, sucrose, maltose and mannose. The model facilitates the exploration of *S. pyogenes* behaviour to environmental perturbations. Based on the model we predict essential amino acids and a minimal medium for the growth of *S. pyogenes*.

Both models, the kinetic and the genome-scale model, facilitate discovering and understanding the similarities and differences between *S. pyogenes* and closely related lactic acid bacteria, especially *L. lactis*. These models will help in the design of strategies to control or reduce growth of the human pathogen *S. pyogenes*.

Zusammenfassung

Streptococcus pyogenes gehört zu den häufigsten Erregern von Haut- und Atemwegserkrankungen beim Menschen und verursacht verschiedene Krankheiten, von leichten Hautinfektionen bis hin zu schweren immunologisch bedingten Folgeerkrankungen der Streptokokkeninfektion, beispielsweise rheumatisches Fieber. Wie alle Milchsäurebakterien gewinnt *S. pyogenes* die zum Wachstum benötigte Energie mittels Substratkettenphosphorylierung in der Glykolyse. Das dabei gebildete Pyruvat wird hauptsächlich zu Lactat reduziert. Bisher ist die Regulation einiger glykolytischer Enzyme von *S. pyogenes* untersucht worden, ein dynamisches Modell der Fermentation ist aber noch nicht aufgestellt worden. Um die Glykolyse von *S. pyogenes* verstehen und mit der anderer Milchsäurebakterien vergleichen zu können, entwickeln wir ein quantitatives Modell des zentralen Stoffwechsels.

Die Konstruktion dieses ersten glykolytischen Modells für *S. pyogenes* erfolgt in enger Zusammenarbeit mit experimentellen und theoretischen Gruppen innerhalb eines SysMO-Konsortiums. Zur Modellentwicklung werden die von unseren Partnern bereitgestellten Daten benutzt. Fehlende Parameter und Regulationen werden von verwandten Organismen, insbesondere von *Lactococcus lactis*, übernommen. Aufgrund unbekannter Enzymmechanismen werden „Convenience Kinetics“ genutzt. Um eine gute Übereinstimmung zwischen unseren experimentellen Daten und dem Modell zu erhalten, wird eine Parameterschätzung durchgeführt.

Unsere Glukosepulsexperimente zeigen, dass mit der extrazellulären Phosphatkonzentration das FBP-Level und die Rate der Glukoseaufnahme steigen. Mit der Erweiterung um ein Phosphataufnahme-System kann unser kinetisches Modell beide Effekte beschreiben. Zur Aufnahme von Phosphat aus dem Medium besitzt *S. pyogenes* zwei Systeme. Zum einen besitzt es einen ATP-abhängigen Uniporter, zum anderen wurde ein Natrium-Phosphat-Symporter vorhergesagt. In bisher veröffentlichten glykolytischen Modellen wurde die Phosphatkonzentration nicht als

freie Variable implementiert, der Einfluss von Phosphat auf die Glykolyse wurde bislang unterschätzt.

Weiterhin wurde ein genomweites Modell zur Simulation von Wachstum und Reproduktion von *S. pyogenes* konstruiert. Diese Rekonstruktion basiert auf der Genomsequenz und bereits existierenden metabolischen Netzwerken von *Escherichia coli*, *Bacillus subtilis*, *Lactobacillus plantarum* und *Lactococcus lactis*.

Zur Auswertung und Simulation wird „Flux Balance Analysis“ angewandt. Gemessene Aminosäure- und Produktflüsse begrenzen die Flüsse des genomweiten Modells. Um Wachstum und Reproduktion zu simulieren, wurde die Produktion von Biomasse als Zielfunktion gewählt. Die Validierung des rekonstruierten Netzwerks erfolgt mit experimentellen Daten. Dazu haben wir das Wachstum auf einem chemisch definierten Medium mit dem Fehlen von ausgesuchten Aminosäuren untersucht. Außerdem haben wir das Substratspektrum von *S. pyogenes* studiert. In Übereinstimmung mit den experimentellen Daten simuliert das Modell Wachstum auf Trehalose, Sucrose, Maltose und Mannose. Das Modell erleichtert die Untersuchung des Verhaltens von *S. pyogenes* auf Veränderungen in seiner Umgebung. Basierend auf dem Modell haben wir essentielle Aminosäuren und ein Minimalmedium für das Wachstum von *S. pyogenes* bestimmt.

Das kinetische und das genomweite Modell erleichtern das Bestimmen und Verstehen der Ähnlichkeiten und Unterschiede zwischen *S. pyogenes* und eng verwandten Milchsäurebakterien, insbesondere *L. lactis*. Diese Modelle erleichtern die Entwicklung von Strategien zur Kontrolle oder Reduktion des Wachstums des Krankheitserregers *S. pyogenes*.

Chapter 1

Introduction

1.1	<i>Streptococcus pyogenes</i>	2
1.2	Modelling strategies and existing glycolytic models	12
1.3	Project and cooperation partners	14
1.4	Goals of the thesis	17

The results presented in this thesis are collected in the context of the SysMO project “Comparative systems biology: Lactic acid bacteria” which focuses on three simple and highly related lactic acid bacteria, namely *Streptococcus pyogenes*, *Lactococcus lactis* and *Enterococcus faecalis*. My task within this project consists in constructing a kinetic as well as a genome-scale model of *S. pyogenes*. These models are used to explore and understand the organism’s metabolism, compare it to related bacteria and propose drug targets. A detailed description of the project can be found in Section 1.3 and the goals of this thesis are defined in Section 1.4.

1.1 *Streptococcus pyogenes*

Streptococcus pyogenes is a Gram-positive, facultative anaerobic, non-motile and non-sporeforming bacteria. Since streptococci divide along a plane they appear in pairs of cells or in chains of varying length. The cell diameter ranges from 0.6 to 1.0 μm [Todar, 2011].

S. pyogenes colonises the skin, tonsils, mucous membrane and deeper tissues and causes many different infections. Acute infections comprise pharyngitis, scarlet fever, impetigo or cellulitis. Invasive infections may present necrotizing fasciitis and streptococcal toxic shock syndrome. *S. pyogenes* can also cause immune-mediated post-streptococcal sequelae, such as acute rheumatic fever and acute glomerulonephritis, which follow acute infections [Todar, 2011]. Detailed information about streptococcal infections and sequelae can be found in [Cunningham, 2000].

Streptococci are classified depending on their cell wall polysaccharides (groups A, B, C, F and G) or lipoteichoic acids (LTA) (group D) via the Lancefield serotyping scheme [Lancefield, 1928]. Streptococci found in humans such as *S. pyogenes* occupy the group A antigen and, therefore, belong to the group A streptococci (GAS). The group A polysaccharide is a polymer of N-acetylglucosamine and rhamnose. The group-specific polysaccharide is also called the C substance or group carbohydrate antigen. GAS are further classified into M protein serotypes. This division bases on the fact that the N-terminal region of the M protein contains a type-specific moiety. The M protein is a virulence factor that extends from the cell membrane of GAS (see Section 1.1.1). More than 80 types of *S. pyogenes* M proteins have been identified [Cunningham, 2000].

A commonly used and fast method for detecting the presence of GAS in the

throat are throat cultures in blood agar. Since GAS are β -hemolytic they can be easily distinguished from normal throat flora which is usually α - or non-hemolytic [Cunningham, 2000]. Hemolysis denotes the break-down of red cell hemoglobin. If hemolysis is associated with hydrogen peroxide production, hemoglobin is oxidised to methemoglobin, changing the agar colour to green. Such a bacterium is called α -hemolytic. β -hemolysis is associated with complete lysis of red cells in the medium surrounding the colony by streptolysin, indicated by a lightened colour. Non-hemolytic or γ -hemolytic colonies do not act on red blood cells and, thus, no change within the agar surrounding the bacteria is observed [Todar, 2011].

1.1.1 Interactions between pathogen and host

S. pyogenes is one of the most widespread human pathogens. It is estimated that 5 to 15% of the population harbour this pathogen without signs of disease. When host defences are impaired or when the organism can penetrate the immune defences *S. pyogenes* is able to infect the host. Contact between the bacteria and vulnerable tissues can lead to a variety of suppurative infections [Todar, 2011].

In the past, *S. pyogenes* infections demanded many lives. Today, due to the antibiotic therapy, acute and invasive infections caused by *S. pyogenes* usually are not fatal. However, *S. pyogenes* is of major concern because of the risk of serious sequelae in untreated infections. There has been a recent increase in diversity, seriousness and sequelae of *S. pyogenes* infections and a resurgence of severe invasive infections [Todar, 2011]. Therefore, an exact knowledge about the interaction of the pathogen with the host is essential.

Virulence factors

The first contact between pathogen and host is assembled by so called virulence factors which are exposed on the cell surface. GAS produce a wide variety of virulence factors that enable them to adhere to host tissues, circumvent immune response and spread by invading host tissue layers. These factors include

- M protein, fibronectin-binding protein and LTA for adherence,
- hyaluronic acid capsule and M protein to inhibit phagocytosis,

- invasins such as streptokinase, streptodornase, hyaluronidase and streptolysins, and
- exotoxins, such as pyrogenic toxin [Cunningham, 2000, Todar, 2011].

Many of the virulence factors are present on the cell surface of *S. pyogenes*, especially those involved in colonisation, avoiding phagocytosis and the host immune responses [Cunningham, 2000]. Antigenic components present on the cell surface include the group-specific polysaccharide, peptidoglycan and LTA and a variety of surface proteins, including M protein, fimbrial proteins, fibronectin-binding proteins and cell-bound streptokinase. The cell wall of *S. pyogenes* contains some antigens similar to those of mammalian muscle and connective tissue, resulting in molecular mimicry and a tolerant or reduced host immune response [Todar, 2011].

The M protein as well as the capsule are considered to play a role in virulence [Cunningham, 2000, Todar, 2011]. The M protein is involved in colonisation and resistance to phagocytosis and is the major cause of antigenic shift and antigenic drift in the GAS. It also binds fibrinogen from serum and inhibits the binding of complement to the underlying peptidoglycan. This enables survival of the pathogen by blocking phagocytosis. The capsule of *S. pyogenes* is built-up of a polymer of hyaluronic acid. Since hyaluronic acid is chemically similar to that of host connective tissue the pathogen can hide its own antigens. Therefore, the capsule also prohibits opsonized phagocytosis by neutrophils or macrophages [Todar, 2011].

GAS can be opsonized by activation of the classical or alternate complement pathway and by anti-streptococcal antibodies. These specific antibodies are able to kill *S. pyogenes* rapidly following phagocytosis since the pathogen is catalase-negative and produces no significant amounts of superoxide dismutase to inactivate the oxygen metabolites produced by the phagocyte. Therefore, the streptococcal defence must prohibit phagocytosis [Todar, 2011].

Adhesion

After the first contact is accomplished, interactions between the pathogen and the host occur due to binding of surface streptococcal ligands to specific receptors on host cells. *S. pyogenes* produces many adhesins differing in specificity. Evidence suggests that *S. pyogenes* exploits LTA, M protein and fibronectin-binding proteins

as adhesins [Todar, 2011]. Strong adherence of GAS to pharyngeal or dermal epithelial cells is the most important initial step in colonisation of the host. Without these mechanisms, the pathogen could not attach to host tissues and would be removed by mucous and salivary fluid flow mechanisms [Cunningham, 2000].

Invasins and toxins

GAS not only adhere to epithelial cells but also invade them. The reason for invasion is not absolutely clear [Cunningham, 2000]. However, two hypothesis have been constructed for the role of internalisation of GAS in disease pathogenesis. First, invasion means to avoid host defence mechanisms and thus may play a role in the carriage and persistence of streptococci. Second, studies imply that internalisation could lead to invasion of deeper tissues [LaPenta et al., 1994], while other studies detected that low virulence was associated with internalisation [Schrager et al., 1996]. Maybe both hypothesis are correct depending on the virulence and properties of the invading bacterium as well as on the invaded epithelium. Perhaps internalisation describes successful containment of the pathogen by the host. This theory is corroborated by the observation that poorly encapsulated strains are internalised most efficiently but are relatively avirulent in infection models [Schrager et al., 1996, Cunningham, 2000].

GAS secrete several proteins including virulence factors, invasins and toxins into its host. These secreted proteins interact with human blood and tissue components in such ways that kill the cells and provoke a damaging inflammatory response. GAS invasins lyse eukaryotic cells and other host macromolecules and enable the bacteria to spread among tissues by dissolving host fibrin and intercellular ground substances. In the following, some of these invasins and protein toxins are shortly described. Streptolysin is one of the streptococcal exotoxins killing leukocytes and includes streptolysin S, an oxygen-stable leukocidin and streptolysin O which is an oxygen-labile leukocidin. NADase also functions as a leukotoxic. *S. pyogenes* produces hyaluronidase which degrades hyaluronic acid and is able to digest the host's as well as the organism's own capsule. Streptokinase binds plasminogen and converts it to plasmin, which further digests fibrin and other proteins. Fibrin plays a role in blood coagulation. The plasminogen-binding activity of streptokinase may also directly contribute to streptococcal virulence and invasion of tissues [Cunningham, 2000]. GAS secrete up to four different streptodornases which possess deoxyribonuclease activity and protect the bacteria from being trapped in neutrophil

extracellular traps. Three streptococcal pyrogenic exotoxins secreted by GAS are identified, namely types A, B and C, which act as superantigens on the immune system. Superantigens are a class of antigens that do not require processing by antigen-presenting cells and release immense amounts of cytokines. Compared to conventional antigen-induced T cell response, superantigens activate a much larger number of T cells [Cunningham, 2000, Todar, 2011].

Immunity

For effective clearance of the group A streptococci by polymorphonuclear leukocytes or neutrophils opsonizing antibodies against type-specific M proteins are essential [Lancefield, 1962]. Type-specific antibodies recognise epitopes in the amino-terminal region of the M protein molecule [Jones & Fischetti, 1988]. Once the host is exposed to the type-specific epitopes, a primary response occurs and long-term immunity to the infecting serotype is acquired [Lancefield, 1959]. Immune responses can also appear to other parts of the M protein molecule but these antibodies are non-opsonic and therefore not protective. Opsonic antibodies are probably produced late in infection while non-opsonic epitopes are produced prior to the opsonic response [Fischetti, 1977]. Non-type-specific epitopes are shared among GAS and a secondary response would occur faster to the epitopes to which the host had been previously exposed. Protective immunity has two major mechanisms. The pathogen can be hindered from adherence to mucosal surfaces preventing colonisation. Second, after invasion GAS is phagocytosed and killed due to opsonisation with type-specific antibody and complement preventing multiplication in the host and elimination of the bacterium in host tissues or blood [Cunningham, 2000].

Vaccination and prevention

Penicillin is still the drug of choice for GAS infections and is used as prophylaxis to prevent streptococcal sequelae. GAS are highly sensitive to penicillin. In severe diseases penicillin can be combined with clindamycin. Macrolides such as erythromycin are an alternative antibiotic for the treatment of GAS infections in patients allergic to penicillin whereby erythromycin-resistance becomes more frequent [Stille et al., 2005].

No vaccines preventing streptococcal infections and their sequelae are available so far but are under study. These vaccines contain streptococcal surface components

like M proteins and C5a peptidase. It was found that immunity to the M protein is protective against GAS infection and that has initiated the study of M protein vaccines. The immune response against the M protein results in the production of antibodies which promote phagocytosis and killing. Due to its role as a major virulence factor the M protein has the potential as a vaccine against streptococcal infections [Cunningham, 2000].

1.1.2 Metabolic capabilities

S. pyogenes belongs to the group of lactic acid bacteria (LAB) which are characterised by their capability to ferment glucose to lactic acid. LAB survive in distinct biotopes, including foods, plants and even the human body. Some of these play an essential role in the fermented food and beverage industry, while others possess pathogenic features. There is a great biodiversity amongst lactic acid-producing bacteria with respect to their genetics and consequent biochemical details, reflected in differences in flavor production, acidification, pathogenicity and health benefits [Levering et al., 2011].

Lactic acid bacteria are Gram-positive rods and cocci that rely primarily on fermentation for energy generation (adenosine triphosphate (ATP) production) and, thus, can grow well anaerobically. Nevertheless, they can also grow in the presence of oxygen as aerotolerant anaerobes. Although they are catalase-negative, LAB possess a superoxide dismutase and have alternative mechanisms to get rid of peroxide radicals, generally through peroxidase enzymes. LAB ferment hexose sugars via the Embden-Meyerhof-Parnas pathway either to lactate alone or to lactate and acetate, ethanol and carbon dioxide [Tittsler et al., 1952].

On the basis of the amount of fermentation end-products lactic acid bacteria can be classified into two groups, homofermentative and heterofermentative bacteria. Under conditions of excess glucose and limited oxygen, homolactic LAB ferment one molecule of glucose to two pyruvate molecules yielding two ATP per glucose consumed. Redox balance is maintained through oxidating reduced nicotinamide adenine dinucleotide (NADH) concomitant with the conversion of pyruvate to lactate. Thereby, lactate is the major end-product (> 85%). The remaining products are carbon dioxide and acetate. Heterofermentative bacteria produce up to 50% lactate, 20 to 25% acetate and 20 to 25% carbon dioxide and ethanol from glucose. Fermentation of pentoses yield equimolecular amounts of lactate and acetate in both

organisms, homofermentative and heterofermentative bacteria [Tittsler et al., 1952].

Two mechanisms for the uptake and phosphorylation of carbon sources occur in lactic acid-producing bacteria. First, the sugar is transported into the cell via a permease and phosphorylated by an ATP-dependent glucokinase. Second, the phosphoenolpyruvate:carbohydrate phosphotransferase system (PTS) mediates the sugar uptake and subsequent phosphorylation with phosphoenolpyruvate (PEP) functioning as phosphoryl donor [Postma et al., 1993]. Thereby, the main part of the sugar is taken up via the PTS system [Cvitkovitch et al., 1995].

The requirement of PEP for sugar uptake and, thus, for initiating glycolysis integrates a loop into the system since PEP is produced in the lower part of glycolysis. The regulation of sugar uptake via the PTS system by a fructose-1,6-bisphosphate (FBP) activated ATP-dependent protein kinase introduces another loop. These feedback loops render the model into a complex system with much richer dynamics and many interdependencies as compared to a linear system. Changes done in the kinetics of one enzyme propagates through the whole system due to modifications in the enzyme's substrate and product concentrations.

In general, lactic acid bacteria have evolved in environments that are rich in amino acids, vitamins, purines and pyrimidines. As a consequence, they have complex nutritional requirements. Species differ in their ability to ferment individual carbohydrates and in their preferred carbon source [Gunnewijk et al., 2001]. The most commonly used sugar for their cultivation is glucose. Growth of LAB requires supply of vitamins and related growth factors like p-aminobenzoic acid, biotin, riboflavin, thiamine, vitamin B₆ and vitamin B₁₂, whereby the amount of required growth factors differ among the organisms [Tittsler et al., 1952].

The amount and combination of amino acids required for growth is characteristic for each LAB and depends upon the medium composition, i.e. upon the supplied vitamins. This explains the often contradicting data about essential amino acids of LAB in literature. Some amino acids are non-essential for growth and can be synthesised by transamination if vitamin B₆ is supplied in high amounts. Biotin is involved in aspartate synthesis and folic acid in serine synthesis. However, even if all vitamins are supplied in excess, lactic acid bacteria still require many amino acids for growth. Among the necessary growth factors are purine and pyrimidine bases which are precursors for nucleic acid synthesis. Besides its function as a buffer, acetic acid stimulates growth of most LAB. Furthermore, inorganic salts

like potassium, manganese, magnesium and phosphate are required by lactic acid bacteria. The complex nutritional requirements indicate that many biochemical byways of metabolism present in other organisms are lacking in lactic acid bacteria. As a consequence, these bacteria represent useful organisms for biochemical research [Tittsler et al., 1952].

These examples of nutritional requirements and their interrelationships point out that each lactic acid bacteria requires a specific medium for optimal growth. Within the SysMO-LAB project, the three different lactic acid bacteria *L. lactis*, *S. pyogenes* and *E. faecalis* are examined. To be able to compare experimental results, especially growth under different cultivation conditions, a specific medium supporting the growth of the examined organisms was designed by collaboration partners (see Section 2.1.3).

As mentioned before, lactic acid bacteria such as *S. pyogenes* essentially ferment glucose to lactic acid. However, under certain conditions, e.g. glucose limitation, the metabolism of these bacteria shifts from homolactic to mixed acid fermentation resulting in the production of formate, acetate and ethanol [Thomas et al., 1979]. This is a more efficient way of fermentation since three molecules of ATP are produced per molecule of glucose. The oxidative part of the pentose phosphate pathway (PPP) and the citrate cycle are missing in *S. pyogenes*. Therefore, this bacterium relies on glycolysis and pyruvate metabolism for energy production. As stated above, *S. pyogenes* is auxotroph for many amino acids and some vitamins. A detailed overview of the genome-scale metabolism of *S. pyogenes* is given in Section 3.5.

1.1.3 Studied kinetics and primary metabolism

As stated above, *S. pyogenes* produces the energy required for growth by fermentation. Thus, one possibility to reduce its growth is inhibiting its glycolysis and pyruvate degradation. The identification of such targets is facilitated by using mathematical models. The development of a reliable model requires a good knowledge about the studied pathway and its enzymes, e.g. the kinetic parameters and regulation. The following section gives an overview about the studied parts of glycolysis in *S. pyogenes*.

So far, the dynamics of *S. pyogenes* metabolism have hardly been studied. Some *S. pyogenes*-specific allosteric regulations of glycolytic processes have been identified, but no dynamic model of *S. pyogenes* glycolysis exists so far. Due to its role

as wide-spread human pathogen, focus of studies on *S. pyogenes* has been particularly on the molecular mechanisms behind virulence rather than on metabolism.

One of the best studied part of energy metabolism in *S. pyogenes* is the control of sugar uptake. One component of the PTS, the histidine containing protein (HPr), plays a crucial role in the sugar uptake control. In low-G+C Gram-positive bacteria, HPr can be phosphorylated on two sites. It can be phosphorylated by PEP at His-15 yielding HPr-His-P but also by ATP at Ser-46 resulting in HPr-Ser-P [Ye et al., 1996]. In response to changes in its phosphorylation state HPr carries out diverse regulatory functions. HPr-His-P is required for sugar uptake while HPr-Ser-P regulates among others the extent of sugar-phosphate accumulation by inhibiting uptake or by activating expulsion of the sugar.

Reizer and Panos demonstrated that *S. pyogenes* has a special mechanism conducting catabolite regulation [Reizer & Panos, 1980]. When *S. pyogenes* is grown on thiomethyl- β -D-galactoside (TMG), a non-metabolisable lactose analogue, the intracellular TMG-6-P pool is stable. When glucose is added, TMG-6-P is dephosphorylated and transported out of the cell. This mechanism, called inducer expulsion, is mediated by a sugar-phosphate phosphatase (PaseII) [Reizer & Saier, 1983]. Under glucose excess conditions, FBP accumulates and inorganic phosphate (P_i) declines. FBP stimulates an ATP-dependent HPr kinase which phosphorylates HPr on a serine residue. The resulting HPr-Ser-P regulates the inducer expulsion mechanism [Ye et al., 1996]. HPr-Ser-P can be dephosphorylated by HPr phosphatase, which is activated by phosphate. Thus, P_i and FBP regulate inducer expulsion [Deutscher et al., 1985].

Inducer expulsion has been demonstrated in species of Lactococci, Enterococci and some Streptococci. *S. pyogenes* and *S. bovis* exhibit inducer expulsion whereas *S. mutans* and *S. salivarius* do not [Ye et al., 1996]. Furthermore, high-G+C Gram-positive bacteria do not show HPr kinase activity. Therefore, the expression of the HPr kinase may be a characteristic feature of low-G+C Gram-positive bacteria [Ye et al., 1996].

Thompson and Saier [Thompson & Saier, 1981] demonstrated that sugar uptake via PTS is strongly inhibited in the presence of high concentrations of any metabolisable PTS sugars. *L. lactis* cells grown on TMG accumulate this non-metabolisable lactose analogue. The simultaneous addition of a PTS sugar such as glucose inhibited the uptake of TMG. This process is called inducer exclusion and provides

a mechanism for creating a hierarchy of preferred sugars. In particular, it prevents the accumulation of non-metabolisable sugar phosphates.

In contrast to *L. lactis* and *E. faecalis*, *S. pyogenes* possesses a non-phosphorylating NADP⁺-dependent glyceraldehyde-3-phosphate dehydrogenase (GAPN) which catalyses the irreversible conversion of glyceraldehyde-3-phosphate (GAP) to 3-phosphoglycerate (3PG) by reducing oxidised nicotinamide adenine dinucleotide phosphate (NADP⁺) to NADPH. Since the oxidative part of the pentose phosphate pathway is missing in *S. pyogenes*, it functions as an alternative mechanism to produce NADPH on the cost of one molecule ATP per molecule of GAP [Iddar et al., 2003]. Originally, GAPN was reported to be exclusively present in green eukaryotes. However, it has been found in various Gram-positive bacteria with a characteristic low-G+C content, including Bacillaceae and Streptococcaceae [Iddar et al., 2005].

Another process which has been reported about in the literature is uptake of phosphate in *S. pyogenes*. This transport reaction is inhibited by ATP and activated by extracellular phosphate (P_i^{ex}) [Reizer & Saier, 1987]. Except for the mentioned paper of Reizer and Saier no further indication of an energy-independent phosphate uptake mechanism could be found in the literature. However, the integration of this transport process was crucial for simulating our experimental data (see Section 3.2.2). Interestingly, only recently the putative gene sequence of a sodium phosphate symporter has been reported for *S. pyogenes* (for prediction see accession number B5XHT4 in UniProt [UniProt Consortium, 2010]). Since sodium is present in excess in our specific medium (see Section 2.1.3), this finding supports our decision for integrating phosphate transport in the model. Additionally, in the genome of *S. pyogenes* genes encoding an active phosphate transport system are present [Ferretti et al., 2001]. No information about regulation was found.

Interestingly, the pyruvate kinases in *S. mutans* and *L. lactis* are regulated differently although the organisms are closely related [Yamada & Carlsson, 1975b, Collins & Thomas, 1974]. Based on this fact and missing information about glycolytic key enzymes in *S. pyogenes* we decided to study the kinetics of pyruvate kinase and lactate dehydrogenase ourselves (see Section 3.1.4).

1.2 Modelling strategies and existing glycolytic models

Since *S. pyogenes* is a human pathogen and no vaccines or specific antibiotics are available so far, the exploration of drug targets is still one aspect of research. To find such targets the metabolism of this pathogen is analysed. For this purpose systems biology provides a variety of tools to explore the metabolism. Systems biology is an interdisciplinary research field that focuses on complex interactions in biological systems and involves the development of mathematical models to analyse for example the interactions between the components of the system or the sensitivities of model components towards perturbations.

Depending on the purpose of the model and the available experimental data, different mathematical models can be used to analyse the system under investigation. In order to study the system behaviour along time under different conditions a kinetic model can be used. Metabolic networks are modelled by a set of metabolites that can be converted into each other through chemical reactions and are mathematically described by ordinary differential equations (ODEs). The velocity of each reaction is defined by a kinetic rate law. These rate laws have to be filled with kinetic parameters. Kinetic parameters can be determined experimentally and can be found in literature and databases such as SABIO-RK [Wittig et al., 2006] and BRENDA [Schomburg et al., 2002]. Kinetic models can be analysed with metabolic control analysis (MCA), sensitivity analysis and dynamic analysis methods such as phase portrait and bifurcation analysis.

Stoichiometric models describe the flux distribution within a network without knowing the rate constants for a particular reaction. As a consequence, these type of models are especially interesting for describing large scale models such as genome-scale models. In order to analyse such models flux balance analysis (FBA) is applied. To be able to apply FBA, the studied system has to be homeostatic meaning that the internal concentrations of metabolites within the system remain constant over time. To reduce the solution space of the FBA model constraints are added to the individual metabolic flux rates within the network and an objective function is defined according to the purpose of the model.

Since the dynamics of *S. pyogenes* metabolism have hardly been studied no kinetic model of *S. pyogenes* glycolysis exists so far. The metabolic network of *S. pyogenes*

has not been reconstructed as well. Therefore, both models were developed within the context of the SysMO-LAB project (see Section 1.3). Another LAB investigated within the project is *E. faecalis*. Although some kinetic studies about this bacterium exist especially about the pyruvate metabolism [Harold & Levin, 1974, Lindmark et al., 1969, Snoep et al., 1990, Wittenberger & Angelo, 1970], no kinetic model has been constructed so far. A genome-scale model is also lacking for this microorganism and is also reconstructed within the framework of the SysMO-LAB project by Nadine Veith (see Section 1.3). In contrast to that, several kinetic models have been developed of *L. lactis* glycolysis, each concentrating on a different aspect. The existing models study either metabolic flux distributions [Hoefnagel et al., 2002a, Hoefnagel et al., 2002b], metabolic regulation [Voit et al., 2006a, Oh et al., 2011] or pH control [Andersen et al., 2009]. The kinetic model published by Hoefnagel *et al.* [Hoefnagel et al., 2002a, Hoefnagel et al., 2002b] comprises glycolysis, pyruvate metabolism and an overall reaction for polysaccharides for cell synthesis. All in all the model gives a qualitative correct behaviour of glycolysis but fails to do so quantitatively [Hoefnagel et al., 2002a]. The model studying regulation of glucose consumption in *L. lactis* developed by Voit *et al.* [Voit et al., 2006a] comprise simple power-law kinetics. To simplify the model ATP and P_i are modelled as constant functions. The Andersen model [Andersen et al., 2009] is based on the existing Hoefnagel model [Hoefnagel et al., 2002a] and extends this model to simulate the effect of lowering extracellular pH. The published models omitted phosphate transport [Andersen et al., 2009, Hoefnagel et al., 2002b, Oh et al., 2011] or considered phosphate as constant [Neves et al., 1999, Voit et al., 2006a].

1.3 Project and cooperation partners

This dissertation is done in the context of the SysMO (Systems Biology of Microorganisms) project “Comparative systems biology: Lactic acid bacteria” which focuses on three relatively simple and highly related lactic acid bacteria, namely

1. *Lactococcus lactis*, the major microorganism used in the dairy industry,
2. *Streptococcus pyogenes*, a human pathogen, and
3. *Enterococcus faecalis*, a major contaminant in food and water as well as a contributor to food fermentation.

Lactococci are not known to be pathogenic or to cause food poisoning in man. A few species of streptococci, especially *S. pyogenes*, are known to be human pathogens. Due to modern sanitary food handling methods food-borne epidemics caused by streptococci have become unusual. Enterococci, one group of streptococci, is intestinal in origin but is also used as a contributor to food fermentation [Tittsler et al., 1952].

Although these microorganisms have a similar primary metabolism, they persist in different environments (milk, skin/mucous membrane/blood and faeces). Furthermore, they exhibit significant differences in their functional relationship with human beings. Within this consortium, detailed mathematical models of the primary metabolism of the three lactic acid bacteria are developed facilitating a thorough understanding of the differences and similarities between the three lactic acid bacteria and the extent to which these differences contribute to different functionalities. These models help in the design of strategies that allow metabolic engineering but also control of growth. Modelling is done in close collaboration with experimental and theoretical groups within this consortium.

Within this project my part is the construction and analysis of a dynamic as well as a genome-scale model of *S. pyogenes*. These models are used to understand on the one hand the similarities and differences between *S. pyogenes* and related lactic acid bacteria and, on the other hand, the growth requirements of this human pathogen with the purpose of reducing its growth and identifying possible drug targets. The strategy for the construction of the kinetic model of the central metabolism of *S. pyogenes* consists in exploiting delivered data from partners (see

Section 3.1.3 and 3.1.4) and the adoption of unknown parameters and allosteric regulation from related organisms, especially from *L. lactis* which is used as a reference organism since it is by far the best studied lactic acid bacterium. Furthermore, several genomes have been sequenced and diverse kinetic models have been developed for its glycolysis including the pyruvate metabolism (see Section 1.2). By using a comparative approach the development of the glycolytic model of *S. pyogenes* can be accelerated starting with already existing models and modify or extend these. The development of the genome-scale model of *S. pyogenes* is facilitated by applying a semi-automatic approach and taking full advantage of already annotated reference models from *Bacillus subtilis*, *Escherichia coli*, *Lactobacillus plantarum* and *L. lactis* (see Section 2.3.1). The constructed model is validated with experimental data delivered by project partners (see Section 3.1.2 and 3.1.7).

The project focuses on the central carbon metabolism, change of carbon source and the knock-out of the L-lactate dehydrogenase gene (*ldh*). Cells are grown in a glucose-limited chemostat at two pHs and two dilution rates as well as under batch conditions with a defined glucose-pulse. A specifically medium used for the SysMO-LAB project, the CDM-LAB medium [Fiedler et al., 2011, Jonsson et al., 2009], was designed to support the growth of all three lactic acid bacteria and to allow the comparison of experimental results and the models of all three studied LAB (see Section 2.1.3).

Table 1.1 gives an overview of the participating institutions and their roles within the SysMO-LAB project. The scheduler project description is divided into the organisms and further into experimental and modelling part. Modelling was done in close collaboration with the experimental groups. The experiments were designed based on modelling results, e.g. the glucose-pulse experiments were performed with varying extracellular phosphate concentration since free phosphate had a crucial role in the model. The construction of the kinetic as well as the genome-scale model of *E. faecalis* was done by Nadine Veith in the context of an internship and a bachelor thesis and was supervised by Ursula Kummer and myself. The kinetic model of *L. lactis* was developed by Mark Musters based on previously published models and was improved and analysed by myself (see Section 3.4.1).

Table 1.1: Overview of all participating institutions and their roles within the SysMO-LAB project

Organism	Type	Part	Person involved	Affiliation
All	Experiments	Design of CDM-LAB	Martijn Bekker, Tomas Fiedler, Maria Jonsson	1, 2, 3
<i>S. pyogenes</i>	Modelling	Conception of this dissertation	Ursula Kummer, Jennifer Levering	4
		Construction of kinetic and genome-scale model	Jennifer Levering	4
	Experiments	Experimental design	Tomas Fiedler, Bernd Kreikemeyer, Araz Zeyniyev	1
			Ursula Kummer, Jennifer Levering	4
		Construction of <i>ldh</i> -negative mutant	Tomas Fiedler	1
		Fermentation experiments	Martijn Bekker, Tomas Fiedler	1, 2
		Glucose-pulse experiments	Martijn Bekker	2
		Measuring kinetics <i>in vitro</i>	Tomas Fiedler	1
Amino acid leave-out experiments	Araz Zeyniyev	1		
<i>L. lactis</i>	Modelling	Construction of kinetic model	Mark Musters, Jennifer Levering	5, 4
	Experiments	Experimental design	Martijn Bekker, Jeroen Hugenholtz, Bas Teusink, Mark Musters,	2 6, 5
			Ursula Kummer, Jennifer Levering	4
		Fermentation and glucose-pulse experiments	Martijn Bekker	3
<i>E. faecalis</i>	Modelling	Construction of kinetic and genome-scale model	Nadine Veith	4
	Experiments	Experimental design	Maria Jonsson, Ibrahim Mehmeti, Ingolf Nes, Ursula Kummer, Jennifer Levering, Nadine Veith	3 4
		Fermentation experiments	Maria Jonsson, Ibrahim Mehmeti	3
		Glucose-pulse experiments	Martijn Bekker	2

Affiliations:

1. Institute of Medical Microbiology, Virology and Hygiene, Rostock, Germany
2. Laboratory for Microbiology, Swammerdam Institute for Life Sciences, Amsterdam, The Netherlands
3. Norwegian University of Life Sciences, Department of Chemistry, Biotechnology and Food Science, Ås, Norway
4. Department of Modelling of Biological Processes, BioQuant / COS Heidelberg, University of Heidelberg, Germany
5. Laboratory of Microbiology, Wageningen University, The Netherlands
6. Systems Bioinformatics IBIVU / Netherlands Consortium for Systems Biology, Faculty of Earth and Life Sciences, Vrije Universiteit Amsterdam, The Netherlands

1.4 Goals of the thesis

The purpose of this thesis is the development of a kinetic and a genome-scale model of *S. pyogenes* and the understanding of the differences and similarities between *S. pyogenes* and *L. lactis* and the extent to which these differences contribute to different functionalities. Since the *E. faecalis* model is still under investigation, the central conclusions are not based on this model. However, it is used for comparison when appropriate. In the following the goals of this thesis are specified.

1. Construct a kinetic model of *S. pyogenes* using ODEs based on an extensive literature survey and delivered experimental data.
 - Simulate our glucose-pulse data.
 - Simulate our fermentation data at two pHs and two dilution rates.
 - Understand the differences and similarities between *S. pyogenes* and *L. lactis* based on the developed kinetic models.
 - Understand the adaption to different environments based on the models of *S. pyogenes* and *L. lactis*.
2. Reconstruct the metabolic network of *S. pyogenes* based on a semi-automatic approach which takes advantage of already existing and manually curated models.
 - Simulate our fermentation data.
 - Understand the growth requirements of *S. pyogenes* and define optimal and suboptimal conditions.
 - Explore the organism's reaction to perturbations in its environment.
 - Find strategies to reduce the growth of the pathogen *S. pyogenes* and propose drug targets.
 - Describe differences and similarities between *S. pyogenes* and *L. lactis*.

Chapter 2

Materials and Methods

2.1	Experimental data	20
2.2	Dynamic modelling	26
2.3	Genome-scale modelling	35

2.1 Experimental data

In this section the experimental methods used within the SysMO-LAB project are described. Since my role in the project consists in modelling *S. pyogenes* and I did no experiments myself, in each paragraph the experimentalist is named. For an overview of all participating institutions and their roles within the project see Section 1.3.

2.1.1 Bacterial strains

Within this project two different strains of *S. pyogenes*, namely *S. pyogenes* M49 591 and *S. pyogenes* M49 591 Δ *ldh* were investigated. Furthermore, *L. lactis* NZ9000 and the *ldh*-deficient strain NZ9010 [Hoefnagel et al., 2002a, Linares et al., 2010] as well as *E. faecalis* V583 and V583 Δ *ldh*-1 [Jonsson et al., 2009] were analysed.

2.1.2 Construction of recombinant vectors and mutant strains

For the construction of a *S. pyogenes* M49 *ldh*-knock-out strain, a 2,977 bp fragment comprising the *ldh* and 1,000 bp of the upstream and 993 bp of the downstream flanking sequences was PCR-amplified from chromosomal DNA of *S. pyogenes*. The resulting PCR fragment was digested with *SacI* and *SphI* and ligated into the equally treated pUC18Erm1 vector [Baev et al., 1999]. The resulting plasmid was used as a template for an outward-PCR. Thus, the resulting PCR product comprised the whole plasmid including the upstream and downstream flanking regions of the *ldh* gene but excluding the *ldh* gene itself. After restriction of this fragment with *BamHI* and *SalI* it was ligated with an equally treated PCR fragment comprising the spectinomycin-resistance gene *aad9* from plasmid pSF152 [Tao et al., 1992]. The resulting recombinant plasmid pUCerm-ldh-ko was transformed into *S. pyogenes* and double crossover events were assayed by selection for erythromycin sensitive but spectinomycin resistant transformants. The correct replacement of the *ldh* gene by the *aad9* gene in the respective transformants was confirmed by appropriate PCR assays and L-lactate dehydrogenase (LDH) activity assays. For all PCR amplifications the Phusion High Fidelity PCR Kit (Finzymes) was used [Fiedler et al., 2011]. The construction of recombinant vectors and the *ldh*-deletion strain for *S. pyogenes* were done by Tomas Fiedler.

2.1.3 CDM-LAB medium

All three bacteria persist in different environments and thus differ in their optima cultivation conditions, e.g. the pH. To be able to compare the experimental results and thus the models, Martijn Bekker, Tomas Fiedler and Maria Jonsson designed a medium used for the SysMO-LAB project, the CDM-LAB medium [Fiedler et al., 2011, Jonsson et al., 2009], supporting the growth of all three lactic acid bacteria. The medium contained per litre: 1 g K_2HPO_4 , 5 g KH_2PO_4 , 0.6 g ammonium citrate, 1 g acetate, 0.25 g tyrosine, 0.24 g alanine, 0.125 g arginine, 0.42 g aspartic acid, 0.13 g cysteine, 0.5 g glutamic acid, 0.15 g histidine, 0.21 g isoleucine, 0.475 g leucine, 0.44 g lysine, 0.275 g phenylalanine, 0.675 g proline, 0.34 g serine, 0.225 g threonine, 0.05 g tryptophan, 0.325 g valine, 0.175 g glycine, 0.125 g methionine, 0.1 g asparagine, 0.2 g glutamine, 10 g glucose, 0.5 g L-ascorbic acid, 35 mg adenine sulfate, 27 mg guanine, 22 mg uracil, 50 mg cystine, 50 mg xanthine, 2.5 mg D-biotin, 1 mg vitamin B₁₂, 1 mg riboflavin, 5 mg pyridoxamine-HCl, 10 μ g p-aminobenzoic acid, 1 mg pantothenate, 5 mg inosine, 1 mg nicotinic acid, 5 mg orotic acid, 2 mg pyridoxine, 1 mg thiamine, 2.5 mg lipoic acid, 5 mg thymidine, 200 mg $MgCl_2$, 50 mg $CaCl_2$, 16 mg $MnCl_2$, 3 mg $FeCl_3$, 5 mg $FeCl_2$, 5 mg $ZnSO_4$, 2.5 mg $CoSO_4$, 2.5 mg $CuSO_4$, 2.5 mg $(NH_4)_6Mo_7O_{24}$. Media was buffered with either 100 mM MES buffer or 100 mM MOPS buffer for growth at pH 6.5 and 7.5, respectively.

2.1.4 Fermentation experiments

S. pyogenes M49 wild-type strain and its *ldh*-negative mutant were grown in anaerobic glucose-limited chemostat cultures in CDM-LAB medium [Fiedler et al., 2011, Jonsson et al., 2009] in a Biostat Bplus fermentor unit with a total volume of 750 and 1000 ml at a stirring rate of 100 and 400 rpm by Tomas Fiedler and Martijn Bekker, respectively. The temperature was kept at 37°C. The pH was maintained at 6.5 and 7.5, respectively, by titrating with sterile 2 M NaOH. The supply of medium occurs with different dilution rates (D) of 0.05 h^{-1} and 0.15 h^{-1} , respectively, controlling growth rates. Culture volume was kept constant by removing culture liquid at the same rate that fresh medium was added. Thus, the number of organisms per volume is constant. The cultures were considered to be in steady state when no detectable glucose remained in the culture supernatant and the optical densities

(ODs), dry weights (DWs) and product concentrations of the cultures were constant on two consecutive days. All chemostat results showed a carbon balance of $80\% \pm 10\%$ on the basis of glucose consumption and organic acid formation. Steady state bacterial DW was measured as described previously [Alexeeva et al., 2000]. Glucose, pyruvate, lactate, formate, acetate, succinate and ethanol were determined by high-pressure liquid chromatography (HPLC, LKB) with a Rezex organic acid analysis column (Phenomenex) at a temperature of 45°C with $7.2\text{ mM H}_2\text{SO}_4$ as the eluent, using a RI 1530 refractive index detector (Jasco) and AZUR chromatography software for data integration. Discrimination between D- and L-lactate was performed using a D-/L-lactate assay kit (Megazyme). Aspartic acid, serine, glutamic acid, glycine, histidine, arginine, threonine, alanine, proline, cysteine, tyrosine, valine, methionine, lysine, isoleucine, leucine and phenylalanine were determined by HPLC (Agilent) by use of the Waters AccQ Tag method. Fluorescence was analysed using a Hitachi F-1080 fluorescence detector set to 250 nm excitation and emission was recorded at 395 nm [Fiedler et al., 2011].

2.1.5 Glucose-pulse experiments

To measure intra- and extracellular metabolite profiles under batch conditions, e.g. glucose-6-phosphate (G6P), fructose-6-phosphate (F6P), FBP, GAP, PEP, pyruvate, ATP, extracellular lactate and extracellular glucose (Glc^{ex}), *S. pyogenes* cells were grown in THY medium. This medium consists of 36.4 g/l Todd-Hewitt Broth (Oxoid) and 5 g/l yeast extract (Oxoid). Mid-exponentially grown cells were harvested by centrifugation at 5000 rpm for 10 minutes at room temperature, washed twice with 50 mM MES buffer ($\text{pH } 6.5$) and finally suspended in the indicated buffer solution. Anaerobic conditions were established by flushing with nitrogen for 10 minutes . Glucose was added and $400\text{ }\mu\text{l}$ samples were taken at regular time intervals. These samples were mixed immediately with $200\text{ }\mu\text{l}$ of a cold perchloric acid (3.5 M) solution. The extracts were kept on ice for maximal 60 minutes . The pH was neutralised with $160\text{ }\mu\text{l}$ 2 M KOH . The pH-adjusted samples were centrifuged and the supernatants were stored at -80°C for subsequent analysis. All metabolites were quantified by enzymatic methods coupled to the spectrophotometric determination of NAD(P)H (M. Bekker, personal communication). Glucose-pulse experiments were performed by Martijn Bekker.

2.1.6 Kinetic measurements of individual enzymes

Kinetic analysis of L-lactate dehydrogenase

Kinetic measurements of L-lactate dehydrogenase of *S. pyogenes* were done by Tomas Fiedler. For heterologous expression of the LDH of *S. pyogenes* chromosomal DNA of the M49 serotype strain was isolated according to the Qiagen Blood and Tissue Kit (Qiagen, Hilden, Germany) and used as a template for PCR amplification with the PhusionTM High Fidelity PCR Kit (Finzymes). The resulting PCR fragment was ligated into the pASK-IBA2 vector (IBA GmbH, Göttingen, Germany) system via *Bam*HI and *Sal*I restriction sites. The recombinant vector was heat-shock transformed in CaCl₂ competent *E. coli* DH5 α cells. Correct insertion of the PCR product was confirmed by plasmid sequencing. For heterologous expression of the corresponding enzyme recombinant *E. coli* strains were grown in 200 ml Luria-Bertani medium at 37°C under vigorous shaking. At an OD of about 0.4 expression was induced by addition of anhydrotetracycline (0.2 μ g/ml) and growth of the bacteria was allowed for another two to four hours. Cells were harvested by centrifugation and bacterial pellets were stored overnight at -20°C, subsequently thawed, suspended in 1 ml of buffer W (100 mM Tris-HCl pH 8.0, 1 mM EDTA, 150 mM NaCl) and disrupted using a Ribolyzer. Cell debris was removed by centrifugation for 10 min at 13,000 g and 4°C. Clear supernatants were diluted 1:10 with buffer W and applied to StrepTactin sepharose (IBA GmbH, Göttingen, Germany) columns. After washing the sepharose 3 times with 10 ml of buffer W recombinant Strep-tagged protein was eluted with 6 \times 0.5 ml of buffer E (buffer W including 2.5 mM desthiobiotin). Elution fractions were checked for recombinant protein by SDS-PAGE and Western Blots using Strep-Tag specific antibodies.

For LDH activity measurements protein concentrations in the purified recombinant protein fractions were determined using the Bradford method (Bio-Rad Protein Assay Kit, Bio-Rad, Munich, Germany). The standard assay for determination of LDH activity was carried out by adding 50 μ l protein solution, 25 μ l FBP (20 mM) and 25 μ l NADH (6.75 mM) to 800 μ l sodium-phosphate buffer (50 mM, pH 6.8). The mixture was heated to 37°C and the reaction was started by adding 100 μ l pre-warmed (37°C) sodium pyruvate (100 mM) to the reaction mixture. The LDH-activity was assayed by measuring the decrease of NADH in the mixture at 340 nm in a spectrophotometer for 5 min. The conversion of 1 μ mol of NADH ($\epsilon_{\text{NADH}} =$

6220 l mol⁻¹ cm⁻¹) to oxidised nicotinamide adenine dinucleotide (NAD⁺) per minute was defined as one unit of LDH activity. The activity was expressed as enzyme unit (U) per mg of protein. For determination of Michaelis binding constants (K_m) and allosteric regulation the standard assay was modified by using varying concentrations of P_i, sodium pyruvate, FBP, NADH, ATP and NAD⁺. For determination of the K_m-values for the reverse reaction, NADH and sodium pyruvate were replaced by varying concentrations of NAD⁺ and L-lactate (T. Fiedler, personal communication).

Kinetic analysis of pyruvate kinase

Kinetic measurements of *S. pyogenes* pyruvate kinase (PYK) were done with protein crude extracts by Tomas Fiedler. For that purpose cells from 50 ml of an exponentially growing *S. pyogenes* culture in CDM-LAB medium [Fiedler et al., 2011, Jonsson et al., 2009] were harvested by centrifugation. Bacteria were washed twice in 1× PBS buffer, suspended in 1× PBS to an OD (600 nm) of 10 and lysed with 100 U of Phagelysin C per ml for 15 min at 37°C [Köller et al., 2008, Nelson et al., 2006]. Subsequently, cell debris was removed by centrifugation (10 min, 15,000 g) and the supernatant was filter-sterilised (0.22 μm). For the standard PYK assay 20 μl of protein crude extract were mixed with 880 μl pre-warmed (37°C) reaction buffer (120 mM cacodylic acid, 120 mM KCl, 12 mM ADP, 1.2 mM FBP, 30 mM MgCl₂, 0.18 mM NADH, 5 U/ml L-LDH). The reaction was started by addition of 100 μl pre-warmed (37°C) PEP (20 mM). The PYK activity was assayed by measuring the decrease of NADH in the mixture at 340 nm in a spectrophotometer for 5 min. The conversion of 1 μmol of NADH ($\epsilon_{\text{NADH}} = 6220 \text{ l mol}^{-1} \text{ cm}^{-1}$) to NAD⁺ per minute was defined as one unit of PYK activity. The activity was expressed as U per mg of protein. For determination of K_m-values the concentrations of the respective substrates were modified in the standard assay (T. Fiedler, personal communication).

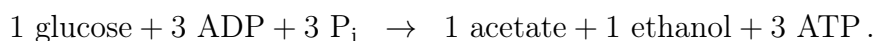
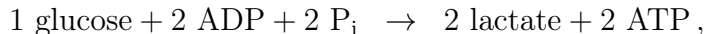
2.1.7 Substrate utilisation assays

For substrate utilisation assays, bacteria were grown overnight in CDM-LAB medium [Fiedler et al., 2011, Jonsson et al., 2009], pelleted by centrifugation, washed twice in phosphate-buffered saline (pH 7.4) and suspended in glucose-free CDM-LAB medium. Optical densities were adjusted to 0.05 and 100 μl bacterial suspension

was applied to each well of Biolog phenotype microarray plates PM1 and PM2. The microarray plates were incubated for 24 h at 37°C in a 5% CO₂ atmosphere and the optical densities of each well were measured. The optical densities in well A1 of the arrays containing no carbon source were subtracted from all values. Optical densities in the wells containing α -D-glucose were set equal to 100% and all other values were related accordingly [Fiedler et al., 2011]. Substrate utilisation assays were done by Tomas Fiedler.

2.1.8 Calculation of specific ATP synthesis rates

The calculation of specific ATP synthesis rates was done by Tomas Fiedler, Martijn Bekker, Maria Jonsson and co-workers [Fiedler et al., 2011]. The rate of ATP synthesised by substrate-level phosphorylation is stoichiometrically coupled to the rate of lactate, acetate and ethanol synthesis. From one molecule of glucose two ATP can be synthesised by producing lactate whereas the mixed-acid fermentation yields three ATP molecules



The rate of energy required for maintenance ($q_{\text{ATP maintenance}}$) was estimated by extrapolating the linear line of dilution rate plotted against the total rate of ATP synthesis to $D = 0$. The ATP production rate at the maximal specific growth rate μ_{max} ($q_{\text{ATP } \mu_{\text{max}}}$) was estimated by extrapolating the same line to the D at which the specific organism has its maximal specific growth rate [Fiedler et al., 2011].

The cell mass in g produced per mol of ATP generated by substrate catabolism (Y_{atp}) was determined at a dilution rate of 0.15 h⁻¹ since Y_{atp} at lower dilution rates is strongly influenced by $q_{\text{ATP maintenance}}$ [Tempest & Neijssel, 1984].

2.1.9 Amino acid leave-out experiments

For amino acid leave-out experiments *S. pyogenes* was grown overnight in CDM-LAB medium [Fiedler et al., 2011, Jonsson et al., 2009], pelleted by centrifugation, washed and suspended in full CDM-LAB medium or CDM-LAB medium with amino acid leave-outs. Bacterial suspension was applied to 96-well plates and incubated at 37°C in atmospheric air and the optical density of each well was measured at

600 nm in a Spectramax Plate reader (T. Fiedler, personal communication). Amino acid leave-out experiments were done in Tomas Fiedler's lab and by Araz Zeyniyev.

2.2 Dynamic modelling

Biochemical networks comprise the chemical reactions converting the metabolites into each other. Such networks are mathematically represented by a set of ODEs which describe the concentration changes along time. Therefore, expressions describing the velocity at which the reactions proceed are needed. Each reaction velocity is described by a rate law and depends on the concentration of substrates, products and modifiers of this reaction. The resulting set of ODEs is used to analyse the model and simulate the metabolite concentrations along time. In the following sections the set-up of the glycolytic model and methods used for simulation and analysis are described.

2.2.1 COPASI

Modelling, simulation and analysis of the glycolytic model of *S. pyogenes* was done in COPASI (**CO**mplex **PA**thway **SI**mulator) [Hoops et al., 2006]. COPASI is free for academic user and is available at <http://www.copasi.org>.

As a first step the general model settings like the units for time, volume and concentration quantities were specified. In the model of *S. pyogenes* the time is defined as seconds, the volume as litre and concentrations are given in mmol. Since the model comprises intra- and extracellular species, a new compartment was added. Thus, the glycolytic model of *S. pyogenes* contains an intra- and extracellular compartment, both with fixed volumes and given by the experimental data. For the continuous cultured cells as well as for the glucose-pulse experiments the ratio of the intra- to extracellular compartment was adjusted for each experimental condition as determined experimentally. Therefore, dry weights were calculated from measured ODs (in arbitrary units (AU)) by multiplication with the *L. lactis* specific correlation factor of 0.33 g DW per litre per AU [Pedersen et al., 2002]. From *E. coli* it is known that the intracellular volume is 2.5 ml per g DW [Winkler & Wilson, 1966]. Thus, the ratio of intra- to extracellular volume, denoted by vol , can be derived

from the OD by the following equation

$$\text{vol} = \text{OD} \cdot 0.33 \frac{\text{g DW}}{\text{l}} \cdot 2.5 \cdot 10^{-3} \frac{\text{l}}{\text{g DW}}.$$

After defining certain parameters for the model the metabolites or species taking part in the glycolysis and pyruvate branching were initialised. For each metabolite its name, the compartment it is localised in, the simulation type and the initial concentration were specified. For all species the concentration is determined by the kinetic laws of the reactions that modify the species. The initial concentrations are listed in Table A.6 and the compartment volumes are given in Section 3.2.1.

With this information the reactions are defined. A reaction is identified by its name, an equation, whether the reaction is reversible or not, a rate law and corresponding parameters for this law. The equation describes the chemical formula and maybe additional modifiers like inhibitors and activators of the reaction. The rate law for each reaction can be either chosen from a list of predefined kinetics or be added by the user. Since the detailed enzymatic mechanism for most *S. pyogenes* enzymes is unknown, convenience kinetics were used (see section 2.2.3). The rate laws used in the glycolytic model of *S. pyogenes* can be found in Appendix A.2.1 and the corresponding parameters are listed in Appendix A.1 in the Tables A.1 – A.6.

2.2.2 Ordinary differential equations

Within the network, each metabolite is represented by an ODE. Each ODE is composed by a sum of terms that represent the velocities of all reactions affecting the metabolite concentration. For a species X the time-dependent concentration change is defined as

$$\frac{d[X]}{dt} = \sum_i s_i \cdot v_i,$$

where s_i is the stoichiometric coefficient and v_i is the velocity of reaction i . The stoichiometric coefficient is the number of molecules of X that participate in reaction i . If X is consumed s_i is negative, positive if X is produced and zero if X is neither produced nor consumed in reaction i .

2.2.3 Kinetics

Most of the kinetic rate equations v (see Appendix A.2.1) were implemented as convenience kinetics [Liebermeister & Klipp, 2006a] due to unknown parameters and detailed underlying enzyme mechanisms.

Convenience kinetics are a general and simple rate law derived from Michaelis-Menten kinetics and hold enzyme saturation for high substrate concentrations. Furthermore, they cover all possible stoichiometries with a small number of parameters and enzyme regulation can be easily modelled by multiplication with a prefixed factor. Convenience kinetics can be derived from a rapid-equilibrium random-order enzyme mechanism. The substrates bind in arbitrary order and are converted to products which dissociate likewise in arbitrary order [Liebermeister & Klipp, 2006a].

For a reversible reaction $S_1 + S_2 + \dots \leftrightarrow P_1 + P_2 + \dots$ with concentration vectors $\mathbf{s} = ([S_1], [S_2], \dots)^T$ and $\mathbf{p} = ([P_1], [P_2], \dots)^T$, convenience kinetics are defined as

$$v = \frac{V_{\max} \cdot \prod_i \frac{s_i}{K_m^{s_i}} - \frac{V_{\max}}{K_{\text{eq}}} \cdot \prod_i \frac{p_i}{K_m^{p_i}}}{\prod_i \left(1 + \frac{s_i}{K_m^{s_i}} \right) + \prod_i \left(1 + \frac{p_i}{K_m^{p_i}} \right) - 1}$$

with V_{\max} measured in $\frac{\text{mM}}{\text{s}}$, the metabolite concentrations s_i and p_i in mM and K_m in mM. The equilibrium constant K_{eq} is dimensionless. The maximal reaction rate V_{\max} can be calculated from the product of enzyme concentration and the rate at which bounded substrate is converted into product per time. The K_m value can be determined from the substrate concentration at which the reaction rate reaches half of its maximal velocity. The equilibrium constant is characteristic for each reaction and indicates the side of the chemical reaction on which the equilibrium is located.

For general stoichiometries $\alpha_1 S_1 + \alpha_2 S_2 + \dots \leftrightarrow \beta_1 P_1 + \beta_2 P_2 + \dots$ the stoichiometric coefficients α_i and β_i appear as exponents in the nominator and the formula reads

$$v = \frac{V_{\max} \cdot \prod_i \frac{s_i}{K_m^{s_i}} - \frac{V_{\max}}{K_{\text{eq}}} \cdot \prod_i \frac{p_i}{K_m^{p_i}}}{\prod_i \left(1 + \frac{s_i}{K_m^{s_i}} + \dots + \left(\frac{s_i}{K_m^{s_i}} \right)^{\alpha_i} \right) + \prod_i \left(1 + \frac{p_i}{K_m^{p_i}} + \dots + \left(\frac{p_i}{K_m^{p_i}} \right)^{\beta_i} \right) - 1}.$$

Regulation terms are incorporated in the kinetic law as prefixed factors. For an activator A with binding constant K_A , both measured in mM, the factor is

$$h_A = \frac{[A]}{K_A + [A]},$$

for an inhibitor I with binding constant K_I , both measured in mM, the regulation term looks like

$$h_I = \frac{K_I}{K_I + [I]}.$$

To fill the rate laws with kinetic parameters an extensive literature search in the SABIO-RK [Wittig et al., 2006] and BRENDA [Schomburg et al., 2002] databases was performed. Enzyme specific activities were converted into V_{\max} values depending on their unit. Specific activities are often measured in U/mg of protein. Since we have no information about the concentration of any glycolytic enzyme in streptococcal cells velocity values having this unit cannot be converted into V_{\max} values. Specific activities with the unit U/mg protein can be converted into V_{\max} values by assuming that 42 % of cellular dry weight consists of protein [Even et al., 2002] and by multiplication with the average measured dry weight of 13.67 g DW per l of reactor volume corrected by the assumed intracellular volume of 30 ml per litre of reactor volume. The average measured dry weight is the mean value of the measured dry weights for 0, 10 and 50 mM P_i^{ex} . The transformation of specific activities measured in U/mg protein into V_{\max} values reads

$$\begin{aligned} \frac{\text{U}}{\text{mg protein}} &= \frac{10^{-3} \text{ mmol}}{60 \text{ s} \cdot \text{mg protein}} \\ &= \frac{10^{-3} \text{ mmol}}{60 \text{ s} \cdot \frac{1}{0.42} \text{ mg DW}} \cdot \frac{13.67 \cdot 10^3 \text{ mg DW}}{30 \cdot 10^{-3} \text{ l}} \\ &= \frac{0.42 \cdot 13.67 \cdot 10^3 \text{ mmol}}{30 \cdot 60 \text{ l} \cdot \text{s}} \\ &= 3.1897 \frac{\text{mM}}{\text{s}}. \end{aligned}$$

Specific activity values in U/mg dried cells can also be converted into V_{\max} values by multiplication with the protein content in *L. lactis* and with the average measured dry weight transformed in g per l intracellular volume as follows

$$\frac{\text{U}}{\text{mg DW}} = \frac{10^{-3} \text{ mmol}}{60 \text{ s} \cdot \text{mg DW}}$$

$$\begin{aligned}
&= \frac{10^{-3} \text{ mmol}}{60 \text{ s} \cdot \text{mg DW}} \cdot \frac{13.67 \cdot 10^3 \text{ mg DW}}{30 \cdot 10^{-3} \text{ l}} \\
&= \frac{13.67 \text{ mmol}}{60 \cdot 30 \cdot 10^{-3} \text{ l} \cdot \text{s}} \\
&= 7.5944 \frac{\text{mM}}{\text{s}}.
\end{aligned}$$

2.2.4 Simulation

Simulations of the biochemical network are achieved by numerical integration of the system of ODEs which were performed with the LSODA algorithm as implemented in COPASI [Hoops et al., 2006]. LSODA is a very robust adaptive step-size solver that uses the non-stiff method initially and automatically switches to a stiff multistep method if necessary [Hoops et al., 2006].

It is challenging to find a definition of stiffness since it is rather a phenomenon showing itself in different behaviours. For some differential equations, application of standard methods exhibit instability in the solutions, though other methods may produce stable solutions. Stiffness is often caused by the presence of different time-scales in the problem. Stiff problems are common among other in chemical kinetics.

For non-stiff problems Adam methods are used to solve the ODEs. For stiff problems the backward differentiation formula is used as solver. Both methods are implicit, linear multistep methods that, for a given function and time, approximate the derivative of the function using information from already computed times and solving a non-linear equation at each time step [Hoops et al., 2006].

2.2.5 Parameter estimation

Since not all kinetic parameters were determined for the glycolytic enzymes of *S. pyogenes* and *in vitro* measurements can deviate considerably from *in vivo* conditions [Teusink et al., 2000], we fitted the parameters to match the time-series data for various levels of extracellular P_i . We therefore consider the parameters as initial estimates for the parameter estimation. To fit the glycolytic model of *S. pyogenes*, parameters found in literature were allowed to vary between 10% and 1,000%. Unknown parameters were modified over a larger range, e.g. binding constants were varied from 0.01 to 100 mM and V_{\max} values from 0.1 to 1,000 mM per s while V_{\max} values of transport reactions were varied in a larger range, e.g. from 0.001 to

1,000 mM per s. Subsequently, our fermentation experiments were used as input for a particle swarm algorithm with an increased swarm size of 100 carried out with the COPASI software [Hoops et al., 2006].

The particle swarm optimisation method written by James Kennedy and Russel Eberhart [Kennedy & Eberhart, 1995] is a stochastic optimisation technique for non-linear functions. This method is inspired by a flock of birds or a school of fish searching for food. The goal of the algorithm is to find a solution with minimal objective function and thus a global minimum in the parameter space. The problem is optimised by having a swarm of candidate solutions, so called particles. Each particle has a position in the parameter space and a velocity. Additionally, it remembers its best achieved objective value and position as well as the position of its best neighbour. With this information in each step of the algorithm for one particle a new velocity is calculated and the position is updated. With this new parameter set P the so called objective value $E(P)$ is calculated as the weighted sum of squares

$$E(P) = \sum_{i,j} \omega_j \cdot (x_{i,j} - y_{i,j}(P))^2,$$

where the indices i and j denote rows and columns in the dataset, ω_j gives the weight for each data column, $x_{i,j}$ is a point in the dataset and $y_{i,j}(P)$ the corresponding simulated value. Thus, the objective value gives the sum of the weighted quadratic distance between simulated and experimentally determined value. If the calculated weights are not satisfactory they can be adapted manually. If the corresponding objective function value of the particle improves, the particle's best known position is updated. If the particle's objective function is better than that of its best neighbour this position is updated as well [Hoops et al., 2006].

2.2.6 Local sensitivity analysis

Sensitivity analysis is often applied to quantify the importance of each parameter of the investigated model on the system's behaviour. This is done by numerical differentiation using finite differences. This approach can be used to identify parameters or parts of a model either having a small impact on the system or that are most sensitive. The sensitivity $S_{X_i}^Y$ of the output Y to an input factor X_i is defined as

$$S_{X_i}^Y = \left| \frac{\partial Y}{\partial X_i} \right|_{X_0},$$

where the subscript X_0 indicates that this is a local method and the derivative is taken at some fixed point in the input space.

Comparisons of sensitivities are difficult by issues of scale. Therefore, COPASI also calculates scaled sensitivities $\|S_{X_i}^Y\|$ describing the proportional effects by applying the log function

$$\begin{aligned}\|S_{X_i}^Y\| &= \left| \frac{\partial \log Y}{\partial \log X_i} \right|_{X_0} \\ &= \frac{X_i}{Y} \cdot S_{X_i}^Y.\end{aligned}$$

A sensitivity higher than one means that a small change in the output factor Y results in a big change of the input factor X_i .

2.2.7 Global sensitivity analysis

To check the impact of each parameter on the metabolic intermediates and products and to be independent of the exact parameter space, we performed a global sensitivity analysis. This approach carries out sensitivity analysis over a wide range of values for all parameters and is therefore computationally expensive especially if the system is high dimensional.

Random sampling

We performed a global sensitivity analysis by applying random sampling of the parameter space for varying extracellular P_i concentrations (0, 10 and 50 mM) using the software package COPASI [Hoops et al., 2006]. To get reliable results for the sensitivities, a parameter scan with 10^6 iterations was done. The parameter values taken from literature were varied in the same range as described for parameter estimation (see Section 2.2.5). For each scanned point in the parameter space the scaled sensitivity (see Section 2.2.6) was calculated under glucose consumption ($t = 100$ s). Scanning the parameter space for this large set of parameters is computationally extremely expensive. Further processing and analyses of the data were performed in MATLAB 7.8 (The Mathworks, Inc.).

Fitting and local sensitivity analysis

To use tighter boundary conditions on the parameter scan, we performed several hundred fits and subjected the best 50 of them to the local sensitivity analysis. We

calculated scaled sensitivities (see Section 2.2.6) of all parameters on the metabolite concentrations and the concentration fluxes for 0, 10 and 50 mM extracellular phosphate under glucose consumption ($t = 100$ s).

2.2.8 Steady state analysis

A system is in steady state when every metabolite M does not change over time meaning that the partial derivative with respect to time is zero

$$\frac{\partial[M]}{\partial t} = 0.$$

This condition holds when the rates of synthesis are in balance with the rates of degradation for every metabolite. If the steady state has zero fluxes the system is in a chemical equilibrium, otherwise the fluxes are finite. Steady states can be found using the Newton-Raphson method which finds the roots of the right-hand side of the ODE. Alternatively steady states can also be calculated by integration of the ODE. COPASI can use either one of these strategies or a combination of the two [Hoops et al., 2006].

2.2.9 Metabolic control analysis

Metabolic control analysis [Heinrich & Rapoport, 1974, Kacser & Burns, 1973] is a sensitivity analysis of metabolic systems and describes the control exerted by network parameters on the system's variables, such as fluxes and species concentrations. This control is measured by applying a perturbation to the parameter under investigation and then measuring the effect on the system's variable (e.g. fluxes or species concentrations) after the system has settled to a new steady state and is defined as

$$C_{v_i}^A = \frac{\partial A}{\partial v_i} \frac{v_i}{A},$$

where A is the system variable, i the reaction and v_i the steady state rate of the perturbed reaction. Two main control coefficients are those for fluxes and species concentrations, but any variable of the system can be analysed with MCA. To run MCA the system does not need to be in steady state since COPASI calculates the steady state before determining control coefficients. In COPASI the calculation of steady state concentration- and flux-control coefficients is implemented, those for other variables can be estimated by simulating small perturbations [Hoops et al., 2006].

A very important property of steady state metabolic systems was uncovered with the MCA formalism. It can be shown that the control is shared by all reactions in the system. For the flux-control coefficients of a pathway it can be demonstrated that the sum of all coefficients is equal to unity

$$\sum_i C_{v_i}^J = 1,$$

where J is the reaction flux, i the reaction and v_i the steady state rate of the perturbed reaction. As a consequence, an increase in one of the flux-control coefficients implicates a decrease of the same rate in at least one other control coefficient. For the species concentration-control coefficients holds that the sum of all concentration-control coefficients over all steps of the system is zero

$$\sum_i C_{v_i}^{[M]} = 0.$$

Analysing the properties of each enzyme can be done by using a sensitivity known as the elasticity coefficient. This coefficient describes the effect of perturbations of a reaction parameter (like substrate or product concentrations) on the reaction rate. Elasticities are local coefficients and are defined as the ratio of relative change in local rate to the relative change in one parameter

$$\epsilon_p^{v_i} = \frac{\partial v_i}{\partial p} \frac{p}{v_i},$$

where v_i is the rate of the enzyme i under investigation and p is the perturbed parameter.

The elasticity coefficients and control coefficients of reactions with common intermediate species can be related through the connectivity theorem which emphasises a close relation between the kinetic properties of the individual reactions and the properties of the whole intact pathway. Two basic theorems exist, one for flux-control coefficients and one for concentration-control coefficients. For a common species S the sum of the products of the flux-control coefficients of all steps i affected by S and its elasticity coefficients towards S vanishes

$$\sum_i C_{v_i}^J \epsilon_{[S]}^{v_i} = 0.$$

The concentration-control coefficients are divided in two equations depending on whether the reference species A is different from the perturbed species S or not

[Westerhoff & Chen, 1984]

$$\begin{aligned}\sum_i C_{v_i}^{[A]} \epsilon_{[S]}^{v_i} &= 0, \quad \text{for } A \neq S, \\ \sum_i C_{v_i}^{[A]} \epsilon_{[A]}^{v_i} &= -1.\end{aligned}$$

The connectivity theorems allow MCA to describe how perturbations on metabolites of a pathway propagate through the chain of enzymes. The kinetic properties of each enzyme effectively propagate the perturbation to and from its immediate neighbours [Hoops et al., 2006].

2.3 Genome-scale modelling

Metabolic networks or genome-scale models comprise associations between genes and metabolic reactions [Notebaart et al., 2006]. Since such a model lacks for *S. pyogenes* we have constructed it. The reconstruction of the metabolism of *S. pyogenes* takes advantage of already existing and curated networks. The first step is the comparison between the genome sequence of the organism of interest and already annotated reference models, here from *Bacillus subtilis*, *Escherichia coli*, *Lactobacillus plantarum* and *Lactococcus lactis*. This step of annotation can be automated by using the AUTOGRAPH method [Notebaart et al., 2006] which uses INPARANOID [Remm et al., 2001] for orthology detection and results in the generation of a putative metabolic network (see Section 2.3.1). The output of the AUTOGRAPH method was supplied by Michiel Wels. This step was followed by a manual curation. The single steps of the reconstruction process are described below.

2.3.1 AUTOGRAPH and INPARANOID

The AUTOGRAPH method (**A**Utomatic **T**ransfer by **O**rthology of **G**ene **A**ssociations of **P**athway **H**euristics) [Notebaart et al., 2006] is applied to the Genbank NCBI [Bilofsky & Burks, 1988] annotation file of *S. pyogenes* M49 together with four manually curated metabolic networks from

- *B. subtilis* subsp. *subtilis* str. 168 [Park et al., 2003],
- *E. coli* K12 [Edwards et al., 2001],

- *L. plantarum* WCFS1 [Teusink et al., 2006] and
- *L. lactis* IL1403 [Notebaart et al., 2006].

The identification of genes having most likely an identical biological function in different organisms bases on orthology detection. By definition orthologous genes are homologs that originate from the same gene in the most recent ancestor of the organisms that are compared. Such genes have often kept identical biological roles. In many cases the sequences have duplicated after the speciation event and there is more than one ortholog in one or both species. In such cases it is difficult to determine which of the orthologs are functionally identical to the ortholog in the other species. Thus, it is crucial to detect all of these homologous genes that arose from a gene duplication, so-called paralogs. Here, one distinguishes between out-paralogs which predate the species split and in-paralogs that arose after the species split and are orthologs by definition [Remm et al., 2001].

To predict orthologs and in-paralogs from two organisms the algorithm INPARANOID (**IN-PAR**alog **ANd** **Orthology** **I**dentification) [Remm et al., 2001] is used. It requires the genome sequences as input which were retrieved from Genbank NCBI [Bilofsky & Burks, 1988]. The INPARANOID method bases on Bidirectional Best Hits and predicts orthologous as well as in-paralogous genes. The idea is that two orthologous sequences score higher with each other than with any other sequence of the genome [Remm et al., 2001]. Here, INPARANOID was applied with the default settings.

The output of the AUTOGRAPH method assigns each gene from the query genome one ortholog from each reference organism's metabolic network and the corresponding score. The *S. pyogenes* genes and the corresponding orthologs in the reference organisms were analysed manually.

2.3.2 Manual curation

The manual curation step comprised the assignment of reactions to each gene of the query genome. To predict gene-reaction associations the annotations of each query gene were compared with the functionality of the corresponding orthologs in the reference organisms with the help of the given score. This score depends on the sequence length and, thus, no general rule for a sufficient high score can be given. Instead, for each gene the scores of all orthologous genes

in the four reference organisms were compared. The function corresponding to the highest scoring ortholog was assigned to the query gene. Furthermore, incorporation of protein complexes was done to be able to use proteomics or gene-expression data. In the case that for one gene no orthologs were found in the reference organisms or the functionality was contradicting, the needed information were taken from Uniprot [UniProt Consortium, 2010], NCBI [Geer et al., 2010], KEGG [Kanehisa & Goto, 2000] or BRENDA [Schomburg et al., 2002]. The reactions and protein complexes were taken from the reconstruction of *L. plantarum* and *L. lactis* which were provided as templates by Bas Teusink.

2.3.3 Flux balance analysis

Flux balance analysis [Price et al., 2004, Varma & Palsson, 1994] is a mathematical method for analysing the flow through a metabolic network. It is suitable to analyse high-dimensional models since it does not require knowledge about enzyme mechanisms and metabolite concentrations; this approach is based on the stoichiometry of the model.

Mathematically, the reconstructed metabolic network is represented by the stoichiometric matrix \mathbf{S} . In this matrix, each column represents a reaction and each row represents a metabolite. The elements of the matrix are the stoichiometric coefficients.

To be able to apply FBA the studied system has to be homeostatic meaning that the internal concentrations of metabolites within the system remain constant over time. Thus, the system is in steady state and it can be represented by

$$\mathbf{S} \cdot \mathbf{v} = 0$$

with the $m \times n$ stoichiometric matrix \mathbf{S} where m is the number of metabolites and n the number of reactions and the vector \mathbf{v} of all fluxes through the network.

To reduce the solution space of the FBA model constraints are added to the individual metabolic flux rates within the network. For a particular reaction a constraint to the flux can be applied by

$$v_i^{\min} < v_i < v_i^{\max}$$

where v_i^{\min} and v_i^{\max} represent lower and upper boundary conditions, respectively, and can be set to zero for irreversible reactions. For measured flux rates v_i^m the

corresponding reaction in the network is constrained within an error ε by

$$v_i^m - \varepsilon < v_i < v_i^m + \varepsilon.$$

The constraints limiting nutrient uptake and excretion and the flux through the reactions in the *S. pyogenes* model are defined according to the experimental set-up. A complete list with lower and upper boundaries is given in Appendix B.3 in Tables B.3 – B.7.

Additionally, an objective function is defined that further reduces the number of possible solutions. Since the network is constructed to simulate growth and reproduction the biomass function denoted $\mathbf{v}_{\text{biomass}}$ is chosen. The biomass reaction describes the rate at which all of the biomass precursors are made in the correct proportions. Thus, the solution is a flux distribution \mathbf{v} maximising the biomass function, fulfilling the steady state condition and satisfying the constraints. This particular flux distribution was found using linear programming provided by Brett Olivier as a script written in the Python programming language [van Rossum, 1995].

Chapter 3

Results

3.1	Experimental results	40
3.2	Kinetic model of <i>S. pyogenes</i>	55
3.3	Comparison between <i>S. pyogenes</i> and <i>L. lactis</i>	76
3.4	Oscillations caused by the stoichiometry	85
3.5	Reconstructing the metabolic network of <i>S. pyogenes</i>	88

3.1 Experimental results

Within the project, different types of data were collected as basis and validation of both computational models, the kinetic and the genome-scale model. These data include concentration of products and amino acids measured in continuous cultured cells, time-series profiles in response to a glucose-pulse, kinetic parameters, utilisation of different substrates and growth rates after amino acid leave-outs. The methods are described in Section 2.1, the results and the corresponding experimentalist are given in the following sections.

3.1.1 Construction of recombinant vectors and mutant strains

S. pyogenes possesses two genes encoding two lactate dehydrogenases, one L-LDH and one D-LDH. Fiedler *et al.* [Fiedler et al., 2011] reported that *S. pyogenes* L-LDH is responsible for over 95% of total lactate synthesis, a fact that was shown for *L. lactis* and *E. faecalis* before [Bongers et al., 2003, Jonsson et al., 2009]. To achieve the *ldh*-deletion strain *S. pyogenes* M49 591 Δldh , this main *ldh* gene was removed by Tomas Fiedler.

The mutant strain showed no significant difference in growth rate compared to the wild-type strain when grown in CDM-LAB medium (see Table 3.1). In THY medium the growth rate of the *ldh*-deletion strain was lower compared to the wild-type at pH 6.5, at pH 7.5 the deletion of *ldh* did not result in a significant decrease in growth. Under the tested conditions, a deletion of *ldh* is no significant disadvantage to the organism [Fiedler et al., 2011].

Table 3.1: Maximal specific growth rates of *S. pyogenes* wild-type and its *ldh*-knock-out mutant in CDM-LAB and THY medium at two pHs. Strains were grown in 96-well plates at 37°C under low micro-aerobic conditions. Values indicate the average $\mu_{\max} \pm$ standard deviation.

Medium	pH	M49	M49 Δldh
CDM-LAB	6.5	0.43 \pm 0.01	0.39 \pm 0.04
	7.5	0.39 \pm 0.02	0.35 \pm 0.01
THY	6.5	0.86 \pm 0.13	0.69 \pm 0.01
	7.5	0.57 \pm 0.06	0.53 \pm 0.03

3.1.2 Fermentation experiments

S. pyogenes M49 wild-type strain and its *ldh*-negative mutant were grown at two dilution rates and two pH values in a bioreactor to which fresh CDM-LAB medium was continuously added, while culture liquid was removed with the same rate to keep the volume constant. As a consequence, the cells were grown in a physiological steady state. Since in steady state the specific growth rate of the organism is equal to the dilution rate [Davies et al., 1965], growth rate can be easily controlled by changing the dilution rate with which medium is added to the fermentor vessel. Here, two different dilution rates, 0.05 h⁻¹ and 0.15 h⁻¹ and two different pHs (6.5 and 7.5) were investigated. Amino acid concentrations were measured once and product levels as well as OD and dry weight were measured twice in the culture supernatant with one exemplary data set displayed in the following tables. Measured OD and dry weight are given in Table 3.2 for both dilution rates and both pH values. The fermentation experiments were performed by Tomas Fiedler and Martijn Bekker.

S. pyogenes mainly exhibited homolactic fermentation but showed more mixed acid fermentation at lower dilution rates at both pH 6.5 and pH 7.5 (see Table 3.3) as compared to *L. lactis* and *E. faecalis* [Fiedler et al., 2011]. However, no significant pH dependent differences were observed in the fermentation pattern. Interestingly, *E. faecalis* showed a strong pH dependency with a more homolactic phenotype at pH 6.5. Deletion of the main *ldh* of *S. pyogenes* resulted in complete mixed acid fermentation in all conditions [Fiedler et al., 2011].

Table 3.2: Measured OD (AU) and dry weight (DW, g/l) of *S. pyogenes* wild-type and *ldh*-knock-out at two dilution rates (D, h⁻¹) and two pHs during continuous cultivation in glucose-limited CDM-LAB medium.

pH	D	M49		M49 Δ <i>ldh</i>	
		OD	DW	OD	DW
6.5	0.05	2.55	1.20	2.27	1.00
	0.15	2.36	0.70	2.94	1.25
7.5	0.05	2.22	0.65	1.65	0.65
	0.15	2.10	1.00	2.43	1.05

Product concentrations

Measured product concentrations comprise glucose, ethanol, acetate, lactate, formate, succinate, pyruvate, acetoin and 2,3-butanediol. Under all four investigated experimental conditions, no glucose remained in the culture supernatant of *S. pyogenes* M49 wild-type strain and its *ldh*-negative mutant. Furthermore, neither succinate nor 2,3-butanediol were detected. The experimental data for the *S. pyogenes* M49 wild-type strain and its *ldh*-negative mutant are shown in Table 3.4 and 3.5, respectively.

The wild-type strain produces high amounts of lactate, ethanol, acetate and formate under all four investigated conditions (see Table 3.4). Glucose, succinate, acetoin and 2,3-butanediol were not detected in the supernatant. The amount of pyruvate in the culture liquid is low and only detectable for the lower dilution rate of 0.05 h^{-1} . The higher the flux towards lactate, the lower is the flux towards the mixed-acid branch. The ratio of ethanol:acetate:formate is approximately 1:1:2 except for pH 7.5, $D = 0.05$. In that case, no ethanol was produced by the wild-type strain.

The *ldh*-knock-out strain is not able to produce lactate and thus the flux is redirected. As a consequence, this mutant produces not only high amounts of ethanol, acetate and formate but also acetoin (see Table 3.5). Glucose and succinate were not detected in the supernatant. Acetoin production may be the result of a reaction performed by pyruvate dehydrogenase. Compared to the wild-type strain, the amount of extracellular pyruvate is explicitly increased.

Table 3.3: Relative flux distribution in *S. pyogenes* at two dilution rates (D , h^{-1}) and two pHs during continuous cultivation in glucose-limited CDM-LAB medium. Values indicate mol product/mol glucose \pm standard deviation.

pH	D	Lactate	Formate
6.5	0.05	0.8 ± 0.4	0.5 ± 0.1
	0.15	1.4 ± 0.1	0.1 ± 0.1
7.5	0.05	0.6 ± 0.3	0.5 ± 0.2
	0.15	1.1 ± 0.3	0.2 ± 0.2

Table 3.4: Product concentrations in *S. pyogenes* wild-type strain at two dilution rates (D , h^{-1}) and two pHs during continuous cultivation in glucose-limited CDM-LAB medium. Values indicate mM end-product.

pH	D	Glucose	Ethanol	Acetate	Lactate	Formate	Succinate	Pyruvate	Acetoin	2,3-Butanediol
6.5	0.05	0.00	19.26	35.10	69.97	35.41	0.00	1.50	0.00	0.00
	0.15	0.00	8.32	22.84	83.79	13.63	0.00	0.00	0.00	0.00
7.5	0.05	0.00	0.00	20.82	99.67	8.14	0.00	1.44	0.00	0.00
	0.15	0.00	11.00	20.22	56.22	20.69	0.00	0.00	0.00	0.00

Table 3.5: Product concentrations in *S. pyogenes* *ldh*-negative mutant at two dilution rates (D , h^{-1}) and two pHs during continuous cultivation in glucose-limited CDM-LAB medium. Values indicate mM end-product.

pH	D	Glucose	Ethanol	Acetate	Lactate	Formate	Succinate	Pyruvate	Acetoin	2,3-Butanediol
6.5	0.05	0.00	44.14	40.34	1.75	65.44	0.00	8.20	3.15	0.00
	0.15	0.00	61.08	40.80	1.72	71.47	0.00	15.35	2.60	0.00
7.5	0.05	0.00	55.65	42.12	2.25	74.60	0.00	19.53	2.98	0.00
	0.15	0.00	55.26	39.59	0.80	69.00	0.00	15.02	2.51	0.00

Table 3.6: Amino acid concentrations in *S. pyogenes* wild-type strain at two dilution rates (D , h^{-1}) and two pHs during continuous cultivation in glucose-limited CDM-LAB medium. Values indicate mM amino acid.

pH	D	Aspartate	Serine	Glutamate	Glycine	Histidine	NH ₃	Arginine	Threonine	Alanine	Proline
6.5	0.05	0.42	0.04	0.51	0.35	0.09	1.70	0.00	0.22	0.38	0.84
	0.15	0.35	0.01	0.42	0.28	0.09	1.94	0.05	0.20	0.38	0.79
7.5	0.05	1.04	0.03	1.15	0.73	0.18	5.58	0.00	0.57	0.74	2.27
	0.15	0.21	0.01	0.26	0.25	0.11	1.24	0.02	0.17	0.22	0.63

pH	D	Cysteine	Tyrosine	Valine	Methionine	Ornithine	Lysine	Isoleucine	Leucine	Phenylalanine
6.5	0.05	0.00	0.26	0.34	0.12	2.55	0.25	0.16	0.39	0.25
	0.15	0.00	0.16	0.32	0.09	1.30	0.22	0.16	0.38	0.23
7.5	0.05	0.00	0.58	0.86	0.24	4.89	0.62	0.09	0.99	0.00
	0.15	0.00	0.27	0.23	0.10	0.47	0.14	0.10	0.27	0.27

Table 3.7: Amino acid concentrations in *S. pyogenes* *ldh*-negative mutant at two dilution rates (D , h^{-1}) and two pHs during continuous cultivation in glucose-limited CDM-LAB medium. Values indicate mM amino acid.

pH	D	Aspartate	Serine	Glutamate	Glycine	Histidine	NH ₃	Arginine	Threonine	Alanine	Proline
6.5	0.05	0.33	0.01	0.37	0.27	0.05	1.59	0.00	0.18	0.44	0.70
	0.15	0.34	0.01	0.39	0.21	0.07	2.12	0.00	0.21	0.71	0.80
7.5	0.05	0.57	0.03	0.60	0.42	0.21	1.69	0.00	0.29	0.65	1.17
	0.15	0.11	0.01	0.11	0.07	0.02	0.68	0.01	0.06	0.21	0.26

pH	D	Cysteine	Tyrosine	Valine	Methionine	Ornithine	Lysine	Isoleucine	Leucine	Phenylalanine
6.5	0.05	0.00	0.19	0.24	0.10	2.05	0.22	0.09	0.28	0.20
	0.15	0.00	0.15	0.17	0.09	0.95	0.22	0.04	0.15	0.22
7.5	0.05	0.00	0.37	0.39	0.16	2.72	0.33	0.13	0.40	0.28
	0.15	0.00	0.07	0.06	0.03	0.39	0.07	0.02	0.06	0.06

Amino acid concentrations

Since *S. pyogenes* is auxotroph for many amino acids, amino acids present in the nutrient-rich CDM-LAB medium are taken up by both, the wild-type strain and the *ldh*-knock-out mutant (see Tables 3.6 and 3.7). From the 17 measured amino acids arginine (Arg), cysteine (Cys) and serine (Ser) are completely consumed in the wild-type as well as in the *ldh*-knock-out strain. Ornithine and ammonia, which are no compounds of CDM-LAB medium, are produced by *S. pyogenes* and transported out of the cell. In these energy limited growth conditions, ornithine production is likely due to use of arginine for ATP production [Fiedler et al., 2011].

All in all we can see for the wild-type strain as well as for the *ldh*-knock-out mutant a difference in amino acid consumption under the investigated conditions. Compared to the wild-type strain, the *ldh*-knock-out mutant consumes less amounts of amino acids except for serine, arginine, alanine (Ala) and cysteine, which are present with the same amounts in the supernatant of both strains.

3.1.3 Glucose-pulse experiments

In order to study the effect of extracellular phosphate on the glycolysis of *S. pyogenes*, approximately 8 mM glucose and 0, 10 or 50 mM phosphate were added to pre-grown cells and samples were taken at regular time intervals. Under these conditions initially all nutrients are in excess but their concentrations decrease during growth and become limiting while the metabolic products accumulate. G6P, F6P, FBP, GAP, PEP, pyruvate, ATP, extracellular lactate and extracellular glucose were quantified in each sample. The glucose-pulse experiments were done by Martijn Bekker and were reproduced several times with an exemplary data set for 0, 10 and 50 mM P_i^{ex} displayed in Tables 3.8, 3.9 and 3.10.

In all experiments glucose is consumed after approximately 5 to 6 minutes whereas the glucose uptake increases with 50 mM extracellular phosphate as compared to 0 mM P_i^{ex} . Interestingly, the uptake rate is slightly inhibited in the presence of 10 mM external phosphate as compared to 0 mM phosphate. The FBP level increases with the phosphate level and reaches a maximum of 5.2 mM, 6.2 mM and 8.2 mM for 0, 10 and 50 mM P_i^{ex} , respectively. We can also see a rise in the GAP level whereas the amount of G6P, F6P and ATP is approximately the same under all experimental conditions. This shows a crucial role of extracellular phosphate on the glycolysis

of *S. pyogenes* and confirms the necessity of including phosphate transport in the model.

Table 3.8: Metabolite concentration time-series in *S. pyogenes* for a glucose-pulse of approximately 8 mM without extracellular phosphate. Values are given in mM, the measured OD is 43.3. n.d., not determined.

Time (min)	FBP	G6P	F6P	ATP	GAP	Glc ^{ex}	Lactate ^{ex}
0	0.1	0.4	n.d.	0.3	n.d.	n.d.	2.8
1	4.6	1.4	1.4	0.6	n.d.	6.6	3.9
2	4.2	1.9	0.6	1.5	n.d.	5.2	4.8
3	4.7	1.2	2.2	1.8	n.d.	3.7	8.1
4	5	1.3	0.8	1.3	n.d.	2.5	9.6
5	5.2	1.3	1	1.5	n.d.	1.4	10.6
10	1.6	0.1	0.6	1.5	n.d.	n.d.	11.1
15	0	0.2	0.6	0.7	n.d.	n.d.	15.3
20	n.d.	0	0.2	0.4	n.d.	n.d.	12.4
25	n.d.	0.9	0.5	0.2	n.d.	n.d.	12.9

Table 3.9: Metabolite concentration time-series in *S. pyogenes* for a glucose-pulse of approximately 10 mM and 10 mM extracellular phosphate. Values are given in mM, the measured OD is 38.5. n.d., not determined.

Time (min)	FBP	G6P	F6P	ATP	GAP	Glc ^{ex}	Lactate ^{ex}
0	n.d.	0.2	n.d.	0.1	1.1	n.d.	1.9
1	4.8	1.5	0	0.4	1.6	4.6	2.7
2	5.3	1.2	1.4	1.6	2.2	3.7	4.4
3	6.2	1	1.5	1.5	2.6	2.6	8.2
4	6.2	1.3	1.2	1.8	3.8	1.9	7.8
5	6.1	1.4	0.2	1.7	3.9	1.0	10.1
10	0.6	0.4	n.d.	0.9	2	n.d.	11.7
15	0.1	0.4	n.d.	0.9	1.6	n.d.	12.9
20	n.d.	0.1	n.d.	0.3	0.5	n.d.	11.1
25	0.6	n.d.	n.d.	0.2	1.1	n.d.	n.d.

Table 3.10: Metabolite concentration time-series in *S. pyogenes* for a glucose-pulse of approximately 8 mM and 50 mM extracellular phosphate. Values are given in mM, the measured OD is 41.5. n.d., not determined.

Time (min)	FBP	G6P	F6P	ATP	GAP	Glc ^{ex}	Lactate ^{ex}
0	0.2	n.d.	0.1	0.2	3.3	n.d.	2.3
1	4	0.6	0	0.4	5	7.3	2.4
2	7.1	1	0.5	1.6	6.9	5.5	4.2
3	7.6	0.5	2.7	2.1	8.6	1.5	6.3
4	8.1	0.6	2.1	2.2	8.3	0.1	9.3
5	8.2	1	0.7	2	8.3	n.d.	12.3
10	0.5	0.6	n.d.	0.6	4.3	n.d.	8.6
15	0.1	n.d.	n.d.	0.6	5.8	n.d.	12
20	0.4	n.d.	n.d.	0.3	4.9	n.d.	8.3
25	n.d.	n.d.	n.d.	0.2	3.6	n.d.	11.7

3.1.4 Kinetic parameters of individual enzymes

Since no information about the regulation of glycolytic enzymes in *S. pyogenes* has been studied so far, we decided to investigate the kinetics of pyruvate kinase and lactate dehydrogenase ourselves. The kinetic measurements *in vitro* were done by Tomas Fiedler.

Kinetic parameters of L-lactate dehydrogenase

Kinetic measurements of LDH were done with heterologous expression. The binding constant of the substrates pyruvate and NADH amounts 0.41 mM and 0.062 mM, respectively, and the K_m values for the products lactate and NAD^+ are 8.8 mM and 0.152 mM. The enzyme specificity of the forward reaction is 6 U/mg of protein.

Since no information about the regulation of LDH in *S. pyogenes* could be found in literature, potential effectors were studied. We found out that FBP and phosphate have a stimulating effect on LDH whereas NAD^+ inhibits this enzyme.

Kinetic parameters of pyruvate kinase

Kinetic measurements of *S. pyogenes* pyruvate kinase were done with protein crude extracts since the heterologous expression was inactive in *E. coli*. The measured binding constants are 0.69 mM for PEP, 0.75 mM for ADP, 21 mM for pyruvate

and 10 mM for ATP. The enzyme specificity of the forward reaction is 6 U/mg of protein.

3.1.5 Substrate utilisation assays

Substrate utilisation assays were done by Tomas Fiedler. Thereto, Biolog Phenotype Microarrays were used to investigate growth of the *S. pyogenes* wild-type and *ldh*-knock-out strains on 190 different carbon sources. There were 20 substrates on which the wild-type was able to grow on. The results from the experiment consisting of four measurements are summarised in Table 3.11. The *ldh*-negative mutant showed a decreased ability of utilising trehalose, sucrose, uridine, inosine, N-acetyl neuramic acid, cyclodextrin and galactopyranosyl-d-arabinose.

S. pyogenes showed optimal growth on glucose and sucrose and ended up at lower ODs after 24 h of growth for all other tested substrates. Compared to the wild-type, the deletion of the *ldh* gene resulted in a significant reduced growth on D-mannose, D-trehalose and sucrose [Fiedler et al., 2011].

3.1.6 Calculation of specific ATP synthesis rates

The energy required for maintenance and the rate of ATP synthesis at the maximal specific growth rate were determined in conditions that varied in growth rate and pH (see Table 3.12).

For the *S. pyogenes* wild-type strain $q_{\text{ATP maintenance}}$ did not show large pH dependent differences. For the *ldh*-knock-out strain $q_{\text{ATP total}}$ was similar to the wild-type strain [Fiedler et al., 2011]. This indicates deletion of *ldh* does not result in an overall increase in ATP dissipating reactions.

Large differences were observed with respect to Y_{atp} . For *S. pyogenes* this value was almost two-fold higher at pH 7.5 as compared to pH 6.5. The calculation of specific ATP synthesis rates was done by Tomas Fiedler, Martijn Bekker and Maria Jonsson *et al.* [Fiedler et al., 2011].

3.1.7 Amino acid leave-out experiments

As a human pathogen *S. pyogenes* is used to live in nutrient rich media such as blood and, therefore, is auxotroph for many amino acids. Little is known about the amino acid requirements of *S. pyogenes*. Studies focussing on the amino acid

metabolism of *S. pyogenes* report rather about limiting amino acid concentrations [Davies et al., 1965] or concentrate on different strains. In general, many conflicting data concerning the amino acid requirements of lactic acid bacteria appear in literature. These are primarily due to the use of different levels of vitamins in media. Thus, we decided to determine essential amino acids ourselves. This was done with amino acid leave-out experiments.

For amino acid leave-out experiments, *S. pyogenes* was grown overnight in CDM-

Table 3.11: Substrate utilisation of *S. pyogenes* wild-type and its *ldh*-knock-out mutant on different carbon sources. Optical densities of the cultures grown on glucose were set to 100% for the wild-type and the *ldh*-mutant strain and optical densities for growth on all other substrates were related to this value.

Substrate	M49	M49 Δ <i>ldh</i>
Sucrose	101.1 \pm 20.4	38.6 \pm 11.3
α -D-Glucose	100.0 \pm 0.0	100.0 \pm 0.0
D-Trehalose	90.4 \pm 16.5	38.4 \pm 9.8
Maltotriose	87.4 \pm 16.5	78.9 \pm 9.0
D-Mannose	82.0 \pm 17.7	41.3 \pm 14.7
N-Acetyl-D-glucoseamine	77.5 \pm 10.7	90.3 \pm 6.8
D-Glucoseamine	63.3 \pm 7.3	68.2 \pm 17.9
β -Methyl-D-glucoside	62.6 \pm 17.1	38.7 \pm 21.7
Maltose	52.3 \pm 14.1	40.5 \pm 15.2
Salicin	46.3 \pm 11.3	24.1 \pm 16.6
D-Fructose	43.0 \pm 39.7	26.5 \pm 32.0
α -D-Lactose	26.6 \pm 24.2	20.9 \pm 19.7
Gelatin	25.7 \pm 42.0	5.3 \pm 2.2
N-Acetyl- β -D-mannosamine	22.9 \pm 17.1	17.7 \pm 14.7
Uridin	17.1 \pm 24.5	10.5 \pm 11.2
3-0- β -D-Galactopyranosyl-D-arabinose	17.0 \pm 26.9	14.0 \pm 11.0
Pectin	13.9 \pm 18.5	44.0 \pm 23.7
Dextrin	13.8 \pm 9.0	12.3 \pm 5.5
2-Hydroxy benzoic acid	7.3 \pm 3.7	11.0 \pm 6.5
Chondroitin sulfate c	6.5 \pm 3.9	19.1 \pm 11.6

LAB medium, pelleted by centrifugation, washed and suspended in full CDM-LAB medium or in CDM-LAB without Ala, Arg, asparagine (Asn), aspartate (Asp), cystine (Cyn), Cys, glutamine (Gln), glutamate (Glu), glycine (Gly), histidine (His), isoleucine (Ile), leucine (Leu), lysine (Lys), methionine (Met), phenylalanine (Phe), proline (Pro), Ser, threonine (Thr), tryptophan (Trp), tyrosine (Tyr) and valine (Val) or in the absence of combinations of amino acids. The optical density of each well was measured at 600 nm for 12 h. The final growth rate measured after 12 h in the different reduced media was compared to the growth rate in full CDM-LAB medium. Table 3.13 summarises the experimental data from two independent experiments. Each experiment consists of eight measurements and, thus, mean value and standard deviation are given.

Table 3.12: Specific ATP synthesis rates of *S. pyogenes* grown in glucose-limited continuous cultures. $q_{\text{ATP maintenance}}$ was calculated according to the methods applied by Tempest et al. [Tempest & Neijssel, 1984]. Y_{atp} was determined at $D = 0.15$. $q_{\text{ATP}\mu_{\text{max}}}$ was estimated by extrapolation of the slope for $q_{\text{ATP total}}$ to the D similar to μ_{max} . Values indicate mean value \pm standard deviation.

pH	$q_{\text{ATP maintenance}}$	Y_{atp}	$q_{\text{ATP}\mu_{\text{max}}}$
6.5	2.6 ± 2.2	5.2 ± 0.7	88 ± 9.2
7.5	2.9 ± 2.1	9.4 ± 2.3	38 ± 7.1

Table 3.13: Final OD at 600 nm after 12 h growth of *S. pyogenes* in full CDM-LAB medium and medium with amino acid leave-outs as indicated. The results from two independent experiments are given whereas each experiment consists of eight measurements. Values indicate mean OD values \pm standard deviation. n.d., not determined.

CDM-LAB medium	Final growth rate	
	Experiment 1	Experiment 2
Full	0.31 ± 0.02	0.81 ± 0.02
w/o Ala	n.d.	0.76 ± 0.00
w/o Arg	n.d.	0.14 ± 0.02
w/o Asn	0.25 ± 0.09	0.32 ± 0.00
w/o Asn, Asp	0.27 ± 0.09	0.32 ± 0.05
w/o Asp	0.4 ± 0.04	0.73 ± 0.00

Table 3.13 – continued from previous page

CDM-LAB medium	Final growth rate	
	Experiment 1	Experiment 2
w/o Cyn	0.33 ± 0.07	0.73 ± 0.01
w/o Cyn, Cys	0.15 ± 0.02	0.51 ± 0.02
w/o Cys	0.25 ± 0.05	0.62 ± 0.10
w/o Cys, Gly	n.d.	0.10 ± 0.00
w/o Cys, Ser	n.d.	0.11 ± 0.00
w/o Cys, Thr	n.d.	0.08 ± 0.00
w/o Gln	0.20 ± 0.08	0.13 ± 0.03
w/o Gln, Glu	0.15 ± 0.02	0.12 ± 0.01
w/o Gln, Thr	n.d.	0.10 ± 0.01
w/o Glu	0.36 ± 0.04	0.64 ± 0.03
w/o Gly	n.d.	0.15 ± 0.01
w/o Gly, Ser	n.d.	0.12 ± 0.00
w/o Gly, Ser, Thr	n.d.	0.12 ± 0.02
w/o Gly, Thr	n.d.	0.09 ± 0.00
w/o His	n.d.	0.15 ± 0.01
w/o Ile	n.d.	0.10 ± 0.00
w/o Leu	n.d.	0.14 ± 0.02
w/o Lys	n.d.	0.13 ± 0.02
w/o Met	n.d.	0.15 ± 0.02
w/o Met, Ser	n.d.	0.13 ± 0.02
w/o Phe	n.d.	0.15 ± 0.02
w/o Pro	n.d.	0.40 ± 0.02
w/o Ser	n.d.	0.13 ± 0.01
w/o Ser, Thr	n.d.	0.14 ± 0.00
w/o Thr	n.d.	0.10 ± 0.01
w/o Trp	n.d.	0.15 ± 0.02
w/o Tyr	n.d.	0.13 ± 0.02
w/o Val	n.d.	0.14 ± 0.01

The first experiment shows that *S. pyogenes* is able to grow in CDM-LAB with single leave-outs of Asp, Asn, Glu, Gln, Cys and Cyn or a double leave-out of

Asp and Asn. Hereby, we defined a final OD lower than 0.15 as loss of growth. When suspended in CDM-LAB medium without Asn, Gln or Cys *S. pyogenes* shows reduced growth. Surprisingly, in CDM-LAB medium without Asp, Glu or Cyn the growth rate is increased. Growth of *S. pyogenes* in the absence of other amino acids have not been tested in this experiment. This study was performed in Tomas Fiedler's lab.

In the second experiment growth of *S. pyogenes* in 35 media omitting the amino acids as specified in Table 3.13 was tested. A final OD lower than 0.3 indicates loss of growth. We found out that leaving out Arg, Gln (alone and in combinations), Gly (alone and in combinations), His, Ile, Leu, Lys, Met, Phe, Ser (alone and in combinations), Thr (alone and in combinations), Trp, Tyr and Val results in complete loss of growth. In contrast, the organism is able to grow without Ala, Asn, Asn and Glu, Asp, Cyn, Cyn and Cys, Cys as well as without Glu, but at a lower growth rate as compared to full medium. The second experiment was performed by Araz Zeyniyev.

From the eight amino acid leave-outs performed in both experiments the results for the omission of Asn, Asp, Cyn, Cys, Glu, Gln and Glu show qualitatively the same results, meaning growth or no growth in both experiments. Taking the standard deviation into account, the second experiment predicts no or at least very low growth by omitting Asn and Asp in agreement with the results of the first experiment. Both experiments give contrary results for growth of *S. pyogenes* in the absence of Cyn and Cys as well as without Gln. Increased growth of *S. pyogenes* in the absence of Asp, Cyn and Glu as seen in the first experiment cannot be reproduced. Table 3.14 summarises essential amino acids for the growth of *S. pyogenes* based on our experimental data. This table shows preliminary data which has to be validated by at least one additional independent experiment, especially for glutamine since our experimental data give contradicting results for growth in the absence of this amino acid.

Table 3.14: Essential amino acids for growth of *S. pyogenes* in CDM-LAB medium based on our experimental data. From the tested amino acids 14 are essential for growth of *S. pyogenes*.

Essential	Non-essential
Arginine	Alanine
Glutamine	Asparagine
Glycine	Aspartate
Histidine	Cysteine
Isoleucine	Cystine
Leucine	Glutamate
Lysine	Proline
Methionine	
Phenylalanine	
Serine	
Threonine	
Tryptophan	
Tyrosine	
Valine	

3.2 Kinetic model of *S. pyogenes*

The kinetic model of *S. pyogenes* comprises glucose uptake, glycolysis and pyruvate branching resulting in the production of lactate, acetate, ethanol and formate. Under anaerobic conditions, the metabolism of one molecule of glucose to two molecules of pyruvate has a net yield of two ATP. The conversion of pyruvate to the final end-products recovers NAD^+ via lactate or via ethanol production and yields one additional molecule ATP by producing acetate. The construction of the glycolytic model is described in the following sections. Modelling, simulating and analysing was done in COPASI [Hoops et al., 2006]. We performed parameter estimation to tune the parameters so that the model reproduces our experimental data (see Sections 3.1.2 and 3.1.3). To analyse the model in more detail, parameter sensitivity analysis and metabolic control analysis were performed. The applied methods are described in Section 2.2.

3.2.1 Setting up the model

In order to set up a computational model on the basis of the experimental data described before (see Section 3.1) the metabolic reactions involved in fermentation and their respective regulation are defined according to the metabolic capabilities of *S. pyogenes*. In a second step this set of reactions is transformed into a mathematical network.

Defining the metabolic reactions of the model

S. pyogenes has at least two glucose uptake systems showing different affinities for its substrate [Cvitkovitch et al., 1995]. The main part of glucose in the medium is taken up via the high-affinity PTS. The PTS is only found in bacteria and catalyses the import and direct phosphorylation of sugar derivatives like mono- and disaccharides or amino sugars [Deutscher et al., 2006]. Thereby, PEP serves as energy source and phosphoryl donor.

The PTS consists of two unspecific cytoplasmic components, enzyme I (EI) and HPr. Carbohydrate specificity resides in enzyme II (EII), and hence, bacteria usually contain many different EIIs. EII is a complex itself and consists of one or two hydrophobic integral membrane domains (domains C and D) and two hydrophilic domains (domains A and B), which together are responsible for the transport of the

carbohydrate across the bacterial membrane as well as its phosphorylation. The glucose-specific EII^{Glc} complex of *S. pyogenes* consists of two distinct proteins, the cytoplasmic protein EIIA^{Glc} and the membrane-associated protein EIICB^{Glc}. Thereby, the EIIB^{Glc} domain is hydrophilic and in contact with the cytoplasm and the EIIC^{Glc} domain is buried within the membrane [Postma et al., 1993].

The first step in transport and subsequent phosphorylation of incoming sugar is the transfer of the phosphate group from PEP to HPr via EI. From there, the phosphate group is delivered to EIIA^{Glc} and further to membrane bound EIIB^{Glc}. The phosphoryl group bound to EIIB^{Glc} is transferred to glucose after translocation of the sugar by EIIC^{Glc} across the membrane. Thus, the incoming sugar is directly converted into G6P [Postma et al., 1993].

As mentioned before, HPr can be phosphorylated on His-15 or Ser-46 by PEP or ATP, respectively, in low-G+C Gram-positive bacteria [Ye et al., 1996]. Consequently, four different forms of HPr exist in these organisms: unphosphorylated HPr, HPr phosphorylated at either His-15 or Ser-46 and doubly phosphorylated HPr [Vadeboncoeur et al., 1991].

In response to changes in its phosphorylation state HPr carries out diverse regulatory functions. HPr-His-P is required for sugar uptake while HPr-Ser-P regulates among others the extent of sugar-phosphate accumulation. This is done either by inhibiting the uptake of less preferred sugars by a rapidly metabolisable substrate, a process denoted inducer exclusion, or by activating inducer expulsion which mediates the efflux of intracellular sugar-phosphates [Reizer & Panos, 1980, Thompson & Saier, 1981].

The ratio of the two phosphorylated HPr forms is mainly adjusted by the bifunctional enzyme HPr kinase/phosphatase (HPrK/P). The kinase catalyses the ATP-dependent phosphorylation of HPr at Ser-46 and is activated by FBP and inhibited by P_i whereas the phosphatase catalyses the dephosphorylation of HPr-Ser-P and is activated by P_i and inhibited by ATP [Deutscher et al., 1985, Reizer et al., 1984]. Thereby, HPr-His-P does not serve as a substrate for the kinase and PEP-dependent phosphorylation of HPr-Ser-P is approximately five thousand times slower compared to that of unphosphorylated HPr [Reizer et al., 1985].

In glycolysing cells, the FBP level is high whereas the P_i concentration is low [Mason et al., 1981]. As a consequence, a major fraction of HPr is present as HPr-Ser-P or doubly phosphorylated HPr, which has a much lower affinity for EIAs

compared to HPr-His-P, but there is little HPr-His-P and undetectable amounts of unphosphorylated HPr [Vadeboncoeur et al., 1991]. Since the expulsion mechanism is activated by HPr-Ser-P, only glycolysing cells hydrolyse the sugar-phosphate followed by expulsion.

The exclusion mechanism is not modelled since the only carbohydrate source in the medium is glucose. The expulsion mechanism preventing sugar-phosphate accumulation is catalysed by PaseII which dephosphorylates G6P to glucose that is subsequently transported out of the cell. This reaction is controlled by HPr-Ser-P [Ye et al., 1996].

Besides the PTS, *S. pyogenes* possesses a low-affinity glucose permease (GlcP) allowing the diffusion of glucose across the membrane [Cvitkovitch et al., 1995]. Intracellular glucose is phosphorylated by glucokinase (GK) yielding G6P. This reaction is coupled to ATP hydrolysis and, thus, is irreversible. Furthermore, GK is regulated by negative feedback [Porter et al., 1982]. G6P is transfigured into F6P by phosphoglucose isomerase (PGI) and is further phosphorylated to FBP. This reaction carried out by the phosphofructokinase (PFK) consumes ATP and is irreversible. FBP is split by fructose-bisphosphate aldolase (ALDO) into two triose phosphates, dihydroxyacetone phosphate (DAP) and GAP. DAP is converted into GAP by the enzyme triosephosphate isomerase (TPI). GAP proceeds further in glycolysis and is transformed into 1,3-bisphosphoglycerate (BPG) catalysed by glyceraldehyde-3-phosphate dehydrogenase (GAPDH). Thereby, the triose phosphate is dehydrogenated and P_i is added while NAD^+ is reduced to NADH. This reaction is inhibited by one of its products, NADH [Pancholi & Fischetti, 1992].

As mentioned before, *S. pyogenes* has a non-phosphorylating $NADP^+$ -dependent glyceraldehyde 3-phosphate dehydrogenase. GAPN catalyses the irreversible conversion of GAP to 3PG with concomitant NADPH production [Iddar et al., 2003].

In the next step of glycolysis a phosphate group from BPG is transferred to adenosine diphosphate (ADP) by phosphoglycerate kinase (PG), forming ATP and 3PG which is further converted into 2-phosphoglycerate (2PG) by phosphoglycerate mutase (PGM). Enolase (ENO) forms PEP from 2PG. PEP and ADP are converted into pyruvate and ATP by the enzyme PYK. This step is inhibited by P_i and activated by G6P [Yamada & Carlsson, 1975b].

The main part of pyruvate is converted into lactate with concomitant interconversion of NADH and NAD^+ catalysed by LDH. The measurement of the kinetics

done in Rostock by Tomas Fiedler yield that this enzyme is negatively regulated by NAD^+ and stimulated by FBP and P_i .

Due to the fact that *S. pyogenes* shows more mixed acid fermentation at lower dilution rates at pH 6.5 and pH 7.5 compared to *L. lactis* and *E. faecalis* (see Section 3.1.2 and [Fiedler et al., 2011]), the mixed acid branch was included in the model. Besides the conversion to lactate, pyruvate and coenzyme A (CoA) can be converted into acetyl-CoA and formate by the pyruvate formate lyase (PFL). This transformation is inhibited by DAP and GAP [Takahashi et al., 1982]. Acetyl-CoA is metabolised to acetate via acetylphosphate yielding one molecule ATP. This conversion is inhibited by FBP [Lopez de Felipe & Gaudu, 2009]. Furthermore, acetyl-CoA is converted into acetaldehyde which is further metabolised to ethanol by the alcohol dehydrogenase (ADH) and is inhibited by ATP [Palmfeldt et al., 2004]. Thereby, two molecules of NADH are recovered.

With the analysis of the experimental data in mind, we investigated the mechanism of P_i uptake in *S. pyogenes* and based on experimental findings incorporated facilitated diffusion of P_i which is inhibited by ATP and activated by P_i^{ex} [Reizer & Saier, 1987] as well as active import of P_i^{ex} [Ferretti et al., 2001].

Furthermore, an ATPase reaction is included as a sink for the ATP generated in glycolysis, replacing all ATP consuming reactions. Additionally, NADPH recovery via the activity of a NADP^+ regenerating reaction (NPOX) is included. To get rid of the products, export reactions for formate, acetate and ethanol as well as pyruvate-controlled export of lactate [Harold & Levin, 1974] were incorporated into the model.

To simplify the model and reduce the number of parameters, some metabolites were lumped based on near-equilibrium time-scale separation:

- double phosphorylated HPr was omitted since HPr-His-P is not a substrate of HPr kinase and PEP-dependent phosphorylation of HPr-Ser-P occurs very slow compared to that of unphosphorylated HPr,
- G6P and F6P were lumped into the G6P pool,
- DAP and GAP are defined as triose-P pool,
- 2PG, 3PG and PEP are collected in the PEP pool,
- acetate and acetylphosphate are summed up in the acetate pool and

- acetaldehyde and ethanol are combined in the ethanol pool.

The ATP/ADP, NAD⁺/NADH, NADP⁺/NADPH and P_i pools are set as free-state variables, in contrast to other kinetic models [Neves et al., 1999, Voit et al., 2006a, Voit et al., 2006b]. Furthermore, the PTS system is modelled as one step to reduce the number of unknown parameters. Fig. 3.1 gives an overview of the molecular interactions of the *S. pyogenes* glycolysis model.

Transformation into a mathematical model

After the reactions of the pathway and their regulation are defined, this set is transformed into a computational model. Modelling was done using the software package COPASI [Hoops et al., 2006]. Two compartments were considered, the extracellular and the intracellular space. According to the experimental OD measurements the ratio of intra- and extracellular volume was adjusted. For simulating the glucose-pulse experiments, the extracellular volume was set to 1 l whereas the intracellular volume was calculated to be 0.036 l for 0 mM P_i^{ex}, 0.032 l for 10 and 0.035 l for 50 mM P_i^{ex}. For the fermentation experiments, the extracellular volume was set to 0.75 l and the intracellular space determined from the measured dry weight was 0.003 l for pH 6.5 and $d = 0.05$, 0.002 l for pH 6.5 and $d = 0.05$ as well as for pH 7.5 and $d = 0.15$ and 0.003 l for pH 7.5 and $d = 0.15$.

Due to unknown detailed enzyme mechanisms convenience rate laws were used for most reactions [Liebermeister & Klipp, 2006b]. However, the glucose permease as well as the passive phosphate transport are modelled as facilitated diffusion and the ATPase is modelled as hill equation. The rate laws of the *S. pyogenes* model are shown in Appendix A.2.1.

S. pyogenes is poorly studied and especially kinetic parameters are rarely described in the literature. However, we were able to find kinetic constants for the passive phosphate transporter and PaseII in the literature. From cooperation partners the kinetics of PYK and LDH were experimentally studied (see Section 3.1.4). All other kinetic parameters were either derived from enzymes of related organisms found in the literature, e.g. from *S. mutans* or *S. thermophilus*, or, if no information was available, we adopted the missing parameters from the *L. lactis* model. Enzyme specific activities were converted into V_{\max} values by assuming that 42% of cellular dry weight consisted of proteins [Even et al., 2002] and by taking an estimated

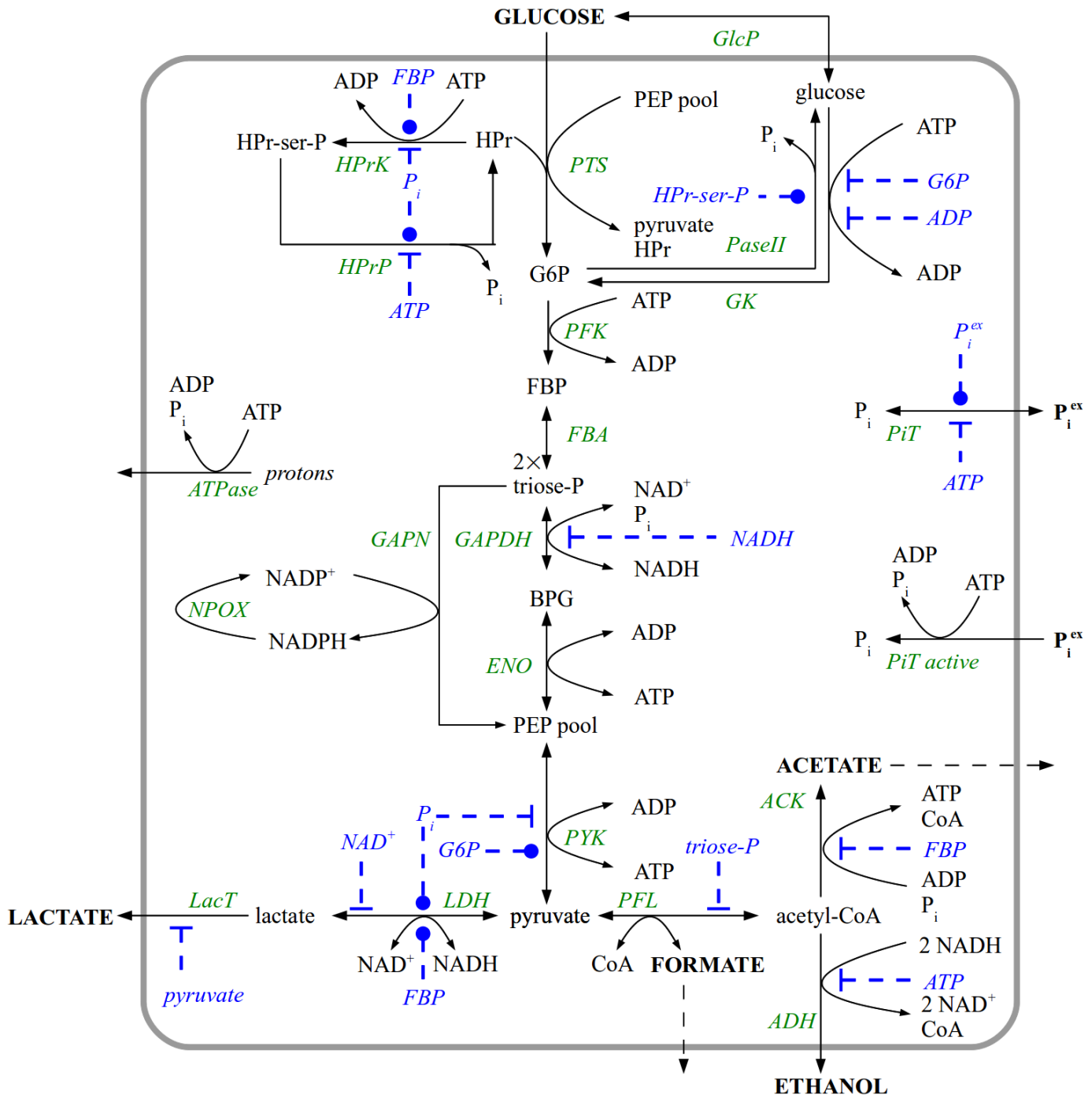


Figure 3.1: Overview of molecular interactions of *S. pyogenes* glycolysis. Allosteric regulation (blue) is divided in barred arrows (inhibition) or open circle-ends (activation). Enzymes are listed in green.

intracellular volume of 30 ml per litre of reactor volume (see Section 2.2.3). The parameters used for the *S. pyogenes* model are listed in Appendix A.1 in Tables A.1 – A.6.

Since the model is also used to simulate our fermentation data (see Section 3.1.2), the experimental set-up has to be integrated into the model. In a chemostat the cultures are constantly supplied with medium. To keep the volume constant culture liquid is removed at the same rate that fresh medium is added. In our experiments the supply of medium occurs with different dilution rates of 0.05 h^{-1} and 0.15 h^{-1} , respectively. A dilution rate of 0.05 h^{-1} indicates that within one hour 5% of the culture volume is exchanged with CDM-LAB medium. The dilution rate multiplied by the volume gives the time needed to replace the whole culture volume. For a total volume of 0.75 l and $D = 0.05 \text{ h}^{-1}$ fresh medium is added with a rate of

$$\frac{0.05}{\text{h}} \cdot 0.75 \text{ l} = \frac{0.05 \cdot 0.75 \text{ l}}{60 \cdot 60 \text{ s}} = 1.0417 \cdot 10^{-5} \frac{\text{l}}{\text{s}}.$$

In the model the permanent supply of CDM-LAB medium is represented by a constant influx of every metabolite contained in the medium. Species included in both compartments are glucose, phosphate and acetate. CDM-LAB medium contains 61.1 mM glucose, 42 mM P_i and 12 mM acetate (see Section 2.1.3). The influx of these metabolites is given by the product of dilution rate and species concentration (see Table 3.15). At the same rate that CDM-LAB medium was added, culture liquid and contained metabolites like glucose, acetate, ethanol, formate, P_i , pyruvate and lactate were removed. The efflux of these metabolites is modelled by mass action kinetics with the medium supply rate (see Table 3.15) as kinetic constant describing the velocity. Since extracellular pyruvate was detected in the supernatant a pyruvate efflux describing the transport from pyruvate out of the cell was added to the model. Due to the lack of knowledge of the detailed enzyme mechanism this reaction was modelled with mass action.

Table 3.15: Rate of medium supply in $\frac{\mu\text{l}}{\text{s}}$, influx of glucose, acetate and phosphate in $\frac{\mu\text{mol}}{\text{l s}}$ for both dilution rates of 0.05 h^{-1} and 0.15 h^{-1} , respectively.

D	Medium supply rate	Glucose inflow	Acetate inflow	P_i inflow
0.05	10.42	0.64	0.13	0.44
0.15	31.25	1.91	0.38	1.31

The kinetic model is able to describe continuous cultured as well as glucose-pulsed cells. For this purpose the dilution rate as well as the velocity constant of the pyruvate efflux reaction are set to zero.

Parameter estimation

Since not all kinetic parameters were determined in *S. pyogenes* and *in vitro* measurements can deviate considerably from *in vivo* conditions [Teusink et al., 2000], we tuned the parameters to match our time-series or fermentation data. We therefore consider the parameters as initial estimates for the parameter estimation. Subsequently, our glucose-pulse and fermentation experiments were used as input for a particle swarm algorithm with an increased swarm size of 100 carried out with the COPASI software package [Hoops et al., 2006].

Reactions describing a transport across the membrane demand attention if the concerning compartments differ in volume since changing the volume affects the concentration. COPASI overcomes this problem by considering particle numbers instead of concentrations for all calculations. For the output the concentration is recalculated from the particle number [Hoops et al., 2006]. In general, V_{\max} values are given per l of intracellular volume. Since the transporters are located within the membrane the V_{\max} has to be corrected by multiplication with a surface dependent factor. As a consequence the velocity constants of transport reactions, i.e. PTS, GlcP, lactate transport, ACK, ADH, passive and active phosphate transport, were varied in a wider range for parameter estimation. Thereby, the lower bound was reduced since the surface dependent correction factor includes the ratio of extracellular to intracellular compartment.

3.2.2 The role of phosphate

Fitting the first version of the *S. pyogenes* glycolytic model of continuous cultured cells to our fermentation data (see Section 3.1.2) resulted in a system in an equilibrium state with zero fluxes. It was impossible to get the system into a steady state with positive fluxes. As a consequence of the vanishing fluxes neither glucose was taken up nor was energy produced due to depleted PEP. The reason for that was an exhausted phosphate pool which stopped the glycolysis at the level of GAPDH.

The depleted phosphate pool motivated us to investigate the role of free inor-

ganic phosphate in more detail. We found out that phosphate possesses a special role in glycolysis. On the one hand, the intracellular P_i concentration depends on the metabolic activity of the cell. In starved streptococcal cells the phosphate level is high but it decreases as soon as a carbon source is present in the medium [Reizer & Saier, 1987]. Therefore, intracellular phosphate cannot be fixed in the model but has to be modelled as an independent variable. On the other hand, P_i regulates glycolytic key enzymes (see Figure 3.1). Phosphate controls, for example, the sugar uptake by inhibiting HPr kinase and activating HPr phosphatase. As a consequence, dephosphorylated HPr is available which is a substrate for the PTS system. Furthermore, phosphate controls the level of PEP by inhibiting PK and activates the break down of pyruvate by activating LDH. Moreover, the availability of P_i determines the flux through glycolysis by virtue of its involvement as essential substrate, i.e. of GAPDH and acetate kinase.

In the first version of the *S. pyogenes* model intracellular phosphate was modelled as a free variable but, as stated above, it was depleted shortly after glucose supply. In order to solve this problem we studied the literature concerning the intracellular phosphate level and its effectors. Thereby, we identified a mismatch between the total measured phosphate pool under starved and glycolysing conditions based on ^{13}C - and ^{31}P -NMR measurements of Neves and co-workers [Neves et al., 2002]. The data reveals that phosphate is primarily incorporated in the PEP pool (15–30 mM) and unbound P_i (45 mM) during starvation but shifts towards FBP (55 mM) and ATP (8 mM) during glycolysis. The sum of total measured phosphate is therefore approximately 60 mM during starvation, but approximately 120 mM during glycolysis. Unidentified phosphorylated compounds [Kulaev et al., 1999, Mijakovic et al., 2002, Sutrina et al., 1988] or phosphate in the cell wall are not likely to explain this difference of approximately 60 mM between these two physiological states, as the disappearance of phosphate upon starvation is so immediate. A subsequent literature survey showed that the concentration of phosphate in the medium has a pronounced effect on the intracellular FBP concentration during glucose consumption. This implies that the pool of free and bound phosphate (in PEP, FBP and so forth) is critically dependent on the external phosphate concentration.

We independently repeated the experiments of Neves *et al.* [Neves et al., 2002] by use of NAD(P) coupled enzymatic assays (see Section 2.1.5). This revealed a de-

pendency of the build-up of FBP on the extracellular phosphate concentration (see Section 3.1.3 and Figure 3.2). Therefore, we concluded that the observed differences in the total phosphate pool between glycolysing and starving cells must be due to differences in external phosphate concentrations. In summary, we have shown that the internal phosphate pool depends on the extracellular phosphate concentrations which implies that the inclusion of phosphate exchange over the membrane is absolutely necessary in the kinetic model.

Thus, we incorporated phosphate uptake in the glycolytic model for *S. pyogenes*. Experimental findings by Reizer and Saier suggest a facilitated diffusion of P_i which is inhibited by ATP and dependent on extracellular phosphate [Reizer & Saier, 1987]. Additionally, we included an ATP-dependent uptake of phosphate since genes encoding this transporter are found in the genome of *S. pyogenes* [Ferretti et al., 2001].

3.2.3 Resulting fit

The developed kinetic model is initialised with the kinetic parameters found in literature (see Appendix A.1). Since not all kinetic parameters were determined, we fitted them to our experimentally obtained time-series profiles and steady state product concentrations (see Section 3.1.3 and 3.1.2).

Glucose-pulsed cells

Firstly, the glycolytic model of *S. pyogenes* was fitted to time-series data. Since the metabolite concentrations are measured at different time points, more data is available as compared to the chemostat experiments. To fit the glucose-pulse data all kinetic parameters of the model except for the equilibrium constants were tuned. Equilibrium constants are dependent on the chemical reaction and thus are valid for all organisms. In order to improve the goodness of the fit we increased the weights for the quadratic distance between the measured and the simulated extracellular glucose level to 1.

For the three different phosphate concentrations, initial concentrations of measured and fitted metabolites were allowed to differ. We have measured initial concentrations for G6P (at 0 and 10 mM P_i^{ex}), FBP, triose-P (at 10 and 50 mM P_i^{ex}), ATP and extracellular lactate. HPr was assumed to be 0.16 mM [Reizer et al., 1984]. HPr-Ser-P, intracellular glucose, BPG, pyruvate, intracellular lactate, acetyl-CoA,

ethanol, formate, acetate, NADH and NADPH are set to zero to reduce the dimension of the parameter space. The remaining initial metabolite concentrations are fitted. The range for initial extracellular glucose is restricted to 5 and 10, initial G6P (at 50 mM P_i^{ex}) can vary between 0.01 and 5, the start values of trioseP (in the absence of P_i^{ex}), intracellular phosphate and CoA are bounded by 1 and 5 and the initial values of PEP, NAD and NADP can vary between 1 and 10. The model with this constraints is able to almost perfectly fit our experimental data (see Figure 3.2), as long as the phosphate uptake system is in place. The experiments were reproduced several times with an exemplary data set displayed in Figure 3.2.

Due to the fact that the experimental data does not allow an unambiguous fit of the data and the parameters are not identifiable (between the different fits, all parameters varied over a wide range within the set boundaries), we performed several hundred fits and subjected the best 50 of them to the analysis below in order to make sure that we are observing robust effects that do not depend on the exact choice of the parameters. The selection of this 50 models is based on the objective value of the parameter estimation and on visual inspection of the resulting fit. All 50 models have an objective value lower than 25. One exemplary simulation of our measured time-series profiles is shown in Figure 3.2 and the corresponding parameter set is displayed in Appendix A.1. In summary, it is clear that P_i exchange plays an important role in sustaining a large intracellular total P_i pool, affecting the levels of phosphorylated metabolic intermediates.

Interestingly, the glucose uptake rate in *S. pyogenes* does not simply correlate with the extracellular phosphate concentration. Rather, low extracellular phosphate concentrations (e.g. around 1 mM) decrease the glucose uptake compared to no phosphate in the environment whereas higher phosphate concentrations increase the glucose uptake rate. This observation is not trivial to explain. Because free phosphate has such a pronounced effect on glycolysis and glucose uptake, we studied the behaviour of intracellular phosphate in our model. Intracellular phosphate is extremely hard to determine experimentally in the presence of extracellular phosphate. Insights from computational models are therefore advantageous. Curiously, we observe that due to the combination of active and passive phosphate transport low extracellular phosphate concentration can lead to a decrease of the intracellular phosphate level in *S. pyogenes*, if the concentration gradient is pointing to the outside of the cell. Figure 3.3 displays a parameter scan of intracellular

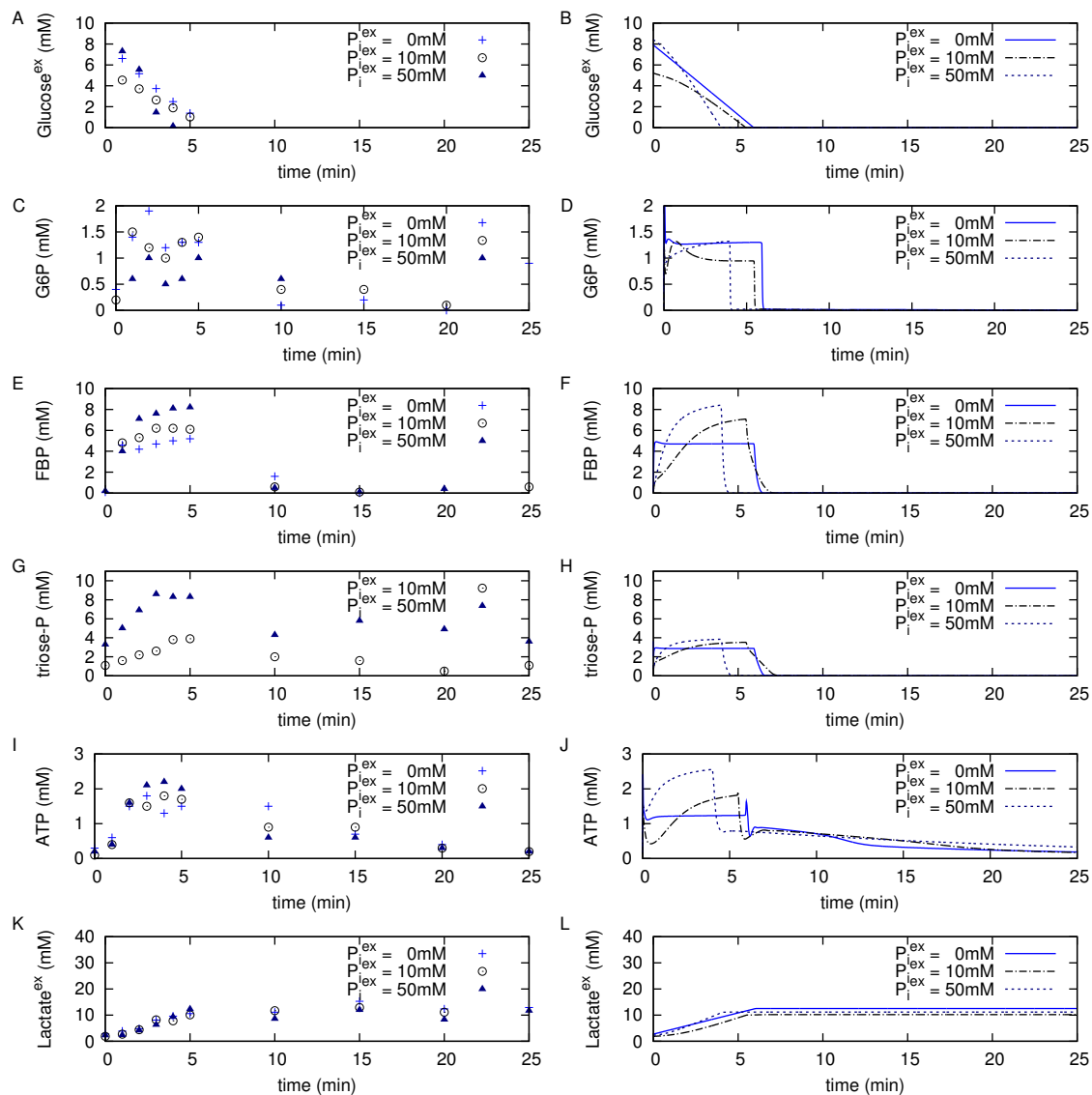


Figure 3.2: Metabolic profiles and model simulations of glucose-pulse experiments in *S. pyogenes*. We measured the influence of 0 mM (crosses), 10 mM (circles) and 50 mM (triangles) extracellular P_i on the dynamics of (A) glucose, (C) G6P, (E) FBP, (G) triose-P, (I) ATP and (K) extracellular lactate. Simulations show similar quantitative trends in (B), (D), (F), (H), (J) and (L), respectively. Initial concentrations are displayed in Table A.6 and the ratio of intra- to extracellular volume was set to 0.036, 0.032 and 0.035 for 0, 10 and 50 mM P_i^{ex} , respectively (based on OD measurements).

phosphate against extracellular phosphate (Figure 3.3A) as well as the effect of extracellular phosphate on the flux of the passive phosphate transport system (Figure 3.3B). For low extracellular phosphate levels (e.g. around 1 mM) the flux through the phosphate transporter is directed towards the outside removing phosphate from the cytosol whereas higher phosphate concentrations result in phosphate uptake. Thus, it is obvious, that certain low concentrations of extracellular phosphate lead to a decreased intracellular phosphate concentration compared to no extracellular phosphate. Intracellular phosphate in turn activates the PTS and is an important substrate for GAPDH and ACK. Therefore, a decreased intracellular phosphate concentration leads to a decreased glucose uptake rate (see Figure 3.3C). The effect on glucose uptake was also observed experimentally and the respective data (which were not used for fitting of the model) are also shown in Figure 3.3D. The experimentally observed effect is however even more pronounced than the computationally predicted one. Due to the non-identifiability of the parameters, we studied the 50 best fits of *S. pyogenes* with respect to this behaviour. The above reported behaviour is the same in many (roughly 50%) of the fits, but not in all. Thus, it is obviously crucial to experimentally verify the observations resulting from our canonical best fit, since the behaviour is not completely robust irrespective of the parameter set. This has been done as described above.

We performed additional *in silico* experiments with our kinetic model of *S. pyogenes* in which extracellular glucose and phosphate levels were varied within physiological ranges. Our experimental studies showed that glucose uptake ceases when extracellular glucose levels rise above 20 mM under the employed conditions. We observed that *S. pyogenes* consumes 5 to 10 mM of the pulse and subsequently stops sugar uptake. We therefore varied the amount of extracellular glucose in our simulation for all fitted parameter sets in the model. In all models if no or low external phosphate was present for *S. pyogenes*, the glucose uptake was completely stopped or severely inhibited at high glucose levels (the exact numerical value varied between the different fits). Often the actual value was much higher (and unphysiological) compared to the experimental set-up (ranging between 25 mM – 963 M), but qualitatively this was robust behaviour irrespective of the exact parameter set. This inhibition could be overcome by adding phosphate, underlining again the crucial importance of this substance for glucose uptake and glycolysis in general.

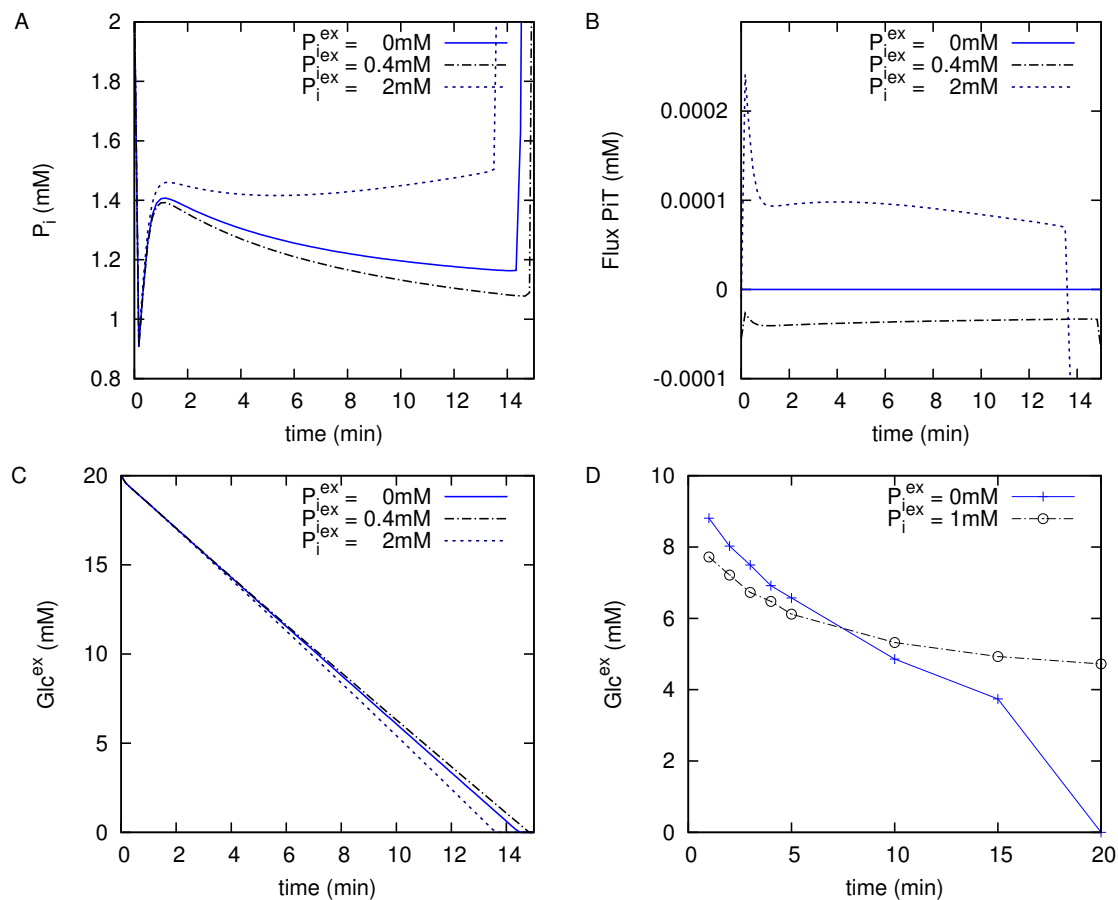


Figure 3.3: Model simulations after a 20 mM and metabolic profiles after a 8 mM glucose-pulse in *S. pyogenes*. Model predictions of intracellular phosphate levels in (A) *S. pyogenes* under 0, 0.4 and 2 mM extracellular phosphate. Due to the presence of a passive phosphate transporter low extracellular phosphate concentrations result in phosphate efflux (B) and, thus, decrease the intracellular phosphate concentration. Since the PTS system is regulated by phosphate, the sugar uptake is slower at low extracellular phosphate concentrations (C) which we also determined experimentally (D).

Continuous culture

The model fitted to the glucose-pulse data (see Section 3.2.3) was subsequently fitted to steady state data. Hereby, only the velocity constants were modified. This makes sense, since the V_{\max} value of an enzyme depends on the amount of enzyme present which will certainly not be exactly the same in both experiments. K_m values are characteristics of the enzymes and independent from the amount of enzyme used in the ansatz. The fitted velocity constants are displayed in Table 3.16. Table 3.17

summarizes the initial metabolite concentrations and compares the simulated steady state species levels with the measured end-product concentrations.

Table 3.16: Velocity constants (in $\frac{\text{mM}}{\text{s}}$) of the steady state model.

Variable	Optimized
V_{\max}^{PTS}	0.58
V_{\max}^{GlcP}	0.003
V_{\max}^{HPrP}	731.28
V_{\max}^{HPrK}	176.47
V_{\max}^{GK}	1.44
V_{\max}^{PFK}	12.45
V_{\max}^{PaseII}	0.13
V_{\max}^{FBA}	247.97
V_{\max}^{GAPDH}	7.92
V_{\max}^{GAPN}	1.14
V_{\max}^{ENO}	20.45
V_{\max}^{PYK}	6.35
V_{\max}^{PyrT}	0.03
V_{\max}^{LDH}	5.75
V_{\max}^{LacT}	289.00
V_{\max}^{PFL}	134.23
V_{\max}^{ACK}	8.67
V_{\max}^{ADH}	29.89
V_{\max}^{PiT}	0.32
$V_{\max}^{\text{PiTactive}}$	0.05
V_{\max}^{ATPase}	112.74
V_{\max}^{NPOX}	210.97

Table 3.17: Initial metabolite concentrations and simulated and measured steady state end-products (mM) in the continuous cultured cells. n.d., not determined.

Species	Initial concentration	End-product concentration	
		Simulation	Measurement
G6P	1.13	1.20	n.d.
FBP	6.20	25.90	n.d.
Triose-P	3.12	6.75	n.d.
BPG	0.20	0.08	n.d.
PEP	13.86	2921.8	n.d.
Pyruvate	3.78	0.008	n.d.
Acetyl-CoA	3.46	$6.14 \cdot 10^{-5}$	n.d.
P _i	17.36	42.00	n.d.
ADP	3.05	4.24	n.d.
ATP	1.95	0.76	n.d.
NAD	8.54	2.14	n.d.
NADH	0	6.40	n.d.
CoA	1.07	4.54	n.d.
Lactate	8.35	$5.97 \cdot 10^{-5}$	n.d.
Glucose	2.40	$9.36 \cdot 10^{-4}$	n.d.
HPr-ser-P	0.16	0.12	n.d.
HPr	0	0.04	n.d.
NADP	0.72	0.72	n.d.
NADPH	0	$2.93 \cdot 10^{-4}$	n.d.
Acetate	12.2	36.19	35.10
Glucose ^{ex}	61.1	$3.37 \cdot 10^{-4}$	0.00
Lactate ^{ex}	7.34	77.36	69.97
P _i ^{ex}	42	42	40.07
Formate	5.20	21.58	35.41
Ethanol	3.03	21.48	19.26
Pyruvate ^{ex}	8.54	23.27	1.50

Although the steady state concentrations of intracellular metabolites are not restricted, all transient species levels show reasonable concentrations compared to literature data (e.g. for *L. lactis* steady state levels are listed in [Even et al., 2001])

except for PEP which is in the molar range and, thus, too high. The simulated cell is not completely glucose-limited since small amounts of glucose remain in the supernatant. Nevertheless, the model is able to reflect the measured end-product concentrations of acetate, extracellular lactate, external phosphate and ethanol. Surprisingly, the formate and extracellular pyruvate levels are too high.

3.2.4 Sensitivity analysis

The developed kinetic model contains many unknown parameters. In order to reduce the search space in parameter estimation we determine the impact of each parameter on the system by performing a sensitivity analysis with the model of glucose-pulsed cells (see Section 3.2.3). If a parameter has a low sensitivity, it exerts a small control on the system and the determination of its exact value is not needed. For a parameter with a high impact, the knowledge of the accurate value improves the model and, therefore, a measurement of this kinetic parameter is essential. Two different sensitivity analysis methods were used to explore the parameter sensitivity of the kinetic model of *S. pyogenes*. We performed a global strategy to identify the general features of all parameters within a physiologically-feasible range and, secondly, fitted the model several times to the experimental data and calculated the local sensitivities of this set of models to use tighter boundary conditions on the parameter scan.

Random sampling

We performed a global sensitivity analysis since the exact parameter set is not known and a local method depends directly on the parameter space. One way to perform a global sensitivity analysis is an extensive random exploration of the parameter space. Thereby, the parameter values were allowed to vary within the physiologically-feasible ranges which we also used for parameter estimation (see Section 3.2.1). In each sampling iteration the parameters were randomly selected within these defined boundaries. With this parameter set we subsequently calculated scaled parameter sensitivities on the species concentrations. To analyse the results of this approach, histograms with non-equidistant bins (being more precise for small sensitivities and having larger ranges for higher sensitivities, e.g. lower or higher than 10, respectively) were plotted using MATLAB 7.8 (The MathWorks, Inc).

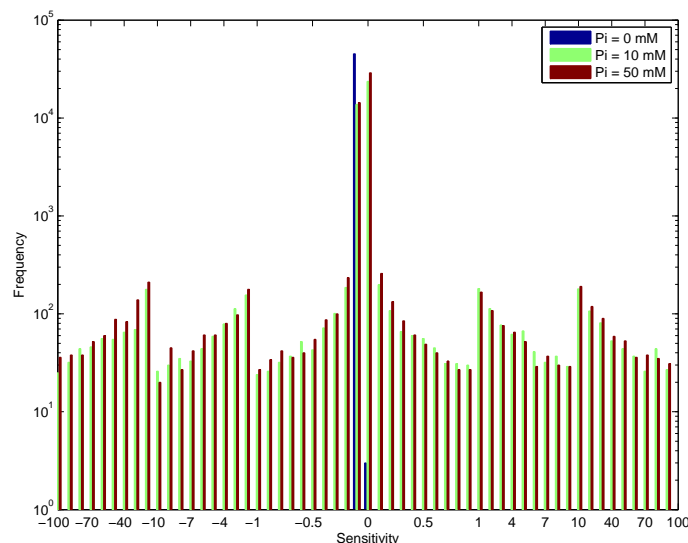


Figure 3.4: Results of the global sensitivity analysis of the velocity constant of the passive phosphate transporter on the FBP level in *S. pyogenes*. The scaled sensitivities of the evaluated models are shown on the x -axis and on the logarithmic y -axis the sensitivities are plotted. This parameters can have a high impact on the FBP concentration.

Exemplary the impact of the velocity constant of the passive phosphate transporter on FBP is shown in Figure 3.4.

Due to the random sampling the calculated sensitivities give the possible impact of the parameters on the system but imply no information about the probabilities of these values. However, if one histogram displays that the parameter has low sensitivities we conclude that the knowledge of the exact parameter value does not improve the model and, thus, the determination is not necessary. Therefore, we concentrate on all parameters which can have high sensitivities. For each parameter we calculated the maximal sensitivity from the data obtained from the random sampling approach. For each species the maximal impact of each parameter on the particular metabolite was plotted. As we focus on the role of phosphate and FBP, Figure 3.5 shows the distribution of the parameter sensitivities on these concentrations. The model parameters are plotted on the x -axis and the sensitivities are shown on the logarithmic y -axis. The figure reveals that almost all parameters can exert a large control on FBP at 0, 10 and 50 mM and on P_i in the absence of external phosphate, respectively, in certain parameter sets. Interestingly, the parameters of the glycolytic model of *S. pyogenes* show a low impact on the phosphate level in the

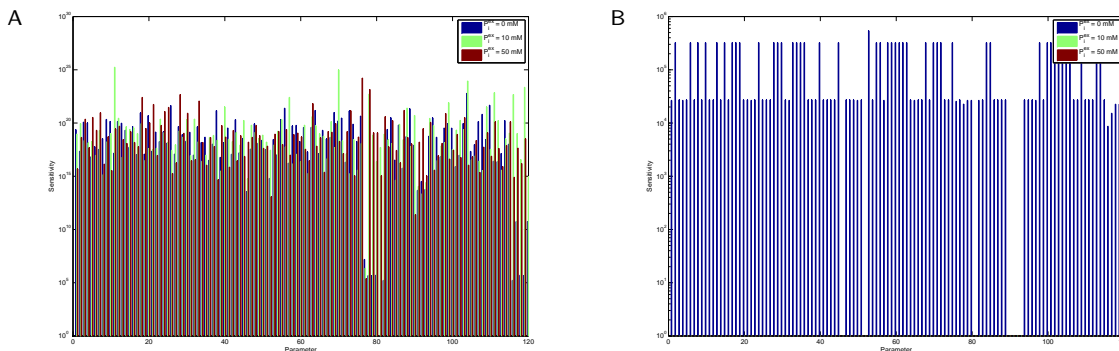


Figure 3.5: Maximal parameter sensitivities on (A) FBP and (B) P_i for *S. pyogenes*. The parameters are shown on the x -axis and on the logarithmic y -axis the sensitivities are plotted. All parameters can have a high impact on FBP at 0, 10 and 50 mM P_i^{ex} . Contrary to FBP, all parameters show a low impact on the P_i level at 10 and 50 mM external phosphate.

presence of 10 or 50 mM P_i^{ex} . Therefore, with this very general approach we are not able to identify crucial parameters and we have to restrict our search space further.

Fitting and local sensitivity analysis

In order to use tighter boundary conditions we calculated scaled sensitivities of the best 50 fits (see Section 3.2.3). Each model describes our experimental data but they differ from each other in the parameter set. From these 50 models scaled parameter sensitivities on all species concentrations and reaction fluxes were calculated for varying extracellular phosphate concentrations (0, 10 and 50 mM) and plotted as histograms. These results represent a subset of the outcome of the random sampling method.

We concentrated on the parameter sensitivities on FBP, P_i , PFK flux and PTS flux. In order to analyse the outcome of this approach we classified the parameters into groups according to their maximal effects on the studied system variable. Thus, we obtain one set of parameters having a high impact on the particular species or flux, one class exerting a medium effect and one set showing a low impact. According to our definition, a parameter having a maximal scaled sensitivity higher than plus or minus one exerts a high impact on the studied model parameter whereas a maximal control lower than plus or minus 0.3 characterises a parameter having a low effect

on the investigated system variable. Parameters showing a sensitivity between plus or minus 0.3 and plus or minus one are classified as exhibiting a medium effect. The results of this approach are summarised in the Tables A.7 – A.10.

As displayed in Table A.7, the control on the FBP concentration is distributed among all parameters. In general, the maximal scaled parameter sensitivities are lower than 10 (data not shown). The sensitivities of both phosphate transport systems, the active and the passive one, are affected by external phosphate. That makes sense since both transporters are dependent on the presence of extracellular phosphate and does not operate in the absence of that metabolite. We can identify the parameters of the lactate transporter and some single parameters such as the equilibrium constant of PFL and PYK as parameters having a low impact on the FBP level. The remaining parameters can have at least a medium effect. In the presence of external phosphate, the parameters of the active and the passive phosphate transport can exert a medium or high impact on FBP.

Considering the sensitivities on internal phosphate (see Table A.8) it is obvious that the parameters have a lower impact on this species as compared to FBP. We can identify the ATPase and the glucose permease as reactions which can have a high impact whereas the mixed acid branch, LDH and the lactate transport have a low effect on the phosphate concentration. The remaining processes are classified in the group showing medium sensitivities.

Both fluxes through PTS and PFK are controlled by many parameters (see Tables A.9 and A.10). Again, we can identify the phosphate uptake systems in the absence of phosphate, the lactate transporter and some single parameters such as the equilibrium constant of ENO as having a low effect on the fluxes. However, the remaining processes can exert at least a medium effect on the PTS and PFK flux, respectively.

In summary, we are not able to identify crucial parameters even with the described analysis and the usage of physiological conditions.

MCA

Having a model describing continuous cultivated cells (see Section 3.2.3), the control exerted by the parameters on a system's variable can be studied by means of MCA (see Section 2.2.9). This local sensitivity analysis facilitates predictions concerning the robustness and validity of a model.

Similar to the global sensitivity analysis of the kinetic model of glucose-pulsed cells, the control on the steady state fluxes and metabolite concentrations is broadly distributed among the reactions of the model. Consequently, the steady state concentrations and fluxes are strongly influenced by small perturbations in the parameters.

However, we can identify some reactions having a low flux and concentration control coefficient. Surprisingly, among these are the reactions involved in sugar uptake such as PTS, GK and glucose permease. Furthermore, we found out that the lactate transporter as well as the reactions describing pyruvate and lactate outflow from the vessel have a small control. Since *S. pyogenes* carries out enhanced mixed acid fermentation as compared to *L. lactis* [Fiedler et al., 2011], the low impact of the lactate transport makes sense.

Reactions showing a particular high impact on the steady state concentrations and fluxes comprise PFK, PYK, ATPase, but also glucose inflow as well as phosphate in- and outflow with the medium. Since the glucose inflow maintains the glucose supply of the system, a high impact makes sense. The high impact of the phosphate in- and outflow on the steady state concentrations and fluxes can be explained by the effect this metabolite exerts on the intermediate FBP and the glucose uptake rate. However, it is surprising that the passive phosphate transport system does not show a high control coefficient.

3.3 Comparison between *S. pyogenes* and *L. lactis*

The kinetic model of *S. pyogenes* glycolysis presented in the last section is used to facilitate inter-species comparison between this lactic acid bacteria and the closely related *L. lactis*. Although both LAB have a similar primary metabolism they persist in different environments. In this section the *L. lactis* model, the similarities and the differences to the model of *S. pyogenes* and the extent to which these differences contribute to different functionalities are described. The *L. lactis* model was developed by Mark Musters and modified by me to be comparable to the *S. pyogenes* model. All analyses were done by myself.

3.3.1 Kinetic model of *L. lactis*

Setting up the kinetic model for *L. lactis* on the basis of existing models necessitated a (re)assessment of all relevant processes and their respective regulation as described in the following. Like in *S. pyogenes*, sugar is mainly taken up via the PTS and directly converted into G6P [Deutscher et al., 2006]. A low-affinity glucose permease is present, but its contribution to the overall glucose uptake is limited in *L. lactis* [Castro et al., 2009]. Therefore, this permease was omitted in our *L. lactis* model. Furthermore, the PTS system is modelled as a single step reaction. The conversion of glucose to its main product pyruvate proceeds via the Embden-Meyerhof-Parnas pathway. Thereby, PYK is allosterically activated by FBP and inhibited by P_i [Crow & Pritchard, 1976].

In glucose excess conditions, the majority of the synthesised pyruvate is converted into lactate, catalysed by LDH. This enzyme is allosterically activated and inhibited by FBP and P_i , respectively, in *L. lactis* [van Niel et al., 2004]. PFL catalyses the conversion of pyruvate and CoA into acetyl-CoA and formate. This reaction is inhibited by GAP [Asanuma & Hino, 2000, Solem et al., 2008]. Acetyl-CoA is metabolised to acetate via acetylphosphate or, alternatively, via acetaldehyde to ethanol [Thomas et al., 1979]. The compounds acetate, ethanol and formate are synthesised and subsequently transported out of the cell. An ATPase reaction is included cleaving the produced ATP into ADP and P_i .

Since our experiments show the significance of including phosphate exchange over the membrane in the kinetic model, we extended the model with an ATP-driven phosphate uniporter which is feedback regulated by the intracellular phosphate level

[Poolman et al., 1987]; phosphate leakage was assumed to be negligible.

To simplify the model and reduce the number of parameters, the following metabolites were lumped:

- G6P and F6P were lumped into the G6P pool,
- DAP and GAP are defined as triose-P pool,
- 2PG, 3PG and PEP are collected in the PEP pool and
- all mixed acid products (formate, ethanol and acetate) were lumped into the mixed acids pool.

Under the conditions for which we developed the model, mixed acid formation was negligible due to the fact that the measured final lactate concentration in the medium corresponds to roughly twice the entered glucose concentration (see Figure 3.7, A and G). The ATP/ADP, NAD⁺/NADH and P_i pools are set as free-state variables, in contrast to other kinetic models [Neves et al., 1999, Voit et al., 2006a, Voit et al., 2006b]. Fig. 3.6 shows the structure of the *L. lactis* model.

As for the *S. pyogenes* model, the parameters in the *L. lactis* model were optimised with parameter estimation to fit *in vivo* time-series data [Levering et al., 2011]. These time-series data comprised our own measurements (see Figure 3.7) as well as the published NMR data by Neves *et al.* (see Figure 3.8) [Neves et al., 2002]. For the two different data sets, initial concentrations of metabolites (both measured and fitted ones), as well as the activity of the ATPase were allowed to differ. In addition, initial concentrations that were not measured in our own or in the NMR data were fitted for the respective data sets. Thus, initial concentrations of PEP, extracellular lactate, ATP (without phosphate in the medium), ADP, intracellular phosphate and NAD were fitted for our experiments (at 0, 10 and 50 mM extracellular phosphate). For the Neves data, initial concentrations of ATP, ADP and phosphate for the ¹³C-NMR data set and FBP, lactate, NAD, PEP and ADP for the ³¹P-NMR data set were fitted. All other parameters stayed the same irrespective of the assumption that the V_{max} values (that include the enzyme expression levels) for the two different experimental data sets will certainly not be exactly the same. However, the model with these constraints is able to almost perfectly fit the dynamics for different strains (i.e. MG1363 for the Neves experiments [Neves et al., 2002] and NZ9000, a MG1363 derivative, for our glucose-pulse experiments) with one single

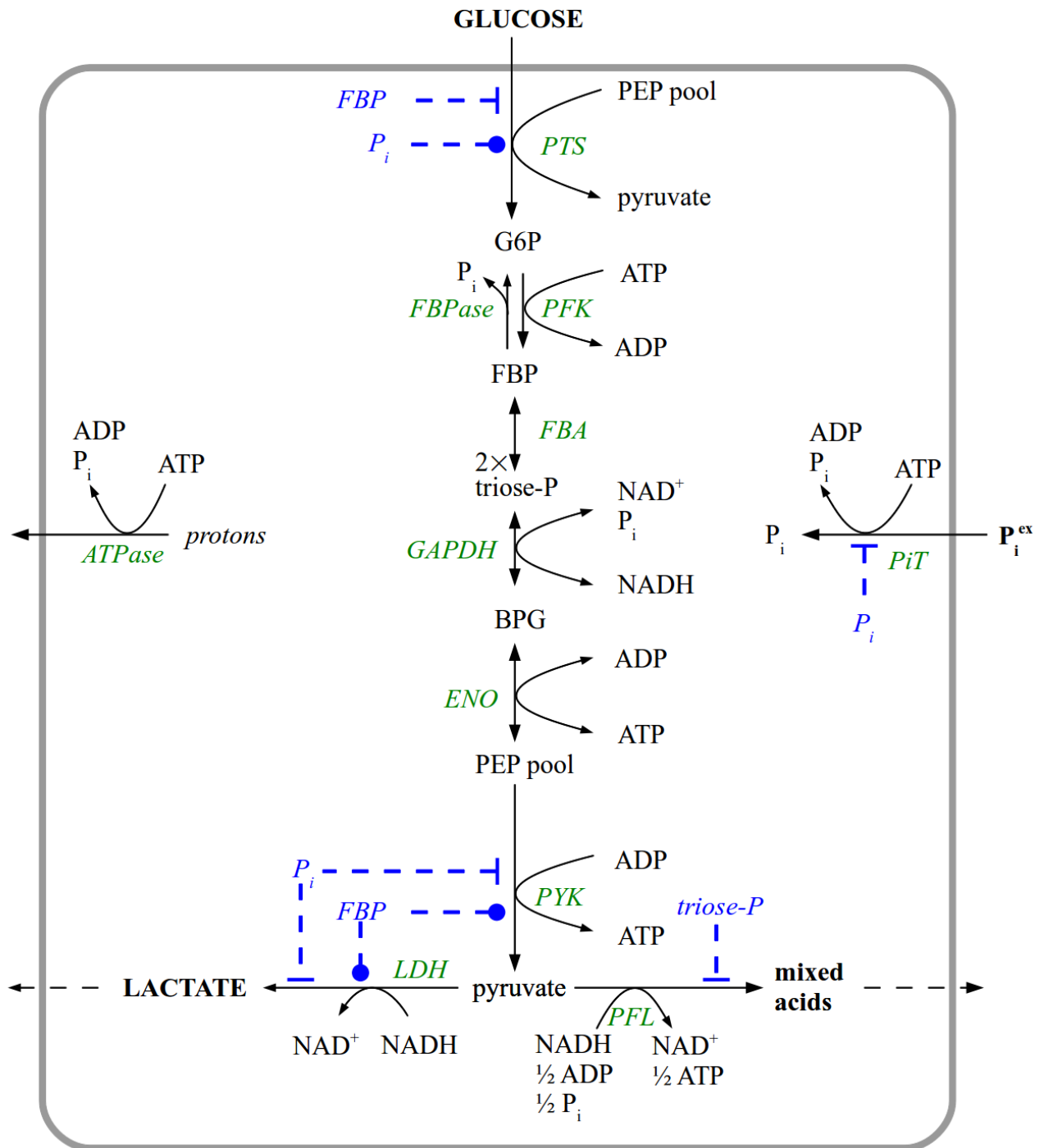


Figure 3.6: Overview of molecular interactions of *L. lactis* glycolysis. Allosteric regulation (blue) is divided in barred arrows (inhibition) or open circle-ends (activation). Enzymes are listed in green.

thermodynamically-consistent parameter set (though with variable ATPase activities) as long as the phosphate uptake is included in the model (see Figure 3.7 and 3.8). Without this reaction, the data cannot be fitted since P_i exchange plays an important role in sustaining a large intracellular total P_i pool, affecting the levels of phosphorylated metabolic intermediates. The parameters of the *L. lactis* model are given in [Levering et al., 2011].

Due to a high number of unknown parameters and little experimental data the optimisation problem is underdetermined and the parameter set resulting from the initial fit is not unique. As done for the *S. pyogenes* model we performed several hundred fits and subjected the best 50 of them to the analysis below to overcome this problem.

3.3.2 Topological and regulatory differences

After the glycolytic models of both LAB, *S. pyogenes* and *L. lactis*, are set up and able to describe our experimental data, they are used to study the differences between the two bacteria. In a first step we concentrate on the topological differences.

In the model for *S. pyogenes* the PTS system is decomposed in HPr and serine-phosphorylated HPr (see Figure 3.1 and 3.6) [Reizer et al., 1985]. In *L. lactis*, the PTS is modelled as a single step. In *S. pyogenes* this refinement was motivated by the presence of the expulsion mechanism.

The gene encoding the FBPase is not present in the genome of *S. pyogenes* and, consequently, this reaction was removed from the model. Instead, an expulsion mechanism of G6P was introduced, which is catalyzed by the HPr-Ser-P-activated sugar-phosphate phosphatase II (PaseII) [Ye et al., 1996]. In *S. pyogenes* this expulsion mechanism yields free inorganic phosphate in glycolysing cells whereas the FBP dephosphorylation is not regulated in *L. lactis*. The incorporation of PaseII led to an inclusion of a GlcP participating in the expulsion mechanism and in the incorporation of a glucokinase that is allosterically inhibited by G6P and ADP [Porter et al., 1982]. For *L. lactis*, GlcP and GK are both omitted.

Interestingly, *S. pyogenes* possesses a GAPN which is not present in the genome of *L. lactis*. This reaction enables *S. pyogenes* to produce PEP required for sugar uptake in the absence of phosphate or ADP.

Since *S. pyogenes* shows a higher heterofermentative capacity than *L. lactis* [Fiedler et al., 2011], the mixed acid branch is subdivided into acetate and ethanol

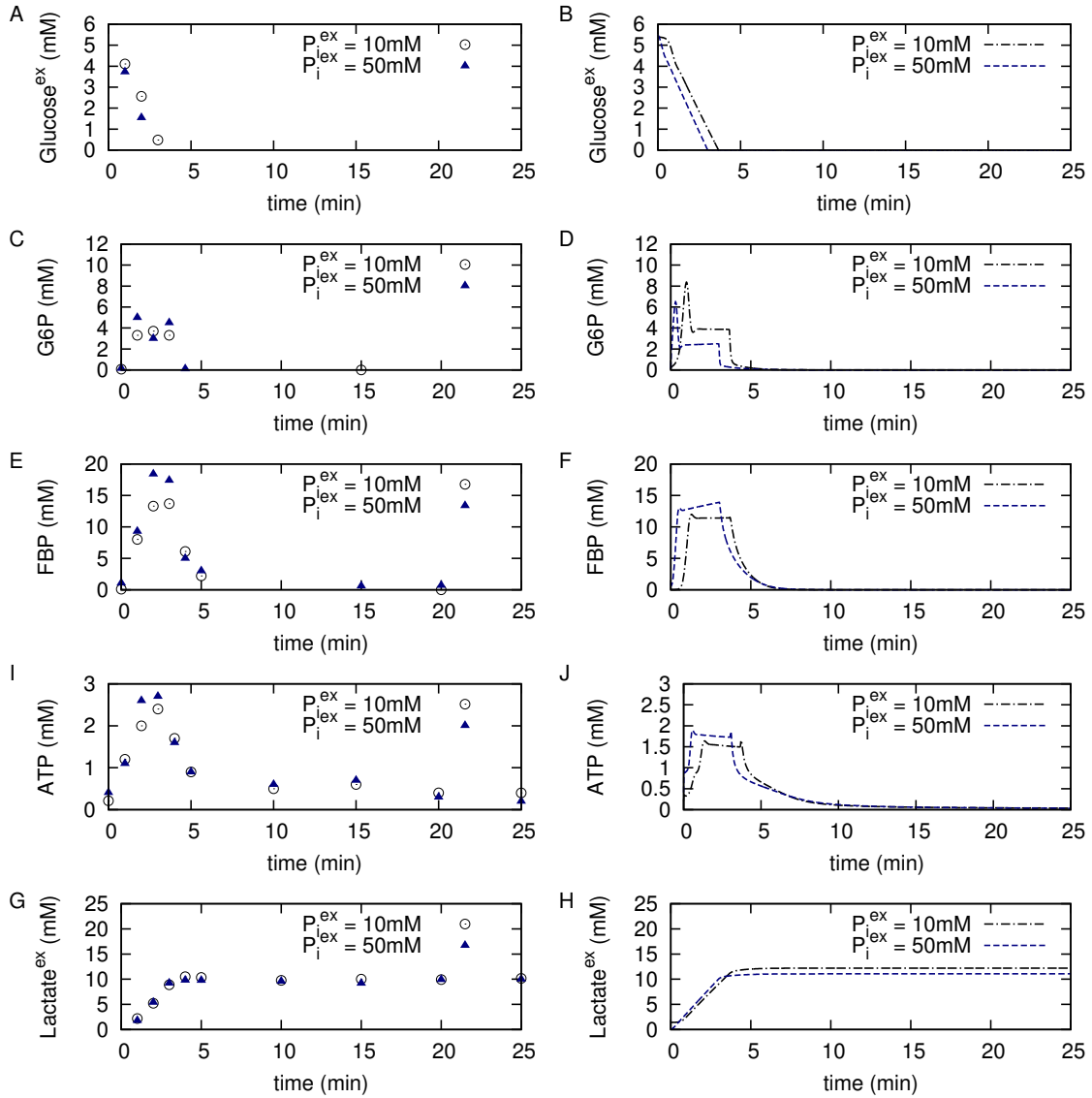


Figure 3.7: Metabolic profiles and model simulations of 5 mM glucose-pulse experiments in *L. lactis*. (A) Extracellular glucose, (C) G6P, (E) FBP, (G) ATP and (I) external lactate profiles as measured in glucose-pulse experiments with extracellular P_i levels of 10 (circles) and 50 mM (triangles) and (B), (D), (F), (H) and (J) show the *L. lactis* model simulations. Initial concentrations are given in [Levering et al., 2011] and the ratio of intra- to extracellular volume was set to 0.0099 and 0.0129, respectively (based on OD measurements).

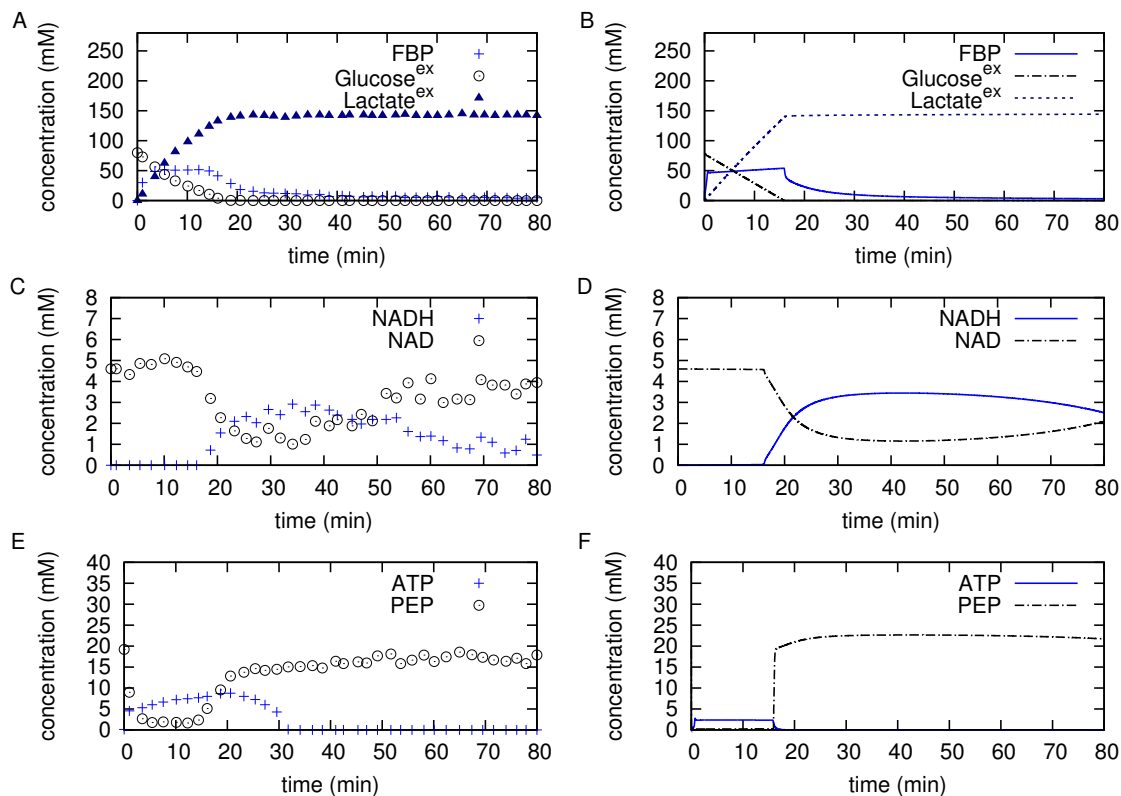


Figure 3.8: Metabolic profiles and model simulations of glucose-pulse experiments in *L. lactis*. ^{13}C - and ^{31}P -NMR time-series profiles [Neves et al., 2002] of (A) FBP, glucose and lactate, (C) NAD^+ and NADH and (E) PEP pool and ATP when 80 mM of glucose is added; (B), (D) and (F) are corresponding model simulations. Simulations were performed with a ratio of intra- to extracellular volume of 0.047 and the following initial concentrations: $[\text{glucose}] = 80 \text{ mM}$, $[\text{PEP pool}] = 20 \text{ mM}$, $[\text{P}_i] = 120 \text{ mM}$, $[\text{P}_i^{\text{ex}}] = 50 \text{ mM}$, $[\text{ATP}] = 0.1 \text{ mM}$, $[\text{ADP}] = 8.9 \text{ mM}$ and $[\text{NAD}^+] = 5 \text{ mM}$. The other metabolic intermediates are set to zero.

production via acetaldehyde whereas it is modelled as one step in *L. lactis*.

Furthermore, the pyruvate-controlled export of lactate [Harold & Levin, 1974] is modelled explicitly in *S. pyogenes* but implicitly as one step with LDH in *L. lactis*.

We can also find differences in the phosphate uptake mechanisms of both LAB. While *S. pyogenes* possesses two phosphate transporters, an active and a passive system [Ferretti et al., 2001, Reizer & Saier, 1987], *L. lactis* is dependent on active phosphate uptake [Poolman et al., 1987].

Additionally, the regulation of some glycolytic enzymes differs between both LAB.

In *S. pyogenes*, sugar uptake is regulated by the availability of unphosphorylated HPr. Thus, it is activated by phosphate and inhibited by FBP and ATP. The model of *L. lactis* lacks the regulation by ATP. GAPDH is inhibited by NADH in *S. pyogenes* [Pancholi & Fischetti, 1992] what is not modelled for *L. lactis*. PYK is also regulated differently in both LAB. In *L. lactis*, it is activated by FBP and inhibited by P_i [Crow & Thomas, 1982] while it is activated by G6P in *S. pyogenes* [Yamada & Carlsson, 1975a]. Interestingly, LDH is activated by FBP and inhibited by P_i in *L. lactis* [van Niel et al., 2004] whereas it is regulated by NAD^+ (inhibition) and FBP and P_i (both activation) in *S. pyogenes*, which we determined experimentally (see Section 3.1.4). Since the mixed acid branch is modelled as one step in *L. lactis* no regulation of acetate kinase or alcohol dehydrogenase is included. These steps are regulated by FBP and ATP, respectively, in the glycolytic model of *S. pyogenes* [Lopez de Felipe & Gaudu, 2009, Palmfeldt et al., 2004].

3.3.3 Comparative systems biology of *L. lactis* and *S. pyogenes* glycolysis

As described above, we can identify differences between both LAB based on the model topology. In the following section the impact of these differences is explored computationally. As stated before (see Section 3.1.3), our glucose-pulse experiments in resting cells with varied extracellular P_i concentration (0, 10 and 50 mM) showed that the FBP levels in both LAB are strongly influenced by the extracellular phosphate concentration. This is reflected and reproduced by our kinetic models. The experiments were reproduced several times with exemplary simulations in Figure 3.2 and 3.7.

The rate of glucose uptake was also slightly altered by extracellular P_i in *L. lactis* and to a much larger extend in *S. pyogenes* with glucose uptake rates that were higher in *S. pyogenes* than in *L. lactis* (Figure 3.2A and 3.7A). Once again, our models reproduce this behaviour very well (see Figure 3.2B and 3.7B). As stated before, the glucose uptake rate in *S. pyogenes* does not simply correlate with the extracellular phosphate concentration but low extracellular phosphate concentrations (e.g. around 1 mM) decreased the glucose uptake slightly compared to no phosphate in the environment whereas higher phosphate concentrations increased the glucose uptake rate (see Figure 3.2A). Due to the fact that free phosphate has such

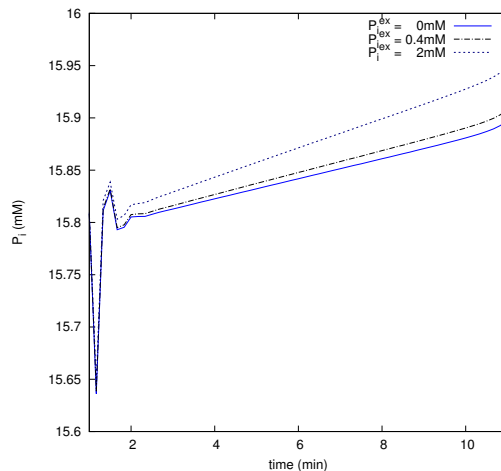


Figure 3.9: Model simulations of intracellular phosphate levels after a 20 mM glucose-pulse in *L. lactis* under 0, 0.4 and 2 mM extracellular phosphate. Due to the presence of an active phosphate transporter low extracellular phosphate concentrations does not result in phosphate efflux as was observed for *S. pyogenes*.

a pronounced effect on glycolysis and glucose uptake in *S. pyogenes*, we studied the behaviour of intracellular phosphate in our kinetic model of *L. lactis*. We observe that the intracellular phosphate level in *L. lactis* raises with the extracellular level (see Figure 3.9).

Our experimental glucose-pulse studies showed that extracellular glucose levels of 20 mM and higher are no obstruction for glucose uptake in *L. lactis* although uptake ceases in *S. pyogenes* as reported before (see Section 3.2.3). We therefore varied the amount of extracellular glucose in our simulation for *L. lactis*. If no or low external phosphate was present, the glucose uptake was completely stopped or severely inhibited at high glucose levels (the exact numerical value varied between the different fits). Often the actual value was much higher than in the experimental set-up (ranging between 60 - 4500 M). As observed in the model of *S. pyogenes*, this inhibition could be overcome by adding phosphate. However, this is not robust behaviour and we have not verified this observation experimentally.

Another interesting observation is the fact that *S. pyogenes* seems to be more efficient in converting glucose to ATP, exhibiting a higher uptake rate than *L. lactis*. The model shows this to be a direct consequence of the antagonistic effects of allosteric regulators (FBP, P_i , NAD^+ , $NADH$). PYK and especially LDH are differently regulated in *L. lactis* (see Figure 3.1) and *S. pyogenes* (see Figure 3.6).

In *L. lactis*, LDH is allosterically regulated by FBP and antagonistically by P_i , indicating that during glycolysis where P_i is low and FBP high, the flux is directed towards the less efficient lactate production. *S. pyogenes* LDH lacks this antagonistic regulation by FBP and P_i . Here, FBP and P_i both activate LDH whereas the product NAD^+ inhibits LDH. This indicates that LDH is running at a submaximal speed during glycolysis and more flux can be diverted to the more efficient mixed acid fermentation.

3.4 Oscillations caused by the stoichiometry

Biological systems such as biochemical networks can show complex behaviours like oscillations. In this context, mathematical models facilitate the understanding of the scope of behaviours that a biological system can exhibit. Glycolytic oscillations have been extensively studied in yeast experimentally and computationally. There are two hypotheses for the occurrence of oscillations. Firstly, oscillations might result from the allosteric regulation of PFK or, secondly, from the stoichiometry of glycolysis [Aon et al., 1991]. The use of PEP for sugar uptake [Aon et al., 1991] but also the autocatalytic feedback loop caused by ATP [Cortassa et al., 1991] are stoichiometric factors which are supposed to introduce oscillatory behaviour.

So far, *E. coli* is the only bacterium for which glycolytic oscillations were studied experimentally [Ju & Trivedi, 1998, Schaefer et al., 1999] and by simulations [Chassagnole et al., 2002, Ricci, 2000]. Both published models include the PTS system and regulation of PFK. Here again the occurrence of glycolytic oscillations is believed to be generated by the regulation of PFK [Ju & Trivedi, 1998] and it is proposed that ADP (and ATP) exerts a major influence on the dynamic behaviour through the regulation of the enzymes PFK and PYK [Ricci, 2000].

While developing the glycolytic model of *S. pyogenes* we observed that some models fitted to our glucose-pulse data show damped oscillations. Since the PFK is not regulated in our model this oscillations are caused by the stoichiometric nature of glycolysis. Since a living cell is mathematically described by a model in steady state we searched for oscillations in the glycolytic model for continuous cultured cells in glucose-limited CDM-LAB medium. In the following the method applied to determine the parameter set for which the model shows oscillations is described.

3.4.1 Finding oscillations in the model

Since oscillations in lactic acid bacteria are not observed experimentally so far, we studied the ability of the glycolytic model of *S. pyogenes* to show oscillations. Therefore, the model of continuous cultured cells was used and the rate of one oscillating species – we have chosen the FBP concentration – was maximised according to the following equation by scanning the model parameters

$$\frac{\text{FBP.Rate} + \text{FBP.Rate} \cdot \text{FBP.Conc}}{1 + \text{FBP.Conc} + (\text{FBP.Conc})^2}$$

whereas FBP.Rate is defined as the integral of the absolute concentration change given by

$$\text{FBP.Rate} = \begin{cases} \int \left| \frac{d}{dt}[\text{FBP}] \right| dt, & \text{if } t > 100, \\ 0, & \text{else} \end{cases}$$

and FBP.conc is the rate of change of the species concentration and is determined by an ODE. In order to prevent a large peak or a depleted FBP concentration as the optimisation result, a time delay of 100 s is introduced in FBP.Rate. After that initial transient phase a spontaneous depletion or accumulation is unlikely. The parameters were allowed to vary in the same physiologically ranges used for the parameter estimation (see Section 3.2.1).

3.4.2 Results

Applying the above described optimisation yields a model showing glycolytic oscillations. Exemplary the profiles of G6P, FBP, ATP, ADP, NADP⁺ and NADPH are shown in Figure 3.10. All metabolites show oscillatory behaviour whereas the amplitude changes between the species. The metabolites glucose, BPG, pyruvate, lactate, CoA, acetyl-CoA, the extracellular metabolites, NAD⁺ and NADH show small amplitudes which are hardly recognisable as compared to the other species such as FBP. Compared to literature data from *E. coli* [Schaefer et al., 1999], the simulated amplitudes are lower in *S. pyogenes*. However, in summary we have shown that, according to our analyses, the glycolytic system of *S. pyogenes* is able to show oscillatory behaviour and that these oscillations are caused by the stoichiometry since a PFK regulation is missing in this organism.

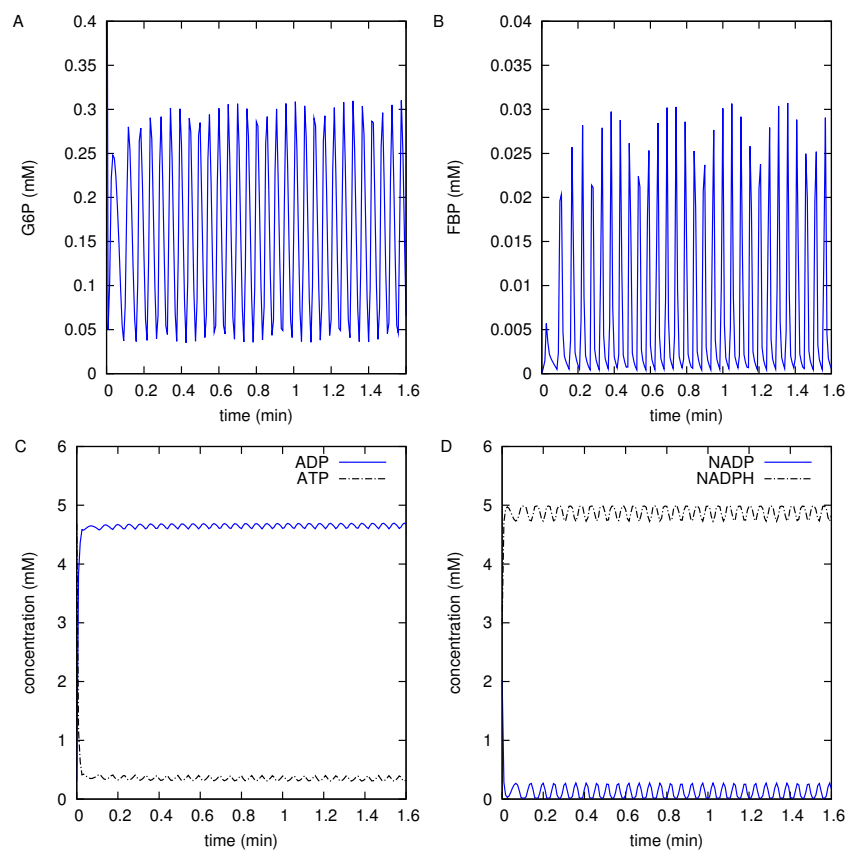


Figure 3.10: Model simulations of (A) G6P, (B) FBP, (C) ATP and ADP and (D) NADP⁺ and NADPH showing glycolytic oscillations.

3.5 Reconstruction of the metabolic network of *S. pyogenes*

Metabolic networks or genome-scale models comprise a list of associations between reactions, enzymes, substrates and products. They can be used among others to explore the response of an organism's metabolism to changes in its environment, gain insights into the genotype-phenotype relationship, identify the physiological states which are achievable by a given metabolic network or to analyse perturbations like gene deletions or drug applications [Durot et al., 2009].

The construction of a genome-scale model is based on the organism's genome and requires a large amount of knowledge about the organism's metabolism. However, the increasing availability of experimental high-throughput data like transcriptomics and proteomics have facilitated the knowledge about metabolic components and the interactions between them and, thus, the development of metabolic networks.

Here, we concentrated on all reactions essential for growth. To speed up the development of the first genome-scale model of *S. pyogenes* the semi-automatic AUTOGRAPH method [Notabaart et al., 2006] (see Section 2.3.1) was used. AUTOGRAPH was applied to the annotated genome sequence of *S. pyogenes* and already annotated reference models from *Bacillus subtilis*, *Escherichia coli*, *Lactobacillus plantarum* and *Lactococcus lactis*. This approach predicts the query gene's function based on orthology detection. This step was followed by a manual curation of the initial reconstruction which includes a consistency check and gap filling (see Sections 2.3.2, 3.5.3 and 3.5.4).

According to the experimental set-up, the growing cell is simulated by a model in steady state with continuous in- and outflow of CDM-LAB medium and metabolic products from the reaction vessel. Nutrients contained in the medium and accumulating products can be transported in and out of the cell, respectively. Consequently, two compartments are considered, i.e. the reaction vessel and the cytosol. So called exchange reactions in the model guarantee a constant supply of fresh medium and contained nutrients but also prevent product accumulation in the reaction vessel. These exchange reactions cover

- uptake reactions for the carbon source, here glucose, and amino acids,
- reversible transport reactions for vitamins, protons, water, carbon dioxide and

- efflux of metabolic products.

Required compounds can be taken up by the organism from the extracellular space by specific transport reactions and metabolic products can be transported into the reaction vessel via efflux reactions. Thus, exchange reactions are defined by the experimental set-up whereas transport reactions cover the abilities of the cultivated organism to take up or secrete substances. Since transporters in *S. pyogenes* are poorly studied, required reactions were incorporated based on experimental findings, e.g. measurement of pyruvate in the supernatant, or adopted from the *L. lactis* model.

3.5.1 Metabolic pathways incorporated in the model

All metabolic reactions essential for cell growth were reconstructed and included in the model to simulate cell growth. The model comprises

- production of DNA and RNA,
- protein biosynthesis,
- synthesis of membrane, cell wall and capsule components,
- primary and (poly)saccharide metabolism,
- amino acid metabolism,
- pathways for the synthesis of fatty acids and
- production of vitamins and cofactors.

An overview of the single pathways is given in Section 3.5.5.

3.5.2 Orthology detection

After the reconstructed pathways are defined we apply the AUTOGRAPH approach [Notebaart et al., 2006] to the genome sequence of *S. pyogenes* to predict the molecular function of genes involved in cell growth based on orthology determination.

The molecular properties of a protein or a gene are encoded by its sequence. Consequently, function prediction methods are often based on the determination of

homology to molecules of known function. Two genes are homologous if they are derived from a common ancestor. Homologous genes can be further classified in orthologs and paralogs. Orthologs are homologous genes in different species that were separated by a speciation event whereas paralogs were separated by a gene duplication event within one species. Hereby, one has to distinguish between out-paralogs which predate the species split and in-paralogs that arose after the species split and are orthologs by definition [Remm et al., 2001]. Orthologous genes will in most cases carry out identical functions, whereas paralogous genes will have similar but possibly distinct functions [Francke et al., 2005].

For function prediction the AUTOGRAPH method is applied to the annotated genome of *S. pyogenes* using four manually curated metabolic networks as input. AUTOGRAPH uses INPARANOID [Remm et al., 2001] for orthology detection. INPARANOID is based on the idea that two orthologous sequences score higher with each other than with any other sequence of the genome [Remm et al., 2001]. Thus, the algorithm searches for most similar sequences in the query and the reference organisms. The most similar sequences are called best hits. Confidence is gained by bi-directional best hits. We predicted 332 genes of *S. pyogenes* to be associated to 351 reactions and 223 non-gene associated reactions (see Appendix B). Non-gene associated reactions comprise both transport reactions and reactions which enzymes are not linked to a gene yet. For the reconstruction, we concentrated on genes encoding enzymes involved in cell growth.

The main problem arising by homology detection are incomplete Enzyme Commission (EC) numbers and annotation errors in databases [Notebaart et al., 2006]. By using manually curated reference networks, errors caused by misannotations can be corrected. However, a manual curation step is crucial.

3.5.3 Manual curation

Manual curation of an initial metabolic reconstruction is laborious and requires the combination of available information on protein sequence, phylogeny, gene context and co-occurrence but also high-throughput data [Francke et al., 2005]. Manual curation is required to

- couple the query gene to one of the orthologous genes from the reference networks and to define its function. Since homology based methods do not always

yield a correct coupling the correctness of the predicted orthologs has to be checked manually.

- trace back the experimental evidence since annotations in the database entries are often incorrect.
- add organism-specific reactions or pathways that are absent in the reference networks.
- check unspecific function identifiers like incomplete EC numbers manually. These can lead to false reaction associations.

For all genes of *S. pyogenes* the enzymes encoded by the best hit were transferred to the query gene. However, for some genes no ortholog was predicted. Missing gene-reaction associations can be divided into two groups. Either the missing association refers to

- organism-specific *S. pyogenes* genes that are not present in the reference organisms or
- predicted orthologs with a missing reaction association in the reference metabolic networks, e.g. due to a lack of experimental evidence [Notebaart et al., 2006].

For manual curation BRENDA [Schomburg et al., 2002], NCBI [Geer et al., 2010] and UniProt [UniProt Consortium, 2010] were used as sources of information on enzymes. Furthermore, KEGG [Kanehisa & Goto, 2000] as a collection of information on genes, enzymes, function and pathways and TransportDB [Ren et al., 2004] to find information on transport functions encoded by many already annotated genomes were used.

Since the reaction stoichiometry is crucial for most quantitative modelling approaches like FBA (see Section 2.3.3) all reactions added to the network has to be balanced with respect to oxygen atoms, hydrogen atoms and charges. Most reactions were copied from the networks of *L. plantarum* [Teusink et al., 2005] and *L. lactis* (unpublished results) which was kindly provided by Bas Teusink. However, some reactions had to be checked in databases. In most databases protons and cofactors are omitted and, thus, the reaction had to be balanced manually.

3.5.4 Filling gaps

Since the reconstruction is used to simulate growth and predict the flux through the network the cell is required to achieve a steady state with balanced production and consumption of all intermediate substrates and products. To ensure this, all reactions have to be balanced and essential pathways have to be complete.

The initial reconstruction had several gaps, e.g. in pathways required for cell wall assembly. In this context, a gap refers to a reaction in a pathway that is not coupled to a gene and prevents the production of one or more essential components of the biomass reaction. A gap in the initial metabolic network occurs because the particular gene is either not present in the organism's genome or it is present but could not be recovered by the automatic reconstruction process due to differences in the sequence. To fill these gaps a good knowledge about the organism's physiology is required.

The functionality of physiologically essential pathways in the reconstruction can be tested using FBA. Therefore, a demand reaction in the form of an artificial sink is added to the model and the flux through this step is maximised. A maximal flux of zero through the end-product demand reaction indicates an unbalanced pathway. To find the unbalanced step, the fluxes through the precursor producing reactions are considered. If the first reaction in the pathway with a maximal flux of zero is identified it has to be established if the flux is zero due to a missing substrate or cofactor or due to an accumulating product. If a substrate or cofactor is missing in most cases this problem is due to a missing reaction producing the species. If a product is accumulating a consuming reaction lacks in the model. To solve this problem a literature search or a search in KEGG [Kanehisa & Goto, 2000] was performed.

3.5.5 Characteristics of *S. pyogenes*

The manually curated metabolic reconstruction facilitates gaining insight into the metabolic capabilities of *S. pyogenes*. In the following paragraphs for all metabolic pathways incorporated in the genome-scale model the characteristics of *S. pyogenes* are described. A list with all compounds and reactions included in the model can be found in Appendix B.1 and B.2.

Production of DNA and RNA

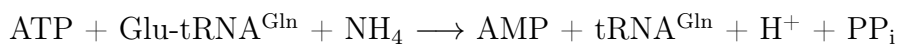
Nucleotides required for DNA and RNA production are synthesised in the pyrimidine and purine biosynthesis. Since DNA and RNA synthesis is conserved, all enzymes required for the synthesis of the according nucleotides are present. Like all other Gram-positive bacteria, *S. pyogenes* lacks the adenylate cyclase and, thus, no cyclic adenosine monophosphate (cAMP) is produced. cAMP is a second messenger which is involved, for example, in the control of the lac operon.

Protein biosynthesis

Protein biosynthesis is represented by the assembly of charged transfer RNAs (tRNA) in the model. tRNAs transport active amino acids to a growing polypeptide chain. The covalent linkage of amino acid to tRNA is catalysed by aminoacyl tRNA synthetases. All genes encoding the synthetase enzymes are included in the initial reconstruction except for the gene encoding a specific glutamyl-tRNA synthetase (tRNA^{Gln}). As in *L. plantarum* and *L. lactis*, no tRNA^{Glu} exists in *S. pyogenes*. Instead, tRNA^{Gln} can be loaded with glutamine and, additionally, with glutamate. The loading of tRNA^{Gln} with glutamine follows the reaction



and is catalysed by the glutamyl-tRNA^{Gln} synthetase whereas discharging



is carried out by glutamyl-tRNA synthetase.

Synthesis of membrane, cell wall and capsule components

Within the reconstructed network the synthesis of membrane, cell wall and capsule components is represented by the production of phospholipid, lipid II, peptidoglycan, lipoteichoic acid and the capsule polysaccharide.

The cell membrane separates the cytosol from the environment and consists of a phospholipid bilayer with integral proteins. Phospholipids contain a diglyceride, a phosphate group and a simple organic molecule which is lysine in *S. pyogenes*, yielding lysylphosphatidyl glycerol. Phospholipids determine the structure and flexibility of the cell membrane [Seltmann & Holst, 2002]. Two lysylphosphatidyl glycerol form

cardiolipin, another component of the cell membrane which is involved in osmotic adaption [Romantsov et al., 2009]. Phosphatidic acid, which is formed by the assembly of all products of the fatty acid metabolism, can also be converted into diacylglycerol which is required for LTA production. Since no information about phospholipid biosynthesis could be found in the literature, but the compounds produced in this pathway are essential for cell wall and LTA production, phospholipid biosynthesis is assumed to be present in *S. pyogenes*. Required enzymes are adopted from the *L. lactis* reconstruction.

The cell wall of Gram-positive organisms is composed of peptidoglycan. This macromolecule is made up of the repeating disaccharide N-acetylmuramic acid-(β 1-4)-N-acetylglucosamine (MurNAc-GlcNAc) whereby the MurNAc component is often linked to short peptides composed of L-alanine, D-iso-glucose, L-lysine and a D-alanine-D-alanine dipeptide [Swoboda et al., 2010]. In *S. pyogenes* this peptide chains are cross-linked via a dialanine bridge. The peptidoglycan synthesis starts with the production of UDP-MurNAc to which L-alanine, D-iso-glucose, L-lysine and the D-alanine-D-alanine dipeptide are linked. In the next step this UDP-MurNAc-pentapeptide is linked to a carrier molecule which is attached to the membrane. The linking of UDP-GlcNAc to the muramoyl moiety results in the formation of the lipid II precursor. By adding amino acids to lysine lipid II is further modified. Lipid II serves as the substrate for the assembly of peptidoglycan [Navarre & Schneewind, 1999].

Teichoic acids are a component of the cell wall or cell membrane of a wide range of Gram-positive bacteria [Knox & Wicken, 1973]. Since Group A teichoic acid is free of ribitol [Matsuno & Slade, 1970] and is present in the form of lipoteichoic acid in *S. pyogenes* [Slabyj & Panos, 1976], reactions including ribitol teichoic acid or WTA were removed from the model. In the model the only teichoic acid *S. pyogenes* produces is lipoteichoic acid with a chain length of 25 and with alanine and glucose substitutions. As indicated by experimental data [Slabyj & Panos, 1973], the formation of teichoic acid is independent of peptidoglycan synthesis.

S. pyogenes is covered by a capsule which is made of polysaccharide. The capsular polysaccharide is built-up of a polymer of hyaluronic acid (see Section 1.1.1). In the model, hyaluronic acid is omitted and the capsule is represented by the capsular polysaccharide which is composed of UDP-galactose, UDP-glucose and dTDP-6-deoxy-L-mannose.

Primary and (poly)saccharide metabolism

In the genome-scale model three pathways producing energy are included: glycolysis followed by pyruvate metabolism, pentose phosphate pathway and the citric acid cycle. The energy production in glycolysis is described in detail in Section 3.2.1. All glycolytic enzymes are present in *S. pyogenes* and were included in the initial reconstruction.

The PPP is divided into two parts. In the first or oxidative part NADPH is generated whereas in the non-oxidative phase pentoses are synthesised. In *S. pyogenes* many genes encoding enzymes of the oxidative part of the PPP are missing.

Furthermore, in *S. pyogenes* many enzymes of the citric acid cycle, also called tricarboxylic acid (TCA) cycle, are missing. This pathway is part of the cellular respiration and converts carbohydrates, fats and proteins into carbon dioxide and water to generate a form of usable energy. The complete respiration pathway includes glycolysis and pyruvate oxidation followed by TCA and oxidative phosphorylation. Within this pathway, precursors for many compounds including amino acids are synthesised. Like all other Gram-positive bacteria, *S. pyogenes* has an incomplete TCA cycle which means that no succinate or succinyl-CoA is produced. Therefore, succinyl-CoA is substituted by acetyl-CoA in the model.

S. pyogenes can grow on several carbon sources. In the model the disaccharides trehalose, sucrose, maltose and lactose and the monosaccharide mannose are included. All saccharides are converted into G6P or F6P and further metabolised in glycolysis.

Glycogen is a polysaccharide that is composed of a branched chain of glucose residues and serves as energy storage. *S. pyogenes* lacks the enzyme synthesising glycogen but possesses the enzyme degrading it. So far, no energy storage mechanism is detected in *S. pyogenes*.

Biosynthesis of non-essential amino acids

From literature it is known that *S. pyogenes* is auxotroph for many amino acids [Slade et al., 1951]. This fact is confirmed by the incomplete reconstructed amino acid synthesis pathways. However, *S. pyogenes* can synthesise some amino acids itself. According to the reactions included in the model, proline can be made of glutamate which can be mutual converted with glutamine. Cysteine can be transformed

into serine which is interconvertible with glycine. The latter one is mutual convertible with threonine. Furthermore, aspartate and asparagine can be transformed into each other.

Fatty acid synthesis

Fatty acids are an important compound of the cell membrane since phospholipids, cardiolipin and LTA are made up of fatty acids. All genes encoding enzymes for the fatty acid biosynthesis are present in *S. pyogenes* except for the gene encoding the cyclopropane fatty acid synthetase (CFAS). This enzyme catalyses the conversion of phospholipid olefinic fatty acid into phospholipid cyclopropane fatty acid. This product, like all other fatty acid synthesis products, is required for phospholipid biosynthesis. CFAS is predicted to be present in *L. lactis*, *L. plantarum*, *S. thermophilus* and *S. agalactiae* but for none of the genes a gene from *S. pyogenes* with a high similarity could be identified based on BLAST [UniProt Consortium, 2010, Geer et al., 2010]. Nevertheless, this enzyme is included in the model since it is required to simulate cell growth.

Production of vitamins and cofactors

Cofactors included in the model comprise NAD(P)⁺, vitamin B₆, thioredoxin, biotin, coenzyme A, riboflavin, folate, molybdopterin and glutathion.

NAD(P)⁺ takes part in many redox reactions. Its production starts with the uptake of nicotinate, also known as vitamin B₃. All enzymes required for the conversion of nicotinate into NAD(P)⁺ are present in *S. pyogenes*.

Pyridoxamine and pyridoxal are precursors of pyridoxal 5'-phosphate, the activated form of vitamin B₆. Pyridoxamine is taken up and converted into pyridoxal 5'-phosphate via pyridoxal. One of the enzymes involved in this conversion is alanine transaminase. For *S. pyogenes*, no information about the presence of this enzyme could be found. However, genes encoding this enzyme are predicted for several strains of *S. pneumoniae* and for *L. lactis*. A BLAST search [Geer et al., 2010] with the *S. pneumoniae* alanine transaminase yielded genes in several strains of *S. pyogenes* having identities of 83% with the *S. pneumoniae* alanine transaminase. The related genes in *S. pyogenes* are annotated to encode the aspartate transaminase. Since annotations are often incorrect and the related genes have a high identity, alanine transaminase is included in the model.

Biotin is involved in fatty acid synthesis and amino acid metabolism. It is one of the essential vitamins that are taken up from the medium, *S. pyogenes* cannot produce it *de novo*.

Thioredoxins are small redox proteins that are reduced by the NADPH-dependent thioredoxin reductase. The reduced form of thioredoxin acts as electron acceptor to ribonucleoside-diphosphate and -triphosphate reductases.

Coenzyme A (CoA) participates in the oxidation of pyruvate and fatty acids. All enzymes catalysing CoA production from pantothenate are annotated. Pantothenate is an essential vitamin and is supplied with CDM-LAB medium.

Since many thiamin synthesis enzymes are missing in *S. pyogenes* we hypothesise that thiamin is essential. Since thiamin is one of the compounds of CDM-LAB medium, it is taken up from the medium.

Riboflavin is also taken up from the medium and is converted into flavin adenine dinucleotide, a redox cofactor. The flavin reductase lacks in *S. pyogenes* and therefore no reduced riboflavin is produced.

Furthermore, *S. pyogenes* cannot produce molybdopterin which serves as a cofactor for some enzymes.

Most enzymes participating in the folate and C1-THF pool synthesis are present. The enzyme catalysing the transformation of dihydropteridine triphosphate into 7,8-dihydropteridine, which is one of the first steps, is missing. In *L. plantarum*, two enzymes, dihydroneopterin triphosphate pyrophosphatase (DNTPPA) and dihydroneopterin monophosphate dephosphorylase (DNMPPA), are catalysing this conversion. DNMPPA is non-gene associated and for DNTPPA an EC number lacks in the *L. plantarum* model. No UniProt [UniProt Consortium, 2010] entry for DNTPPA in *L. plantarum* was found. As a consequence, no BLAST search of DNTPPA against the genome of *S. pyogenes* could be performed. In *L. lactis* the transformation of dihydropteridine triphosphate into 7,8-dihydropteridine is catalysed by an enzyme which is not present in the provided reconstructed network. A KEGG [Kanehisa & Goto, 2000] search yielded that this step can be catalysed by the membrane-bound alkaline phosphatase (EC 3.1.3.1). This enzyme is not listed for any lactococcal species but for *Streptococcus dysgalactiae* subsp. *equisimilis* (strain GGS_124) in UniProt. A BLAST search of this enzyme against the *S. pyogenes* genome results in genes having a very low score. It is likely that *S. pyogenes* lacks a membrane-bound alkaline phosphatase. However, since all other

enzymes are present in the pathway, it is likely that *S. pyogenes* possesses a mechanism converting dihydropteridine triphosphate into 7,8-dihydropteridine. Therefore, the transformation was adopted from the model of *L. plantarum*. Furthermore, the NADPH-dependent enzyme methylenetetrahydrofolate reductase catalysing the conversion of 5,10-methylenetetrahydrofolate into 5-methyltetrahydrofolate, i.e. the active form of folate, is missing in *S. pyogenes*.

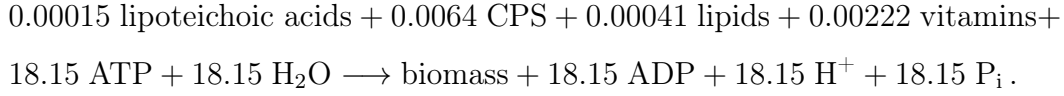
In most Gram-positive bacteria glutathione is not found but some bacteria like *S. mutans* import it [Sherrill & Fahey, 1998]. However, some bacteria are able to synthesise glutathione, e.g. *L. plantarum*. *S. pyogenes* possesses the enzymes glutathione reductase and glutathione peroxidase which enables it to convert glutathione into glutathione disulfide and back to glutathione with concomitant reduction of NADPH to NADP⁺. Since no information about glutathione synthase in *S. pyogenes* could be found, a BLAST search against the genome was performed which indicated that this enzyme is not present in *S. pyogenes*. Since glutathione is not present in CDM-LAB medium, no exchange and transport reaction is included in the model. Glutathione is not essential for growth of *S. pyogenes* in CDM-LAB medium.

Composition of the biomass reaction used in the model

In order to reduce the number of possible solutions and obtain a physiologically solution of the reconstructed metabolic network, an objective function is specified. Since the model is used to simulate growth, the flux towards the formation of biomass is maximised. The biomass reaction comprises biomass components and growth-associated ATP consumption. Among the biomass reactants are common biomass components included in the biomass equation for all organisms, e.g. nucleotides for DNA and RNA and amino acids for protein biosynthesis, but also reactants which are specific for the organism like cell wall components.

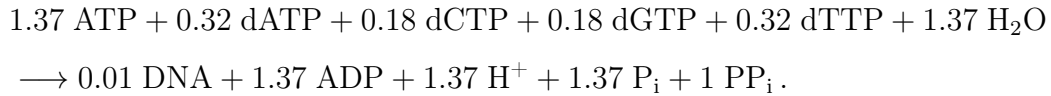
Since no information about the biomass composition of *S. pyogenes* could be found in literature, the biomass reaction of *L. lactis* is used. Biomass components that are explicitly taken into account in this equation are DNA, RNA, protein, cell wall components, membrane constituents and vitamins. The *L. lactis* specific biomass production equation is given by

$$0.00074 \text{ DNA} + 0.00329 \text{ RNA} + 0.004201 \text{ protein} + 0.1192 \text{ peptidoglycans} +$$

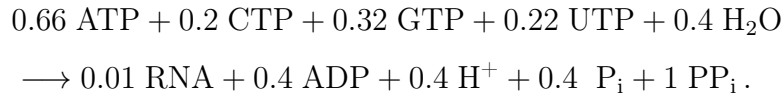


The stoichiometric coefficients in mmol per gDW indicate the relative proportion of each component in an organism's biomass. The individual composition of the biomass components was maintained at a fixed stoichiometry and, for simplicity, is independent of the growth rate [Oliveira et al., 2005]. The coefficients are based on data available from the literature (see Additional file 2 from [Oliveira et al., 2005]). The growth-associated ATP maintenance is set to 18.15 mmol per gDW per hour as for *L. lactis*. In the following the biomass components are described.

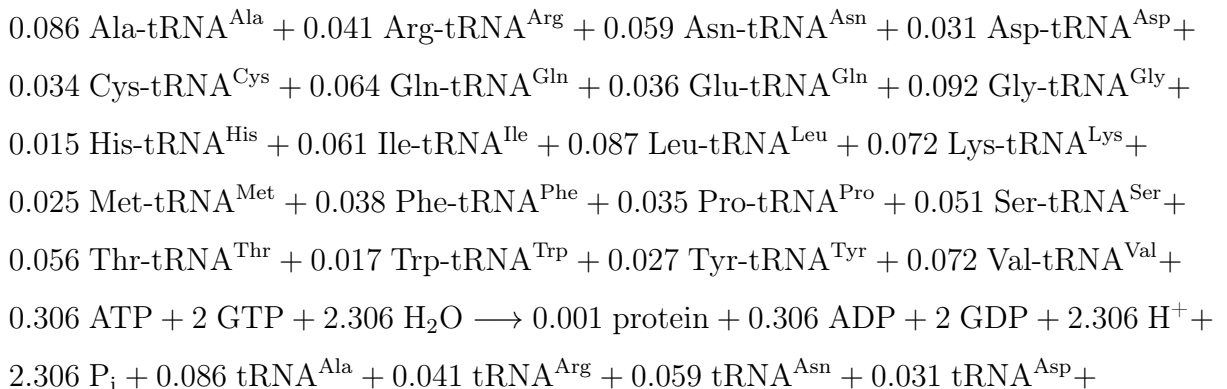
DNA assembly is modelled as the hydrolysis of the four nucleotides deoxyadenosine triphosphate (dATP), deoxycytidine triphosphate (dCTP), deoxyguanosine triphosphate (dGTP) and deoxythymidine triphosphate (dTTP) with concomitant energy consumption summarised in the following equation



Analogously to DNA assembly, RNA synthesis is modelled by the hydrolysis of the four nucleotides adenosine triphosphate (ATP), cytidine triphosphate (CTP), guanosine triphosphate (GTP) and uridine triphosphate (UTP) by



In general, proteins are assembled from amino acids using information encoded in genes. Within the model, protein biosynthesis is modelled by the assembly of loaded transfer RNAs (tRNAs) concomitant with ATP and GTP consumption by



$$0.034 \text{ tRNA}^{\text{Cys}} + 0.064 \text{ tRNA}^{\text{Gln}} + 0.036 \text{ tRNA}^{\text{Glu}} + 0.092 \text{ tRNA}^{\text{Gly}} + 0.015 \text{ tRNA}^{\text{His}} + \\ 0.061 \text{ tRNA}^{\text{Ile}} + 0.087 \text{ tRNA}^{\text{Leu}} + 0.072 \text{ tRNA}^{\text{Lys}} + 0.025 \text{ tRNA}^{\text{Met}} + 0.038 \text{ tRNA}^{\text{Phe}} + \\ 0.035 \text{ tRNA}^{\text{Pro}} + 0.051 \text{ tRNA}^{\text{Ser}} + 0.056 \text{ tRNA}^{\text{Thr}} + 0.017 \text{ tRNA}^{\text{Trp}} + 0.027 \text{ tRNA}^{\text{Tyr}} + \\ 0.072 \text{ tRNA}^{\text{Val}}$$

whereas the superscript defines the specificity and the prefix indicates charging of the tRNA.

The cell wall of Gram-positive organisms is a thick peptidoglycan layer to which molecules like proteins and polysaccharides are anchored [Swoboda et al., 2010].

One of the major surface proteins are teichoic acids which are specific components of the cell wall of Gram-positive bacteria. *S. pyogenes* possesses only LTA which may be involved in the control of cell shape, autolytic enzyme activity and maintenance of cation homeostasis [Kristian et al., 2005].

S. pyogenes is covered by a capsule which is made of polysaccharide and is denoted in the model by CPS. The capsule belongs to the virulence factors and masks the pathogen's antigens [Todar, 2011].

In the model, cellular lipids of lactobacilli are mainly composed of five types of phospholipids: 0.000061 mmol gDW⁻¹ phosphatidylglycerol, 0.000013 mmol gDW⁻¹ 1-lysyl phosphatidylglycerol, 0.000138 mmol gDW⁻¹ cardiolipin, 0.000096 mmol gDW⁻¹ 1,2-diacylglycerol and 0.000013 mmol gDW⁻¹ 1,2-monoacylglycerol. The acyl chain is composed of seven different fatty acids: tetradecanoic acid (14:0), dodecanoic acid (12:0), hexadecanoic acid (16:0), hexadecanoic acid (16:1), octodecanoic acid (18:0), octodecanoic acid (18:1) and cyclopropanoyl octadecanoic acid.

As mentioned before, lactic acid bacteria are auxotroph for many vitamins. To model the vitamin and vitamin-derived cofactor requirements these components were included in the biomass equation. Vitamins and cofactors included in the biomass equation were 0.00001 mmol gDW⁻¹ tetrahydrofolate, 0.00001 mmol gDW⁻¹ thiamin diphosphate, 0.0002 mmol gDW⁻¹ CoA, 0.002 mmol gDW⁻¹ NAD⁺.

3.5.6 Results from flux balance analysis

After checking the consistency of the reconstructed metabolic network, the model is validated and the metabolic capabilities of *S. pyogenes* are explored. One approach to analyse metabolic networks is FBA (see Section 2.3.3). Therefore, exchange and transport reactions are restricted with experimental measured values taking a

measurement error into account and the growth rate is optimised. In continuous cultures the time-dependent population change is given by

$$\frac{db}{dt} = \alpha \cdot b - D \cdot b,$$

where b is the bacterial dry weight per litre, α is the growth rate per hour and D is the dilution rate (h^{-1}). Under steady state conditions the time-dependent population change equals zero and as a consequence equals the growth rate the dilution rate [Davies et al., 1965]. Therefore, the predicted growth rate is compared to the measured value and – if predicted and measured value differ – the metabolic model can be corrected accordingly. After the model resembles the experimental data, FBA can be used among others to investigate the organism’s behaviour to environmental perturbations.

Incorporation of measured ATP synthesis rates

Before the model can be used to predict growth rates, the energy required for growth and maintenance has to be specified [Teusink et al., 2006]. The amount of ATP required for biomass formation is determined in the biomass equation (see Section 3.5.5). The maintenance-associated ATP consumption coefficient was estimated from measured ATP production rates at different growth rates (see Section 3.1.6). In the model, setting the ATP maintenance rate to 1.35 at pH 6.5 and to 0.8 at pH 7.5 accurately predicts the growth rate. These values are in accordance with experimentally determined ATP maintenance rates (see Table 3.12).

Applying constraints to measured fluxes

S. pyogenes M49 wild-type and its *ldh*-negative strain were grown in a bioreactor at two dilution rates and two pH values and the concentrations of amino acids and products were measured (see Section 3.1.2). In order to apply FBA, these concentrations are transformed into fluxes of utilisation given in $\text{mmol h}^{-1} \text{gDW}^{-1}$. These fluxes were calculated as

$$q_i = D \cdot \frac{[M]_{\text{supernatant}} - [M]_{\text{CDM-LAB}}}{[\text{biomass}]}$$

where $[M]$ is the concentration of metabolite M in mmol per litre , $[\text{biomass}]$ is the measured biomass concentration in gDW per litre and D is the dilution rate

per hour. These fluxes are used to restrict the reaction rates in the genome-scale model (see Section 2.3.3). Since the product concentrations are measured twice but amino acid levels are determined once, the upper and lower boundaries are given by the measured fluxes taking a measurement error of 20% into account. If one has performed three or more measurements the mean value plus or minus the standard deviation would be used to limit the fluxes.

Some metabolites can be exchanged with the environment and are transported in or out of the system through specific exchange reactions that can have lower and upper bounds on their throughput. We restrict the following reactions

- glucose uptake,
- transport of amino acids and nucleotides which are taken up but not excreted,
- transport of precursors for vitamins and cofactors,
- citrate is taken up but not produced since the TCA cycle is incomplete in *S. pyogenes*,
- water, CO₂ and protons are transported in and out of the cells,
- transport of metabolic byproducts like NH₄, NO₂, NO₃, SO₄, spermidine and glycolate, and
- glycolytic end-products like lactate, formate and so on

according to measured values taking the measurement error into account.

Applying all calculated upper and lower boundaries results in an infeasible problem meaning that no solution exists which satisfies all the constraints. In order to solve this problem and to find an optimal solution the constraints were widened, e.g. from -1 to 0 for amino acid or from 0 to 10 for end-product exchange reactions. After simulating the model it was checked which exchange reactions have their simulated value falling within the specified ranges. Fixing the bounds of those reactions by taking the measurement error into account results in a feasible problem and an optimal solution. The remaining reactions would give infeasible solutions if their bounds would be fixed with experimentally measured values and have to be further explored either experimentally or in the model. This strategy leads to the lists of constraints for *S. pyogenes* wild-type and *ldh*-deletion strain given in Appendix B.3. The predicted growth rates are shown in Table 3.18.

Simulation results

For both strains, *S. pyogenes* wild-type and its *ldh*-deletion, the model is able to predict the accurate growth rate of approximately 0.05 at pH 6.5 and about 0.15 at both pHs, 6.5 and 7.5. The model fails to predict the growth rate of 0.05 at pH 7.5 for the wild-type and the knock-out mutant.

Product fluxes. Table B.8 and B.9 summarise the uptake or production fluxes at both pHs, 6.5 and 7.5, for the wild-type and the *ldh*-knock-out strain, respectively. The flux distribution for the *ldh*-negative mutant was simulated by setting the flux through L-LDH to zero.

The model predicts that acetate, ethanol and formate production increases with the dilution rate. Although acetoin production is measured in the *ldh*-negative mutant strain at both pHs and both dilution rates, the flux through acetoin producing reactions is zero under all simulated conditions. The model further predicts no uptake or production of biotin, pyridoxamine, pyridoxine and riboflavin and no production of NO₂, NO₃, SO₄ and spermidine under all simulated conditions. Furthermore, xanthine is not taken up. The *ldh*-knock-out strain shows an increased flux through D-LDH compared to the wild-type. Under all conditions, the model predicts an uptake of phosphate.

Amino acid fluxes. According to the model simulations the amino acid uptake fluxes decrease with increasing dilution rate in the wild-type. Thus, a higher amount of amino acids is taken up for higher dilution rates. The *ldh*-deletion strain does

Table 3.18: Predicted growth rates of *S. pyogenes* wild-type and its *ldh*-deletion at two pHs and two dilution rates (D, h⁻¹) during continuous cultivation in glucose-limited CDM-LAB medium. Values indicate mmol/gDW.

Experiment		Simulation	
pH	D	M49	M49 Δ <i>ldh</i>
6.5	0.05	0.0506	0.0656
	0.15	0.1577	0.1330
7.5	0.05	0.1443	0.1637
	0.15	0.1505	0.1721

not show this trend; the fluxes are comparable for both measured dilution rates in the wild-type and the mutant strain. Cysteine is not taken up under all simulated conditions.

Growth on different carbon sources

Biolog Phenotype Microarrays were applied to test the ability of *S. pyogenes* wild-type and *ldh*-knock-out mutant to utilise different substrates. From the 20 carbon sources *S. pyogenes* was able to grow on (see Table 3.11) trehalose, sucrose, maltose and mannose were already included in the model. In a first step, exchange reactions were added for all of these sugars. In the following the degradation of these sugars is described.

Trehalose is a disaccharide consisting of two glucose molecules which are linked in a $\beta(1\rightarrow1)$ bond. Trehalose is transported into the cell via a specific PTS system yielding trehalose-6-phosphate. Trehalose-6-phosphate is hydrolysed into glucose and G6P. All required enzymes for uptake and conversion of trehalose were present in the initial reconstruction.

Sucrose is a disaccharide composed of fructose and glucose linked via an α, β -1,2-glycolytic bond. Sucrose is taken up via a specific PTS uptake system and the resulting sucrose-6-phosphate is dephosphorylated by sucrose-6-phosphate hydrolase and subsequently hydrolysed to fructose and glucose. In the initial reconstruction sucrose-6-phosphate hydrolase was missing. We included this enzyme based on homology studies [UniProt Consortium, 2010].

Maltose is a disaccharide consisting of two glucose molecules which are linked by an $\alpha(1\rightarrow4)$ bond. Contrary to all previously mentioned disaccharides it is taken up by an ATP-dependent system. Intracellular maltose is broken down into glucose and β -D-glucose-1-phosphate (β -G1P) by a phosphorylase. This enzyme is predicted to be present in *L. lactis* and *E. faecalis* but no information about a gene encoding it in *S. pyogenes* could be found [UniProt Consortium, 2010]. The enzyme β -phosphoglucomutase catalyses the mutual conversion of β -G1P into β -G6P which is further transformed into G6P. This enzyme is predicted to be present in other streptococcal serotypes and a BLAST search [Geer et al., 2010] revealed a similarity of 100% to one gene from the here studied serotype M49.

Mannose is an epimer of glucose taken up via a PTS system and subsequently rearranged to F6P. The mannose PTS as well as the mannose-6-phosphate isomerase

were included in the initial reconstruction.

Since the remaining 16 sugars are neither present in the model of *L. lactis* nor in the model of *L. plantarum* and *S. pyogenes* showed lower growth on these sugars compared to the included ones, we decided to leave these sugars out and include them perhaps at a later stage.

In accordance with experimental data the model predicts that *S. pyogenes* wild-type and *ldh*-deletion strain can grow on trehalose, sucrose, maltose and mannose. The uptake fluxes were constrained between $[-2.4957, -2.4929]$ in the case of the monosachharides glucose and mannose and between $[-1.29735, -1.24645]$ for the disaccharides trehalose, sucrose and maltose at pH 6.5 and $D = 0.05$. Growth on the mentioned sugars was found to be the same as on glucose (data not shown).

Modelling amino acid leave-outs

For amino acid leave-out experiments *S. pyogenes* was grown in CDM-LAB medium lacking specified amino acids. The optical density was monitored at 600 nm for 12 h (see Section 2.1.9). In the model the leave-out of amino acids was realised by setting the uptake fluxes of the corresponding compounds to zero. The simulated growth rates under the different conditions are given in Table 3.19. Although the experimental data was measured under batch conditions we can compare it to the simulated steady state data at pH 6.5 and $D = 0.05 \text{ h}^{-1}$ qualitatively.

Table 3.19: Simulated growth rates (h^{-1}) of *S. pyogenes* wild-type grown in full CDM-LAB medium and medium without the indicated amino acids at $D = 0.05 \text{ h}^{-1}$ and pH 6.5.

CDM-LAB medium	Simulated growth rate
Full	0.0506
w/o Ala	0
w/o Arg	0
w/o Asn	0.0504
w/o Asn, Asp	0
w/o Asp	0.0506
w/o Cyn	0.0506
w/o Cyn, Cys	0
w/o Cys	0.0506

Table 3.19 – continued from previous page

CDM-LAB medium	Simulated growth rate
w/o Cys, Gly	0.0524
w/o Cys, Ser	0.0506
w/o Cys, Thr	0.0521
w/o Gln	0.0506
w/o Gln, Glu	0
w/o Gln, Thr	0.0521
w/o Glu	0.0505
w/o Gly	0.0524
w/o Gly, Ser	0.0480
w/o Gly, Ser, Thr	0
w/o Gly, Thr	0
w/o His	0
w/o Ile	0
w/o Leu	0
w/o Lys	0
w/o Met	0
w/o Met, Ser	0
w/o Phe	0
w/o Pro	0.0504
w/o Ser	0.0506
w/o Ser, Thr	0.0497
w/o Thr	0.0521
w/o Trp	0
w/o Tyr	0
w/o Val	0

In accordance to experimental data (see Section 3.1.7), the model predicts no growth in the absence of Arg, Gln and Glu, Gly and Ser and Thr, Gly and Thr, His, Ile, Leu, Lys, Met, Met and Ser, Phe, Trp, Tyr and Val. Furthermore, simulation and experimental data agree that *S. pyogenes* can grow in the absence of Asp, Asn, Cyn, Cys, Glu and Pro. The simulated and measured growth rate give contrary results for the omission of Ala, Cys and Cyn, Cys and Gly, Cys and Ser, Cys and

Thr, Gln, Gln and Thr, Gly, Gly and Ser, Ser, Ser and Thr, and Thr alone.

Predictions from the model

The constructed genome-scale model of *S. pyogenes* is used to explore its metabolism and the response to environmental perturbations in more detail. Since this is recent work and we are in the stage of model validation, we present preliminary results which will be studied further in SysMO-LAB II.

Our first experimental data (see Section 3.1.7, Table 3.13, Experiment 1) show that *S. pyogenes* is able to grow in the absence of Cys or Cyn whereas the omission of both, Cys and Cyn, results in complete loss of growth. This finding indicates that these amino acids are interconvertible. We could not find any information about the uptake or metabolism of cystine in *S. pyogenes* in literature. Based on an extensive literature search and BLAST [Geer et al., 2010] we propose that Cyn is taken up via an ATP-dependent cystine transporter. A BLAST search for a L-cystine import ATP-binding protein of *Streptococcus pneumoniae* (strain Hungary19A-6) against the *S. pyogenes* genome yields a hit with an amino acid ABC transporter having an identity of 80%. Cystine is converted into thiocysteine by cystathionine γ -lyase. Studies on *Lactobacillus fermentum DT41* revealed that this enzyme has a wide substrate specificity whereby cystine was the best substrate [Smacchi & Gobetti, 1998]. Thiocysteine is non-enzymatically degraded to Cys and H₂S [Łowicka & Bełtowski, 2007]. Based on these experimental results we incorporated the described transformation of cystine into cysteine. Surprisingly, the following experiment suggests that *S. pyogenes* can grow in the absence of cystine and cysteine. Since these data contradicts our first measurements we will perform another independent experiment before changing the *in silico* model.

The model can also be used to determine essential amino acids for growth of *S. pyogenes* in CDM-LAB medium by omission of each amino acid at a time. A list defining essential and non-essential amino acids is given in Table 3.20. Referring to the literature [Slade et al., 1951], 15 amino acids are essential for growth of *S. pyogenes*. The model predicts 12 amino acids to be essential, 11 of them are identical with literature data. Thereby, we define a proteinogenic amino acid that cannot be produced from another standard one as essential. Although Cys can be made of Cyn in the model we listed it as essential amino acid since Cyn is non-proteinogenic. Referring to the model predictions but contrary to the literature,

cystine is not essential for growth of *S. pyogenes* in CDM-LAB. Surprisingly, in the literature serine, glycine and threonine are listed as essential amino acids although they are interconvertible according to the model. The corresponding reactions were incorporated in the model based on orthology detection. Experimentally we validated that Arg, His, Ile, Leu, Lys, Met, Phe, Trp, Tyr and Val are essential amino acids whereas the model and the measurements give contrary results with respect to Ala, Glu, Gly, Thr and Ser. Discrepancies between experimental and literature data [Slade et al., 1951] concern Cys, Glu and Ser.

Additionally to essential amino acids, the minimal amino acid requirement was determined. Adding the essential amino acids was not found to result in growth. Growth occurs if Asn (or Asp), Gln (or Glu) and Gly (or Thr) can be taken up in the presence of the essential amino acids. Therefore, glucose, Ala, Arg, Asn (or Asp),

Table 3.20: Essential amino acids for growth of *S. pyogenes* in CDM-LAB medium based on simulations compared to literature data [Slade et al., 1951]. Referring to the literature, 15 amino acids are essential for growth of *S. pyogenes* while the model predicts 12 amino acids to be essential, 11 of them are identical with literature data.

Model predictions	Literature data
Arginine	Arginine
Cysteine	Cystine
Histidine	Histidine
Isoleucine	Isoleucine
Leucine	Leucine
Lysine	Lysine
Methionine	Methionine
Phenylalanine	Phenylalanine
Tryptophan	Tryptophan
Tyrosine	Tyrosine
Valine	Valine
Alanine	Glycine
	Proline
	Serine
	Threonine

Cys, Gln (or Glu), Gly (or Thr), His, Ile, Leu, Lys, Met, Phe, Trp, Tyr and Val were found to be the minimal required medium for growth of *S. pyogenes*. Growth in the minimal media is 8.54% lower as compared to rich media.

3.5.7 Topological comparison with *L. lactis* and *L. plantarum*

Compared on the sequence level, *S. pyogenes* is more similar to *L. lactis* than to any remaining reference organism. Thus, many reactions could be copied from the metabolic network of *L. lactis*. However, there are some differences on the enzymatic level. In the following a short and preliminary overview over the differences between the whole cell metabolism of *S. pyogenes*, *L. lactis* and *L. plantarum* is given. This will be further studied in SysMO-LAB II. The differences are based on the topology of the models.

Since DNA and RNA synthesis are conserved, there are no significant differences in purine and pyrimidine metabolism in *S. pyogenes*, *L. lactis* and *L. plantarum*.

The cell wall composition differs among the three organisms. Like in *L. lactis*, in *S. pyogenes* the peptide chains of peptidoglycan are cross-linked by dialanine bridges whereas they are linked by D-lactate in *L. plantarum*. The latter organism produces wall and lipoteichoic acids whereas *L. lactis* and *S. pyogenes* possess only lipoteichoic acids. Neither *L. lactis* nor *S. pyogenes* produce ribitol-containing teichoic acids whereas *L. plantarum* does. In *L. plantarum* and *S. pyogenes* two forms of lipoteichoic acids are present, i.e. LTA with alanine substitutions and with glucose residues. *L. lactis* produces LTA with alanine substitutions as well but also LTA with galactose residues.

The lipid II and fatty acid synthesis is similar in all three organisms but they show differences in the phospholipid biosynthesis. *L. lactis* and *S. pyogenes* produce the LTA precursor in that pathway whereas *L. plantarum* produces the required diacylglycerol compounds within the teichoic acid synthesis.

L. plantarum and *L. lactis* use glycogen as energy storage while *S. pyogenes* probably lacks the enzyme synthesising glycogen. Furthermore, *L. plantarum* and *L. lactis* have an almost complete pentose phosphate pathway while in *S. pyogenes* the oxidative phase is missing. Instead, *S. pyogenes* possesses GAPN which is again lacking in *L. plantarum* and *L. lactis*. Like all other Gram-positive bacteria, *S. pyogenes* and *L. lactis* have an incomplete TCA cycle while *L. plantarum* can run this cycle.

We can also find differences in the amino acid metabolism. Again, there is a clear hierarchy concerning the present enzymes. *L. plantarum* has a more complete amino acid biosynthesis pathway than *L.lactis*. *S. pyogenes* lacks more genes encoding enzymes involved in this pathway compared to *L. lactis*. For *L. lactis*, the leave-out of arginine, methionine and valine was found to prevent *in silico* growth [Oliveira et al., 2005], whereas we identified twelve amino acids as being essential for *S. pyogenes*.

L. plantarum is able to synthesise thiamin, molybdopterin and glutathion whereas both, *S. pyogenes* and *L. lactis*, lack the genes for molybdopterin and glutathion production. Furthermore, *S. pyogenes* relies on thiamin supply.

Compared on the enzyme level, *L. plantarum* has a more complex metabolic pathway than *L. lactis*. Compared to *L. plantarum* and *L. lactis*, the model of *S. pyogenes* covers less reactions which indicates more complex requirements and a simpler metabolism.

Chapter 4

Discussion

4.1	Kinetic model	112
4.2	Comparison to <i>L. lactis</i>	121
4.3	Genome-scale model	124
4.4	Discussion of thesis goals	132

4.1 Kinetic model

We have developed a kinetic model of *S. pyogenes* energy metabolism (see Section 3.2.1) which is able to capture dynamic profiles of intracellular metabolites after glucose-pulse experiments (see Figure 3.2) and compared this to a related lactic acid bacteria, i.e. the well-studied *L. lactis* (see Section 3.3.1). *S. pyogenes* derives energy from fermentation and, thus, the developed kinetic model covers glucose uptake, glycolysis and pyruvate metabolism. Since the sum of measured fermentation products equals approximately the supplied glucose concentration (see Section 2.1.4), side-pathways such as the pentose phosphate pathway can be neglected. This fact also points out that anabolic precursors are imported from the medium and only a minor fraction is synthesised *de novo* from glucose. Due to its role as human pathogen the investigation of *S. pyogenes* metabolism can help to identify possible drug targets and facilitate the development of specific antibiotics.

4.1.1 Model set-up, topology and regulation

Mathematically the model is represented by a set of ODEs since we assume that all metabolites are uniformly distributed in the cell and spatial effects can be neglected. We decided to use COPASI [Hoops et al., 2006] as modelling framework since it is free for academic user, available for the usual platforms and includes algorithms for simulation as well as for optimisation. Since the model is deterministic, LSODA was used for time-course simulation (see Section 2.2.4). The other algorithms implemented in COPASI are either stochastic or hybrid methods. The steady state analysis was performed with a combination of the Newton-Raphson method and integration of the ODE which is set as default in COPASI (see Section 2.2.8). The method applied for parameter estimation is discussed in Section 4.1.3.

Modelling is aggravated by the fact that very little is known about *S. pyogenes* on the metabolic level. This involves also the regulation of many glycolytic enzymes. Although glycolysis and pyruvate metabolism are conserved among bacteria, regulation may differ even between two related species. Kinetic studies performed by Tomas Fiedler revealed that LDH is activated by FBP and P_i and inhibited by NAD^+ in *S. pyogenes* (see Section 3.1.4) whereas this enzyme is stimulated by FBP and blocked by P_i in *L. lactis* [van Niel et al., 2004]. NAD^+ does not effect LDH in *L. latcis*. However, since the characteristics and regulation of glycolytic enzymes

in *S. pyogenes* have not been studied before, kinetic parameters as well as enzyme regulations were adopted from related organisms such as *S. mutans* and *L. lactis*. Discrepancies between simulated and experimental data might be due to incorrect parameter values or regulation.

Kinetic parameters often differ between various experimental conditions such as temperature or pH value. Both have a high impact on the velocity of an enzyme. Moreover, kinetic measurements are often performed *in vitro* and the parameters can deviate considerably from *in vivo* conditions [Teusink et al., 2000]. Especially the experimental determination of V_{\max} values is difficult. In most cases specific activities having the unit U/mg of protein are measured. Since we have no information about the concentration of any glycolytic enzyme in streptococcal cells, this velocity cannot be converted into V_{\max} values required for modelling.

Since detailed enzyme mechanisms for the glycolytic enzymes in *S. pyogenes* have not been studied, convenience kinetics are used [Liebermeister & Klipp, 2006a] (see Section 2.2.3). These rate laws describe a generalised form of the Michaelis-Menten kinetics and hold enzyme saturation for high substrate concentrations. Due to the little information about *S. pyogenes* glycolytic enzymes, the small number of parameters required to implement all possible stoichiometries with convenience kinetics is an obvious advantage. Comparing the convenience kinetics to ordered and ping-pong mechanisms shows that the three rate laws differ mathematically in their denominators. The latter two mechanisms contain mixed terms with a combination of substrate and product concentrations and, furthermore, in ping-pong kinetics the term ‘+1’ symbolising the free enzyme is missing. If the denominator of convenience kinetics is multiplied out it contains all products of normalised substrate and product concentrations but no mixed terms. In general, the convenience kinetics resemble the ping-pong mechanism and the similarity between them is greater than that between the ordered and ping-pong mechanisms [Liebermeister & Klipp, 2006a]. Consequently, choosing convenience kinetics instead of a ordered or a ping-pong mechanism is as risky as an incorrect choice between the latter two kinetics.

In order to reduce the number of parameters we summed up reactions, e.g. PGI and PFK, and omitted species, e.g. F6P. However, in contrast to other glycolytic models, the levels of ADP, ATP, NAD^+ , NADH and phosphate are set as free variables since these metabolites determine the end-product pattern. As mentioned before, acetate production yields one additional ATP whereas NAD^+ can be syn-

thesised either via lactate or ethanol composition.

The sugar uptake and its control have been extensively studied in lactic acid producing bacteria [Deutscher et al., 1985, Reizer & Panos, 1980, Reizer & Saier, 1983, Thompson & Saier, 1981, Ye et al., 1996]. Therefore, this part, especially the control by HPr, was modelled in more detail. Interestingly, in oral streptococci such as *S. mutans* and *S. salivarius* inducer expulsion does not occur [Thevenot et al., 1995, Ye, 1996]. Although *B. subtilis* lacks the sugar-phosphate phosphatase and, therefore, does not show expulsion, inducer exclusion could be observed. The exclusion mechanism regulates the uptake of sugars by changing the direction and the rate of transport depending on the energy concentration and metabolite levels [Reizer et al., 1985]. Inducer exclusion guarantees the uptake of the preferred sugar such as glucose and inhibits transport of less preferred carbon sources. However, the findings in *B. subtilis* suggest that inducer exclusion is not likely solely mediated by the stimulation of the sugar-phosphate phosphatase and subsequent expulsion. Since we studied growth of *S. pyogenes* on glucose we modelled inducer expulsion but omitted inducer exclusion.

Like all lactic acid bacteria *S. pyogenes* uses the PTS system to import sugars from the medium (see Section 3.2.1). This uptake mechanism neither uses a membrane potential nor ATP. Instead, the PTS is driven by PEP. Sugar uptake via the PTS system is dependent on HPr and PEP. The HPr level is controlled by the bi-functional enzyme HPr kinase/phosphatase. Under glucose-limited conditions HPr kinase is inactive; HPr phosphatase is active and ensures the presence of unphosphorylated HPr required for sugar uptake. Under glucose excess conditions HPr kinase is active and phosphorylates HPr at a serine residue. As a consequence, the level of free HPr declines and limits the glucose uptake rate. Simultaneously, inducer expulsion is activated by HPr-Ser-P. Both effects, limiting the sugar uptake rate and stimulating inducer expulsion, prevent a sugar shock caused by sugar phosphate accumulation.

Recent studies on HPr-kinase discovered that the dephosphorylation is not a hydrolysis reaction as stated in [Deutscher et al., 1985], but a phospho-phospholysis which requires P_i and releases pyrophosphate (PP_i) [Deutscher et al., 2006]. HPr-Ser-P dephosphorylation is reversible and, thus, PP_i can replace ATP as the phosphoryl donor for HPr phosphorylation. Interestingly, PP_i -dependent HPr phosphorylation is the energetically favoured reaction resulting in an increased ATP level.

The incorporation of the described phospho-phospholysis requires the addition of metabolites, i.e. AMP and PP_i , and reactions describing PP_i hydrolysis to the model. We decided to leave the model as described in Section 3.2.1 since it is able to describe our experimental data (see Section 3.2.3), the incorporation would introduce more unknown parameters and we have not identified one reaction hydrolysing PP_i in *S. pyogenes*.

To ensure a sufficient high PEP pool and, thus, carbon source uptake the PEP level is controlled via the regulation of PYK. Under energy limited conditions, early glycolytic intermediates such as FBP decline and P_i increases resulting in PYK inhibition [Thompson & Torchia, 1984]. This mechanism prevents further conversion of PEP into pyruvate. Since PYKs and LDHs of lactic acid bacteria are often allosterically regulated in a similar way, LDHs also appear to be activated by early glycolytic intermediates and are strongly inhibited by phosphate (see Fig. 3.1) [Russell et al., 1996]. PFL is inhibited by triose-P but is unaffected by FBP and P_i . However, triose-P is in equilibrium with FBP and, thus, increases with FBP. Acetate production is inhibited by FBP and ethanol production by ATP. The level of both regulators is high under glucose excess conditions and consequently acts in alignment with the PFL regulation.

This regulation by FBP and P_i allows a shift in fermentation pattern depending on the energy availability. As stated above, FBP and triose-P levels are low whereas P_i is high under energy limiting conditions. As a consequence, LDH is inhibited and PFL converts pyruvate into acetate and ethanol. NAD^+ regeneration is catalysed concomitant with ethanol production by alcohol dehydrogenase and acetate production yields one additional ATP. Under energy excess conditions, FBP and triose-P levels are high and P_i is low. In that case, LDH is active and converts pyruvate to lactate assuring NAD^+ availability. The crucial role of FBP as a regulator in glycolysis might be due to the fact that it is the first common intermediate of all metabolisable sugars [Reizer et al., 1984].

Lactate transport is regulated by pyruvate (see Fig. 3.1). To prohibit lactate accumulation the pyruvate concentration has to be low under glucose excess conditions. Our model predicts low intracellular lactate concentrations (lower than 0.0035 mM). The pyruvate level shows a fast build-up upon glucose up to 9 mM which decreases immediately under 4 mM and vanishes after glucose consumption.

S. pyogenes lacks the oxidative part of the pentose phosphate pathway. Con-

sequently, it must have an alternative mechanism to produce NADPH which is required for the biosynthesis of cellular components, e.g. amino acid biosynthesis. One candidate is GAPN which has been reported to occur in green eukaryotes and Gram-positive bacteria with a characteristic low-G+C content [Iddar et al., 2005]. This reaction introduces an alternative route into glycolysis whereby GAPDH and PG are left out and NADPH is synthesized. As a consequence, this process enables *S. pyogenes* to produce PEP required for sugar uptake in the absence of phosphate. Indeed, removing the GAPN reaction from our model led to a much stronger reduction of glucose uptake at low external phosphate concentrations. The role of GAPN will be further studied by constructing a *gapn*-knock-out strain. If our hypotheses about the crucial role of GAPN in the energy metabolism of *S. pyogenes* holds and the *gapn*-deletion mutant shows reduced or no growth at low extracellular phosphate levels, GAPN is essential for treatment. Inhibiting this reaction would lead to a decreased growth of *S. pyogenes* at low extracellular phosphate concentrations which resemble the conditions this bacterium encounters in the human body. Therefore, GAPN represents a possible drug target.

In our experiments we observe that *S. pyogenes* mainly exhibits homolactic fermentation but shows more mixed acid fermentation at lower dilution rates at both pH 6.5 and pH 7.5 (see Table 3.3) as compared to *L. lactis* and *E. faecalis* [Fiedler et al., 2011]. This fact supports our decision to include the mixed acid fermentation pathway in more detail in the model of *S. pyogenes* (see Section 3.3.2). Our model is able to simulate this enhanced mixed acid fermentation (see Fig. 3.2).

Although one of the published glycolytic models for *L. lactis* studies the pH control [Andersen et al., 2009] we decided not to include this aspect into our *S. pyogenes* model based on the fact that no significant pH dependent differences in the fermentation pattern of this organism were observed experimentally [Fiedler et al., 2011]. Interestingly, *E. faecalis* showed a strong pH dependency with a more homolactic phenotype at pH 6.5 [Fiedler et al., 2011]. Thus, the integration of protons in the model to simulate the pH dependent effect on glycolysis is not necessary for *S. pyogenes* but could improve the model of *E. faecalis*. So far, the glycolytic model of *E. faecalis* lacks the pH effect and, interestingly, fails to simulate our glucose-pulse data (N. Veith, personal communication).

4.1.2 The role of phosphate

The developed kinetic model was used to analyse the primary metabolism of *S. pyogenes* in more detail (see Sections 3.2.1 and 3.2.3). Both the modelling studies and our experimental data reveal a crucial impact of intra- and extracellular phosphate on glycolysis in *S. pyogenes* (see Section 3.2.2). Interestingly, the observed trend of increasing FBP with increasing P_i^{ex} was also noticed for *L. lactis* [Levering et al., 2011] (see also Section 4.2.2) and *E. faecalis* (unpublished results). In order to model this effect of P_i^{ex} on the intracellular phosphorylated glycolytic intermediates the incorporation of a phosphate uptake system turned out to be key.

Phosphate uptake seems also to prevent an incomplete or slow glucose metabolism in both species, *S. pyogenes* and *L. lactis*, which is a consequence of phosphate becoming limiting (see Section 3.3.3). This is also demonstrated in our model simulations. The experimentally observed inability of *S. pyogenes* to ferment at high glucose concentrations might be due to too low phosphate concentration in the medium to counterbalance the high sugar level, such that phosphate becomes very rapidly a limiting substrate.

Especially the large FBP concentration during glycolysis is crucial for the regulation of several glycolytic enzymes and the glucose uptake rate and is a direct result of extracellular phosphate. So far, metabolite measurements were performed in medium with defined but varying phosphate concentrations without considering its effect on the system (e.g. *L. lactis*, measurement of metabolites in buffers with 25 mM [Thomas et al., 1979, Mason et al., 1981, Thompson, 1978] and 50 mM [Garrigues et al., 2001, Melchiorsen et al., 2001, Neves et al., 2005] P_i^{ex}). Our studies indicate that especially the comparison of metabolite levels measured at various phosphate concentrations in the medium is not possible. Furthermore, in glycolytic models in other organisms inorganic phosphate is rarely a free metabolite (e.g. yeast [Teusink et al., 2000]). Our study suggests that major improvements can be made by studying phosphate dynamics more carefully also in these cases.

4.1.3 Parameter estimation and resulting fit

The parameters in the model were optimised to fit our glucose-pulse data (see Section 3.2.1). Since many different optimisation algorithms are available and it is known that the optimal method for global optimisation depends on the specific

optimisation problem [Wolpert & Macready, 1997], it is important to use several algorithms to verify that the solution obtained is the global minimum or at least a good local optimum. Here, the particle swarm proved to be the best suited optimisation strategy. All other optimisation methods implemented in COPASI finished with higher objective values. The applied increased swarm size also ensures that the solution is the global (or at least a good local) minimum even if the landscape of the objective function covers many local optima. The drawback of using particle swarm for such a high dimensional optimisation problem is the computation time which was approximately 50 hours per fit.

Since hardly any kinetic parameter of *S. pyogenes* glycolytic enzymes had been identified beforehand, we were not able to use tight boundary conditions for parameter estimation. Due to the high number of unknown parameters compared to the little amount of experimental data the resulting optimisation problem is underdetermined and the parameters are not identifiable. Therefore, we decided to fit several models to our experimental data and used the best 50 of them for our analyses since different parameter combinations are capable of describing the same dynamic behaviour. This set of models describing our data enables us to predict robust behaviour independent of the parameter set. Effects observed in all of the models are caused by the model structure and, thus, are characteristics of the system. This enables us to predict robust behaviour even if the parameters are not identifiable.

Even though little is known about *S. pyogenes* and the regulation was adopted from related organisms, the model is able to simulate our glucose-pulse experiments (see Section 3.2.3). The kinetic model captures the increase in FBP concentration and glucose uptake rate when more extracellular P_i is present. This trend is robust in all obtained fits. Due to the combination of active and passive phosphate transport, low extracellular phosphate concentrations can lead to a decrease of intracellular phosphate, if the concentration gradient is pointing to the outside of the cell. It is obvious that certain low levels of extracellular phosphate lead to a decreased intracellular phosphate concentration compared to no extracellular phosphate. This behaviour is the same in roughly 50% of the fits, but not in all. However, we were able to verify this effect experimentally (see Section 3.2.3). Intracellular phosphate in turn activates the PTS and is an important substrate for GAPDH and ACK. Therefore, a decreased intracellular phosphate concentration leads to a decreased glucose uptake rate which we can also see in our experimental data (see Figure 3.2

A and B).

After incorporating the chemostat set-up in the model, e.g. reactions describing the medium in- and outflow, our glycolytic model is able to reproduce the measured acetate, extracellular lactate, external phosphate and ethanol end-product concentrations at steady state but fails to reflect the formate and extracellular pyruvate levels (see Section 3.2.3). Surprisingly, the ratio of the simulated end-product concentrations of acetate, ethanol and formate is 1:1:1 and not 1:1:2 which was observed experimentally. This is caused by the PFL reaction which produces formate and directly releases it in the extracellular space. Formate is subsequently transported out of the medium whereas this reaction is implemented with irreversible mass action kinetics and the velocity is given by the dilution rate. The more formate is present, the more is transported out of the supernatant. Thus, reducing the velocity of the PFL or adjusting the binding constant for formate might solve the problem. Due to the fact that the PEP level is as well too high, the model might miss a glycolytic branch point at the level of pyruvate. This might be the production of acetoin which was experimentally observed for the *ldh*-negative mutant. It is possible that the wild-type produces little amounts of acetoin which were not detected with the applied HPLC. Further measurements of end-product concentrations will be done to solve this problem.

4.1.4 Sensitivity analysis

Sensitivity analysis can be exploited to determine those parts of a system that are crucial and have the potential of becoming a drug target. Often a local sensitivity analysis method is applied to identify these parts of a network. One disadvantage of these local methods is their direct dependency on the actual parameter set. Due to the fact that the exact parameter set is unknown for many biochemical systems, global approaches have to be exploited in which the sensitivity analysis is carried out over a wider parameter range to circumvent the dependency on the actual parameter set. However, the interpretation of the results of a global sensitivity analysis is crucial. Since this method is based on a sampling of the parameter space the results from the global approach does not contain any statements about the probability of parameters or sensitivity values but give an overview about the system's achievable sensitivities. Since we have only little knowledge about the kinetic parameters of our glycolytic model of *S. pyogenes* we defined wide parameter ranges and a high

iteration number for the parameter scan to obtain a robust result. One obvious drawback of that method is the high computation time which is about two weeks for 10^6 iterations.

With this random sampling method we were not able to identify any parameter exerting a small control on metabolite concentrations such as FBP or internal phosphate. This might be caused by the large parameter ranges. In order to use tighter boundary conditions on the sensitivity analysis we concentrated on our set of 50 fitted models and performed a local sensitivity analysis with each of it. Hereby, we considered the distribution of the local sensitivities within the set of fitted models. However, even by applying this approach we were not able to identify parameters which always have a small impact on metabolite concentrations such as FBP or internal phosphate or on reaction fluxes like PTS and PFK fluxes (see Section 3.2.4). Every single model from the whole set has individual parameters exerting a high impact on the system variables but is robust. However, the distribution of local sensitivities in our set of models is not robust.

Additionally, we performed MCA which denotes the sensitivity analysis of the steady state model. Hereby, control coefficients are calculated which are defined for infinitesimal small perturbations. Therefore, their predictive power for effects of larger changes, like enzyme concentrations, is limited. However, applying MCA on our steady state model shows that already small perturbations in the parameters have a strong influence on the steady state fluxes and concentrations. This indicates that the model is not robust. Due to the fact that biological systems are permanently exposed to perturbations, robustness is a significant characteristic to ensure stability. Accordingly, our fitted steady state model does not describe the physiological state of the glycolytic system. In order to obtain the steady state model we fitted the velocity constants of our glucose-pulse model to our fermentation data. Incorrect kinetic binding constants might cause the observed sensitivity to perturbations. This might be solvable by exploiting more data and by determining kinetic parameters by performing additional enzymatic measurements.

In order to make sure that the lack of robustness in the chemostat model is not caused by the actual set of V_{\max} values, we will fit several models to our fermentation data and study the best 50 of them by means of MCA like already done for the glucose-pulse model.

4.2 Comparison to *L. lactis*

We have developed an improved kinetic model of the well-studied *L. lactis* which takes into account the effects of varying amounts of extracellular phosphate and quantitatively describes the dynamics of extracellular metabolites (glucose and lactate), main glycolytic intermediates (FBP, G6P, PEP) and co-factors (ADP, ATP, NAD⁺, NADH, P_i). This model was compared to the model of *S. pyogenes*.

4.2.1 Kinetic model of *L. lactis*

Previously published *L. lactis* models omitted P_i transport [Hoefnagel et al., 2002b, Hoefnagel et al., 2002a, Oh et al., 2011, Andersen et al., 2009] or considered phosphate as a constant input [Neves et al., 1999, Voit et al., 2006a, Voit et al., 2006b]. Consequently, the simulated FBP and intracellular phosphate levels were considerably lower in these studies, which affects the regulation of glycolytic processes such as the PTS [Deutscher et al., 2006], PYK [Crow & Pritchard, 1976] and LDH [van Niel et al., 2004]. Especially the large FBP concentration during glycolysis was crucial for the regulation of several glycolytic enzymes as well as for the glucose uptake rate and was a direct result of extracellular phosphate.

We developed a substantially improved kinetic model of *L. lactis* glycolysis, which accurately simulates our measured metabolite profiles quantitatively at different extracellular phosphate concentrations and is also consistent with published ¹³C- and ³¹P-NMR measured by Neves and co-workers [Neves et al., 2002]. Interestingly, the Neves experiments were performed with MG1363 and we used NZ9000, a MG1363 derivative, for our glucose-pulse experiments. For both data sets, the initial concentrations as well as the activity of the ATPase were allowed to differ. All other parameters stayed the same irrespective of the assumption that the V_{max} values for the two different experimental data sets will certainly not be exactly the same. However, the model with these constraints is able to almost perfectly fit the data as long as phosphate uptake is included in the model. Without this reaction, the data cannot be fitted.

Thus, our developed model is able to capture dynamic profiles of intracellular metabolites after glucose-pulse experiments with strongly improved accuracy (see Section 3.3.1) and fits the dynamics for different strains with one single thermodynamically-consistent parameter (though with variable ATPase activities). Like

for *S. pyogenes*, we used a set of 50 models for our analyses described below due to the non-identifiability of the parameters.

4.2.2 Role of phosphate in *L. lactis* and *S. pyogenes*

The role of phosphate is crucial in *L. lactis* and *S. pyogenes* even though uptake and regulation show some differences. We can ascribe these to the phosphate uptake mechanisms differing in both species. A passive transport (even a well regulated one) as present in *S. pyogenes* will allow phosphate outflux, if the concentration gradient points in this direction.

Having revealed the fundamental role of free phosphate for the metabolism of these species, it is interesting to see, how the two bacteria cope with the phosphate available in their respective natural environment. *S. pyogenes* which resides in the human body (e.g. skin, mucous membrane and blood (0.8 - 1.8 mM phosphate in the latter)) at relatively constant and low concentrations of phosphate has two phosphate uptake mechanisms, a passive and an active transport. Both have to supply sufficient phosphate to the cells to enable them to efficiently metabolise glucose in order to grow and multiply. However, according to the above, the relatively low phosphate concentrations are not the optimal conditions for glucose uptake for this organism. This raises the question why *S. pyogenes* still uses the passive transport that causes this effect. The answer might be the fairly constant supply of phosphate and glucose in the compartments of the human body. Thus, while not allowing optimal glucose uptake rates, the passive transport system allows a cheap and guaranteed minimal phosphate uptake (the phosphate concentration in its natural environment will certainly never drop much) that is sufficient to sustain glycolysis.

L. lactis on the other hand encounters relatively high phosphate levels (ca. 20 mM) in fresh milk initially. However, here, the situation is more like in batch experiments, since there is no further supply of phosphate once the milk has left the body and *L. lactis* starts to reside in it. Thus, an active mechanism as found for phosphate uptake in these bacteria makes sense, even though one may wonder, why the bacteria do not own a passive one which would allow them to make use of the initially high phosphate concentration without wasting ATP. As seen for *S. pyogenes*, a passive transporter can slow down glucose uptake, if the extracellular phosphate concentration starts to deplete. This might be dangerous for a species that encounters highly variable environmental conditions. For *L. lactis*, no putative

sodium phosphate symporter has been identified so far.

The above observations about the phosphate regulation of LDH are supported on the kinetic level by the differences between plant- and dairy-strains of *L. lactis*. Van Niel et al. [van Niel et al., 2004] measured that LDH activity in plant- and dairy-strains of *L. lactis* are differentially regulated: dairy strains use FBP and P_i , whereas LDH of plant isolates are regulated by the NADH/NAD⁺ ratio. As a plant environment is virtually devoid from phosphate [Asher & Loneragan, 1967], these observations support a close link between the organism's natural environment and its metabolic regulation.

In summary, the interspecies comparison gains insight in the crucial role of P_i transport and P_i regulation of glycolysis, which we could relate to the phosphate availability in the environmental niches of these organisms.

4.3 Genome-scale model

In order to explore the whole-cell metabolism of *S. pyogenes* we have developed a genome-scale model with predictive capabilities based on genomic, physiological and biochemical information (see Section 3.5). Very little is known about the metabolism of *S. pyogenes* due to the fact that it is a human pathogen and its cultivation is subject to strict instructions. Moreover, our experiments show that the cultivation of this organism is more difficult than the cultivation of *L. lactis* and *E. faecalis*. We have not identified the reason for that yet. Therefore insights from a computational model are very helpful. The model comprises 574 reactions and 552 metabolites (see Appendix B.1 and B.2). The manual consistency check of the network (see Section 3.5.3) has taken much effort but guarantees high quality of the reconstruction. Since the biomass components have not been measured yet, the biomass equation and its stoichiometric coefficients are adopted from the closely related *L. lactis* (see Section 3.5.5). We have measured input and output fluxes under defined experimental conditions. Finally, we used the model to explore the organism's metabolism and propose strategies to control growth. The presence or absence of functional pathways can be predicted based on the model and will be validated experimentally. Hereby, we concentrated on the investigation of essential amino acids.

4.3.1 Orthology detection

The quality of the reconstructed metabolic network depends on the orthology detection method and on the quality of the reference networks selected for this purpose. We used INPARANOID [Remm et al., 2001] for orthology detection which is based on bi-directional best hits and does not use multiple alignments or phylogenetic trees and, therefore, avoids errors that might be introduced at these steps [Remm et al., 2001]. The chosen networks are manually curated and, thus, guarantee a high quality of the reconstructed network.

Several automatic methods for the reconstruction of genome-scale metabolic networks are available. Here, we used the AUTOGRAPH method. Notebaart *et al.* compared this method to the well established Pathologic approach [Karp et al., 2002]. Pathologic takes annotated genomes as input and predicts gene-reaction associations based on EC numbers and name comparisons. It is the first step in the development of so-called pathway-genome-databases. Notebaart *et al.* found out that the recon-

struction based on AUTOGRAPH contained organism specific genes and transport system components which were absent in the automatic Pathologic reconstruction. Since transport reactions often do not have complete EC numbers, the lack of these reactions have to be expected in a network constructed with Pathologic and, consequently, the according reactions have to be added manually. The prediction of organism specific genes demonstrates the strength of the AUTOGRAPH method [Notebaart et al., 2006].

4.3.2 Network composition

The purpose of the network reconstruction is to simulate cell growth and, consequently, all metabolic reactions essential for cell growth were included in the model. Due to simplicity, inorganic ions were negligible for modelling. The biomass production was used as objective function. This reaction relates the maximal energy production to the organism's growth rate and was adapted from the *L. lactis* reconstruction since the biomass composition of *S. pyogenes* is not available from experiments. According to this reaction, biomass is composed of six compounds, namely DNA, RNA, protein, cell wall components, membrane constituents and vitamins. Even though *L. lactis* and *S. pyogenes* are closely related we already identified some differences, e.g. in their energy metabolism (see Section 3.3.2 and 3.3.3). Consequently, it is likely that their biomass composition will differ, especially the stoichiometric coefficients.

Reconstructing the whole-cell metabolism was complicated by the fact that little is known about *S. pyogenes* metabolism. Membrane and cell wall synthesis is well studied due to the role of some of their components as virulence factors. Especially the composition and role of teichoic acids was investigated [Knox & Wicken, 1973, Navarre & Schneewind, 1999, Swoboda et al., 2010, Cunningham, 2000]. It is speculated that teichoic acids serve as specific decorations differentiating Gram-positive bacteria from other organisms possessing an identical peptidoglycan composition [Navarre & Schneewind, 1999]. Wide gaps exist, for example, in the folate and C1-THF pool synthesis where information about an enzyme catalysing one of the first steps is missing (see Section 3.5.5). Due to incomplete EC numbers and missing annotation in UniProt [UniProt Consortium, 2010] we could not figure out how this step is catalysed in *S. pyogenes* even though the genome-scale models of *L. lactis* and *L. plantarum* served as a template. Consequently, we will study this part of the

folate synthesis in more detail.

4.3.3 Simulation of experimental data

One approach to explore such large metabolic networks is FBA (see Section 2.3.3). This method calculates the flux through the network based on its stoichiometry. To reduce the number of possible solutions we specify an objective function and constraints on uptake and product fluxes (see Sections 3.5.5 and 3.5.6). The objective function is defined as the flux towards the biomass formation and the constraints on the fluxes are set according to our measured amino acid and end-product fluxes.

Without further constraints on the fermentation products, enhanced mixed-acid formation would be observed. Since the acetate production yields one additional ATP, mixed-acid fermentation is energetically more favourable for the cell than lactate production. This points out that limiting the uptake and production fluxes is essential; in general, the optimal solution found with FBA does not reflect a physiological solution. To validate the reconstructed metabolic network of *S. pyogenes* we simulated our fermentation data (see Section 3.1.2). Additionally, we studied the substrate spectrum and growth in the absence of amino acids of *S. pyogenes* (see Sections 3.1.5 and 3.1.7).

Fermentation data. The model correctly simulates the growth rate of approximately 0.05 at pH 6.5 and about 0.15 at both pHs, 6.5 and 7.5, but fails to predict the growth rate of 0.05 at pH 7.5 for the wild-type and the *ldh*-knock-out mutant (see Section 3.5.6). This might be due to an error in the measurements since all other experimental set-ups could be simulated accurately. We will perform additional fermentation experiments to verify the measured fluxes and validate the computational model. More than three measurements under each experimental condition will facilitate the use of mean values and standard deviation to restrict the uptake or production fluxes. So far, we assumed an error of 20% but had to widen the upper boundaries of the amino acid fluxes to find an optimal solution (see Section 3.5.6). This again points to a measurement problem.

In all simulations under the objective of maximising the biomass formation, the amino acid cysteine is not taken up even if it is present in the medium. The *in silico* model prefers to synthesise it from cystine. This might be due to the fact that in the model cystine can only be degraded into cysteine. We will concentrate on the

cystine metabolism during the ongoing model improvement and validation.

Furthermore, no acetoin is produced by the computational model although it is measured during growth of the *ldh*-negative mutant. According to the computational model, the mutant ferments glucose to acetate, ethanol, formate and mainly to D-lactate. The last mentioned flux is not limited since we have not measured it. Under the simulated conditions, biotin, pyridoxamine, pyridoxine, riboflavin and xanthine are not taken up although the first four compounds are essential for growth; according to the model, xanthine can be synthesised *de novo*.

All in all, more experimental data is needed to apply tighter constraints on the fluxes and, thus, reduce the achievable physiological states. Smaller ranges will also decrease the possibility of having multiple model states showing identical objective values.

Growth on different carbon sources. We identified 20 sugars out of 190 on which the wild-type and the *ldh*-negative mutant are able to grow (see Section 3.1.5). Out of the 20 carbon sources four were already included in the model. After integrating exchange, uptake and degradation of these sugars, the *in silico* model predicts growth of *S. pyogenes* wild-type and *ldh*-deletion strain on these sugars (see Section 3.5.6). However, no quantitative prediction can be done due to the experimentally determined growth rate under batch conditions. Tomas Fiedler will measure product and amino acid concentrations in *S. pyogenes* wild-type and *ldh*-negative mutant at two dilution rates and two pHs during continuous cultivation in CDM-LAB medium with trehalose, sucrose, maltose and mannose as carbon source. These data will be used to validate the model predictions.

Omission of amino acids. The amino acid leave-out experiments were carried out in batch cultures (see Section 2.1.9). Consequently, we compare the outcome of the two independent experiments (see Table 3.13) qualitatively to the model predictions. Surprisingly, our first experiment indicates that the growth rate in the absence of aspartate and glutamine is higher than in full medium. As described in Section 3.5.6, the model fails to predict this increase. This might be due to a measurement error, a missing connection between these two amino acids or to a loss of competition for a single transport system which might occur under batch conditions [Davies et al., 1965]. The formation of correctly charged Asn-tRNA^{Asn}

through the transamidation of misacylated Asp-tRNA^{Asn} establishes a connection between aspartate and glutamine through the following reaction



However, due to the missing information regarding the presence of the non-discriminating aspartyl tRNA synthetase (EC 6.1.1.23) in *S. pyogenes* and the contradicting data from our second experiment the reaction is not incorporated in the model. Furthermore, the *in silico* model predicts no change in growth rate in the absence of cysteine or glutamate as compared to full medium. Taking the standard deviation into account, the difference in the measured growth rates of *S. pyogenes* in full medium or medium without the mentioned amino acids is negligible.

The model predictions agree with our experimental data (see Section 3.1.7) for growth in the absence of most tested amino acids. Thus, the model correctly predicts Arg, His, Ile, Leu, Lys, Met, Phe, Trp, Tyr and Val to be essential for growth of *S. pyogenes*.

However, the simulation and the measured data give contrary results for some amino acid leave-outs. While growth occurs in the absence of alanine in the measurements, the *in silico* model does not grow in this medium. So far, we did not identify the reaction producing Ala. Furthermore, our data give contrary results concerning growth in the absence of cysteine and cystine. According to the first experiment these amino acids are interconvertible whereas the second experiment indicates that there must be an alternative way producing Cys.

The experimental data indicate that Gly, Ser and Thr are not interconvertible. A database survey using BLAST [Geer et al., 2010] points out that the gene encoding the enzyme converting threonine into glycine is not present in the genome of *S. pyogenes*. However, the enzyme converting glycine and serine is available. Although this reaction is reversible, the flux only occurs in the direction of serine production. The conversion of serine into glycine proceeds concomitant with the transformation of tetrahydrofolate into 5,10-methylenetetrahydrofolate. Since the enzyme metabolising 5,10-methylenetetrahydrofolate is missing in *S. pyogenes* (see Section 3.5.5), this metabolite would accumulate while producing glycine from serine. Furthermore, referring to experimental data, serine is essential whereas the model predicts it to be synthesised from cysteine.

According to both of our experiments, *S. pyogenes* can grow in the absence of Glu. The first experiment also indicates growth omitting Gln whereas in the sec-

ond experiment no growth occurs under this condition. Thus, the first experiment indicates a conversion of Gln and Glu whereas the second experiment points out that Gln cannot be produced from Glu. Additional experiments will be performed to sort out mismatches between both data sets and the model simulations. Discrepancies between the validated data and the computational model will be resolved by removing or adding reactions.

4.3.4 Predictions from the model

We used the genome-scale model to predict essential amino acids and to propose a minimal medium for growth of *S. pyogenes* (see Section 3.5.6). Based on the developed model, we identified 12 amino acids to be essential for the growth of *S. pyogenes* in CDM-LAB medium, 10 of them are identical with literature data (see Table 3.19 and [Slade et al., 1951]). Referring to literature, 15 amino acids are required for the growth of *S. pyogenes*. Discrepancies between the model prediction and literature data concern Ala, Gly, Pro, Ser and Thr. In order to validate the model predictions we performed amino acid leave-out experiments ourselves (see Section 2.1.9 and 3.1.7) and were able to validate 9 of the 12 amino acids predicted to be essential (see Table 3.13). Although alanine, cysteine and valine are predicted to be essential by the computational model, our experimental findings show that *S. pyogenes* is able to grow in the absence of these amino acid. Thus, trusting the data, the computational model lacks reactions catalysing the production of these amino acids. However, we have not identified the missing steps based on a KEGG search [Kanehisa & Goto, 2000]. Furthermore, according to our experimental and the literature data [Slade et al., 1951], glycine, serine and threonine are essential for growth of *S. pyogenes*. Referring to the model, these amino acids are interconvertible. The reactions catalysing the mutual transformation are included in the model based on orthology detection. However, this is preliminary data and we will independently repeat the amino acid leave-out experiments and adapt our model to our experimental results. Furthermore, the amino acid requirements might differ depending on the medium, especially on the vitamin content [Tittsler et al., 1952] which likely explains the discrepancies between our data and literature [Slade et al., 1951].

Based on the predicted essential amino acids a minimal medium was proposed. No *in silico* growth was observed when only the essential amino acids were allowed to be taken up. If glutamine (or glutamate), glycine (or threonine) and asparagine

(or aspartate) are supplied additionally to the essential amino acids, growth occurs (see Section 3.5.6).

4.3.5 Differences and similarities between *S. pyogenes* and related bacteria

As described in Section 3.5.7, *L. lactis* has an almost complete pentose phosphate pathway while the oxidative phase is missing in *S. pyogenes*. Concentrating on related bacteria, we found out that *S. bovis*, *S. mutans* and *S. thermophilus* also lack the oxidative portion of the hexose monophosphate pathway [Asanuma & Hino, 2006, Crow & Wittenberger, 1979, Kanehisa & Goto, 2000]. Interestingly, this incompleteness seems to be related to the presence of the enzyme GAPN which is annotated in the latter four organisms. On the other hand, *L. plantarum* and *L. lactis* have a complete hexose monophosphate pathway for generating NADPH and lack GAPN [Kanehisa & Goto, 2000]. This underlines the significance of GAPN in NADPH synthesis.

GAPN produces NADPH on the cost of one ATP. Therefore, this mechanism is inefficient for the growing cell. We investigated the amino acid metabolism to discover a more efficient way for NADPH recovery. NADPH can be generated concomitant with the conversion of proline into glutamate, as is done in *L. plantarum*. However, *S. pyogenes* lacks the required enzymes. So far, we could not identify any NADPH recovery process neither in the amino acid metabolism nor in another pathway. Interestingly, the same holds for *S. bovis* and *S. mutans*. Both have genes encoding GAPN but do not have any other NADPH-producing systems such as the pentose phosphate pathway or the NADPH:NAD⁺ oxidoreductase [Asanuma & Hino, 2006, Crow & Wittenberger, 1979]. The lack of any other NADPH regenerating reaction underlines the crucial role of GAPN in *S. pyogenes* and the suggestion of GAPN as drug target (see Section 4.1.1).

Based on the comparison between *L. lactis* and *S. pyogenes*, we propose that the presence of GAPN can be further linked to nutritional requirements. This hypothesis is supported by the higher number of essential amino acids for the growth of *S. pyogenes* compared to *L. lactis*. Concerning required vitamins, *S. pyogenes* is not able to synthesise thiamin while *L. lactis* can produce it *de novo*. However, this hypothesis has to be verified by means of bioinformatic approaches in which the

genomes of bacteria possessing GAPN as well as lacking it are investigated regarding their nutritional requirements, e.g. the presence of enzymes involved in vitamin or cofactor synthesis.

4.4 Discussion of thesis goals

The purpose of this thesis was the development of a kinetic and a genome-scale model of *S. pyogenes* and the understanding of the differences and similarities between *S. pyogenes* and *L. lactis*. The following objectives have been investigated within the scope of this thesis.

- 1. Construct a kinetic model of *S. pyogenes* using ODEs based on an extensive literature survey and delivered experimental data.**
 - **Simulate our glucose-pulse data.** Our computational model is able to reflect the effect of extracellular phosphate on glycolysis. In accordance with our experimental data, the FBP level and the glycolytic flux increase with the extracellular phosphate concentration (see Section 3.2.3).
 - **Simulate our fermentation data at two pHs and two dilution rates.** The developed glycolytic model is able to simulate our measured acetate, extracellular lactate, external phosphate and ethanol end-product concentrations at steady state but fails to reflect the formate and extracellular pyruvate levels (see Section 3.2.3).
 - **Understand the differences and similarities between *S. pyogenes* and *L. lactis* based on the developed kinetic models.** Based on the models we could identify crucial differences in the regulation of glycolytic key enzymes such as LDH. Furthermore, both LAB show differences in the phosphate uptake and the way phosphate affects glycolysis (see Sections 3.3.2 and 3.3.3).
 - **Understand the adaption to different environments based on the models of *S. pyogenes* and *L. lactis*.** Free inorganic phosphate has a crucial role on the metabolism of both *S. pyogenes* and *L. lactis*. The uptake and impact of phosphate can be related to its availability in the respective natural environments (see Sections 3.3.2, 3.3.3 and 4.2).
- 2. Reconstruct the metabolic network of *S. pyogenes* based on a semi-automatic approach which takes advantage of already existing and manually curated models.**

- **Simulate our fermentation data.** Our genome-scale model is able to simulate the correct growth rates of approximately 0.05 at pH 6.5 and about 0.15 at both pHs, 6.5 and 7.5, for the wild-type and the mutant strain. It fails to predict the growth rate of 0.05 at pH 7.5 for the wild-type and the *ldh*-knock-out mutant (see Section 3.5.6). This might be due to a measurement error and will be studied in more detail.
- **Understand the growth requirements of *S. pyogenes* and define optimal and suboptimal conditions.** Based on the *in silico* model, we identified 12 amino acids to be essential for the growth of *S. pyogenes* in CDM-LAB medium. Furthermore, we propose a minimal medium containing three additional amino acids (see Section 3.5.6).
- **Explore the organism's reaction to perturbations in its environment.** We have studied the growth of *S. pyogenes* on different carbon sources (see Section 3.5.6) and in the absence of selected amino acids (see Section 3.5.6).
- **Find strategies to reduce the growth of the pathogen *S. pyogenes* and propose drug targets.** We propose GAPN as drug target since it seems the only possibility to recover NADPH but also effects glucose uptake (see Section 4.3.5 and 4.1.1).
- **Describe differences and similarities between *S. pyogenes* and *L. lactis*.** Although *S. pyogenes* and *L. lactis* are closely related, we can identify differences in their metabolism, e.g. in the cell wall composition and the pentose phosphate pathway (see Section 3.5.7).

Chapter 5

Outlook

We have presented the first kinetic model of *S. pyogenes* glycolysis. The computational model was formulated using ordinary differential equations and was implemented in the software package COPASI. We performed glucose-pulse and fermentation experiments under varying conditions and measured the kinetics of PYK and LDH *in vitro* to parametrise our model. In accordance with experimental data, the kinetic model captures the effect of extracellular phosphate on FBP and the glycolytic flux. We performed sensitivity analysis and emphasised differences and similarities with *L. lactis* based on the kinetic models.

The sensitivity analyses revealed that all parameters are basically non-identifiable with the available data and, thus, yielded no information about crucial parameters. In order to gain more insight one could investigate the relationships between the parameters. With this information, the dimensionality of the parameter space can be reduced. Furthermore, we will concentrate on the arginine metabolism and include this amino acid in the kinetic model since it limits the growth of *S. pyogenes*.

Besides, we have presented the reconstruction of the metabolic network of *S. pyogenes* based on its annotated genome sequence and existing manually curated reference networks. Network reactions were collected from the reconstructed networks of *L. plantarum* and *L. lactis* and from biochemical and metabolic pathway databases. The constructed genome-scale model was analysed using FBA. We investigated essential amino acids and the substrate spectrum of *S. pyogenes*. Simulation results were compared with experimental data delivered from consortium partners.

Improvement of the genome-scale model remains. For the validation of the model more data are needed. In the first place, additional fermentation experiments are important. Furthermore, an independent repeat of the amino acid leave-out experiments is required since our data are conflicting. The scope of the reconstruction will increase and transcriptional regulation will be incorporated. The metabolic network will be used to simulate proteomic and transcriptomic data. Further advancements will be achieved by measuring biomass components and parameters describing the energy required for growth under the same experimental conditions.

Since we propose GAPN as a possible drug target, the construction of a *gapn*-deletion strain and the study of its growth at different phosphate concentrations will be done.

Furthermore, we will combine the kinetic and the genome-scale model to a hybrid system. The kinetic model will replace the primary metabolism in the whole-cell model and will constraint end-product fluxes and ATP maintenance.

Bibliography

- [Alexeeva et al., 2000] Alexeeva S, de Kort B, Sawers G, Hellingwerf KJ & de Mattos MJ, Effects of limited aeration and of the ArcAB system on intermediary pyruvate catabolism in *Escherichia coli*. *J. Bacteriol*, 182: 4934–4940, 2000.
- [Andersen et al., 2009] Andersen AZ, Carvalho AL, Neves AR, Santos H, Kummer U & Olsen LF, The metabolic pH response in *Lactococcus lactis*: an integrative experimental and modelling approach. *Comput Biol Chem*, 33: 71–83, 2009.
- [Aon et al., 1991] Aon MA, Cortassa S, Westerhoff HV, Berden JA, Spronsen EV & Dam KV, Dynamic regulation of yeast glycolytic oscillations by mitochondrial functions. *J Cell Sci*, 99: 325–334, 1991.
- [Asanuma & Hino, 2000] Asanuma N & Hino T, Effects of pH and energy supply on activity and amount of pyruvate formate-lyase in *Streptococcus bovis*. *Appl Environ Microbiol*, 66(9): 3773–3777, 2000.
- [Asanuma & Hino, 2006] Asanuma N & Hino T, Presence of NAD⁺-specific glyceraldehyde-3-phosphate dehydrogenase and CcpA-dependent transcription of its gene in the ruminal bacterium *Streptococcus bovis*. *FEMS Microbiol Lett*, 257(1): 17–23, 2006.
- [Asher & Loneragan, 1967] Asher C & Loneragan J, Response of plants to phosphate concentration in solution culture: growth and phosphorus content. *Soil Science*, 103: 225–233, 1967.
- [Baev et al., 1999] Baev D, England R & Kuramitsu HK, Stress-induced membrane association of the *Streptococcus mutans* GTP-binding protein, an essential G protein, and investigation of its physiological role by utilizing an antisense RNA strategy. *Infect Immun*, 67: 4510–4516, 1999.

- [Bilofsky & Burks, 1988] Bilofsky HS & Burks C, The GenBank genetic sequence data bank. *Nucleic Acids Res*, 16(5): 1861–1863, 1988.
- [Bongers et al., 2003] Bongers RS, Hoefnagel MHN, Starrenburg MJC, Siemerink MAJ, Arends JGA, Hugenholtz J & Kleerebezem M, IS981-mediated adaptive evolution recovers lactate production by *ldhB* transcription activation in a lactate dehydrogenase-deficient strain of *Lactococcus lactis*. *J Bacteriol*, 185(15): 4499–4507, 2003.
- [Brown et al., 1998] Brown CK, Kuhlman PL, Mattingly S, Slaters K, Calie PJ & Farrar WW, A model of the quaternary structure of enolases, based on structural and evolutionary analysis of the octameric enolase from *Bacillus subtilis*. *J Protein Chem*, 17(8): 855–866, 1998.
- [Castro et al., 2009] Castro R, Neves A, Fonseca L, Pool W, Kok J, Kuipers O & Santos H, Characterization of the individual glucose uptake systems of *Lactococcus lactis*: mannose-PTS, cellobiose-PTS and the novel GlcU permease. *Mol Microbiol*, 71: 795–806, 2009.
- [Chassagnole et al., 2002] Chassagnole C, Noisommit-Rizzi N, Schmid JW, Mauch K & Reuss M, Dynamic modeling of the central carbon metabolism of *Escherichia coli*. *Biotechnol Bioeng*, 79(1): 53–73, 2002.
- [Collins & Thomas, 1974] Collins LB & Thomas TD, Pyruvate kinase of *Streptococcus lactis*. *J Bacteriol*, 120(1): 52–58, 1974.
- [Cortassa et al., 1991] Cortassa S, Aon MA & Westerhoff HV, Linear nonequilibrium thermodynamics describes the dynamics of an autocatalytic system. *Biophys J*, 60(4): 794–803, 1991.
- [Crow & Pritchard, 1976] Crow VL & Pritchard GG, Purification and properties of pyruvate kinase from *Streptococcus lactis*. *Biochim Biophys Acta*, 438(1): 90–101, 1976.
- [Crow & Pritchard, 1982] Crow VL & Pritchard GG, Pyruvate kinase from *Streptococcus lactis*. *Methods Enzymol*, 90 Pt E: 165–170, 1982.

- [Crow & Thomas, 1982] Crow VL & Thomas TD, D-tagatose 1,6-diphosphate aldolase from lactic streptococci: purification, properties, and use in measuring intracellular tagatose 1,6-diphosphate. *J Bacteriol*, 151(2): 600–608, 1982.
- [Crow & Wittenberger, 1979] Crow VL & Wittenberger CL, Separation and properties of NAD⁺- and NADP⁺-dependent glyceraldehyde-3-phosphate dehydrogenases from *Streptococcus mutans*. *J Biol Chem*, 254(4): 1134–1142, 1979.
- [Cunningham, 2000] Cunningham MW, Pathogenesis of group A streptococcal infections. *Clin Microbiol Rev*, 13(3): 470–511, 2000.
- [Cvitkovitch et al., 1995] Cvitkovitch DG, Boyd DA, Thevenot T & Hamilton IR, Glucose transport by a mutant of *Streptococcus mutans* unable to accumulate sugars via the phosphoenolpyruvate phosphotransferase system. *J Bacteriol*, 177(9): 2251–2258, 1995.
- [Davies et al., 1965] Davies HC, Karush F & Rudd JH, Effect of amino acids on steady-state growth of a group A hemolytic streptococcus. *J Bacteriol*, 89: 421–427, 1965.
- [Deutscher et al., 2006] Deutscher J, Francke C & Postma PW, How phosphotransferase system-related protein phosphorylation regulates carbohydrate metabolism in bacteria. *Microbiol Mol Biol Rev*, 70(4): 939–1031, 2006.
- [Deutscher et al., 1985] Deutscher J, Kessler U & Hengstenberg W, Streptococcal phosphoenolpyruvate:sugar phosphotransferase system: purification and characterization of a phosphoprotein phosphatase which hydrolyzes the phosphoryl bond in seryl-phosphorylated histidine-containing protein. *J Bacteriol*, 163(3): 1203–1209, 1985.
- [Durot et al., 2009] Durot M, Bourguignon PY & Schachter V, Genome-scale models of bacterial metabolism: reconstruction and applications. *FEMS Microbiol Rev*, 33(1): 164–190, 2009.
- [Edwards et al., 2001] Edwards JS, Ibarra RU & Palsson BO, In silico predictions of *Escherichia coli* metabolic capabilities are consistent with experimental data. *Nat Biotechnol*, 19(2): 125–130, 2001.

- [Even et al., 2001] Even S, Lindley ND & Coccagn-Bousquet M, Molecular physiology of sugar catabolism in *Lactococcus lactis* IL1403. *J Bacteriol*, 183(13): 3817–3824, 2001.
- [Even et al., 2002] Even S, Lindley ND, Loubière P & Coccagn-Bousquet M, Dynamic response of catabolic pathways to autoacidification in *Lactococcus lactis*: transcript profiling and stability in relation to metabolic and energetic constraints. *Mol Microbiol*, 45(4): 1143–1152, 2002.
- [Ferretti et al., 2001] Ferretti JJ, McShan WM, Ajdic D, Savic DJ, Savic G, Lyon K, Primeaux C, Sezate S, Suvorov AN, Kenton S, Lai HS, Lin SP, Qian Y, Jia HG, Najjar FZ, Ren Q, Zhu H, Song L, White J, Yuan X, Clifton SW, Roe BA & McLaughlin R, Complete genome sequence of an M1 strain of *Streptococcus pyogenes*. *Proc Natl Acad Sci U S A*, 98(8): 4658–4663, 2001.
- [Fiedler et al., 2011] Fiedler T, Bekker M, Jonsson M, Mehmeti I, Pritzsckke A, Siemens N, Nes I, Hugenholtz J & Kreikemeyer B, Characterization of three lactic acid bacteria and their isogenic *ldh* deletion mutants shows optimization for YATP (cell mass produced per mole of ATP) at their physiological pHs. *Appl Environ Microbiol*, 77(2): 612–617, 2011.
- [Fischetti, 1977] Fischetti VA, Streptococcal M protein extracted by nonionic detergent. II. Analysis of the antibody response to the multiple antigenic determinants of the M-protein molecule. *J Exp Med*, 146(4): 1108–1123, 1977.
- [Francke et al., 2005] Francke C, Siezen RJ & Teusink B, Reconstructing the metabolic network of a bacterium from its genome. *Trends Microbiol*, 13(11): 550–558, 2005.
- [Garrigues et al., 2001] Garrigues C, Goupil-Feuillerat N, Coccagn-Bousquet M, Renault P, Lindley ND & Loubiere P, Glucose metabolism and regulation of glycolysis in *Lactococcus lactis* strains with decreased lactate dehydrogenase activity. *Metab Eng*, 3(3): 211–217, 2001.
- [Geer et al., 2010] Geer LY, Marchler-Bauer A, Geer RC, Han L, He J, He S, Liu C, Shi W & Bryant SH, The NCBI BioSystems database. *Nucleic Acids Res*, 38(Database issue): D492–D496, 2010.

- [Gunnewijk et al., 2001] Gunnewijk MG, van den Bogaard PT, Veenhoff LM, Heuberger EH, de Vos WM, Kleerebezem M, Kuipers OP & Poolman B, Hierarchical control versus autoregulation of carbohydrate utilization in bacteria. *J Mol Microbiol Biotechnol*, 3(3): 401–413, 2001.
- [Harold & Levin, 1974] Harold FM & Levin E, Lactic acid translocation: terminal step in glycolysis by *Streptococcus faecalis*. *J Bacteriol*, 117: 1141–1148, 1974.
- [Heinrich & Rapoport, 1974] Heinrich R & Rapoport TA, A linear steady-state treatment of enzymatic chains. General properties, control and effector strength. *Eur J Biochem*, 42(1): 89–95, 1974.
- [Hoefnagel et al., 2002a] Hoefnagel MH, van der Burgt A, Martens DE, Hugenholtz J & Snoep JL, Time dependent responses of glycolytic intermediates in a detailed glycolytic model of *Lactococcus lactis* during glucose run-out experiments. *Mol Biol Rep*, 29: 157–161, 2002a.
- [Hoefnagel et al., 2002b] Hoefnagel MHN, Starrenburg MJC, Martens DE, Hugenholtz J, Kleerebezem M, van Swam II, Bongers R, Westerhoff HV & Snoep JL, Metabolic engineering of lactic acid bacteria, the combined approach: kinetic modelling, metabolic control and experimental analysis. *Microbiology*, 148(Pt 4): 1003–1013, 2002b.
- [Hoops et al., 2006] Hoops S, Sahle S, Gauges R, Lee C, Pahle J, Simus N, Singhal M, Xu L, Mendes P & Kummer U, COPASI – a COmplex PATHway SIMulator. *Bioinformatics*, 22(24): 3067–3074, 2006.
- [Iddar et al., 2002] Iddar A, Serrano A & Soukri A, A phosphate-stimulated NAD(P)⁺-dependent glyceraldehyde-3-phosphate dehydrogenase in *Bacillus cereus*. *FEMS Microbiol Lett*, 211: 29–35, 2002.
- [Iddar et al., 2005] Iddar A, Valverde F, Assobhei O, Serrano A & Soukri A, Widespread occurrence of non-phosphorylating glyceraldehyde-3-phosphate dehydrogenase among Gram-positive bacteria. *Int Microbiol*, 8(4): 251–258, 2005.
- [Iddar et al., 2003] Iddar A, Valverde F, Serrano A & Soukri A, Purification of recombinant non-phosphorylating NADP-dependent glyceraldehyde-

- 3-phosphate dehydrogenase from *Streptococcus pyogenes* expressed in *E. coli*. *Mol Cell Biochem*, 247(1-2): 195–203, 2003.
- [Jones & Fischetti, 1988] Jones KF & Fischetti VA, The importance of the location of antibody binding on the M6 protein for opsonization and phagocytosis of group A M6 streptococci. *J Exp Med*, 167(3): 1114–1123, 1988.
- [Jonsson et al., 2009] Jonsson M, Saleihan Z, Nes IF & Holo H, Construction and characterization of three lactate dehydrogenase-negative *Enterococcus faecalis* V583 mutants. *Appl Environ Microbiol*, 75(14): 4901–4903, 2009.
- [Ju & Trivedi, 1998] Ju LK & Trivedi H, Oscillations of NAD(P)H fluorescence in *Escherichia coli* culture performing dissimilative nitrate/nitrite reduction. *World Journal of Microbiology and Biotechnology*, 14: 263–269, 1998.
- [Kacser & Burns, 1973] Kacser H & Burns JA, The control of flux. *Symp Soc Exp Biol*, 27: 65–104, 1973.
- [Kanehisa & Goto, 2000] Kanehisa M & Goto S, KEGG: kyoto encyclopedia of genes and genomes. *Nucleic Acids Res*, 28(1): 27–30, 2000.
- [Karp et al., 2002] Karp PD, Paley S & Romero P, The Pathway Tools software. *Bioinformatics*, 18 Suppl 1: S225–S232, 2002.
- [Kennedy & Eberhart, 1995] Kennedy J & Eberhart R, Particle swarm optimization. *Proceedings of the Fourth IEEE International Conference on Neural Networks, Perth, Australia, 1942–1948*, 1995.
- [Knox & Wicken, 1973] Knox KW & Wicken AJ, Immunological properties of teichoic acids. *Bacteriol Rev*, 37(2): 215–257, 1973.
- [Köller et al., 2008] Köller T, Nelson D, Nakata M, Kreutzer M, Fischetti VA, Glocker MO, Podbielski A & Kreikemeyer B, PlyC, a novel bacteriophage lysin for compartment-dependent proteomics of group A streptococci. *Proteomics*, 8(1): 140–148, 2008.
- [Kristian et al., 2005] Kristian SA, Datta V, Weidenmaier C, Kansal R, Fedtke I, Peschel A, Gallo RL & Nizet V, D-alanylation of teichoic acids promotes group A streptococcus antimicrobial peptide resistance, neutrophil survival, and epithelial cell invasion. *J Bacteriol*, 187(19): 6719–6725, 2005.

- [Kulaev et al., 1999] Kulaev I, Vagabov V & Kulakovskaya T, New aspects of inorganic polyphosphate metabolism and function. *J Biosci Bioeng*, 88(2): 111–129, 1999.
- [Lancefield, 1928] Lancefield RC, The antigenic complex of *Streptococcus hemolyticus*. I. Demonstration of a type-specific substance in extracts of *Streptococcus hemolyticus*. *J Exp Med*, 47: 9–10, 1928.
- [Lancefield, 1959] Lancefield RC, Persistence of type-specific antibodies in man following infection with group A streptococci. *J Immunol*, 110: 271–292, 1959.
- [Lancefield, 1962] Lancefield RC, Current knowledge of type-specific M antigens of group A streptococci. *J Immunol*, 89: 307–313, 1962.
- [LaPenta et al., 1994] LaPenta D, Rubens C, Chi E & Cleary PP, Group A streptococci efficiently invade human respiratory epithelial cells. *Proc Natl Acad Sci U S A*, 91(25): 12115–12119, 1994.
- [Levering et al., 2011] Levering J, Musters MW, Bekker M, Fiedler T, Bellomo D, de Vos WM, Hugenholtz J, Kreikemeyer B, Kummer U & Teusink B, Role of phosphate in the central metabolism of two lactic acid bacteria – a comparative systems biology approach. *FEBS J*, 2011, submitted.
- [Liebermeister & Klipp, 2006a] Liebermeister W & Klipp E, Bringing metabolic networks to life: convenience rate law and thermodynamic constraints. *Theor Biol Med Model*, 3: 41, 2006a.
- [Liebermeister & Klipp, 2006b] Liebermeister W & Klipp E, Bringing metabolic networks to life: integration of kinetic, metabolic, and proteomic data. *Theor Biol Med Model*, 3: 42, 2006b.
- [Linares et al., 2010] Linares DM, Kok J & Poolman B, Genome sequences of *Lactococcus lactis* MG1363 (revised) and NZ9000 and comparative physiological studies. *J. Bacteriol.*, 192: 5806–5812, 2010.
- [Lindmark et al., 1969] Lindmark DG, Paoletta P & Wood NP, The pyruvate formate-lyase system of *Streptococcus faecalis*. I. Purification and properties of the formate-pyruvate exchange enzyme. *J Biol Chem*, 244(13): 3605–3612, 1969.

- [Lopez de Felipe & Gaudu, 2009] Lopez de Felipe F & Gaudu P, Multiple control of the acetate pathway in *Lactococcus lactis* under aeration by catabolite repression and metabolites. *Appl Microbiol Biotechnol*, 82: 1115–1122, 2009.
- [Łowicka & Bełtowski, 2007] Łowicka E & Bełtowski J, Hydrogen sulfide (H₂S) – the third gas of interest for pharmacologists. *Pharmacol Rep*, 59(1): 4–24, 2007.
- [Mason et al., 1981] Mason PW, Carbone DP, Cushman RA & Waggoner AS, The importance of inorganic phosphate in regulation of energy metabolism of *Streptococcus lactis*. *J Biol Chem*, 256(4): 1861–1866, 1981.
- [Matsuno & Slade, 1970] Matsuno T & Slade H, Composition and properties of a group A streptococcal teichoic acid. *J Bacteriol*, 102: 747–752, 1970.
- [Melchiorsen et al., 2001] Melchiorsen CR, Jensen NB, Christensen B, Jokumsen KV & Villadsen J, Dynamics of pyruvate metabolism in *Lactococcus lactis*. *Biotechnol Bioeng*, 74(4): 271–279, 2001.
- [Mijakovic et al., 2002] Mijakovic I, Poncet S, Galinier A, Monedero V, Fieulaine S, Janin J, Nessler S, Marquez JA, Scheffzek K, Hasenbein S, Hengstenberg W & Deutscher J, Pyrophosphate-producing protein dephosphorylation by HPr kinase/phosphorylase: a relic of early life? *Proc Natl Acad Sci U S A*, 99(21): 13442–13447, 2002.
- [Navarre & Schneewind, 1999] Navarre WW & Schneewind O, Surface proteins of gram-positive bacteria and mechanisms of their targeting to the cell wall envelope. *Microbiol Mol Biol Rev*, 63(1): 174–229, 1999.
- [Nelson et al., 2006] Nelson D, Schuch R, Chahales P, Zhu S & Fischetti VA, PlyC: a multimeric bacteriophage lysin. *Proc Natl Acad Sci U S A*, 103(28): 10765–10770, 2006.
- [Neves et al., 2005] Neves AR, Pool WA, Kok J, Kuipers OP & Santos H, Overview on sugar metabolism and its control in *Lactococcus lactis* – the input from in vivo NMR. *FEMS Microbiol Rev*, 29(3): 531–554, 2005.
- [Neves et al., 1999] Neves AR, Ramos A, Nunes MC, Kleerebezem M, Hugenholtz J, de Vos WM, Almeida J & Santos H, In vivo nuclear magnetic resonance

- studies of glycolytic kinetics in *Lactococcus lactis*. *Biotechnol Bioeng*, 64(2): 200–212, 1999.
- [Neves et al., 2002] Neves AR, Ventura R, Mansour N, Shearman C, Gasson MJ, Maycock C, Ramos A & Santos H, Is the glycolytic flux in *Lactococcus lactis* primarily controlled by the redox charge? Kinetics of NAD⁺ and NADH pools determined in vivo by ¹³C NMR. *J Biol Chem*, 277(31): 28088–28098, 2002.
- [van Niel et al., 2004] van Niel EW, Palmfeldt J, Martin R, Paese M & Hahn-Hägerdal B, Reappraisal of the regulation of lactococcal L-lactate dehydrogenase. *Appl Environ Microbiol*, 70: 1843–1846, 2004.
- [Notebaart et al., 2006] Notebaart RA, van Enckevort FHJ, Francke C, Siezen RJ & Teusink B, Accelerating the reconstruction of genome-scale metabolic networks. *BMC Bioinformatics*, 7: 296, 2006.
- [Oh et al., 2011] Oh E, Lu M, Park C, Park C, Oh HB, Lee SY & Lee J, Dynamic modeling of lactic acid fermentation metabolism with *Lactococcus lactis*. *J Microbiol Biotechnol*, 21(2): 162–169, 2011.
- [Oliveira et al., 2005] Oliveira AP, Nielsen J & Förster J, Modeling *Lactococcus lactis* using a genome-scale flux model. *BMC Microbiol*, 5: 39, 2005.
- [Palmfeldt et al., 2004] Palmfeldt J, Paese M, Hahn-Hägerdal B & Niel EWJV, The pool of ADP and ATP regulates anaerobic product formation in resting cells of *Lactococcus lactis*. *Appl Environ Microbiol*, 70(9): 5477–5484, 2004.
- [Pancholi & Fischetti, 1992] Pancholi V & Fischetti VA, A major surface protein on group A streptococci is a glyceraldehyde-3-phosphate-dehydrogenase with multiple binding activity. *J Exp Med*, 176(2): 415–426, 1992.
- [Park et al., 2003] Park S, Schilling C & Palsson B, Compositions and methods for modeling *Bacillus subtilis* metabolism. *US Patent and Trademark Office*, 2003.
- [Pedersen et al., 2002] Pedersen MB, Koebmann BJ, Jensen PR & Nilsson D, Increasing acidification of nonreplicating *Lactococcus lactis* deltathya mutants by incorporating ATPase activity. *Appl Environ Microbiol*, 68(11): 5249–5257, 2002.

- [Poolman et al., 1987] Poolman B, Bosman B, Kiers J & Konings WN, Control of glycolysis by glyceraldehyde-3-phosphate dehydrogenase in *Streptococcus cremoris* and *Streptococcus lactis*. *J Bacteriol*, 169(12): 5887–5890, 1987.
- [Porter et al., 1982] Porter EV, Chassy BM & Holmlund CE, Purification and kinetic characterization of a specific glucokinase from *Streptococcus mutans* OMZ70 cells. *Biochim Biophys Acta*, 709(2): 178–186, 1982.
- [Postma et al., 1993] Postma PW, Lengeler JW & Jacobson GR, Phosphoenolpyruvate:carbohydrate phosphotransferase systems of bacteria. *Microbiol Rev*, 57(3): 543–594, 1993.
- [Price et al., 2004] Price ND, Reed JL & Palsson B, Genome-scale models of microbial cells: evaluating the consequences of constraints. *Nat Rev Microbiol*, 2(11): 886–897, 2004.
- [Reizer et al., 1985] Reizer J, Deutscher J, Sutrina S, Thompson J & M H Saier J, Sugar accumulation in gram-positive bacteria: Exclusion and expulsion mechanisms. *Trends in Biochemical Sciences*, 10(1): 32–34, 1985.
- [Reizer et al., 1984] Reizer J, Novotny MJ, Hengstenberg W & Saier MH, Properties of ATP-dependent protein kinase from *Streptococcus pyogenes* that phosphorylates a seryl residue in HPr, a phosphocarrier protein of the phosphotransferase system. *J Bacteriol*, 160(1): 333–340, 1984.
- [Reizer & Panos, 1980] Reizer J & Panos C, Regulation of beta-galactoside phosphate accumulation in *Streptococcus pyogenes* by an expulsion mechanism. *Proc Natl Acad Sci U S A*, 77(9): 5497–5501, 1980.
- [Reizer & Saier, 1983] Reizer J & Saier MH, Involvement of lactose enzyme II of the phosphotransferase system in rapid expulsion of free galactosides from *Streptococcus pyogenes*. *J Bacteriol*, 156(1): 236–242, 1983.
- [Reizer & Saier, 1987] Reizer J & Saier MH, Mechanism and regulation of phosphate transport in *Streptococcus pyogenes*. *J Bacteriol*, 169(1): 297–302, 1987.
- [Remm et al., 2001] Remm M, Storm CE & Sonnhammer EL, Automatic clustering of orthologs and in-paralogs from pairwise species comparisons. *J Mol Biol*, 314(5): 1041–1052, 2001.

- [Ren et al., 2004] Ren Q, Kang KH & Paulsen IT, TransportDB: a relational database of cellular membrane transport systems. *Nucleic Acids Res*, 32(Database issue): D284–D288, 2004.
- [Ricci, 2000] Ricci JCD, ADP modulates the dynamic behavior of the glycolytic pathway of *Escherichia coli*. *Biochem Biophys Res Commun*, 271(1): 244–249, 2000.
- [Romantsov et al., 2009] Romantsov T, Guan Z & Wood JM, Cardiolipin and the osmotic stress responses of bacteria. *Biochim Biophys Acta*, 1788(10): 2092–2100, 2009.
- [van Rossum, 1995] van Rossum G, Python reference manual. *CWI Report*, 1995.
- [Russell et al., 1996] Russell JB, Bond DR & Cook GM, The fructose diphosphate/phosphate regulation of carbohydrate metabolism in low G + C gram-positive anaerobes. *Res Microbiol*, 147(6-7): 528–535, 1996.
- [Schaefer et al., 1999] Schaefer U, Boos W, Takors R & Weuster-Botz D, Automated sampling device for monitoring intracellular metabolite dynamics. *Anal Biochem*, 270(1): 88–96, 1999.
- [Schomburg et al., 2002] Schomburg I, Chang A & Schomburg D, BRENDA, enzyme data and metabolic information. *Nucleic Acids Res*, 30(1): 47–49, 2002.
- [Schrager et al., 1996] Schrager HM, Rheinwald JG & Wessels MR, Hyaluronic acid capsule and the role of streptococcal entry into keratinocytes in invasive skin infection. *J Clin Invest*, 98(9): 1954–1958, 1996.
- [Seltmann & Holst, 2002] Seltmann G & Holst O, *The bacterial cell wall*. Springer, Berlin, 2002.
- [Sherrill & Fahey, 1998] Sherrill C & Fahey RC, Import and metabolism of glutathione by *Streptococcus mutans*. *J Bacteriol*, 180(6): 1454–1459, 1998.
- [Simon & Hofer, 1981] Simon WA & Hofer HW, Phosphofructokinases from *Lactobacteriaceae*. II. Purification and properties of phosphofructokinase from *Streptococcus thermophilus*. *Biochim Biophys Acta*, 661(1): 158–163, 1981.

- [Slabyj & Panos, 1973] Slabyj BM & Panos C, Teichoic acid of a stabilized L-form of *Streptococcus pyogenes*. *J Bacteriol*, 114(3): 934–942, 1973.
- [Slabyj & Panos, 1976] Slabyj BM & Panos C, Membrane lipoteichoic acid of *Streptococcus pyogenes* and its stabilized L-form and the effect of two antibiotics upon its cellular content. *J Bacteriol*, 127(2): 855–862, 1976.
- [Slade et al., 1951] Slade HD, Knox GA & Slamp WC, The amino acid nutrition of group A hemolytic *Streptococci*, with reference to the effect of glutathione on the cystine requirement. *J Bacteriol*, 62(5): 669–675, 1951.
- [Smacchi & Gobbetti, 1998] Smacchi E & Gobbetti M, Purification and characterization of cystathionine gamma-lyase from *Lactobacillus fermentum* DT41. *FEMS Microbiol Lett*, 166(2): 197–202, 1998.
- [Snoep et al., 1990] Snoep JL, de Mattos MJT, Postma PW & Neijssel OM, Involvement of pyruvate dehydrogenase in product formation in pyruvate-limited anaerobic chemostat cultures of *Enterococcus faecalis* NCTC 775. *Arch Microbiol*, 154(1): 50–55, 1990.
- [Solem et al., 2008] Solem C, Koebmann B & Jensen PR, Control analysis of the role of triosephosphate isomerase in glucose metabolism in *Lactococcus lactis*. *IET Syst Biol*, 2(2): 64–72, 2008.
- [Sommer et al., 1985] Sommer P, Klein JP, Schöller M & Frank RM, Lactate dehydrogenase from *Streptococcus mutans*: purification, characterization, and crossed antigenicity with lactate dehydrogenases from *Lactobacillus casei*, *Actinomyces viscosus*, and *Streptococcus sanguis*. *Infect Immun*, 47(2): 489–495, 1985.
- [Stille et al., 2005] Stille W, Brodt HR, Groll A & Just-Nübling G, *Antibiotika-Therapie: Klinik und Praxis der antiinfektiösen Behandlung*. Schattauer, 2005.
- [Sutrina et al., 1988] Sutrina SL, Reizer J & Saier MH, Inducer expulsion in *Streptococcus pyogenes*: properties and mechanism of the efflux reaction. *J Bacteriol*, 170(4): 1874–1877, 1988.

- [Sutton & Marquis, 1987] Sutton SV & Marquis RE, Membrane-associated and solubilized ATPases of *Streptococcus mutans* and *Streptococcus sanguis*. *J Dent Res*, 66(6): 1095–1098, 1987.
- [Swoboda et al., 2010] Swoboda JG, Campbell J, Meredith TC & Walker S, Wall teichoic acid function, biosynthesis, and inhibition. *Chembiochem*, 11(1): 35–45, 2010.
- [Takahashi et al., 1982] Takahashi S, Abbe K & Yamada T, Purification of pyruvate formate-lyase from *Streptococcus mutans* and its regulatory properties. *J Bacteriol*, 149(3): 1034–1040, 1982.
- [Tao et al., 1992] Tao L, LeBlanc DJ & Ferretti JJ, Novel streptococcal-integration shuttle vectors for gene cloning and inactivation. *Gene*, 120(1): 105–110, 1992.
- [Tempest & Neijssel, 1984] Tempest DW & Neijssel OM, The status of YATP and maintenance energy as biologically interpretable phenomena. *Annu Rev Microbiol*, 38: 459–486, 1984.
- [Teusink et al., 2005] Teusink B, van Enckevort FHJ, Francke C, Wiersma A, Wegkamp A, Smid EJ & Siezen RJ, In silico reconstruction of the metabolic pathways of *Lactobacillus plantarum*: comparing predictions of nutrient requirements with those from growth experiments. *Appl Environ Microbiol*, 71(11): 7253–7262, 2005.
- [Teusink et al., 2000] Teusink B, Passarge J, Reijenga CA, Esgalhado E, van der Weijden CC, Schepper M, Walsh MC, Bakker BM, van Dam K, Westerhoff HV & Snoep JL, Can yeast glycolysis be understood in terms of in vitro kinetics of the constituent enzymes? Testing biochemistry. *Eur J Biochem*, 267(17): 5313–5329, 2000.
- [Teusink et al., 2006] Teusink B, Wiersma A, Molenaar D, Francke C, de Vos WM, Siezen RJ & Smid EJ, Analysis of growth of *Lactobacillus plantarum* WCFS1 on a complex medium using a genome-scale metabolic model. *J Biol Chem*, 281(52): 40041–40048, 2006.
- [Thevenot et al., 1995] Thevenot T, Brochu D, Vadeboncoeur C & Hamilton IR, Regulation of ATP-dependent P-(Ser)-HPr formation in *Streptococcus mutans* and *Streptococcus salivarius*. *J Bacteriol*, 177(10): 2751–2759, 1995.

- [Thomas et al., 1979] Thomas TD, Ellwood EC & Longyear VM, Change from homo- to heterolactic fermentation by *Streptococcus lactis* resulting from glucose limitation in anaerobic chemostat cultures. *J Bacteriol*, 138: 109–117, 1979.
- [Thompson, 1978] Thompson J, In vivo regulation of glycolysis and characterization of sugar: phosphotransferase systems in *Streptococcus lactis*. *J Bacteriol*, 136(2): 465–476, 1978.
- [Thompson & Saier, 1981] Thompson J & Saier MH, Regulation of methyl-beta-d-thiogalactopyranoside-6-phosphate accumulation in *Streptococcus lactis* by exclusion and expulsion mechanisms. *J Bacteriol*, 146(3): 885–894, 1981.
- [Thompson & Torchia, 1984] Thompson J & Torchia DA, Use of ^{31}P nuclear magnetic resonance spectroscopy and ^{14}C fluorography in studies of glycolysis and regulation of pyruvate kinase in *Streptococcus lactis*. *J Bacteriol*, 158(3): 791–800, 1984.
- [Tittsler et al., 1952] Tittsler RP, Pederson CS, Snell EE, Hendlin D & Niven CF, Symposium on the lactic acid bacteria. *Bacteriol Rev*, 16(4): 227–260, 1952.
- [Todar, 2011] Todar K, Todar's Online Textbook of Bacteriology. 2011, URL <http://www.textbookofbacteriology.net>.
- [UniProt Consortium, 2010] UniProt Consortium, The Universal Protein Resource (UniProt) in 2010. *Nucleic Acids Res*, 38(Database issue): D142–D148, 2010.
- [Vadeboncoeur et al., 1991] Vadeboncoeur C, Brochu D & Reizer J, Quantitative determination of the intracellular concentration of the various forms of HPr, a phosphocarrier protein of the phosphoenolpyruvate: sugar phosphotransferase system in growing cells of oral streptococci. *Anal Biochem*, 196(1): 24–30, 1991.
- [Varma & Palsson, 1994] Varma A & Palsson BO, Stoichiometric flux balance models quantitatively predict growth and metabolic by-product secretion in wild-type *Escherichia coli* W3110. *Appl Environ Microbiol*, 60(10): 3724–3731, 1994.

- [Voit et al., 2006a] Voit EO, Almeida J, Marino S, Lall R, Goel G, Neves AR & Santos H, Regulation of glycolysis in *Lactococcus lactis*: an unfinished systems biological case study. *Syst Biol (Stevenage)*, 153(4): 286–298, 2006a.
- [Voit et al., 2006b] Voit EO, Neves AR & Santos H, The intricate side of systems biology. *Proc Natl Acad Sci USA*, 103(4): 9452–9457, 2006b.
- [Westerhoff & Chen, 1984] Westerhoff HV & Chen YD, How do enzyme activities control metabolite concentrations? An additional theorem in the theory of metabolic control. *Eur J Biochem*, 142(2): 425–430, 1984.
- [Winkler & Wilson, 1966] Winkler HH & Wilson TH, The role of energy coupling in the transport of beta-galactosides by *Escherichia coli*. *J Biol Chem*, 241(10): 2200–2211, 1966.
- [Wittenberger & Angelo, 1970] Wittenberger CL & Angelo N, Purification and properties of a fructose-1,6-diphosphate-activated lactate dehydrogenase from *Streptococcus faecalis*. *J Bacteriol*, 101(3): 717–724, 1970.
- [Wittig et al., 2006] Wittig U, Golebiewski M, Kania R, Krebs O, Mir S, Weidemann A, Anstein S, Saric J & Rojas I, SABIO-RK: Integration and curation of reaction kinetics data. In: *In proceedings of the 3rd International workshop on Data Integration in the Life Sciences 2006 (DILS'06)*. Hinxton, UK. *Lecture Notes in Bioinformatics*, vol. 4075, 94–103, 2006.
- [Wolpert & Macready, 1997] Wolpert DH & Macready WG, No free lunch theorems for optimization. *IEEE Trans. Evol. Comp.*, 1: 67–82, 1997.
- [Yamada & Carlsson, 1975a] Yamada T & Carlsson J, Glucose-6-phosphate-dependent pyruvate kinase in *Streptococcus mutans*. *J Bacteriol*, 124(1): 562–563, 1975a.
- [Yamada & Carlsson, 1975b] Yamada T & Carlsson J, Regulation of lactate dehydrogenase and change of fermentation products in streptococci. *J Bacteriol*, 124(1): 55–61, 1975b.
- [Ye, 1996] Ye J, Regulation of carbohydrate transport in *Lactococcus* and *Lactobacillus*. *Res Microbiol*, 147(6-7): 523–527, 1996.

- [Ye et al., 1996] Ye J, Minarcik J & Saier MJ, Inducer expulsion and the occurrence of an HPr(Ser-P)-activated sugar-phosphate phosphatase in *Enterococcus faecalis* and *Streptococcus pyogenes*. *Microbiology*, 142: 585–592, 1996.

Acknowledgements

This thesis would not have been possible without the support and the help of several individuals who contributed and extended their valuable assistance in the preparation and completion of this study.

First and foremost I offer my sincerest gratitude to my supervisor, Ursula Kummer, for her sincerity, the support throughout my thesis and the steadfast encouragement to complete this study whilst allowing me scope for my scientific development.

I would like to thank Mark Musters for providing the model of *L. lactis* as a blueprint and for the insights he has shared. Especially at the beginning of my PhD and while writing our paper he was a great convenience.

I wish to show my gratitude to Tomas Fiedler, Araz Zeyniyev and Martijn Bekker who provided me with experimental data and answered all my endless questions about the experimental set-up. In particular, I would like to thank Tomas Fiedler for measuring extracellular metabolites and amino acids in continuous culture, cloning enzymes and measuring the kinetics *in vitro*, Araz Zeyniyev for performing amino acid leave-out experiments and Martijn Bekker for doing the glucose-pulse and fermentation experiments.

I owe my deepest gratitude to Bas Teusink for giving me the opportunity to work with him in Amsterdam for two weeks and his assistance in the development of the *S. pyogenes* genome-scale model. He saved me a lot of time and frustration with sharing his experience in developing a genome-scale model and his knowledge about biochemical pathways. Furthermore, he provided helpful literature as well as the genome-scale models of *L. plantarum* and *L. lactis* which were indispensable during the reconstruction process.

I would like to thank Domenico Bellomo for detailed review, constructive criticism and excellent advice regarding our manuscript but also the model.

Last but not least I would like to thank my colleagues in the Modelling of Bio-

logical Processes Department for their support, help and fruitful discussions; Brett Olivier for implementing the flux balance analysis in Python and preparing a framework to simulate the genome-scale model; Michiel Wels for providing the AUTOGRAPH output; Nadine Veith and Susanne Roth for extensive literature search on *S. pyogenes*.

This work was part of research conducted for the SysMO-LAB project. It was funded by the Federal Ministry of Education and Research (BMBF), Germany; the Netherlands Organization for Scientific Research (NWO); the Research Council of Norway (RCN); and the United Kingdom Biotechnology and Biological Research Council (BBSRC).

Appendix A

Glycolytic model of *S. pyogenes*

A.1 Kinetic parameters and initial concentrations	156
A.2 Rate laws, differential equations and moiety conservation	162
A.3 Results from sensitivity analysis	168

A.1 Kinetic parameters and initial concentrations

Initial estimates of the parameters were obtained from literature, as indicated. Parameter fitting was performed to tune the parameters to fit our own profiles.

Table A.1: Velocity constants (in $\frac{\text{mM}}{\text{s}}$). Parameters with missing reference from literature are indicated by “-”. Exemplary the parameters of one of the 50 fitted models are shown.

Variable	Original	Optimised	Reference
V_{\max}^{PTS}	0.49	26.83	[Cvitkovitch et al., 1995]
V_{\max}^{GlcP}	0.007	0.0001	[Cvitkovitch et al., 1995]
V_{\max}^{HPrP}	-	464.6	-
V_{\max}^{HPrK}	-	399.02	-
V_{\max}^{GK}	4.40	0.57	[Porter et al., 1982]
V_{\max}^{PFK}	1.66	16.44	[Simon & Hofer, 1981]
V_{\max}^{PaseII}	0.175	0.92	[Ye et al., 1996]
V_{\max}^{FBA}	71.43	713.97	[Crow & Pritchard, 1982]
V_{\max}^{GAPDH}	8.12	72.32	[Pancholi & Fischetti, 1992]
V_{\max}^{GAPN}	6.06	2.06	[Iddar et al., 2003]
V_{\max}^{ENO}	2.23	3.82	[Brown et al., 1998]
V_{\max}^{PYK}	9.72	78.38	[Hoefnagel et al., 2002b]
V_{\max}^{LDH}	2.46	11.22	[Sommer et al., 1985]
V_{\max}^{LacT}	-	433.63	-
V_{\max}^{PFL}	1.53	12.16	[Takahashi et al., 1982]
V_{\max}^{ACK}	8.93	735.64	[Hoefnagel et al., 2002b]
V_{\max}^{ADH}	1.93	59.79	[Hoefnagel et al., 2002b]
V_{\max}^{PiT}	0.35	0.03	[Reizer & Saier, 1987]
$V_{\max}^{\text{PiTactive}}$	-	0.01	-
V_{\max}^{ATPase}	2.73	25.84	[Sutton & Marquis, 1987]
V_{\max}^{NPOX}	-	295.68	-

Table A.2: Reversible processes: K_{eq} . These parameters were not optimised.

Variable	Value	Reference
K_{eq}^{FBA}	0.056	[Andersen et al., 2009]
K_{eq}^{GAPDH}	0.0007	[Andersen et al., 2009]
K_{eq}^{ENO}	27.55	[Andersen et al., 2009]
K_{eq}^{PYK}	6500	[Andersen et al., 2009]
K_{eq}^{LDH}	36000	[Andersen et al., 2009]
K_{eq}^{PFL}	650	[Andersen et al., 2009]

Table A.3: Michaelis constants: K_m (mM). Parameters with missing reference from literature are indicated by “-”. Exemplary the parameters of one of the 50 fitted models are shown.

Variable	Original	Optimised	Reference
$K_{m\text{ glucose}_{ex}}^{PTS}$	0.0068	0.0007	[Cvitkovitch et al., 1995]
$K_{m\text{ HPr}}^{PTS}$	-	12.22	-
$K_{m\text{ PEP}}^{PTS}$	-	1.08	-
$K_{m\text{ pyruvate}}^{PTS}$	-	14.09	-
$K_{m\text{ HPr}}^{PTS}$	-	74.43	-
$K_{m\text{ G6P}}^{PTS}$	-	43.66	-
$K_{m\text{ HPr}}^{HPrK}$	0.066	0.42	[Reizer et al., 1984]
$K_{m\text{ ATP}}^{HPrK}$	0.061	0.02	[Reizer et al., 1984]
$K_{m\text{ HPr-ser-P}}^{HPrK}$	-	79.01	-
$K_{m\text{ ADP}}^{HPrK}$	-	0.65	-
$K_{m\text{ HPr-ser-P}}^{HPrP}$	-	13.16	-
$K_{m\text{ HPr}}^{HPrP}$	-	26.05	-
$K_{m\text{ P}_i}^{HPrP}$	-	0.52	-
$K_{m\text{ glucose}}^{GK}$	0.61	2.70	[Porter et al., 1982]
$K_{m\text{ ATP}}^{GK}$	0.21	1.46	[Porter et al., 1982]
$K_{m\text{ G6P}}^{GK}$	-	0.01	-
$K_{m\text{ ADP}}^{GK}$	-	0.58	-
$K_{m\text{ G6P}}^{PFK}$	1.44	7.61	[Simon & Hofer, 1981]

TableA.3 – continued from previous page

Variable	Original	Optimised	Reference
$K_{m\text{ATP}}^{\text{PFK}}$	5.8	0.25	[Hoefnagel et al., 2002b]
$K_{m\text{FBP}}^{\text{PFK}}$	0.23	58.00	[Simon & Hofer, 1981]
$K_{m\text{ADP}}^{\text{PFK}}$	0.3	0.27	[Hoefnagel et al., 2002b]
$K_{m\text{G6P}}^{\text{PaseII}}$	-	0.01	-
$K_{m\text{glucose}}^{\text{PaseII}}$	-	60.23	-
$K_{m\text{P}_i}^{\text{PaseII}}$	-	5.80	-
$K_{m\text{FBP}}^{\text{FBA}}$	1.1	0.63	[Crow & Pritchard, 1982]
$K_{m\text{triose-P}}^{\text{FBA}}$	2.8	4.46	[Hoefnagel et al., 2002b]
$K_{m\text{triose-P}}^{\text{GAPDH}}$	1.33	0.79	[Crow & Wittenberger, 1979]
$K_{m\text{NAD}}^{\text{GAPDH}}$	0.16	0.17	[Crow & Wittenberger, 1979]
$K_{m\text{P}_i}^{\text{GAPDH}}$	1.44	0.30	[Crow & Wittenberger, 1979]
$K_{m\text{BPG}}^{\text{GAPDH}}$	0.05	0.43	[Hoefnagel et al., 2002b]
$K_{m\text{NADH}}^{\text{GAPDH}}$	0.067	0.12	[Hoefnagel et al., 2002b]
$K_{m\text{triose-P}}^{\text{GAPN}}$	0.67	6.69	[Iddar et al., 2002]
$K_{m\text{NADP}}^{\text{GAPN}}$	0.39	3.90	[Iddar et al., 2002]
$K_{m\text{PEP}}^{\text{GAPN}}$	-	97.97	-
$K_{m\text{NADPH}}^{\text{GAPN}}$	-	2.99	-
$K_{m\text{BPG}}^{\text{ENO}}$	0.44	0.15	[Brown et al., 1998]
$K_{m\text{ADP}}^{\text{ENO}}$	0.53	0.02	[Hoefnagel et al., 2002b]
$K_{m\text{PEP}}^{\text{ENO}}$	0.2	1.12	[Hoefnagel et al., 2002b]
$K_{m\text{ATP}}^{\text{ENO}}$	0.3	2.98	[Hoefnagel et al., 2002b]
$K_{m\text{PEP}}^{\text{PYK}}$	0.69	1.12	T. Fiedler (Section 3.1.4)
$K_{m\text{ADP}}^{\text{PYK}}$	21	7.45	T. Fiedler (Section 3.1.4)
$K_{m\text{pyruvate}}^{\text{PYK}}$	0.75	12.22	T. Fiedler (Section 3.1.4)
$K_{m\text{ATP}}^{\text{PYK}}$	10	92.89	T. Fiedler (Section 3.1.4)
$K_{m\text{pyruvate}}^{\text{LDH}}$	0.41	0.04	T. Fiedler (Section 3.1.4)
$K_{m\text{NADH}}^{\text{LDH}}$	8.8	0.01	T. Fiedler (Section 3.1.4)

TableA.3 – continued from previous page

Variable	Original	Optimised	Reference
$K_{m \text{ lactate}}^{\text{LDH}}$	0.062	83.31	T. Fiedler (Section 3.1.4)
$K_{m \text{ NAD}}^{\text{LDH}}$	0.152	1.12	T. Fiedler (Section 3.1.4)
$K_{m \text{ lactate}}^{\text{LacT}}$	2	6.41	[Harold & Levin, 1974]
$K_{m \text{ lactate}_{\text{ex}}}^{\text{LacT}}$	1.93	33.84	[Harold & Levin, 1974]
$K_{m \text{ pyruvate}}^{\text{PFL}}$	5.4	53.98	[Takahashi et al., 1982]
$K_{m \text{ CoA}}^{\text{PFL}}$	0.02	0.15	[Takahashi et al., 1982]
$K_{m \text{ acetylCoA}}^{\text{PFL}}$	0.05	0.37	[Hoefnagel et al., 2002b]
$K_{m \text{ formate}}^{\text{PFL}}$	24	47.69	[Hoefnagel et al., 2002b]
$K_{m \text{ acetylCoA}}^{\text{ACK}}$	0.06	0.02	[Hoefnagel et al., 2002b]
$K_{m \text{ P}_i}^{\text{ACK}}$	5	9.68	[Hoefnagel et al., 2002b]
$K_{m \text{ ADP}}^{\text{ACK}}$	0.5	3.86	[Hoefnagel et al., 2002b]
$K_{m \text{ acetate}}^{\text{ACK}}$	7	12.84	[Hoefnagel et al., 2002b]
$K_{m \text{ CoA}}^{\text{ACK}}$	0.1	0.24	[Hoefnagel et al., 2002b]
$K_{m \text{ ATP}}^{\text{ACK}}$	7	64.13	[Hoefnagel et al., 2002b]
$K_{m \text{ acetylCoA}}^{\text{ADH}}$	0.007	0.03	[Hoefnagel et al., 2002b]
$K_{m \text{ NADH}}^{\text{ADH}}$	0.025	0.05	[Hoefnagel et al., 2002b]
$K_{m \text{ ethanol}}^{\text{ADH}}$	1	1.94	[Hoefnagel et al., 2002b]
$K_{m \text{ NAD}}^{\text{ADH}}$	0.08	0.03	[Hoefnagel et al., 2002b]
$K_{m \text{ CoA}}^{\text{ADH}}$	0.008	0.07	[Hoefnagel et al., 2002b]
$K_{m \text{ P}_i \text{ ex}}^{\text{PiT}}$	1.1	5.75	[Reizer & Saier, 1987]
$K_{m \text{ P}_i}^{\text{PiT}}$	5	0.79	[Reizer & Saier, 1987]
$K_{m \text{ P}_i \text{ ex}}^{\text{PiTactive}}$	-	71.18	-
$K_{m \text{ ATP}}^{\text{PiTactive}}$	-	55.66	-
$K_{m \text{ P}_i}^{\text{PiTactive}}$	-	8.12	-
$K_{m \text{ ADP}}^{\text{PiTactive}}$	-	5.77	-
$K_{m \text{ ATP}}^{\text{ATPase}}$	0.9	5.26	[Sutton & Marquis, 1987]
$K_{m \text{ NADPH}}^{\text{NPOX}}$	-	9.32	-

Table A.3 – continued from previous page

Variable	Original	Optimised	Reference
K_{mNADP}^{NPOX}	-	99.46	-

Table A.4: Allosteric regulation binding constants (mM). Exemplary the parameters of one of the 50 fitted models are shown.

Variable	Optimised	Reference
K_{aPi}^{HPrP}	0.04	[Reizer et al., 1984]
K_{iATP}^{HPrP}	20.01	[Reizer et al., 1984]
K_{aFBP}^{HPrK}	86.97	[Crow & Pritchard, 1976]
K_{iPi}^{HPrK}	1.03	[Crow & Pritchard, 1976]
K_{iG6P}^{GK}	0.02	[Porter et al., 1982]
K_{iADP}^{GK}	0.05	[Porter et al., 1982]
$K_{aHPr-ser-P}^{PaseII}$	25.15	[Ye et al., 1996]
K_{iNADH}^{GAPDH}	44.59	[Pancholi & Fischetti, 1992]
K_{aG6P}^{PYK}	6.97	[Yamada & Carlsson, 1975a]
K_{iPi}^{PYK}	72.05	[Yamada & Carlsson, 1975a]
K_{aFBP}^{LDH}	58.57	T. Fiedler (Section 3.1.4
K_{aPi}^{LDH}	0.03	T. Fiedler (Section 3.1.4
K_{iNAD}^{LDH}	67.24	T. Fiedler (Section 3.1.4
$K_{i\text{pyruvate}}^{LacT}$	1.10	[Harold & Levin, 1974]
$K_{i\text{trioseP}}^{PFL}$	0.08	[Takahashi et al., 1982]
K_{iFBP}^{ACK}	7.42	[Lopez de Felipe & Gaudu, 2009]
K_{iATP}^{ADH}	8.13	[Palmfeldt et al., 2004]
$K_{aPi\text{extra}}^{PiT}$	90.15	[Reizer & Saier, 1987]
K_{iATP}^{PiT}	16.04	[Reizer & Saier, 1987]

Table A.5: Hill coefficients. This parameter was not optimised.

Variable	Value	Reference
n_{ATPase}	3	[Andersen et al., 2009]

Table A.6: Initial concentrations (mM) for 0, 10 and 50 mM extracellular phosphate. Exemplary the parameters of one of the 50 fitted models are shown.

Species	Optimised		
	$P_i^{\text{ex}} = 0 \text{ mM}$	$P_i^{\text{ex}} = 10 \text{ mM}$	$P_i^{\text{ex}} = 50 \text{ mM}$
G6P	0.36	0.21	0.07
FBP	0.12	0.12	0.25
Triose-P	3.64	1.13	1.10
BPG	0	0	0
PEP	9.99	1.06	1.11
Pyruvate	0.46	0.02	0.11
Acetyl-CoA	0	0	0
P_i	2.06	4.49	4.41
ADP	4.74	4.87	4.83
ATP	0.26	0.14	0.17
NAD	3.50	6.97	9.89
NADH	0	0	0
CoA	1.17	4.51	4.81
Lactate	0	0	0
Glucose	0	0	0
HPr-ser-P	0	0	0
HPr	0.16	0.16	0.16
NADP	6.97	1.00	8.77
NADPH	0	0	0
Glucose ^{ex}	8.08	5.26	8.44
Lactate ^{ex}	2.76	1.90	2.34
P_i^{ex}	0	10	50
Formate	0	0	0
Ethanol	0	0	0
Acetate	0.43	0.49	0.45

A.2 Rate laws, differential equations and moiety conservation

Due to unknown enzyme mechanism convenience kinetics were used for most reactions (see Section 2.2.3) [Liebermeister & Klipp, 2006b]. The kinetic laws and the differential equations of the *S. pyogenes* glycolytic model are described in the following.

A.2.1 Rate laws

$$v_{\text{PTS}} = \frac{V_{\text{max}}^{\text{PTS}} \cdot \frac{[\text{HPr}]}{K_{\text{m HPr}}^{\text{PTS}}} \cdot \frac{[\text{PEP}]}{K_{\text{m PEP}}^{\text{PTS}}} \cdot \frac{[\text{glucose}_{\text{ex}}]}{K_{\text{m glucose}_{\text{ex}}}^{\text{PTS}}}}{\left(1 + \frac{[\text{HPr}]}{K_{\text{m HPr}}^{\text{PTS}}}\right) \cdot \left(1 + \frac{[\text{PEP}]}{K_{\text{m PEP}}^{\text{PTS}}}\right) \cdot \left(1 + \frac{[\text{glucose}_{\text{ex}}]}{K_{\text{m glucose}_{\text{ex}}}^{\text{PTS}}}\right) + \left(1 + \frac{[\text{HPr}]}{K_{\text{m HPr}}^{\text{PTS}}}\right) \cdot \left(1 + \frac{[\text{pyruvate}]}{K_{\text{m pyruvate}}^{\text{PTS}}}\right) \cdot \left(1 + \frac{[\text{G6P}]}{K_{\text{m G6P}}^{\text{PTS}}}\right) - 1}$$

$$v_{\text{GlcP}} = V_{\text{max}}^{\text{GlcP}} \cdot ([\text{glucose}_{\text{ex}}] - [\text{glucose}])$$

$$v_{\text{HPrK}} = \frac{K_{\text{i Pi}}^{\text{HPrK}}}{K_{\text{i Pi}}^{\text{HPrK}} + [\text{P}_i]} \cdot \frac{[\text{FBP}]}{K_{\text{a FBP}}^{\text{HPrK}} + [\text{FBP}]} \cdot \frac{V_{\text{max}}^{\text{HPrK}} \cdot \frac{[\text{HPr}]}{K_{\text{m HPr}}^{\text{HPrK}}} \cdot \frac{[\text{ATP}]}{K_{\text{m ATP}}^{\text{HPrK}}}}{\left(1 + \frac{[\text{HPr}]}{K_{\text{m HPr}}^{\text{HPrK}}}\right) \cdot \left(1 + \frac{[\text{ATP}]}{K_{\text{m ATP}}^{\text{HPrK}}}\right) + \left(1 + \frac{[\text{HPr} - \text{ser} - \text{P}]}{K_{\text{m HPr} - \text{ser} - \text{P}}^{\text{HPrK}}}\right) \cdot \left(1 + \frac{[\text{ADP}]}{K_{\text{m ADP}}^{\text{HPrK}}}\right) - 1}$$

$$v_{\text{HPrP}} = \frac{K_{\text{i ATP}}^{\text{HPrP}}}{K_{\text{i ATP}}^{\text{HPrP}} + [\text{ATP}]} \cdot \frac{[\text{P}_i]}{K_{\text{a FBP}}^{\text{HPrP}} + [\text{P}_i]} \cdot \frac{V_{\text{max}}^{\text{HPrP}} \cdot \frac{[\text{HPr} - \text{ser} - \text{P}]}{K_{\text{m HPr} - \text{ser} - \text{P}}^{\text{HPrP}}}}{\frac{[\text{HPr} - \text{ser} - \text{P}]}{K_{\text{m HPr} - \text{ser} - \text{P}}^{\text{HPrP}}} + \left(1 + \frac{[\text{HPr}]}{K_{\text{m HPr}}^{\text{HPrP}}}\right) \cdot \left(1 + \frac{[\text{P}_i]}{K_{\text{m P}_i}^{\text{HPrP}}}\right)}$$

$$v_{\text{GK}} = \frac{K_{\text{i G6P}}^{\text{GK}}}{K_{\text{i G6P}}^{\text{GK}} + [\text{G6P}]} \cdot \frac{K_{\text{i ADP}}^{\text{GK}}}{K_{\text{i ADP}}^{\text{GK}} + [\text{ADP}]} \cdot \frac{V_{\text{max}}^{\text{GK}} \cdot \frac{[\text{glucose}]}{K_{\text{m glucose}}^{\text{GK}}} \cdot \frac{[\text{ATP}]}{K_{\text{m ATP}}^{\text{GK}}}}{\left(1 + \frac{[\text{glucose}]}{K_{\text{m glucose}}^{\text{GK}}}\right) \cdot \left(1 + \frac{[\text{ATP}]}{K_{\text{m ATP}}^{\text{GK}}}\right) + \left(1 + \frac{[\text{G6P}]}{K_{\text{m G6P}}^{\text{GK}}}\right) \cdot \left(1 + \frac{[\text{ADP}]}{K_{\text{m ADP}}^{\text{GK}}}\right) - 1}$$

$$v_{\text{PFK}} = \frac{V_{\text{max}}^{\text{PFK}} \cdot \frac{[\text{G6P}]}{K_{\text{m G6P}}^{\text{PFK}}} \cdot \frac{[\text{ATP}]}{K_{\text{m ATP}}^{\text{PFK}}}}{\left(1 + \frac{[\text{G6P}]}{K_{\text{m G6P}}^{\text{PFK}}}\right) \cdot \left(1 + \frac{[\text{ATP}]}{K_{\text{m ATP}}^{\text{PFK}}}\right) + \left(1 + \frac{[\text{FBP}]}{K_{\text{m FBP}}^{\text{PFK}}}\right) \cdot \left(1 + \frac{[\text{ADP}]}{K_{\text{m ADP}}^{\text{PFK}}}\right) - 1}$$

$$v_{\text{PaseII}} = \frac{[\text{HPr} - \text{ser} - \text{P}]}{K_{\text{a HPr-ser-P}}^{\text{PaseII}} + [\text{HPr} - \text{ser} - \text{P}]} \cdot \frac{V_{\text{max}}^{\text{PaseII}} \cdot \frac{[\text{G6P}]}{K_{\text{m G6P}}^{\text{PaseII}}}}{\frac{[\text{G6P}]}{K_{\text{m G6P}}^{\text{PaseII}}} + \left(1 + \frac{[\text{glucose}]}{K_{\text{m glucose}}^{\text{PaseII}}}\right) \cdot \left(1 + \frac{[\text{P}_i]}{K_{\text{m P}_i}^{\text{PaseII}}}\right)}$$

$$v_{\text{FBA}} = \frac{V_{\text{max}}^{\text{FBA}} \cdot \frac{[\text{FBP}]}{K_{\text{m FBP}}^{\text{FBA}}} - \frac{V_{\text{max}}^{\text{FBA}}}{K_{\text{eq}}^{\text{FBA}}} \cdot \left(\frac{[\text{triose} - \text{P}]}{K_{\text{m triose-P}}^{\text{FBA}}}\right)^2}{1 + \frac{[\text{FBP}]}{K_{\text{m FBP}}^{\text{FBA}}} + \frac{[\text{triose} - \text{P}]}{K_{\text{m triose-P}}^{\text{FBA}}} + \left(\frac{[\text{triose} - \text{P}]}{K_{\text{m triose-P}}^{\text{FBA}}}\right)^2}$$

$$v_{\text{GAPDH}} = \frac{K_{\text{i NADH}}^{\text{GAPDH}}}{K_{\text{i NADH}}^{\text{GAPDH}} + [\text{NADH}]} \cdot \frac{V_{\text{max}}^{\text{GAPDH}} \cdot \frac{[\text{triose} - \text{P}]}{K_{\text{m triose-P}}^{\text{GAPDH}}} \cdot \frac{[\text{NAD}]}{K_{\text{m NAD}}^{\text{GAPDH}}} \cdot \frac{[\text{P}_i]}{K_{\text{m P}_i}^{\text{GAPDH}}} - \frac{V_{\text{max}}^{\text{GAPDH}}}{K_{\text{eq}}^{\text{GAPDH}}} \cdot \frac{[\text{BPG}]}{K_{\text{m BPG}}^{\text{GAPDH}}} \cdot \frac{[\text{NADH}]}{K_{\text{m NADH}}^{\text{GAPDH}}}}{\left(1 + \frac{[\text{triose} - \text{P}]}{K_{\text{m triose-P}}^{\text{GAPDH}}}\right) \cdot \left(1 + \frac{[\text{NAD}]}{K_{\text{m NAD}}^{\text{GAPDH}}}\right) \cdot \left(1 + \frac{[\text{P}_i]}{K_{\text{m P}_i}^{\text{GAPDH}}}\right) + \left(1 + \frac{[\text{BPG}]}{K_{\text{m BPG}}^{\text{GAPDH}}}\right) \cdot \left(1 + \frac{[\text{NADH}]}{K_{\text{m NADH}}^{\text{GAPDH}}}\right) - 1}$$

$$v_{\text{GAPN}} = \frac{V_{\text{max}}^{\text{GAPN}} \cdot \frac{[\text{triose} - \text{P}]}{K_{\text{m triose-P}}^{\text{GAPN}}} \cdot \frac{[\text{NADP}]}{K_{\text{m NADP}}^{\text{GAPN}}}}{\left(1 + \frac{[\text{triose} - \text{P}]}{K_{\text{m triose-P}}^{\text{GAPN}}}\right) \cdot \left(1 + \frac{[\text{NADP}]}{K_{\text{m NADP}}^{\text{GAPN}}}\right) + \left(1 + \frac{[\text{PEP}]}{K_{\text{m PEP}}^{\text{GAPN}}}\right) \cdot \left(1 + \frac{[\text{NADPH}]}{K_{\text{m NADPH}}^{\text{GAPN}}}\right) - 1}$$

$$v_{\text{ENO}} = \frac{V_{\text{max}}^{\text{ENO}} \cdot \frac{[\text{BPG}]}{K_{\text{m BPG}}^{\text{ENO}}} \cdot \frac{[\text{ADP}]}{K_{\text{m ADP}}^{\text{ENO}}} - \frac{V_{\text{max}}^{\text{ENO}}}{K_{\text{eq}}^{\text{ENO}}} \cdot \frac{[\text{PEP}]}{K_{\text{m PEP}}^{\text{ENO}}} \cdot \frac{[\text{ATP}]}{K_{\text{m ATP}}^{\text{ENO}}}}{\left(1 + \frac{[\text{BPG}]}{K_{\text{m BPG}}^{\text{ENO}}}\right) \cdot \left(1 + \frac{[\text{ADP}]}{K_{\text{m ADP}}^{\text{ENO}}}\right) + \left(1 + \frac{[\text{PEP}]}{K_{\text{m PEP}}^{\text{ENO}}}\right) \cdot \left(1 + \frac{[\text{ATP}]}{K_{\text{m ATP}}^{\text{ENO}}}\right) - 1}$$

$$v_{\text{PYK}} = \frac{K_{\text{i Pi}}^{\text{PYK}}}{K_{\text{i Pi}}^{\text{PYK}} + [\text{Pi}]} \cdot \frac{[\text{G6P}]}{K_{\text{a G6P}}^{\text{PYK}} + [\text{G6P}]} \cdot \frac{V_{\text{max}}^{\text{PYK}} \cdot \frac{[\text{PEP}]}{K_{\text{m PEP}}^{\text{PYK}}} \cdot \frac{[\text{ADP}]}{K_{\text{m ADP}}^{\text{PYK}}} - \frac{V_{\text{max}}^{\text{PYK}}}{K_{\text{eq}}^{\text{PYK}}} \cdot \frac{[\text{pyruvate}]}{K_{\text{m pyruvate}}^{\text{PYK}}} \cdot \frac{[\text{ATP}]}{K_{\text{m ATP}}^{\text{PYK}}}}{\left(1 + \frac{[\text{PEP}]}{K_{\text{m PEP}}^{\text{PYK}}}\right) \cdot \left(1 + \frac{[\text{ADP}]}{K_{\text{m ADP}}^{\text{PYK}}}\right) + \left(1 + \frac{[\text{pyruvate}]}{K_{\text{m pyruvate}}^{\text{PYK}}}\right) \cdot \left(1 + \frac{[\text{ATP}]}{K_{\text{m ATP}}^{\text{PYK}}}\right) - 1}$$

$$v_{\text{LDH}} = \frac{[\text{FBP}]}{K_{\text{a FBP}}^{\text{LDH}} + [\text{FBP}]} \cdot \frac{[\text{Pi}]}{K_{\text{a Pi}}^{\text{LDH}} + [\text{Pi}]} \cdot \frac{K_{\text{i NAD}}^{\text{LDH}}}{K_{\text{i NAD}}^{\text{LDH}} + [\text{NAD}]} \cdot \frac{\left(V_{\text{max}}^{\text{LDH}} \cdot \frac{[\text{pyruvate}]}{K_{\text{m pyruvate}}^{\text{LDH}}} \cdot \frac{[\text{NADH}]}{K_{\text{m NADH}}^{\text{LDH}}} - \frac{V_{\text{max}}^{\text{LDH}}}{K_{\text{eq}}^{\text{LDH}}} \cdot \frac{[\text{lactate}]}{K_{\text{m lactate}}^{\text{LDH}}} \cdot \frac{[\text{NAD}]}{K_{\text{m NAD}}^{\text{LDH}}}\right)}{\left(1 + \frac{[\text{pyruvate}]}{K_{\text{m pyruvate}}^{\text{LDH}}}\right) \cdot \left(1 + \frac{[\text{NADH}]}{K_{\text{m NADH}}^{\text{LDH}}}\right) + \left(1 + \frac{[\text{lactate}]}{K_{\text{m lactate}}^{\text{LDH}}}\right) \cdot \left(1 + \frac{[\text{NAD}]}{K_{\text{m NAD}}^{\text{LDH}}}\right) - 1}$$

$$v_{\text{LacT}} = \frac{K_{\text{i pyruvate}}^{\text{LacT}}}{K_{\text{i pyruvate}}^{\text{LacT}} + [\text{pyruvate}]} \cdot \frac{V_{\text{max}}^{\text{LacT}} \cdot \frac{[\text{lactate}]}{K_{\text{m lactate}}^{\text{LacT}}}}{1 + \frac{[\text{lactate}]}{K_{\text{m lactate}}^{\text{LacT}}} + \frac{[\text{lactate}_{\text{ex}}]}{K_{\text{m lactate}_{\text{ex}}^{\text{LacT}}}}$$

$$v_{\text{PFL}} = \frac{K_{\text{i triose-P}}^{\text{PFL}}}{K_{\text{i triose-P}}^{\text{PFL}} + [\text{triose-P}]} \cdot \frac{V_{\text{max}}^{\text{PFL}} \cdot \frac{[\text{pyruvate}]}{K_{\text{m pyruvate}}^{\text{PFL}}} \cdot \frac{[\text{CoA}]}{K_{\text{m CoA}}^{\text{PFL}}} - \frac{V_{\text{max}}^{\text{PFL}}}{K_{\text{eq}}^{\text{PFL}}} \cdot \frac{[\text{acetyl-CoA}]}{K_{\text{m acetyl-CoA}}^{\text{PFL}}} \cdot \frac{[\text{formate}]}{K_{\text{m formate}}^{\text{PFL}}}}{\left(1 + \frac{[\text{pyruvate}]}{K_{\text{m pyruvate}}^{\text{PFL}}}\right) \cdot \left(1 + \frac{[\text{CoA}]}{K_{\text{m CoA}}^{\text{PFL}}}\right) + \left(1 + \frac{[\text{acetyl-CoA}]}{K_{\text{m acetyl-CoA}}^{\text{PFL}}}\right) \cdot \left(1 + \frac{[\text{formate}]}{K_{\text{m formate}}^{\text{PFL}}}\right) - 1}$$

$$v_{\text{ACK}} = \frac{K_{\text{i FBP}}^{\text{ACK}}}{K_{\text{i FBP}}^{\text{ACK}} + [\text{FBP}]} \cdot \frac{V_{\text{max}}^{\text{ACK}} \cdot \frac{[\text{acetyl-CoA}]}{K_{\text{m acetyl-CoA}}^{\text{ACK}}} \cdot \frac{[\text{Pi}]}{K_{\text{m Pi}}^{\text{ACK}}} \cdot \frac{[\text{ADP}]}{K_{\text{m ADP}}^{\text{ACK}}}}{\left(1 + \frac{[\text{acetyl-CoA}]}{K_{\text{m acetyl-CoA}}^{\text{ACK}}}\right) \cdot \left(1 + \frac{[\text{Pi}]}{K_{\text{m Pi}}^{\text{ACK}}}\right) \cdot \left(1 + \frac{[\text{ADP}]}{K_{\text{m ADP}}^{\text{ACK}}}\right) + \left(1 + \frac{[\text{acetate}]}{K_{\text{m acetate}}^{\text{ACK}}}\right) \cdot \left(1 + \frac{[\text{CoA}]}{K_{\text{m CoA}}^{\text{ACK}}}\right) \cdot \left(1 + \frac{[\text{ATP}]}{K_{\text{m ATP}}^{\text{ACK}}}\right) - 1}$$

$$v_{\text{ADH}} = \frac{K_{\text{iATP}}^{\text{ADH}}}{K_{\text{iATP}}^{\text{ADH}} + [\text{ATP}]} \cdot \frac{V_{\text{max}}^{\text{ADH}} \cdot \frac{[\text{acetyl-CoA}]}{K_{\text{m acetyl-CoA}}^{\text{ADH}}} \cdot \left(\frac{[\text{NADH}]}{K_{\text{m NADH}}^{\text{ADH}}} \right)^2}{\left(1 + \frac{[\text{acetyl-CoA}]}{K_{\text{m acetyl-CoA}}^{\text{ADH}}} \right) \cdot \left(1 + \frac{[\text{NADH}]}{K_{\text{m NADH}}^{\text{ADH}}} + \left(\frac{[\text{NADH}]}{K_{\text{m NADH}}^{\text{ADH}}} \right)^2 \right) + \left(1 + \frac{[\text{ethanol}]}{K_{\text{m ethanol}}^{\text{ADH}}} \right) \cdot \left(1 + \frac{[\text{NAD}]}{K_{\text{m NAD}}^{\text{ADH}}} + \left(\frac{[\text{NAD}]}{K_{\text{m NAD}}^{\text{ADH}}} \right)^2 \right) \cdot \left(1 + \frac{[\text{CoA}]}{K_{\text{m CoA}}^{\text{ADH}}} \right) - 1}$$

$$v_{\text{PiT}} = \frac{K_{\text{iATP}}^{\text{PiT}}}{K_{\text{iATP}}^{\text{PiT}} + [\text{ATP}]} \cdot \frac{[\text{P}_{\text{i ex}}]}{K_{\text{a P}_{\text{i ex}}}^{\text{PiT}} + [\text{P}_{\text{i ex}}]} \cdot \frac{V_{\text{max}}^{\text{PiT}} \cdot ([\text{P}_{\text{i ex}}] - [\text{P}_{\text{i}}])}{1 + \frac{[\text{P}_{\text{i ex}}]}{K_{\text{m P}_{\text{i ex}}}^{\text{PiT}}} + \frac{[\text{P}_{\text{i}}]}{K_{\text{m P}_{\text{i}}}^{\text{PiT}}}}$$

$$v_{\text{PiT.active}} = \frac{V_{\text{max}}^{\text{PiT.active}} \cdot \frac{[\text{P}_{\text{i ex}}]}{K_{\text{m P}_{\text{i ex}}}^{\text{PiT.active}}} \cdot \frac{[\text{ATP}]}{K_{\text{m ATP}}^{\text{PiT.active}}}}{\left(1 + \frac{[\text{P}_{\text{i ex}}]}{K_{\text{m P}_{\text{i ex}}}^{\text{PiT.active}}} \right) \cdot \left(1 + \frac{[\text{ATP}]}{K_{\text{m ATP}}^{\text{PiT.active}}} \right) + \left(1 + \frac{[\text{P}_{\text{i}}]}{K_{\text{m P}_{\text{i}}}^{\text{PiT.active}}} + \left(\frac{[\text{P}_{\text{i}}]}{K_{\text{m P}_{\text{i}}}^{\text{PiT.active}}} \right)^2 \right) \cdot \left(1 + \frac{[\text{ADP}]}{K_{\text{m ADP}}^{\text{PiT.active}}} \right) - 1}$$

$$v_{\text{ATPase}} = \frac{V_{\text{ATPase}} \cdot \left(\frac{[\text{ATP}]}{K_{\text{m ATP}}^{\text{ATPase}}} \right)^{n_{\text{ATPase}}}}{1 + \left(\frac{[\text{ATP}]}{K_{\text{m ATP}}^{\text{ATPase}}} \right)^{n_{\text{ATPase}}}}$$

$$v_{\text{NPOX}} = \frac{V_{\text{max}}^{\text{NPOX}} \cdot \frac{[\text{NADPH}]}{K_{\text{m NADPH}}^{\text{NPOX}}}}{1 + \frac{[\text{NADPH}]}{K_{\text{m NADPH}}^{\text{NPOX}}} + \frac{[\text{NADP}]}{K_{\text{m NADP}}^{\text{NPOX}}}}$$

A.2.2 Differential equations and moiety conservation

$$\frac{d[\text{Glc}^{\text{ex}}]}{dt} = -v_{\text{PTS}} - v_{\text{GlcP}}$$

$$\frac{d[\text{HPr} - \text{Ser} - \text{P}]}{dt} = +v_{\text{HPrK}} - v_{\text{HPrP}}$$

$$\frac{d[\text{HPr}]}{dt} = -v_{\text{HPrK}} + v_{\text{HPrP}}$$

$$\frac{d[\text{Glc}]}{dt} = -v_{\text{GK}} + v_{\text{GlcP}} + v_{\text{PaseII}}$$

$$\frac{d[\text{G6P}]}{dt} = +v_{\text{PTS}} - v_{\text{PFK}} + v_{\text{GK}} - v_{\text{PaseII}}$$

$$\frac{d[\text{FBP}]}{dt} = +v_{\text{PFK}} - v_{\text{FBA}}$$

$$\frac{d[\text{Triose} - \text{P}]}{dt} = -v_{\text{GAPN}} + 2 \cdot v_{\text{FBA}} - v_{\text{GAPDH}}$$

$$\frac{d[\text{BPG}]}{dt} = +v_{\text{GAPDH}} - v_{\text{ENO}}$$

$$\frac{d[\text{PEP}]}{dt} = -v_{\text{PTS}} + v_{\text{GAPN}} + v_{\text{ENO}} - v_{\text{PYK}}$$

$$\frac{d[\text{Pyruvate}]}{dt} = +v_{\text{PTS}} + v_{\text{PYK}} - v_{\text{PFL}} - v_{\text{LDH}}$$

$$\frac{d[\text{Lactate}]}{dt} = -v_{\text{LacT}} + v_{\text{LDH}}$$

$$\frac{d[\text{Lactate}^{\text{ex}}]}{dt} = +v_{\text{LacT}}$$

$$\frac{d[\text{Acetyl} - \text{CoA}]}{dt} = -v_{\text{ADH}} + v_{\text{PFL}} - v_{\text{ACK}}$$

$$\frac{d[\text{CoA}]}{dt} = +v_{\text{ADH}} - v_{\text{PFL}} + v_{\text{ACK}}$$

$$\frac{d[\text{Formate}]}{dt} = +v_{\text{PFL}}$$

$$\frac{d[\text{Acetate}]}{dt} = +v_{\text{ACK}}$$

$$\frac{d[\text{Ethanol}]}{dt} = +v_{\text{ADH}}$$

$$\frac{d[\text{ATP}]}{dt} = -v_{\text{PFK}} - v_{\text{ATPase}} - v_{\text{GK}} - v_{\text{HPrK}} - v_{\text{PiT.active}} + v_{\text{ENO}} + v_{\text{PYK}} + v_{\text{ACK}}$$

$$\frac{d[\text{NAD}^+]}{dt} = +2 \cdot v_{\text{ADH}} - v_{\text{GAPDH}} + v_{\text{LDH}}$$

$$\frac{d[\text{NADP}^+]}{dt} = -v_{\text{GAPN}} + v_{\text{NPOX}}$$

$$\frac{d[\text{Pi}]}{dt} = +v_{\text{ATPase}} + v_{\text{PiT}} + v_{\text{HPrP}} + 2 \cdot v_{\text{PiT.active}} + v_{\text{PaseII}} - v_{\text{GAPDH}} - v_{\text{ACK}}$$

$$\frac{d[\text{Pi}_{\text{ex}}]}{dt} = -v_{\text{PiT}} - v_{\text{PiT.active}}$$

$$[\text{ADP}] = 9 - \text{ATP}$$

$$[\text{NADH}] = [\text{NAD}^+]_0 - [\text{NADH}]$$

$$[\text{NADPH}] = [\text{NADP}^+]_0 - [\text{NADPH}]$$

A.3 Results from sensitivity analysis

At first we performed a global sensitivity analysis by means of a random exploration of the parameter space. Since this analysis did not allow to identify crucial parameters we decided to use tighter boundary conditions. Therefore, we took our set of 50 fitted models and calculated scaled sensitivities on the species concentrations and reaction fluxes for varying extracellular phosphate concentrations (0, 10 and 50 mM) and plotted these as histograms. These results represent a subset of the outcome of the random sampling method. The parameters were classified into groups according to their maximal effects on the studied system variable. Thus, we obtain one set of parameters having a high impact on the particular species or flux, one class exerting a medium effect and one set showing a low impact. The results from that analysis are summarised in the following tables.

Table A.7: Parameter sensitivities on FBP. For each parameter the scaled sensitivity on FBP at $t = 100$ s was calculated and classified based on its maximal value in all 50 models in one of three groups.

High effect ($> \pm 1$)	Medium effect (± 0.3 to ± 1)	Low effect ($< \pm 0.3$)
	$K_{i\text{FBP}}^{\text{ACK}}$	
	$K_{m\text{acetate}}^{\text{ACK}}$	
	$K_{m\text{CoA}}^{\text{ACK}}$	
		$K_{m\text{ATP}}^{\text{ACK}}$
$K_{m\text{acetylCoA}}^{\text{ACK}}$		
	$K_{m\text{P}_i}^{\text{ACK}}$	
	$K_{m\text{ADP}}^{\text{ACK}}$	
	$V_{\text{max}}^{\text{ACK}}$	
	$K_{i\text{ATP}}^{\text{ADH}}$	
	$K_{m\text{ethanol}}^{\text{ADH}}$	
$K_{m\text{NAD}}^{\text{ADH}}$		
$K_{m\text{CoA}}^{\text{ADH}}$		
	$K_{m\text{acetylCoA}}^{\text{ADH}}$	
	$K_{m\text{NADH}}^{\text{ADH}}$	
$V_{\text{max}}^{\text{ADH}}$		
η_{ATPase}		
$K_{m\text{ATP}}^{\text{ATPase}}$		
$V_{\text{max}}^{\text{ATPase}}$		
$K_{\text{eq}}^{\text{ENO}}$		
$K_{m\text{PEP}}^{\text{ENO}}$		
$K_{m\text{ATP}}^{\text{ENO}}$		
$K_{m\text{BPG}}^{\text{ENO}}$		
	$K_{m\text{ADP}}^{\text{ENO}}$	
$V_{\text{max}}^{\text{ENO}}$		

Table A.7 – continued from previous page

High effect ($> \pm 1$)	Medium effect (± 0.3 to ± 1)	Low effect ($< \pm 0.3$)
K_{eq}^{FBA}		
$K_{m\text{ trioseP}}^{FBA}$		
$K_{m\text{ FBP}}^{FBA}$		
V_{max}^{FBA}		
K_{eq}^{GAPDH}		
	$K_{i\text{ NADH}}^{GAPDH}$	
$K_{m\text{ BPG}}^{GAPDH}$		
$K_{m\text{ NADH}}^{GAPDH}$		
$K_{m\text{ triose-P}}^{GAPDH}$		
$K_{m\text{ NAD}}^{GAPDH}$		
$K_{m\text{ P}_i}^{GAPDH}$		
	V_{max}^{GAPDH}	
$K_{m\text{ PEP}}^{GAPN}$		
	$K_{m\text{ NADPH}}^{GAPN}$	
$K_{m\text{ triose-P}}^{GAPN}$		
$K_{m\text{ NADP}}^{GAPN}$		
V_{max}^{GAPN}		
	$K_{i\text{ G6P}}^{GK}$	
	$K_{i\text{ ADP}}^{GK}$	
	$K_{m\text{ G6P}}^{GK}$	
$K_{m\text{ ADP}}^{GK}$		
	$K_{m\text{ glucose}}^{GK}$	
	$K_{m\text{ ATP}}^{GK}$	
V_{max}^{GK}		
V_{max}^{GlcP}		
$K_{a\text{ FBP}}^{HPrK}$		
$K_{i\text{ P}_i}^{HPrK}$		
	$K_{m\text{ HPr-ser-P}}^{HPrK}$	
$K_{m\text{ ADP}}^{HPrK}$		
$K_{m\text{ HPr}}^{HPrK}$		
$K_{m\text{ ATP}}^{HPrK}$		
V_{max}^{HPrK}		
	$K_{a\text{ P}_i}^{HPrP}$	
	$K_{i\text{ ATP}}^{HPrP}$	
	$K_{m\text{ HPr}}^{HPrP}$	
$K_{m\text{ P}_i}^{HPrP}$		
$K_{m\text{ HPr-ser-P}}^{HPrP}$		
V_{max}^{HPrP}		
		$K_{i\text{ pyruvate}}^{LacT}$
		$K_{m\text{ lactate}_{ex}}^{LacT}$
		$K_{m\text{ lactate}}^{LacT}$
	V_{max}^{LacT}	
		K_{eq}^{LDH}
$K_{a\text{ FBP}}^{LDH}$		
	$K_{a\text{ P}_i}^{LDH}$	
$K_{i\text{ NAD}}^{LDH}$		
	$K_{m\text{ lactate}}^{LDH}$	
	$K_{m\text{ NAD}}^{LDH}$	

Table A.7 – continued from previous page

High effect ($> \pm 1$)	Medium effect (± 0.3 to ± 1)	Low effect ($< \pm 0.3$)
$K_{m \text{ pyruvate}}^{\text{LDH}}$		
	$K_{m \text{ NADH}}^{\text{LDH}}$	
$V_{\text{max}}^{\text{LDH}}$		
	$K_{m \text{ NADP}}^{\text{NPOX}}$	
	$K_{m \text{ NADPH}}^{\text{NPOX}}$	
$V_{\text{max}}^{\text{NPOX}}$		
$K_{a \text{ HPr-ser-P}}^{\text{PaseII}}$		
	$K_{m \text{ glucose}}^{\text{PaseII}}$	
	$K_{m \text{ P}_i}^{\text{PaseII}}$	
$K_{m \text{ G6P}}^{\text{PaseII}}$		
$V_{\text{max}}^{\text{PaseII}}$		
	$K_{m \text{ FBP}}^{\text{PFK}}$	
$K_{m \text{ ADP}}^{\text{PFK}}$		
$K_{m \text{ G6P}}^{\text{PFK}}$		
$K_{m \text{ ATP}}^{\text{PFK}}$		
$V_{\text{max}}^{\text{PFK}}$		
		$K_{\text{eq}}^{\text{PFL}}$
	$K_{i \text{ triose-P}}^{\text{PFL}}$	
		$K_{m \text{ acetyl-CoA}}^{\text{PFL}}$
		$K_{m \text{ formate}}^{\text{PFL}}$
$K_{m \text{ pyruvate}}^{\text{PFL}}$		
	$K_{m \text{ CoA}}^{\text{PFL}}$	
	$V_{\text{max}}^{\text{PFL}}$	
$K_{a \text{ P}_i^{\text{ex}}}^{\text{PiT}}$ for 10 and 50 mM P_i^{ex}		$K_{a \text{ P}_i^{\text{ex}}}^{\text{PiT}}$ for 0 mM P_i^{ex}
	$K_{i \text{ ATP}}^{\text{PiT}}$ for 10 and 50 mM P_i^{ex}	$K_{i \text{ ATP}}^{\text{PiT}}$ for 0 mM P_i^{ex}
	$K_{m \text{ P}_i}^{\text{PiT}}$ for 10 and 50 mM P_i^{ex}	$K_{m \text{ P}_i}^{\text{PiT}}$ for 0 mM P_i^{ex}
	$K_{m \text{ P}_i^{\text{ex}}}^{\text{PiT}}$ for 10 and 50 mM P_i^{ex}	$K_{m \text{ P}_i^{\text{ex}}}^{\text{PiT}}$ for 0 mM P_i^{ex}
$V_{\text{max}}^{\text{PiT}}$ for 10 and 50 mM P_i^{ex}		$V_{\text{max}}^{\text{PiT}}$ for 0 mM P_i^{ex}
	$K_{m \text{ P}_i}^{\text{PiT.active}}$ for 10 and 50 mM P_i^{ex}	$K_{m \text{ P}_i}^{\text{PiT.active}}$ for 0 mM P_i^{ex}
$K_{m \text{ ADP}}^{\text{PiT.active}}$ for 10 and 50 mM P_i^{ex}		$K_{m \text{ ADP}}^{\text{PiT.active}}$ for 0 mM P_i^{ex}
	$K_{m \text{ P}_i^{\text{ex}}}^{\text{PiT.active}}$ for 10 and 50 mM P_i^{ex}	$K_{m \text{ P}_i^{\text{ex}}}^{\text{PiT.active}}$ for 0 mM P_i^{ex}
$K_{m \text{ ATP}}^{\text{PiT.active}}$ for 10 and 50 mM P_i^{ex}		$K_{m \text{ ATP}}^{\text{PiT.active}}$ for 0 mM P_i^{ex}
	$V_{\text{max}}^{\text{PiT.active}}$ for 10 and 50 mM P_i^{ex}	$V_{\text{max}}^{\text{PiT.active}}$ for 0 mM P_i^{ex}
	$K_{m \text{ HPr}}^{\text{PTS}}$	
	$K_{m \text{ pyruvate}}^{\text{PTS}}$	
	$K_{m \text{ G6P}}^{\text{PTS}}$	
$K_{m \text{ HPr}}^{\text{PTS}}$		
$K_{m \text{ PEP}}^{\text{PTS}}$		
	$K_{m \text{ glucose}_{\text{ex}}}^{\text{PTS}}$	
$V_{\text{max}}^{\text{PTS}}$		
		$K_{\text{eq}}^{\text{PYK}}$
$K_{a \text{ G6P}}^{\text{PYK}}$		
$K_{i \text{ P}_i}^{\text{PYK}}$		
	$K_{m \text{ pyruvate}}^{\text{PYK}}$	
	$K_{m \text{ ATP}}^{\text{PYK}}$	
$K_{m \text{ PEP}}^{\text{PYK}}$		
$K_{m \text{ ADP}}^{\text{PYK}}$		
$V_{\text{max}}^{\text{PYK}}$		

Table A.8: Parameter sensitivities on P_i . For each parameter the scaled sensitivity on phosphate at $t = 100$ s was calculated and classified based on its maximal value in all 50 models in one of three groups.

High effect ($> \pm 1$)	Medium effect (± 0.3 to ± 1)	Low effect ($< \pm 0.3$)
		K_{iFBP}^{ACK}
		$K_{m\text{ acetate}}^{ACK}$
		$K_{m\text{ CoA}}^{ACK}$
		$K_{m\text{ ATP}}^{ACK}$
	$K_{m\text{ acetylCoA}}^{ACK}$	
		$K_{m\text{ P}_i}^{ACK}$
		$K_{m\text{ ADP}}^{ACK}$
		V_{max}^{ACK}
		$K_{i\text{ ATP}}^{ADH}$
	$K_{m\text{ ethanol}}^{ADH}$	
		$K_{m\text{ NAD}}^{ADH}$
	$K_{m\text{ CoA}}^{ADH}$	
	$K_{m\text{ acetylCoA}}^{ADH}$	
		$K_{m\text{ NADH}}^{ADH}$
	V_{max}^{ADH}	
n_{ATPase}		
$K_{m\text{ ATP}}^{\text{ATPase}}$		
	V_{max}^{ATPase}	
		K_{eq}^{ENO}
		$K_{m\text{ PEP}}^{\text{ENO}}$
		$K_{m\text{ ATP}}^{\text{ENO}}$
	$K_{m\text{ BPG}}^{\text{ENO}}$	
	$K_{m\text{ ADP}}^{\text{ENO}}$	
	V_{max}^{ENO}	
	K_{eq}^{FBA}	
	$K_{m\text{ trioseP}}^{\text{FBA}}$	
	$K_{m\text{ FBP}}^{\text{FBA}}$	
		V_{max}^{FBA}
	K_{eq}^{GAPDH}	
		$K_{i\text{ NADH}}^{\text{GAPDH}}$
	$K_{m\text{ BPG}}^{\text{GAPDH}}$	
	$K_{m\text{ NADH}}^{\text{GAPDH}}$	
	$K_{m\text{ triose-P}}^{\text{GAPDH}}$	
	$K_{m\text{ NAD}}^{\text{GAPDH}}$	
	$K_{m\text{ P}_i}^{\text{GAPDH}}$	
		V_{max}^{GAPDH}
	$K_{m\text{ PEP}}^{\text{GAPN 6}}$	
		$K_{m\text{ NADPH}}^{\text{GAPN}}$
	$K_{m\text{ triose-P}}^{\text{GAPN}}$	
	$K_{m\text{ NADP}}^{\text{GAPN}}$	
	V_{max}^{GAPN}	
		$K_{i\text{ G6P}}^{\text{GK}}$
	$K_{i\text{ ADP}}^{\text{GK}}$	
		$K_{m\text{ G6P}}^{\text{GK}}$

Table A.8 – continued from previous page

High effect ($> \pm 1$)	Medium effect (± 0.3 to ± 1)	Low effect ($< \pm 0.3$)
	K_{mADP}^{GK}	
		$K_{m\text{ glucose}}^{GK}$
		K_{mATP}^{GK}
$V_{\text{GlcP max}}$	V_{max}^{GK}	
	K_{aFBP}^{HPrK}	
	$K_{iP_i}^{HPrK}$	
		$K_{mHPr-ser-P}^{HPrK}$
		K_{mADP}^{HPrK}
	K_{mHPr}^{HPrK}	
	K_{mATP}^{HPrK}	
	V_{max}^{HPrK}	
		$K_{aP_i}^{HPrP}$
		K_{aATP}^{HPrP}
		K_{mHPr}^{HPrP}
	$K_{mP_i}^{HPrP}$	
		$K_{mHPr-ser-P}^{HPrP}$
	V_{max}^{HPrP}	
		$K_{i\text{ pyruvate}}^{\text{LacT}}$
		$K_{m\text{ lactate ex}}^{\text{LacT}}$
		$K_{m\text{ lactate}}^{\text{LacT}}$
		$V_{\text{max}}^{\text{LacT}}$
		K_{eq}^{LDH}
		K_{aFBP}^{LDH}
		$K_{aP_i}^{\text{LDH}}$
		K_{iNAD}^{LDH}
		$K_{m\text{ lactate}}^{\text{LDH}}$
		K_{mNAD}^{LDH}
	$K_{m\text{ pyruvate}}^{\text{LDH}}$	
		K_{mNADH}^{LDH}
	$V_{\text{max}}^{\text{LDH}}$	
		K_{mNADP}^{NPOX}
	K_{mNADPH}^{NPOX}	
		$V_{\text{max}}^{\text{NPOX}}$
	$K_{aHPr-ser-P}^{\text{PaseII}}$	
		$K_{m\text{ glucose}}^{\text{PaseII}}$
		$K_{mP_i}^{\text{PaseII}}$
	K_{mG6P}^{PaseII}	
		$V_{\text{max}}^{\text{PaseII}}$
		K_{mFBP}^{PFK}
	K_{mADP}^{PFK}	
	K_{mG6P}^{PFK}	
	K_{mATP}^{PFK}	
	$V_{\text{max}}^{\text{PFK}}$	
		K_{eq}^{PFL}
	$K_{i\text{ triose-P}}^{\text{PFL}}$	
		$K_{m\text{ acetyl-CoA}}^{\text{PFL}}$

Table A.8 – continued from previous page

High effect ($> \pm 1$)	Medium effect (± 0.3 to ± 1)	Low effect ($< \pm 0.3$)
		$K_m^{\text{PFL}}_{\text{formate}}$
	$K_m^{\text{PFL}}_{\text{pyruvate}}$	
	$V_{\text{max}}^{\text{PFL}}$	$K_m^{\text{PFL}}_{\text{CoA}}$
	$K_{aP_i}^{\text{PiT}}$ for 10 and 50 mM P_i^{ex}	$K_{aP_i}^{\text{PiT}}$ for 0 mM P_i^{ex}
		$K_{i\text{ATP}}^{\text{PiT}}$
		$K_{mP_i}^{\text{PiT}}$
	$K_{mP_i}^{\text{PiT}}$ for 10 and 50 mM P_i^{ex}	$K_{mP_i}^{\text{PiT}}$ for 0 mM P_i^{ex}
	$V_{\text{max}}^{\text{PiT}}$ for 10 and 50 mM P_i^{ex}	$V_{\text{max}}^{\text{PiT}}$ for 0 mM P_i^{ex}
		$K_{mP_i}^{\text{PiT,active}}$
	$K_{m\text{ADP}}^{\text{PiT,active}}$ for 10 and 50 mM P_i^{ex}	$K_{m\text{ADP}}^{\text{PiT,active}}$ for 0 mM P_i^{ex}
	$K_{mP_i}^{\text{PiT,active}}$ for 10 and 50 mM P_i^{ex}	$K_{mP_i}^{\text{PiT,active}}$ for 0 mM P_i^{ex}
	$K_{m\text{ATP}}^{\text{PiT,active}}$ for 10 and 50 mM P_i^{ex}	$K_{m\text{ATP}}^{\text{PiT,active}}$ for 0 mM P_i^{ex}
		$V_{\text{max}}^{\text{PiT,active}}$
		$K_{m\text{HPr}}^{\text{PTS}}$
		$K_{m\text{pyruvate}}^{\text{PTS}}$
		$K_{m\text{G6P}}^{\text{PTS}}$
	$K_{m\text{HPr}}^{\text{PTS}}$	
		$K_{m\text{PEP}}^{\text{PTS}}$
		$K_{m\text{glucoseex}}^{\text{PTS}}$
	$V_{\text{max}}^{\text{PTS}}$	
		$K_{\text{eq}}^{\text{PYK}}$
	$K_{a\text{G6P}}^{\text{PYK}}$	
		$K_{iP_i}^{\text{PYK}}$
		$K_{m\text{pyruvate}}^{\text{PYK}}$
		$K_{m\text{ATP}}^{\text{PYK}}$
	$K_{m\text{PEP}}^{\text{PYK}}$	
	$K_{m\text{ADP}}^{\text{PYK}}$	
	$V_{\text{max}}^{\text{PYK}}$	

Table A.9: Parameter sensitivities on the PFK flux. For each parameter the scaled sensitivity on the PFK flux at $t = 100$ s was calculated and classified based on its maximal value in all 50 models in one of three groups.

High effect ($> \pm 1$)	Medium effect (± 0.3 to ± 1)	Low effect ($< \pm 0.3$)
	$K_{i\text{FBP}}^{\text{ACK}}$	
	$K_{m\text{acetate}}^{\text{ACK}}$	
	$K_{m\text{CoA}}^{\text{ACK}}$	
	$K_{m\text{ATP}}^{\text{ACK}}$	
$K_{m\text{acetylCoA}}^{\text{ACK}}$		
$K_{mP_i}^{\text{ACK}}$		
$K_{m\text{ADP}}^{\text{ACK}}$		
$V_{\text{max}}^{\text{ACK}}$		
	$K_{i\text{ATP}}^{\text{ADH}}$	
	$K_{m\text{ethanol}}^{\text{ADH}}$	
$K_{m\text{NAD}}^{\text{ADH}}$		

Table A.9 – continued from previous page

High effect ($> \pm 1$)	Medium effect (± 0.3 to ± 1)	Low effect ($< \pm 0.3$)
	K_{mCoA}^{ADH}	
$K_{m\text{acetylCoA}}^{ADH}$		
	K_{mNADH}^{ADH}	
V_{max}^{ADH}		
n_{ATPase}		
K_{mATP}^{ATPase}		
V_{max}^{ATPase}		
		K_{eq}^{ENO}
	K_{mPEP}^{ENO}	
	K_{mATP}^{ENO}	
K_{mBPG}^{ENO}		
	K_{mADP}^{ENO}	
V_{max}^{ENO}		
K_{eq}^{FBA}		
$K_{m\text{trioseP}}^{FBA}$		
K_{mFBP}^{FBA}		
		V_{max}^{FBA}
K_{eq}^{GAPDH}		
	K_{iNADH}^{GAPDH}	
K_{mBPG}^{GAPDH}		
K_{mNADH}^{GAPDH}		
$K_{m\text{triose-P}}^{GAPDH}$		
K_{mNAD}^{GAPDH}		
$K_{mP_i}^{GAPDH}$		
V_{max}^{GAPDH}		
K_{mPEP}^{GAPN}		
K_{mNADPH}^{GAPN}		
$K_{m\text{triose-P}}^{GAPN}$		
K_{mNADP}^{GAPN}		
V_{max}^{GAPN}		
	K_{iG6P}^{GK}	
K_{iADP}^{GK}		
K_{mG6P}^{GK}		
K_{mADP}^{GK}		
$K_{m\text{glucose}}^{GK}$		
K_{iATP}^{GK}		
V_{max}^{GK}		
V_{max}^{GlcP}		
$K_{aFBP}^{HP_rK}$		
$K_{iP_i}^{HP_rK}$		
$K_{mHP_r-ser-P}^{HP_rK}$		
$K_{mADP}^{HP_rK}$		
$K_{mHP_r}^{HP_rK}$		
$K_{mATP}^{HP_rK}$		
$V_{max}^{HP_rK}$		
$K_{aP_i}^{HP_rP}$		
	$K_{aATP}^{HP_rP}$	
	$K_{mHP_r}^{HP_rP}$	

Table A.9 – continued from previous page

High effect ($> \pm 1$)	Medium effect (± 0.3 to ± 1)	Low effect ($< \pm 0.3$)
$K_{m P_i}^{HPrP}$		
V_{max}^{HPrP}	$K_{m HPr-ser-P}^{HPrP}$	
		$K_{i pyruvate}^{LacT}$
		$K_{m lactate,ex}^{LacT}$
		$K_{m lactate}^{LacT}$
		V_{max}^{LacT}
		K_{eq}^{LDH}
$K_{a FBP}^{LDH}$		
	$K_{a P_i}^{LDH}$	
$K_{i NAD}^{LDH}$		$K_{m lactate}^{LDH}$
	$K_{m NAD}^{LDH}$	
$K_{m pyruvate}^{LDH}$		
	$K_{m NADH}^{LDH}$	
V_{max}^{LDH}		
	$K_{m NADP}^{NPOX}$	
	$K_{m NADPH}^{NPOX}$	
	V_{max}^{NPOX}	
$K_{a HPr-ser-P}^{PaseII}$		
	$K_{m glucose}^{PaseII}$	
	$K_{m P_i}^{PaseII}$	
$K_{m G6P}^{PaseII}$		
V_{max}^{PaseII}		
	$K_{m FBP}^{PFK}$	
$K_{m ADP}^{PFK}$		
$K_{m G6P}^{PFK}$		
$K_{m ATP}^{PFK}$		
V_{max}^{PFK}		
		K_{eq}^{PFL}
$K_{i triose-P}^{PFL}$		
	$K_{m acetyl-CoA}^{PFL}$	
	$K_{m formate}^{PFL}$	
$K_{m pyruvate}^{PFL}$		
	$K_{m CoA}^{PFL}$	
V_{max}^{PFL}		
	$K_{a P_i,ex}^{PiT}$ for 10 and 50 mM P_i^{ex}	$K_{a P_i,ex}^{PiT}$ for 0 mM P_i^{ex}
	$K_{i ATP}^{PiT}$ for 10 and 50 mM P_i^{ex}	$K_{i ATP}^{PiT}$ for 0 mM P_i^{ex}
	$K_{m P_i}^{PiT}$ for 10 and 50 mM P_i^{ex}	$K_{m P_i}^{PiT}$ for 0 mM P_i^{ex}
$K_{m P_i,ex}^{PiT}$ for 10 and 50 mM P_i^{ex}		$K_{m P_i,ex}^{PiT}$ for 0 mM P_i^{ex}
V_{max}^{PiT} for 10 and 50 mM P_i^{ex}		V_{max}^{PiT} for 0 mM P_i^{ex}
		$K_{m P_i}^{PiT,active}$
	$K_{m ADP}^{PiT,active}$ for 10 and 50 mM P_i^{ex}	$K_{m ADP}^{PiT,active}$ for 0 mM P_i^{ex}
$K_{m P_i,ex}^{PiT,active}$ for 10 and 50 mM P_i^{ex}		$K_{m P_i,ex}^{PiT,active}$ for 0 mM P_i^{ex}
$K_{m ATP}^{PiT,active}$ for 10 and 50 mM P_i^{ex}		$K_{m ATP}^{PiT,active}$ for 0 mM P_i^{ex}
$V_{max}^{PiT,active}$ for 10 and 50 mM P_i^{ex}		$V_{max}^{PiT,active}$ for 0 mM P_i^{ex}
	$K_{m HPr}^{PTS}$	

Table A.9 – continued from previous page

High effect ($> \pm 1$)	Medium effect (± 0.3 to ± 1)	Low effect ($< \pm 0.3$)
	$K_{m \text{ pyruvate}}^{\text{PTS}}$	
		$K_{m \text{ G6P}}^{\text{PTS}}$
$K_{m \text{ HPr}}^{\text{PTS}}$		
$K_{m \text{ PEP}}^{\text{PTS}}$		
$V_{\text{max}}^{\text{PTS}}$		$K_{m \text{ glucose}_{\text{ex}}}^{\text{PTS}}$
		$K_{\text{eq}}^{\text{PYK}}$
$K_{a \text{ G6P}}^{\text{PYK}}$		
$K_{i \text{ P}_i}^{\text{PYK}}$		
		$K_{m \text{ pyruvate}}^{\text{PYK}}$
		$K_{m \text{ ATP}}^{\text{PYK}}$
$K_{m \text{ PEP}}^{\text{PYK}}$		
$K_{m \text{ ADP}}^{\text{PYK}}$		
$V_{\text{max}}^{\text{PYK}}$		

Table A.10: Parameter sensitivities on the PTS flux. For each parameter the scaled sensitivity on the PTS flux at $t = 100$ s was calculated and classified based on its maximal value in all 50 models in one of three groups.

High effect ($> \pm 1$)	Medium effect (± 0.3 to ± 1)	Low effect ($< \pm 0.3$)
	$K_{i \text{ FBP}}^{\text{ACK}}$	
$K_{m \text{ acetate}}^{\text{ACK}}$		
$K_{m \text{ CoA}}^{\text{ACK}}$		
	$K_{m \text{ ATP}}^{\text{ACK}}$	
$K_{m \text{ acetylCoA}}^{\text{ACK}}$		
$K_{m \text{ P}_i}^{\text{ACK}}$		
$K_{m \text{ ADP}}^{\text{ACK}}$		
$V_{\text{max}}^{\text{ACK}}$		
		$K_{i \text{ ATP}}^{\text{ADH}}$
		$K_{m \text{ ethanol}}^{\text{ADH}}$
$K_{m \text{ NAD}}^{\text{ADH}}$		
	$K_{m \text{ CoA}}^{\text{ADH}}$	
	$K_{m \text{ acetylCoA}}^{\text{ADH}}$	
	$K_{m \text{ NADH}}^{\text{ADH}}$	
$V_{\text{max}}^{\text{ADH}}$		
n_{ATPase}		
$K_{m \text{ ATP}}^{\text{ATPase}}$		
$V_{\text{max}}^{\text{ATPase}}$		
$K_{\text{eq}}^{\text{ENO}}$		
$K_{m \text{ PEP}}^{\text{ENO}}$		
$K_{m \text{ ATP}}^{\text{ENO}}$		
$K_{m \text{ BPG}}^{\text{ENO}}$		
$K_{m \text{ ADP}}^{\text{ENO}}$		
$V_{\text{max}}^{\text{ENO}}$		
$K_{\text{eq}}^{\text{FBA}}$		
$K_{m \text{ trioseP}}^{\text{FBA}}$		
$K_{m \text{ FBP}}^{\text{FBA}}$		

Table A.10 – continued from previous page

High effect ($> \pm 1$)	Medium effect (± 0.3 to ± 1)	Low effect ($< \pm 0.3$)
		V_{FBAMax}
$K_{\text{eq}}^{\text{GAPDH}}$		
	$K_{\text{iNADH}}^{\text{GAPDH}}$	
$K_{\text{mBPG}}^{\text{GAPDH}}$		
$K_{\text{mNADH}}^{\text{GAPDH}}$		
$K_{\text{mtriose-P}}^{\text{GAPDH}}$		
$K_{\text{mNAD}}^{\text{GAPDH}}$		
$K_{\text{mPi}}^{\text{GAPDH}}$		
	$V_{\text{max}}^{\text{GAPDH}}$	
$K_{\text{mPEP}}^{\text{GAPN}}$		
	$K_{\text{mNADPH}}^{\text{GAPN}}$	
$K_{\text{mtriose-P}}^{\text{GAPN}}$		
$K_{\text{mNADP}}^{\text{GAPN}}$		
$V_{\text{max}}^{\text{GAPN}}$		
$K_{\text{iG6P}}^{\text{GK}}$		
$K_{\text{iADP}}^{\text{GK}}$		
$K_{\text{mG6P}}^{\text{GK}}$		
$K_{\text{mADP}}^{\text{GK}}$		
$K_{\text{mglucose}}^{\text{GK}}$		
$K_{\text{iATP}}^{\text{GK}}$		
$V_{\text{max}}^{\text{GK}}$		
$V_{\text{max}}^{\text{GlcP}}$		
$K_{\text{aFBP}}^{\text{HPrK}}$		
	$K_{\text{iPi}}^{\text{HPrK}}$	
$K_{\text{mHPr-ser-P}}^{\text{HPrK}}$		
$K_{\text{mADP}}^{\text{HPrK}}$		
$K_{\text{mHPr}}^{\text{HPrK}}$		
$K_{\text{mATP}}^{\text{HPrK}}$		
$V_{\text{max}}^{\text{HPrK}}$		
	$K_{\text{aPi}}^{\text{HPrP}}$	
	$K_{\text{aATP}}^{\text{HPrP}}$	
		$K_{\text{mHPr}}^{\text{HPrP}}$
$K_{\text{mPi}}^{\text{HPrP}}$		
	$K_{\text{mHPr-ser-P}}^{\text{HPrP}}$	
$V_{\text{max}}^{\text{HPrP}}$		
		$K_{\text{i pyruvate}}^{\text{LacT}}$
		$K_{\text{m lactate ex}}^{\text{LacT}}$
		$K_{\text{m lactate}}^{\text{LacT}}$
		$V_{\text{max}}^{\text{LacT}}$
		$K_{\text{eq}}^{\text{LDH}}$
	$K_{\text{aFBP}}^{\text{LDH}}$	
	$K_{\text{aPi}}^{\text{LDH}}$	
$K_{\text{iNAD}}^{\text{LDH}}$		
		$K_{\text{m lactate}}^{\text{LDH}}$
$K_{\text{mNAD}}^{\text{LDH}}$		
	$K_{\text{m pyruvate}}^{\text{LDH}}$	
	$K_{\text{mNADH}}^{\text{LDH}}$	
$V_{\text{max}}^{\text{LDH}}$		

Table A.10 – continued from previous page

High effect ($> \pm 1$)	Medium effect (± 0.3 to ± 1)	Low effect ($< \pm 0.3$)
K_{mNADP}^{NPOX}		
	K_{mNADPH}^{NPOX}	
V_{max}^{NPOX}		
$K_{aHPr-ser-P}^{PaseII}$		
		$K_{mglucose}^{PaseII}$
	$K_{mP_i}^{PaseII}$	
K_{mG6P}^{PaseII}		
V_{max}^{PaseII}		
	K_{mFBP}^{PFK}	
K_{mADP}^{PFK}		
K_{mG6P}^{PFK}		
K_{mATP}^{PFK}		
V_{max}^{PFK}		
		K_{eq}^{PFL}
	$K_{itriose-P}^{PFL}$	
		$K_{m acetyl-CoA}^{PFL}$
		$K_{m formate}^{PFL}$
$K_{m pyruvate}^{PFL}$		
	$K_{m CoA}^{PFL}$	
V_{max}^{PFL}		
	$K_{aP_i^{ex}}^{PiT}$ for 10 and 50 mM P_i^{ex}	$K_{aP_i^{ex}}^{PiT}$ for 0 mM P_i^{ex}
K_{iATP}^{PiT} for 10 and 50 mM P_i^{ex}		K_{iATP}^{PiT} for 0 mM P_i^{ex}
	$K_{mP_i}^{PiT}$ for 10 and 50 mM P_i^{ex}	$K_{mP_i}^{PiT}$ for 0 mM P_i^{ex}
$K_{mP_i^{ex}}^{PiT}$ for 10 and 50 mM P_i^{ex}		$K_{mP_i^{ex}}^{PiT}$ for 0 mM P_i^{ex}
V_{max}^{PiT} for 10 and 50 mM P_i^{ex}		V_{max}^{PiT} for 0 mM P_i^{ex}
		$K_{mP_i}^{PiT.active}$
$K_{mADP}^{PiT.active}$ for 10 and 50 mM P_i^{ex}		$K_{mADP}^{PiT.active}$ for 0 mM P_i^{ex}
	$K_{mP_i^{ex}}^{PiT.active}$ for 10 and 50 mM P_i^{ex}	$K_{mP_i^{ex}}^{PiT.active}$ for 0 mM P_i^{ex}
$K_{mATP}^{PiT.active}$ for 10 and 50 mM P_i^{ex}		$K_{mATP}^{PiT.active}$ for 0 mM P_i^{ex}
$V_{max}^{PiT.active}$ for 10 and 50 mM P_i^{ex}		$V_{max}^{PiT.active}$ for 0 mM P_i^{ex}
		K_{mHPr}^{PTS}
$K_{m pyruvate}^{PTS}$		
		K_{mG6P}^{PTS}
	K_{mHPr}^{PTS}	
	K_{mPEP}^{PTS}	
		$K_{m glucose_{ex}}^{PTS}$
V_{max}^{PTS}		
		K_{eq}^{PYK}
K_{aG6P}^{PYK}		
$K_{iP_i}^{PYK}$		
		$K_{m pyruvate}^{PYK}$
		K_{mATP}^{PYK}
	K_{mPEP}^{PYK}	
	K_{mADP}^{PYK}	
V_{max}^{PYK}		

Appendix B

Genome-scale model of *S. pyogenes*

B.1	Compounds	180
B.2	Reactions	188
B.3	Constraints	198
B.4	Simulation results	203

B.1 Compounds

The denotation of the metabolites of our genome-scale model was done analogously to the reconstruction of *L. plantarum* since this network served as template. The following table gives the abbreviation and the common name of each metabolite of the *S. pyogenes* metabolic network.

Table B.1: Compounds included in the genome-scale model.

Abbreviation	Official name
10fthf	10-Formyltetrahydrofolate
13dpg	3-Phospho-D-glyceroyl phosphate
13ppd	Propane-1,3-diol
1pyr5c	1-Pyrroline-5-carboxylate
23dhdp	2,3-Dihydrodipicolinate
25aics	(S)-2-[5-Amino-1-(5-phospho-D-ribose)]imidazole-4-carboxamido]succinate
26dap-LL	LL-2,6-Diaminoheptanedioate
26dap-M	meso-2,6-Diaminoheptanedioate
2aepnp	(2-Aminoethyl)phosphonate
2ahbut	(S)-2-Aceto-2-hydroxybutanoate
2ahhmd	2-Amino-4-hydroxy-6-hydroxymethyl-7,8-dihydropteridine diphosphate
2ahhmp	2-Amino-4-hydroxy-6-hydroxymethyl-7,8-dihydropteridine
2beacp	But-2-enoyl-[acyl-carrier protein]
2c25dho	2-Carboxy-2,5-dihydro-5-oxofuran-2-acetate
2chdeacp	cis-Hexadec-2-enoyl-[acyl-carrier protein]
2cocdacp	cis-Octadec-2-enoyl-[acyl-carrier-protein]
2cpr5p	1-(2-Carboxyphenylamino)-1-deoxy-D-ribose 5-phosphate
2dda7p	2-Dehydro-3-deoxy-D-arabino-heptonate 7-phosphate
2ddg6p	2-Dehydro-3-deoxy-D-gluconate 6-phosphate
2ddglcn	2-Dehydro-3-deoxy-D-gluconate
2dhp	2-Dehydropantoate
2dr1p	2-Deoxy-D-ribose 1-phosphate
2dr5p	2-Deoxy-D-ribose 5-phosphate
2hxic-L	L-2-hydroxyisocaproate
2ins	2-Inosose
2mahmp	2-Methyl-4-amino-5-hydroxymethylpyrimidine diphosphate
2mba	2-Methyl butanoic acid
2mbal	2-Methylbutanal
2mbol	2-Methylbutanol
2mop	2-Methyl-3-oxopropanoate
2mpa	2-Methylpropanoic acid
2mpal	2-Methylpropanal
2mpol	2-Methylpropanol
2obut	2-Oxobutanoate
2oph	2-Octaprenylphenol
2p4c2me	2-phospho-4-(cytidine 5'-diphospho)-2-C-methyl-D-erythritol
2pg	D-Glycerate 2-phosphate
2pglyc	2-Phosphoglycolate
2tddacp	trans-Dodec-2-enoyl-[acyl-carrier protein]
2tdeacp	trans-Dec-2-enoyl-[acyl-carrier protein]
2thdeacp	trans-Hexadec-2-enoyl-[acyl-carrier protein]
2theacp	trans-Hex-2-enoyl-[acp]
2tocdacp	trans-Octadec-2-enoyl-[acyl-carrier-protein]
2toceacp	trans-Oct-2-enoyl-[acp]
2ttdeacp	trans-Tetradec-2-enoyl-[acyl-carrier protein]
34dhpha	3,4-Dihydroxyphenylacetate
34hplac	(R)-3-(4-Hydroxyphenyl)lactate
34hpp	3-(4-Hydroxyphenyl)pyruvate
35ccmp	3',5'-Cyclic CMP
35cdamp	3',5'-Cyclic dAMP
35cgmp	3',5'-Cyclic GMP
35cimp	3',5'-Cyclic IMP
3dhq	3-Dehydroquininate
3dhsk	3-Dehydroshikimate

Table B.1 – continued from previous page

Abbreviation	Official name
3hbacp	(3R)-3-Hydroxybutanoyl-[acyl-carrier protein]
3hddacp	(R)-3-Hydroxydodecanoyl-[acyl-carrier protein]
3hdeacp	(3R)-3-Hydroxydecanoyl-[acyl-carrier protein]
3hhacp	(R)-3-Hydroxyhexanoyl-[acp]
3hmp	3-Hydroxy-2-methylpropanoate
3hocacp	(R)-3-Hydroxyoctanoyl-[acyl-carrier protein]
3hocdacp	(3R)-3-Hydroxyoctadecanoyl-[acyl-carrier protein]
3hpaacp	(3R)-3-Hydroxypalmitoyl-[acyl-carrier protein]
3hppnl	3-Hydroxypropanal
3htdacp	(3R)-3-Hydroxytetradecanoyl-[acyl-carrier protein]
3ig3p	C ⁻ -(3-Indolyl)-glycerol 3-phosphate
3mba	3-Methylbutanoic acid
3mbal	3-Methylbutanal
3mbol	3-Methylbutanol
3mob	3-Methyl-2-oxobutanoate
3mop	(S)-3-Methyl-2-oxopentanoate
3ophb	3-Octaprenyl-4-hydroxybenzoate
3oxddacp	3-Oxododecanoyl-[acyl-carrier protein]
3oxdeacp	3-Oxodecanoyl-[acyl-carrier protein]
3oxhacp	3-Oxohexanoyl-[acyl-carrier protein]
3oxhdacp	3-Oxohexadecanoyl-[acp]
3oxocacp	3-Oxoctanoyl-[acyl-carrier protein]
3oxocdacp	3-Oxoctadecanoyl-[acp]
3oxtdacp	3-Oxotetradecanoyl-[acyl-carrier protein]
3pg	3-Phospho-D-glycerate
3php	3-Phosphohydroxypyruvate
3psme	5-O-(1-Carboxyvinyl)-3-phosphoshikimate
4abut	4-Aminobutanoate
4abz	4-Aminobenzoate
4adcho	4-Amino-4-deoxychorismate
4ahmmp	4-Amino-5-hydroxymethyl-2-methylpyrimidine
4ampm	4-Amino-2-methyl-5-phosphomethylpyrimidine
4c2me	4-(Cytidine 5'-diphospho)-2-C-methyl-D-erythritol
4coum	4-Coumarate
4h2oxg	D-4-Hydroxy-2-oxoglutarate
4hglu	4-Hydroxy-L-glutamate
4hphac	4-Hydroxyphenylacetate
4met2obut	4-Methylthio-2-oxobutanoate
4mhetz	4-Methyl-5-(2-hydroxyethyl)-thiazole
4mop	4-Methyl-2-oxopentanoate
4mpetz	4-Methyl-5-(2-phosphoethyl)-thiazole
4pasp	4-Phospho-L-aspartate
4ppan	D-4'-Phosphopantothenate
4ppcys	N-((R)-4-Phosphopantothenoyl)-L-cysteine
4vcoum	4-Vinyl p-coumaric acid
5aizc	5-Amino-1-(5-phospho-D-ribosyl)imidazole-4-carboxylate
5dpmev	(R)-5-Diphosphomevalonate
5fothf	5-Formyltetrahydrofolate
5mta	5-Methylthioadenosine
5mthf	5-Methyltetrahydrofolate
5mthglu	5-Methyltetrahydropteroyltri-L-glutamate
5mtr	5-Methylthio-D-ribose
5odhf2a	5-Oxo-4,5-dihydrofuran-2-acetate
5pmev	(R)-5-Phosphomevalonate
6pgc	6-Phospho-D-gluconate
6pgg	6-Phospho-β-D-glucosyl-(1,4)-D-glucose
6pgl	6-phospho-D-glucono-1,5-lactone
a-gal-D	α-D galactose
aaacp	Acetoacetyl-[acyl-carrier protein]
aacoa	Acetoacetyl-CoA
ac	Acetate
acald	Acetaldehyde
acamoxm	N-Acetyl-L-2-amino-6-oxopimelate
accoa	Acetyl-CoA
acetone	Acetone
acg5p	N-Acetyl-L-glutamyl 5-phosphate
acg5sa	N-Acetyl-L-glutamate 5-semialdehyde
acgal6p	N-Acetylgalactosamine 6-phosphate

Table B.1 – continued from previous page

Abbreviation	Official name
acgala	N-Acetyl-D-galactosamine
acgam	N-Acetyl-D-glucosamine
acgam1p	N-Acetyl-D-glucosamine 1-phosphate
acgam6p	N-Acetyl-D-glucosamine 6-phosphate
acglu	N-Acetyl-L-glutamate
achms	O-Acetyl-L-homoserine
acmalt	Acetyl-maltose
acmam	N-Acetyl-D-muramoate
acmama	N-Acetyl-D-muramoyl-L-alanine
acmana	N-Acetyl-D-mannosamine
acmanap	N-Acetyl-D-mannosamine 6-phosphate
acnam	N-Acetylneuraminic acid
acorn	N2-Acetyl-L-ornithine
acp	Acyl-carrier Protein
acser	O-Acetyl-L-serine
actn-R	(R)-Acetoin
actp	Acetyl phosphate
ade	Adenine
adn	Adenosine
adp	ADP
adpglc	ADPglucose
adprib	ADPribose
agly3p_LLA	1-Acyl-sn-glycerol 3-phosphate (<i>L. lactis</i> specific)
ahcys	S-Adenosyl-L-homocysteine
ahdt	2-Amino-4-hydroxy-6-(erythro-1,2,3-trihydroxypropyl)dihydropteridine triphosphate
aicar	5-Amino-1-(5-Phospho-D-ribose)imidazole-4-carboxamide
air	5-amino-1-(5-phospho-D-ribose)imidazole
akg	2-Oxoglutarate
al26da	N6-Acetyl-LL-2,6-diaminoheptanedioate
ala-B	β -Alanine
ala-D	D-Alanine
ala-L	L-Alanine
alac-S	(S)-2-Acetolactate
alalac	D-Alanyl-D-lactate
alatrna	L-Alanyl-tRNA(Ala)
amet	S-Adenosyl-L-methionine
amp	AMP
anth	Anthranilate
apoACP	Apoprotein [acyl carrier protein]
aps	Adenosine 5'-phosphosulfate
arab-L	L-Arabinose
arg-L	L-Arginine
argsuc	N(omega)-(L-Arginino)succinate
argtrna	L-Arginyl-tRNA(Arg)
asn-L	L-Asparagine
asnrna	L-Asparaginyl-tRNA(Asn)
asp-D	D-Aspartate
asp-L	L-Aspartate
aspsa	L-Aspartate 4-semialdehyde
asptrna	L-Aspartyl-tRNA(Asp)
atp	ATP
btd-RR	(R,R)-2,3-Butanediol
btn	Biotin
butacp	Butyryl-[acyl-carrier protein]
bzal	Benzaldehyde
camp	cAMP
cbasp	N-Carbamoyl-L-aspartate
cbp	Carbamoyl phosphate
cdp	CDP
cdpdag_LLA	CDPdiacylglycerol (<i>L. lactis</i> specific)
cdpglyc	CDPglycerol
cdprbtl	CDPriitol
cellb	Cellobiose
chol	Choline
chor	Chorismate
cit	Citrate
citr-L	L-Citrulline
clpn_LLA	Cardiolipin (<i>L. lactis</i> specific)

Table B.1 – continued from previous page

Abbreviation	Official name
cmp	CMP
co2	CO ₂
coa	Coenzyme A
cdpdag_LLA	CDP-Diacylglycerol, <i>L. lactis</i> specific
cpocdacp	Cyclopropanoyl octadecanoyl-[acyl-carrier protein]
CPS_LLA	Capsular polysaccharide linkage unit, <i>L. lactis</i> specific
csn	Cytosine
ctp	CTP
cyn	Cystine
cys-L	L-Cysteine
cysth-L	L-Cystathionine
cystrna	L-Cysteinyl-tRNA(Cys)
cytd	Cytidine
dad-2	Deoxyadenosine
dadp	dADP
damp	dAMP
datp	dATP
db4p	3,4-dihydroxy-2-butanone 4-phosphate
dcamp	N6-(1,2-Dicarboxyethyl)-AMP
dcdp	dCDP
dcmp	dCMP
dctp	dCTP
dcyt	Deoxycytidine
ddeacp	Dodecanoyl-[acyl-carrier protein]
decacp	Decanoyl-[acyl-carrier protein]
dgdp	dGDP
dgmp	dGMP
dgsn	Deoxyguanosine
dgtp	dGTP
dha	Dihydroxyacetone
dhap	Dihydroxyacetone phosphate
dhf	7,8-Dihydrofolate
dhnpt	2-Amino-4-hydroxy-6-(D-erythro-1,2,3-trihydroxypropyl)-7,8-dihydropteridine
dhor-S	(S)-Dihydroorotate
dhpmp	Dihydroneopterin monophosphate
dhpt	Dihydropteroate
diact	Diacetyl
dimp	dIMP
din	Deoxyinosine
dmpp	Dimethylallyl diphosphate
DNA_LLA	DNA, <i>L. lactis</i> specific
dnad	Deamino-NAD ⁺
dpcoa	Dephospho-CoA
drib	Deoxyribose
dtdp	dTDP
dtdp6dm	dTDP-6-deoxy-L-mannose
dtdpddg	dTDP-4-dehydro-6-deoxy-D-glucose
dtdpddm	dTDP-4-dehydro-6-deoxy-L-mannose
dtdpglc	dTDPglucose
dtmp	dTMP
dttp	dTTP
dudp	dUDP
dump	dUMP
duri	Deoxyuridine
dutp	dUTP
dxyl5p	1-Deoxy-D-xylulose 5-phosphate
e4p	D-Erythrose 4-phosphate
eig3p	D-Erythro-1-(Imidazol-4-yl)glycerol 3-phosphate
etha	Ethanolamine
etoh	Ethanol
f1p	D-Fructose 1-phosphate
f6p	D-Fructose 6-phosphate
fad	FAD
fdp	D-Fructose 1,6-bisphosphate
fgam	N2-Formyl-N1-(5-phospho-D-ribose)glycinamide
fmet	N-Formyl-L-methionine
fmn	Flavin mononucleotide
fol	Folate

Table B.1 – continued from previous page

Abbreviation	Official name
for	Formate
fpram	2-(Formamido)-N1-(5-phospho-D-ribosyl)acetamide
fprica	5-Formamido-1-(5-phospho-D-ribosyl)imidazole-4-carboxamide
frdp	Farnesyl diphosphate
fru	D-Fructose
fuc-L	L-Fucose
fum	Fumarate
glp	D-Glucose 1-phosphate
glp-B	β -D-Glucose 1-phosphate
g3p	Glyceraldehyde 3-phosphate
g3pc	sn-Glycero-3-phosphocholine
g3pe	sn-Glycero-3-phosphoethanolamine
g3pg	Glycerophosphoglycerol
g3pi	sn-Glycero-3-phospho-1-inositol
g3ps	Glycerophosphoserine
g6p	D-Glucose 6-phosphate
g6p-B	β -D-glucose 6-phosphate
gal	D-Galactose
gal1p	α -D-Galactose 1-phosphate
galt	Galactitol
galt1p	Galactitol 1-phosphate
gam1p	D-Glucosamine 1-phosphate
gam6p	D-Glucosamine 6-phosphate
gar	N1-(5-Phospho-D-ribosyl)glycinamide
gcald	Glycolaldehyde
gdp	GDP
gdptp	Guanosine 3'-diphosphate 5'-triphosphate
glc-D	D-Glucose
glcn-D	D-Gluconate
gln-L	L-Glutamine
glntrna	L-Glutaminyl-tRNA(Gln)
glu-D	D-Glutamate
glu-L	L-Glutamate
glu5p	L-Glutamate 5-phosphate
glu5sa	L-Glutamate 5-semialdehyde
glucys	γ -L-Glutamyl-L-cysteine
glutrna	L-Glutamyl-tRNA(Glu)
gly	Glycine
glyald	D-Glyceraldehyde
glyb	Glycine betaine
glyc	Glycerol
glyc-R	(R)-Glycerate
glyc3p	sn-Glycerol 3-phosphate
glyclt	Glycolate
glycogen	Glycogen
glytrna	Glycyl-tRNA(Gly)
gmp	GMP
grdp	Geranyl diphosphate
gsn	Guanosine
gthox	Oxidised glutathione
gthrd	Reduced glutathione
gtp	GTP
gua	Guanine
h	H ⁺
h2o	H ₂ O
h2o2	Hydrogen peroxide
h2s	Hydrogen sulfide
hco3	Bicarbonate
hcys-L	L-Homocysteine
hdeacp	Hexadecanoyl-[acyl-carrier protein]
hexacp	Hexanoyl-[acyl-carrier protein]
his-L	L-Histidine
hisp	L-Histidinol phosphate
hista	Histamine
histd	L-Histidinol
histrna	L-Histidyl-tRNA(His)
hmgcoa	Hydroxymethylglutaryl-CoA
hom-L	L-Homoserine

Table B.1 – continued from previous page

Abbreviation	Official name
hxan	Hypoxanthine
idp	IDP
idt	L-Iditol
ile-L	L-Isoleucine
iletrna	L-Isoleucyl-tRNA(Ile)
imacp	3-(Imidazol-4-yl)-2-oxopropyl phosphate
imlac	Imidazole lactate
imp	IMP
impyr	Imidazole pyruvate
indlac	Indolelactate
indpyr	Indolepyruvate
inost	myo-Inositol
ins	Inosine
ipdp	Isopentenyl diphosphate
itp	ITP
lac-D	D-Lactate
lac-L	L-Lactate
lald-L	L-Lactaldehyde
lcts	Lactose
leu-L	L-Leucine
leutrna	L-Leucyl-tRNA(Leu)
LTA_LLA	lipoteichoic acid (n=25, <i>L. lactis</i> specific)
LTAala_LLA	Lipoteichoic acid (n=25) with 100% D-Ala substitutions (<i>L. lactis</i> specific)
LTAglc_LLA	Lipoteichoic acid (n=25 with glucose residues, <i>L. lactis</i> specific)
LTAAlaGAL_LLA	Lipoteichoic acid (n=25 with alanine and galactose residues, <i>L. lactis</i> specific)
lys-L	L-Lysine
lyspg_LLA	1-Lysyl-phosphatidyl glycerol (<i>L. lactis</i> specific)
lystrna	L-Lysine-tRNA (Lys)
mal-L	L-Malate
malacp	Malonyl-[acyl-carrier protein]
malcoa	Malonyl-CoA
malt	Maltose
man	D-Mannose
man1p	D-Mannose 1-phosphate
man6p	D-Mannose 6-phosphate
MCOOH	MPT synthase small subunit MoaD
MCOSH	MPT synthase sulfurylated small subunit (MoaD-SH)
melib	Melibiose
mercppyr	Mercaptopyruvate
met-L	L-Methionine
methal	Methional
methf	5,10-Methenyltetrahydrofolate
mettrna	L-Methionyl-tRNA (Met)
mev-R	(R)-Mevalonate
MGD	Moldybdopterin guanine dinucleotide
milp-D	1D-myo-Inositol 1-phosphate
mlthf	5,10-Methylenetetrahydrofolate
mn2	Mn ²⁺
mnl	D-Mannitol
mnl1p	D-Mannitol 1-phosphate
Moco	Molybdenum cofactor
MPT	Molybdopterin
mql7	Menaquinol 7
mqn7	Menaquinone 7
n2ppn	2-Nitropropane
na1	Sodium
nac	Nicotinate
nad	Nicotinamide adenine dinucleotide
nadh	Nicotinamide adenine dinucleotide - reduced
nadp	Nicotinamide adenine dinucleotide phosphate
nadph	Nicotinamide adenine dinucleotide phosphate - reduced
ncam	Nicotinamide
nh3	Ammonia
nh4	Ammonium
nicrnt	Nicotinate D-ribonucleotide
no2	Nitrite
no3	Nitrate
o2	O ₂

Table B.1 – continued from previous page

Abbreviation	Official name
oaa	Oxaloacetate
ocdacp	Octadecanoyl-[acyl-carrier protein]
octacp	Octanoyl-[acyl-carrier protein]
orn-L	L-Ornithine
orot	Orotate
orot5p	Orotidine 5'-phosphate
oxa	Oxalate
pa_LLA	Phosphatidic acid (<i>L. lactis</i> specific)
pacald	Phenylacetaldehyde
pan4p	Pantetheine 4'-phosphate
pant-R	(R)-Pantoate
pap	Adenosine 3',5'-bisphosphate
paps	3'-Phosphoadenylyl sulfate
pea	Phenylethyl alcohol
pep	Phosphoenolpyruvate
pg_LLA	Phosphatidylglycerol (<i>L. lactis</i> specific)
PGlac2	Peptidoglycan with D-lac as C-terminal residue to form pentadepsipeptide
pgp_LLA	Phosphatidylglycerophosphate (<i>L. lactis</i> specific)
phe-L	L-Phenylalanine
phenol	Phenol
phetrna	L-Phenylalanyl-tRNA(Phe)
phlac	Phenyl lactate
phom	O-Phospho-L-homoserine
phpyr	Phenylpyruvate
pi	Phosphate
pnto-R	(R)-Pantothenate
polypi	Polyphosphate
ppaca	Phosphonoacetaldehyde
pphn	Prephenate
ppi	Diphosphate
pppi	Inorganic triphosphate
pram	5-Phospho- β -D-ribosylamine
pran	N-(5-Phospho-D-ribosyl)anthranilate
prbamp	1-(5-Phosphoribosyl)-AMP
prbatp	1-(5-Phosphoribosyl)-ATP
PreZ	Precursor Z in molybdenum cofactor biosynthesis
prfp	1-(5-Phosphoribosyl)-5-[(5-phosphoribosylamino)methylideneamino]imidazole-4-carboxamide
prlp	5-[(5-phospho-1-deoxyribulos-1-ylamino)methylideneamino]-1-(5-phosphoribosyl)imidazole-4-carboxamide
pro-L	L-Proline
PROT_LLA	<i>L. lactis</i> -specific protein composition for biomass
protrna	L-Prolyl-tRNA(Pro)
prpp	5-Phospho- α -D-ribose 1-diphosphate
psd5p	Pseudouridine 5'-phosphate
pser-L	O-Phospho-L-serine
ptrc	Putrescine
pyam5p	Pyridoxamine 5'-phosphate
pydam	Pyridoxamine
pydx	Pyridoxal
pydx5p	Pyridoxal 5'-phosphate
pydxn	Pyridoxine
pyr	Pyruvate
r1p	α -D-Ribose 1-phosphate
r5p	α -D-Ribose 5-phosphate
raffin	Raffinose
rbl-L	L-Ribulose
rbit	Ribitol
rbit5p	D-Ribitol 5-phosphate
rhcys	S-Ribosyl-L-homocysteine
rib-D	D-Ribose
ribflv	Riboflavin
ribflvRD	Reduced riboflavin
rml	L-Rhamnulose
rml1p	L-Rhamnulose 1-phosphate
rmn	L-Rhamnose
RNA_LLA	RNA, <i>L. lactis</i> specific
RTA	Teichoic acid containing ribitol-P
RTAala	Ribitol teichoic acid (n=25) with D-Ala substitutions
RTAglc	Ribitol teichoic acid (n=25) with glucose substitutions

Table B.1 – continued from previous page

Abbreviation	Official name
ru5p-D	D-Ribulose 5-phosphate
ru5p-L	L-Ribulose 5-phosphate
s7p	Sedoheptulose 7-phosphate
sbt-D	D-Sorbitol
sbt-L	L-Sorbitol
sbt6p	D-Sorbitol 6-phosphate
ser-D	D-Serine
ser-L	L-Serine
sertrna	L-Seryl-tRNA(Ser)
skm	Shikimate
skm5p	Shikimate 5-phosphate
sl26da	N-Succinyl-LL-2,6-diaminoheptanedioate
sl2a6o	N-Succinyl-2-L-amino-6-oxoheptanedioate
so4	Sulfate
spmd	Spermidine
srb-L	L-Sorbose
suc6p	Sucrose 6-phosphate
succ	Succinate
succoa	Succinyl-CoA
sucr	Sucrose
sucsal	Succinic semialdehyde
tartr-L	L-tartarate
tcys	Thiocysteine
tdeacp	Tetradecanoyl-[acyl-carrier protein]
thdp	2,3,4,5-Tetrahydrodipicolinate
thf	5,6,7,8-Tetrahydrofolate
thfglu	Tetrahydrofolyl-[Glu](2)
thglu	Tetrahydropteroyltri-L-glutamate
thm	Thiamin
thmmp	Thiamin monophosphate
thmpp	Thiamine diphosphate
thr-L	L-Threonine
thrtrna	L-Threonyl-tRNA(Thr)
thymd	Thymidine
trdox	Oxidised thioredoxin
trdrd	Reduced thioredoxin
tre	Trehalose
tre6p	α, α' -Trehalose 6-phosphate
trnaala	tRNA(Ala)
trnaarg	tRNA(Arg)
trnaasn	tRNA(Asn)
trnaasp	tRNA(Asp)
trnacys	tRNA(Cys)
trnaglu	tRNA(Glu)
trnagly	tRNA(Gly)
trnahis	tRNA(His)
trnaile	tRNA(Ile)
trnaleu	tRNA(Leu)
trnalys	tRNA(Lys)
trnamet	tRNA(Met)
trnaphe	tRNA(Phe)
trnapro	tRNA(Pro)
trnaser	tRNA(Ser)
trnathr	tRNA(Thr)
trnatrp	tRNA(Trp)
trnatyr	tRNA(Tyr)
trnaval	tRNA(Val)
trp-L	L-Tryptophan
trptrna	L-Tryptophanyl-tRNA(Trp)
tyr-L	L-Tyrosine
tyrtrna	L-Tyrosyl-tRNA(Tyr)
uaagmdalac	Undecaprenyl-diphospho-N-acetylmuramoyl-(N-acetylglucosamine)-L-alanyl-D-glutamyl-meso-2,6-diaminopimeloyl-D-alanyl-D-lactate
uaccg	UDP-N-acetyl-3-O-(1-carboxyvinyl)-D-glucosamine
uacgam	UDP-N-acetyl-D-glucosamine
uacmam	UDP-N-acetyl-D-mannosamine
uAgl	UDP-N-acetylmuramoyl-L-alanyl-D-glutamyl-L-lysine
uagmdalac	Undecaprenyl-diphospho-N-acetylmuramoyl-L-alanyl-D-glutamyl-meso-2,6-diaminopimeloyl-D-alanyl-D-lactate

Table B.1 – continued from previous page

Abbreviation	Official name
uama	UDP-N-acetylmuramoyl-L-alanine
uamag	UDP-N-acetylmuramoyl-L-alanyl-D-glutamate
uamr	UDP-N-acetylmuramate
udcp	Undecaprenol
udcpdp	Undecaprenyl diphosphate
udcpp	Undecaprenyl phosphate
udp	UDP
udpg	UDPglucose
udpgal	UDPGalactose
udpgalfur	UDP-D-galacto-1,4-furanose
ugmd	UDP-N-acetylmuramoyl-L-alanyl-D- γ -glutamyl-meso-2,6-diaminopimelate
ugmdalac	UDP-N-acetylmuramoyl-L-alanyl-D-glutamyl-meso-2,6-diaminopimeloyl-D-alanyl-D-lactate
ump	UMP
unaga	Undecaprenyl diphospho N-acetyl-glucosamine
unagama	Undecaprenyl-diphospho-N-acetylglucosamine-N-acetylmannosamine
unagamagp	Undecaprenyl-diphospho-N-acetylglucosamine-N-acetylmannosamine-glycerolphosphate
unRTA	Undecaprenyl-teichoic acid with ribitol
ura	Uracil
uri	Uridine
utp	UTP
val-L	L-Valine
valtrna	L-Valyl-tRNA(Val)
xan	Xanthine
xmp	Xanthosine 5'-phosphate
xtsn	Xanthosine
xu5p-D	D-Xylulose 5-phosphate

B.2 Reactions

Since the reaction stoichiometry is crucial for most quantitative modelling approaches like FBA all reactions added to the network has to be balanced with respect to oxygen atoms, hydrogen atoms and charges. Most reactions were copied from the networks of *L. plantarum* [Teusink et al., 2005] and *L. lactis* (unpublished results). However, some reactions had to be checked in databases. In most databases protons and cofactors are omitted and, thus, the reaction had to be balanced manually. The reactions included in the *S. pyogenes* metabolic network are given in the following table.

Table B.2: Reactions included in the genome-scale model.

Name	Equation
L-2-Hydroxyisocaproate transport (H^+ symport)	$2\text{hxic-L}[c] + \text{h}[c] \leftrightarrow 2\text{hxic-L}[e] + \text{h}[e]$
2-Methylbutanal dehydrogenase (acid forming)	$[c] : 2\text{mbal} + \text{h}_2\text{o} + \text{nad} \leftrightarrow 2\text{mba} + (2) \text{h} + \text{nadh}$
2-Methylbutanal transport	$2\text{mbal}[c] \leftrightarrow 2\text{mbal}[e]$
2-Methylbutanoic acid transport (H^+ -symport)	$2\text{mba}[c] + \text{h}[c] \leftrightarrow 2\text{mba}[e] + \text{h}[e]$
2-Methylbutanol dehydrogenase	$[c] : 2\text{mbal} + \text{h} + \text{nadh} \leftrightarrow 2\text{mbol} + \text{nad}$
2-Methylbutanol transport	$2\text{mbol}[c] \leftrightarrow 2\text{mbol}[e]$
2-Methylpropanal dehydrogenase (acid forming)	$[c] : 2\text{mpal} + \text{h}_2\text{o} + \text{nad} \leftrightarrow 2\text{mpa} + (2) \text{h} + \text{nadh}$
2-Methylpropanal transport	$2\text{mpal}[c] \leftrightarrow 2\text{mpal}[e]$
2-Methylpropanoic acid transport (H^+ -symport)	$2\text{mpa}[c] + \text{h}[c] \leftrightarrow 2\text{mpa}[e] + \text{h}[e]$
2-Methylpropanol dehydrogenase	$[c] : 2\text{mpal} + \text{h} + \text{nadh} \leftrightarrow 2\text{mpol} + \text{nad}$
2-Methylpropanol transport	$2\text{mpol}[c] \leftrightarrow 2\text{mpol}[e]$
3-Methylbutanal dehydrogenase (acid forming)	$[c] : 3\text{mbal} + \text{h}_2\text{o} + \text{nad} \leftrightarrow 3\text{mba} + (2) \text{h} + \text{nadh}$
3-Methylbutanal transport	$3\text{mbal}[c] \leftrightarrow 3\text{mbal}[e]$

Table B.2 – continued from previous page

Name	Equation
3-Methylbutanoic acid transport (H^+ -symport)	$3mba[c] + h[c] \leftrightarrow 3mba[e] + h[e]$
3-Methylbutanol dehydrogenase	$[c] : 3mbal + h + nadh \leftrightarrow 3mbol + nad$
3-Methylbutanol transport	$3mbol[c] \leftrightarrow 3mbol[e]$
3-Methyl-2-oxobutanoate decarboxylase	$[c] : 3mob + h \rightarrow 2mpal + co2$
3-Methyl-2-oxopentanoate decarboxylase	$[c] : 3mop + h \rightarrow 2mbal + co2$
4-Methyl-2-oxopentanoate decarboxylase	$[c] : 4mop + h \rightarrow 3mbal + co2$
4-Methylthio 2 oxobutyrate decarboxylase	$[c] : 4met2obut \rightarrow co2 + methal$
Aryl-alcohol dehydrogenase	$[c] : h + nadh + pacald \leftrightarrow nad + pea$
Acetyl-CoA C-acetyltransferase	$[c] : (2) accoa \rightarrow aacoa + coa$
Acetaldehyde dehydrogenase (acetylating)	$[c] : acald + coa + nad \leftrightarrow accoa + h + nadh$
Acetaldehyde reversible transport	$acald[e] \leftrightarrow acald[c]$
Acetyl-CoA carboxylase	$[c] : accoa + atp + hco3 \rightarrow adp + h + malcoa + pi$
N-Acetylglucosamine PTS	$acgala[e] + pep[c] \rightarrow acgal6p[c] + pyr[c]$
N-Acetyl-D-glucosamine transport via PEP:Pyr PTS	$acgam[e] + pep[c] \rightarrow acgam6p[c] + pyr[c]$
Acetate kinase	$[c] : ac + atp \leftrightarrow actp + adp$
N-Acetylneuraminate lyase	$[c] : acnam \rightarrow acmana + pyr$
Acetylornithine deacetylase	$[c] : acorn + h2o \rightarrow ac + orn-L$
Acyl-carrier protein synthase	$[c] : apoACP + coa \rightarrow acp + h + pap$
Acetolactate decarboxylase	$[c] : alac-S + h \rightarrow actn-R + co2$
(R)-Acetoin diffusion	$actn-R[e] \leftrightarrow actn-R[c]$
Acetate transport in/out via proton symport	$ac[e] + h[e] \leftrightarrow ac[c] + h[c]$
Acylphosphatase	$[c] : actp + h2o \rightarrow ac + h + pi$
4-Amino-4-deoxychorismate synthase	$[c] : chor + gln-L \rightarrow 4adcho + glu-L$
Adenine transport via proton symport (reversible)	$ade[e] + h[e] \leftrightarrow ade[c] + h[c]$
Adenylate kinase	$[c] : amp + atp \leftrightarrow (2) adp$
Adenylate kinase (Inorganic triphosphate)	$[c] : amp + pppi \leftrightarrow adp + ppi$
ADPribose diphosphatase	$[c] : adprib + h2o \rightarrow amp + (2) h + r5p$
Adenine phosphoribosyltransferase	$[c] : ade + prpp \rightarrow amp + ppi$
Adenylosuccinate lyase	$[c] : dcamp \rightarrow amp + fum$
Adenylosuccinate lyase	$[c] : 25aics \rightarrow aicar + fum$
Adenylosuccinate synthetase	$[c] : asp-L + gtp + imp \rightarrow dcamp + gdp + (2) h + pi$
1-Acyl-glycerol-3-phosphate acyltransferase (lactis specific)	$[c] : (0.03) 2chdeacp + (0.44) 2cocdacp + (0.005) 2ctdeacp + (0.01) agly3p_LLA + (0.13) cpocdacp + (0.295) hdeacp + (0.01) ocdacp + (0.09) tdeacp \rightarrow acp + (0.01) pa_LLA$
N-Acetylglucosamine-6-phosphate deacetylase	$[c] : acgam6p + h2o \rightarrow ac + gam6p$
Adenosylhomocysteine nucleosidase	$[c] : ahcys + h2o \rightarrow ade + rhcys$
Phosphoribosylaminoimidazolecarboxamide formyltransferase	$[c] : 10ftfh + aicar \leftrightarrow fprica + thf$
Phosphoribosylaminoimidazole carboxylase	$[c] : air + co2 \rightarrow 5aizc + h$
L-Alanine transport in/out via proton symport	$ala-L[e] + h[e] \leftrightarrow ala-L[c] + h[c]$
D-Alanine-D-alanine ligase (reversible)	$[c] : (2) ala-D + atp \leftrightarrow adp + alaala + h + pi$
D-Alanine-D-lactate ligase (reversible)	$[c] : ala-D + atp + lac-D \leftrightarrow adp + alalac + pi$
Alanine racemase	$[c] : ala-L \leftrightarrow ala-D$
L-Alanine transaminase	$[c] : akc + ala-L \leftrightarrow glu-L + pyr$
Alanyl-tRNA synthetase	$[c] : ala-L + atp + trnaala \rightarrow alatrna + amp + h + ppi$
Alcohol dehydrogenase (glycerol)	$[c] : glyald + h + nadh \leftrightarrow glyc + nad$
Alcohol dehydrogenase (ethanol: NAD)	$[c] : etoh + nad \leftrightarrow acald + h + nadh$
N-Acetylmannosamine 6-phosphate epimerase	$[c] : acmanap \rightarrow acgam6p$
N-Acetyl-D-mannosamine kinase	$[c] : acmana + atp \rightarrow acmanap + adp + h$
Anthranilate synthase	$[c] : chor + gln-L \rightarrow anth + glu-L + h + pyr$
L-Arginine transport via ABC system	$arg-L[e] + atp[c] + h2o[c] \rightarrow adp[c] + arg-L[c] + h[c] + pi[c]$
Arginine deiminase	$[c] : arg-L + h2o \rightarrow citr-L + h + nh3$
L-Arginine transport in via proton symport	$arg-L[e] + h[e] \leftrightarrow arg-L[c] + h[c]$
Arginyl-tRNA synthetase	$[c] : arg-L + atp + trnaarg \rightarrow amp + argtrna + h + ppi$
L-Asparaginase	$[c] : asn-L + h2o \rightarrow asp-L + nh4$
Asparagine synthetase	$[c] : asp-L + atp + nh4 \rightarrow amp + asn-L + h + ppi$
L-Asparagine transport in/out via proton symport	$asn-L[e] + h[e] \leftrightarrow asn-L[c] + h[c]$
Asparaginyl-tRNA synthetase	$[c] : asn-L + atp + trnaasn \rightarrow amp + asntrna + h + ppi$
Aspartate carbamoyltransferase	$[c] : asp-L + cbp \rightarrow cbasp + h + pi$
L-Aspartate transport in via proton symport	$asp-L[e] + h[e] \leftrightarrow asp-L[c] + h[c]$
Aspartate transaminase	$[c] : akc + asp-L \leftrightarrow glu-L + oaa$
Aspartate transaminase	$[c] : 4hglu + akc \leftrightarrow 4h2oxg + glu-L$
Aspartate transaminase	$[c] : akc + cys-L + h \leftrightarrow glu-L + mercppyr$
Aspartate transaminase	$[c] : akc + tyr-L \leftrightarrow 34hpp + glu-L$
Aspartate transaminase	$[c] : akc + phe-L \leftrightarrow glu-L + phpyr$
Aspartyl-tRNA synthetase	$[c] : asp-L + atp + trnaasp \rightarrow amp + asptrna + h + ppi$
ATP maintenance requirement	$[c] : atp + h2o \rightarrow adp + h + pi$
ATP synthase (three protons for one ATP)	$adp[c] + (3) h[e] + pi[c] \leftrightarrow atp[c] + (2) h[c] + h2o[c]$
β -Glucosidase (cellobiose)	$[e] : cellb + h2o \rightarrow (2) glc-D$

Table B.2 – continued from previous page

Name	Equation
Biomass equation LLA specific	$[c] : (0.0064) \text{CPS_LLA} + (0.00074) \text{DNA_LLA} + (0.00015) \text{LTAAlaGal_LLA} + (0.119) \text{PG} + (0.00329) \text{RNA_LLA} + (60) \text{atp} + (0.000138) \text{clpn_LLA} + (0.0002) \text{coa} + (0.000096) \text{d12dg_LLA} + (60) \text{h2o} + (0.000013) \text{lyspg_LLA} + (0.000013) \text{m12dg_LLA} + (0.002) \text{nad} + (0.000061) \text{pg_LLA} + (0.004201) \text{prot_LLA} + (0.00001) \text{thf} + (0.00001) \text{thmpp} + (0.0002) \text{udcpdp} \rightarrow (60) \text{adp} + (60) \text{h} + (60) \text{pi}$
(R,R)-butanediol dehydrogenase	$[c] : \text{btd-RR} + \text{nad} \leftrightarrow \text{actn-R} + \text{h} + \text{nadh}$
(R,R)-butanediol transport in/out via diffusion reversible	$\text{btd-RR}[c] \leftrightarrow \text{btd-RR}[e]$
Butyryl-[acyl-carrier protein]:malonyl-CoA C-acyltransferase	$[c] : 2\text{beacp} + \text{h} + \text{nadh} \rightarrow \text{butacp} + \text{nad}$
Biotin uptake	$\text{btn}[e] + \text{h}[e] \rightarrow \text{btn}[c] + \text{h}[c]$
Benzaldehyde transport	$\text{bzal}[c] \leftrightarrow \text{bzal}[e]$
Carbamate kinase	$[c] : \text{atp} + \text{co2} + \text{nh4} \rightarrow \text{adp} + \text{cbp} + (2) \text{h}$
Carbamoyl-phosphate synthase (glutamine-hydrolysing)	$[c] : (2) \text{atp} + \text{gln-L} + \text{h2o} + \text{hco3} \rightarrow (2) \text{adp} + \text{cbp} + \text{glu-L} + (2) \text{h} + \text{pi}$
4-(Cytidine 5'-diphospho)-2-C-methyl-D-erythritol kinase	$[c] : 4\text{c2me} + \text{atp} \rightarrow 2\text{p4c2me} + \text{adp} + \text{h}$
Cellulose transport via PEP:Pyr PTS	$\text{cellb}[e] + \text{pep}[c] \rightarrow 6\text{pgg}[c] + \text{pyr}[c]$
Cyclopropane fatty acid synthase (n18:0)	$[c] : 2\text{cocdacp} + \text{amet} \rightarrow \text{ahcys} + \text{cpocdacp} + \text{h}$
Chorismate mutase	$[c] : \text{chor} \rightarrow \text{pphn}$
Chorismate synthase	$[c] : 3\text{psme} \rightarrow \text{chor} + \text{pi}$
Citrate lyase	$[c] : \text{cit} \rightarrow \text{ac} + \text{oaa}$
Citrate transport in/out via proton symport	$\text{cit}[e] + \text{h}[e] \leftrightarrow \text{cit}[c] + \text{h}[c]$
Cardiolipin Synthase (lactis specific)	$[c] : (0.02) \text{pg_LLA} \leftrightarrow (0.01) \text{clpn_LLA} + \text{glyc}$
CO ₂ transport out via diffusion	$\text{co2}[e] \leftrightarrow \text{co2}[c]$
CPS synthase complex, LLA specific	$[c] : \text{dtdp6dm} + (4) \text{h2o} + (2) \text{udpg} + \text{udpgal} \leftrightarrow \text{CPS_LLA} + \text{dtdp} + (5) \text{h} + (2) \text{udp} + \text{ump}$
Cytosine deaminase	$[c] : \text{csn} + \text{h} + \text{h2o} \rightarrow \text{nh4} + \text{ura}$
Cytosine transport in/out via proton symporter	$\text{csn}[e] + \text{h}[e] \leftrightarrow \text{csn}[c] + \text{h}[c]$
CTP synthase (NH ₃)	$[c] : \text{atp} + \text{nh4} + \text{utp} \rightarrow \text{adp} + \text{ctp} + (2) \text{h} + \text{pi}$
CTP synthase (glutamine)	$[c] : \text{atp} + \text{gln-L} + \text{h2o} + \text{utp} \rightarrow \text{adp} + \text{ctp} + \text{glu-L} + (2) \text{h} + \text{pi}$
Cystine transport in via proton symport	$\text{cyn}[e] + \text{h}[e] \leftrightarrow \text{cyn}[c] + \text{h}[c]$
cysteine synthase	$[c] : \text{acser} + \text{h2s} \rightarrow \text{ac} + \text{cys-L} + \text{h}$
L-Cysteine transport in via proton symport	$\text{cys-L}[e] + \text{h}[e] \leftrightarrow \text{cys-L}[c] + \text{h}[c]$
Cystathionine g-lyase	$[c] : \text{cysth-L} + \text{h2o} \rightarrow 2\text{obut} + \text{cys-L} + \text{nh4}$
Cystathionine g-lyase	$[c] : \text{cyn} + \text{h2o} \rightarrow \text{tcys} + \text{nh3} + \text{pyr}$
Cystathionine b-lyase	$[c] : \text{cysth-L} + \text{h2o} \rightarrow \text{hcys-L} + \text{nh4} + \text{pyr}$
CysteinyI-tRNA synthetase	$[c] : \text{atp} + \text{cys-L} + \text{trnacys} \rightarrow \text{amp} + \text{cysrna} + \text{h} + \text{ppi}$
Cytidine kinase (ATP)	$[c] : \text{atp} + \text{cytd} \rightarrow \text{adp} + \text{cmp} + \text{h}$
Cytidine kinase (GTP)	$[c] : \text{cytd} + \text{gtp} \rightarrow \text{cmp} + \text{gdp} + \text{h}$
Cytidine kinase (ITP)	$[c] : \text{cytd} + \text{itp} \rightarrow \text{cmp} + \text{h} + \text{idp}$
Cytidylate kinase (CMP)	$[c] : \text{atp} + \text{cmp} \leftrightarrow \text{adp} + \text{cdp}$
Cytidylate kinase (dCMP)	$[c] : \text{atp} + \text{dcmp} \leftrightarrow \text{adp} + \text{dcdp}$
D-Lactate transport via proton symport	$\text{h}[e] + \text{lac-D}[e] \leftrightarrow \text{h}[c] + \text{lac-D}[c]$
Deoxyadenosine kinase	$[c] : \text{atp} + \text{dad-2} \rightarrow \text{adp} + \text{damp} + \text{h}$
1,2-Diacylglycerol 3-glucosyltransferase (Lactis specific)	$[c] : (0.01) 12\text{dgr_LLA} + (2) \text{udpg} \rightarrow (0.01) \text{d12dg_LLA} + (2) \text{h} + (2) \text{udp}$
Diacylglycerol kinase (Lactis specific)	$[c] : (0.01) 12\text{dgr_LLA} + \text{atp} \rightarrow \text{adp} + \text{h} + (0.01) \text{pa_LLA}$
3-deoxy-D-Arabino-heptulosonate 7-phosphate synthetase	$[c] : \text{e4p} + \text{h2o} + \text{pep} \rightarrow 2\text{dda7p} + \text{pi}$
D-Alanine lipoteichoic acid ligase	$[c] : (0.01) \text{LTA_LLA} + (6) \text{ala-D} + (6) \text{atp} \rightarrow (0.01) \text{LTAala_LLA} + (6) \text{adp} + (6) \text{pi}$
CDP-Diacylglycerol synthetase (Lactis specific)	$[c] : \text{ctp} + \text{h} + (0.01) \text{pa_LLA} \leftrightarrow (0.01) \text{cdpdag_LLA} + \text{ppi}$
2-dehydro-3-deoxy-Gluconokinase	$[c] : 2\text{ddgln} + \text{atp} \rightarrow 2\text{ddg6p} + \text{adp} + \text{h}$
Dodecanoyl-[acyl-carrier protein]: malonyl-CoA C-acyltransferase	$[c] : 2\text{tddacp} + \text{h} + \text{nadh} \rightarrow \text{ddeacp} + \text{nad}$
Decanoyl-[acyl-carrier protein]:malonyl-CoA C-acyltransferase	$[c] : 2\text{tdeacp} + \text{h} + \text{nadh} \rightarrow \text{decacp} + \text{nad}$
Deoxyguanosine kinase (dgsn)	$[c] : \text{atp} + \text{dgsn} \rightarrow \text{adp} + \text{dgmp} + \text{h}$
Deoxyguanosine kinase (gmp)	$[c] : \text{atp} + \text{gmp} \rightarrow \text{adp} + \text{gsn} + \text{h}$
Deoxyguanosine kinase (xmp)	$[c] : \text{atp} + \text{xmp} \rightarrow \text{adp} + \text{xtn} + \text{h}$
Deoxyguanosine kinase (imp)	$[c] : \text{atp} + \text{imp} \rightarrow \text{adp} + \text{ins} + \text{h}$
Deoxyguanosine kinase (amp)	$[c] : \text{atp} + \text{amp} \rightarrow \text{adp} + \text{adn} + \text{h}$
Deoxyguanosine kinase (damp)	$[c] : \text{atp} + \text{damp} \rightarrow \text{adp} + \text{dadn} + \text{h}$
Deoxyguanosine kinase (cmp)	$[c] : \text{atp} + \text{cmp} \rightarrow \text{adp} + \text{cytd} + \text{h}$
Deoxyguanosine kinase (dtmp)	$[c] : \text{atp} + \text{dtmp} \rightarrow \text{adp} + \text{thymd} + \text{h}$
Dihydroxyacetone phosphotransferase	$[c] : \text{dha} + \text{pep} \rightarrow \text{dhap} + \text{pyr}$
Dihydroxyacetone transport via facilitated diffusion	$\text{dha}[e] \leftrightarrow \text{dha}[c]$
Dihydrofolate reductase	$[c] : \text{dhf} + \text{nadp} \leftrightarrow \text{fol} + \text{nadph}$
Dihydrofolate reductase	$[c] : \text{dhf} + \text{h} + \text{nadph} \leftrightarrow \text{nadp} + \text{thf}$

Table B.2 – continued from previous page

Name	Equation
Dihydrofolate synthase	[c] : atp + dhpt + glu-L → adp + dhf + h + pi
Dihydroneopterin aldolase	[c] : dhnpt → 2ahhmp + gcald
Dihydroorotic acid dehydrogenase (NAD)	[c] : dhor-S + nad ↔ h + nadh + orot
Dihydroorotic acid dehydrogenase (O ₂)	[c] : dhor-S + o2 ↔ h2o2 + orot
Dihydroorotase	[c] : dhor-S + h2o ↔ cbasp + h
Dihydropteroate synthase	[c] : 2ahhmd + 4abz → dhpt + ppi
3-Dehydroquininate dehydratase	[c] : 3dhq ↔ 3dhsq + h2o
3-Dehydroquininate synthase	[c] : 2dda7p → 3dhq + pi
Diacetyl diffusion	diact[c] ↔ diact[e]
Dimethylallyltranstransferase	[c] : dmpp + ipdp → grdp + ppi
DNA synthesis, LLA specific	[c] : (1.37) atp + (0.32) datp + (0.18) dctp + (0.18) dgtp + (0.32) dttp + (1.37) h2o → (0.01) DNA_LLA + (1.37) adp + (1.37) h + (1.37) pi + ppi
Dihydroneopterin monophosphate dephosphorylase	[c] : dhpmp + h2o → dhnpt + h + pi
Dihydroneopterin triphosphate pyrophosphatase	[c] : ahdt + h2o → dhpmp + ppi
Dephospho-CoA kinase	[c] : atp + dpcoa → adp + coa + h
Diphosphomevalonate decarboxylase	[c] : 5dpmev + atp → adp + co2 + ipdp + pi
2-Dehydropantoate 2-reductase	[c] : 2dhp + h + nadph → nadp + pant-R
Deoxyribose-phosphate aldolase	[c] : 2dr5p → acald + g3p
dTMP kinase	[c] : atp + dtmp ↔ adp + dtdp
Deoxyuridine kinase (ATP:Deoxyuridine)	[c] : atp + duri → adp + dump + h
Purine-nucleoside phosphatase (deoxyuridine)	[c] : duri + pi ↔ 2dr1p + ura
dUTP diphosphatase	[c] : dutp + h2o → dump + h + ppi
2-dehydro-3-deoxy-Phosphogluconate aldolase	[c] : 2ddg6p → g3p + pyr
Enolase	[c] : 2pg ↔ h2o + pep
Ethanol transport in/out via diffusion	etoh[e] ↔ etoh[c]
4-Aminobenzoate exchange	[e] : 4abz ↔
Acetate exchange	[e] : ac ↔
(R)-Acetoin exchange	[e] : actn-R ↔
Adenine exchange	[e] : ade ↔
L-Alanine exchange	[e] : ala-L ↔
L-Arginine exchange	[e] : arg-L ↔
L-Asparagine exchange	[e] : asn-L ↔
L-Aspartate exchange	[e] : asp-L ↔
(R,R)-2,3-Butanediol exchange	[e] : btd-RR ↔
Biotin exchange	[e] : btn ↔
Cellobiose exchange	[e] : cellb ↔
Citrate exchange	[e] : cit ↔
CO ₂ exchange	[e] : co2 ↔
Cytosine exchange	[e] : csn ↔
Cystine exchange	[e] : cyn ↔
L-Cysteine exchange	[e] : cys-L ↔
Ethanol exchange	[e] : etoh ↔
Formate exchange	[e] : for ↔
D-Glucose exchange	[e] : glc-D ↔
L-Glutamine exchange	[e] : gln-L ↔
L-Glutamate exchange	[e] : glu-L ↔
Glycine exchange	[e] : gly ↔
Glycolate exchange	[e] : glyclt ↔
Guanine exchange	[e] : gua ↔
H ⁺ exchange	[e] : h ↔
H ₂ O exchange	[e] : h2o ↔
L-Histidine exchange	[e] : his-L ↔
L-Isoleucine exchange	[e] : ile-L ↔
Inosine exchange	[e] : ins ↔
D-lactate exchange	[e] : lac-D ↔
L-Lactate exchange	[e] : lac-L ↔
L-Leucine exchange	[e] : leu-L ↔
L-Lysine exchange	[e] : lys-L ↔
Maltose exchange	[e] : malt ↔
D-Mannose exchange	[e] : man ↔
L-Methionine exchange	[e] : met-L ↔
Nicotinate exchange	[e] : nac ↔
NH ₃ exchange	[e] : nh3 ↔
Ammonium exchange	[e] : nh4 ↔
Nitrite exchange	[e] : no2 ↔
Nitrate exchange	[e] : no3 ↔
O ₂ exchange	[e] : o2 ↔

Table B.2 – continued from previous page

Name	Equation
Ornithine exchange	orn-L[e] ↔ orn-L[c]
Orotate exchange	[e] : orot ↔
L-Phenylalanine exchange	[e] : phe-L ↔
Phosphate exchange	[e] : pi ↔
(R)-Pantothenate exchange	[e] : pnto-R ↔
L-Proline exchange	[e] : pro-L ↔
Pyridoxamine exchange	[e] : pydam ↔
Pyridoxine exchange	[e] : pydxn ↔
Pyruvate exchange	[e] : pyr ↔
Riboflavin exchange	[e] : ribflv ↔
Exchange for Serine	[e] : ser-L ↔
Sulfate exchange	[e] : so4 ↔
Spermidine exchange	[e] : spmd ↔
Succinate exchange	[e] : succ ↔
Sucrose exchange	[e] : sucr ↔
Thiamin exchange	[e] : thm ↔
L-Threonine exchange	[e] : thr-L ↔
Thymidine exchange	[e] : thymd ↔
Trehalose exchange	[e] : tre ↔
L-Tryptophan exchange	[e] : trp-L ↔
L-Tyrosine exchange	[e] : tyr-L ↔
L-Valine exchange	[e] : val-L ↔
Xanthine exchange	[e] : xan ↔
Fructose-1-phosphate kinase	[c] : atp + flp → adp + fdp + h
Fatty acid enoyl isomerase (FabM reaction)	[c] : 2ttdeacp ↔ 2ctdeacp
Fatty acid enoyl isomerase (FabM reaction)	[c] : 2thdeacp ↔ 2chdeacp
Fatty acid enoyl isomerase (FabM reaction, 18:1)	[c] : 2tocdacp ↔ 2cocdacp
Fructose-bisphosphate aldolase	[c] : fdp ↔ dhap + g3p
β-Fructofuranosidase	[c] : h2o + suc6p → fru + g6p
Flavin reductase	[c] : h + nadph + ribflv → nadp + ribflvRD
Formylmethionine deformylase	[c] : fmet + h2o → for + met-L
Acid phosphatase / phosphotransferase (FMN)	[c] : fmn + h2o → ribflv + pi
FMN adenyltransferase	[c] : atp + fmn + h → fad + ppi
Methionyl-tRNA formyltransferase	[c] : 10fthf + mettrna + h2o → fmet + thf
Folate transport via proton symport	fol[e] + h[e] ↔ fol[c] + h[c]
Formate transport in via proton symport	for[e] + h[e] ↔ for[c] + h[c]
Fructokinase	[c] : atp + fru → adp + f6p + h
D-Fructose transport via PEP:Pyr PTS	fru[e] + pep[c] → flp[c] + pyr[c]
Formate-tetrahydrofolate ligase	[c] : atp + for + thf → 10fthf + adp + pi
Glucosamine-1-phosphate N-acetyltransferase	[c] : accoa + gam1p → acgam1p + coa + h
Glucose-1-phosphate thymidyltransferase	[c] : dttp + g1p + h → dtdpglc + ppi
Glycerol-3-phosphate dehydrogenase (NAD)	[c] : gly3p + nad ↔ dhap + h + nadh
Glycerol 3-phosphate oxidase	[c] : gly3p + o2 → dhap + h2o2
L-Glutamate 5-semialdehyde dehydratase (spontaneous)	[c] : glu5sa ↔ 1pyr5c + h + h2o
Glutamate-5-semialdehyde dehydrogenase	[c] : glu5p + h + nadph → glu5sa + nadp + pi
Glucosamine-6-phosphate deaminase	[c] : gam6p + h2o → f6p + nh4
Glucose-6-phosphate isomerase	[c] : g6p ↔ g6p-B
4-Aminobutyrate transport in/out via proton symport	4abut[e] + h[e] ↔ 4abut[c] + h[c]
Galactose lipoteichoic acid ligase	[c] : (0.01) LTAala_LLA + (9.8) udpgal → (0.01) LTAala-Gal_LLA + (9.8) h + (9.8) udp
Galactitol transport via PEP:Pyr PTS	galt[e] + pep[c] → galt1p[c] + pyr[c]
UTP-glucose-1-phosphate uridylyltransferase	[c] : g1p + h + utp ↔ ppi + udpg
Glyceraldehyde-3-phosphate dehydrogenase (NAD)	[c] : g3p + nad + pi ↔ 13dpg + h + nadh
Non-phosphorylating glyceraldehyde-3-phosphate dehydrogenase (NADP)	[c] : g3p + nadp + h2o → 3pg + nadph + (2) h
Phosphoribosylglycinamide formyltransferase	[c] : 10fthf + gar ↔ fgam + h + thf
Phosphoribosylglycinamide formyltransferase (metthf)	[c] : methf + h2o + gar → fgam + (2) h + thf
Glycerol 3-phosphate acyltransferase (Lactis specific)	[c] : (0.03) 2chdeacp + (0.44) 2cocdacp + (0.005) 2ctdeacp + (0.13) cpocdacp + gly3p + (0.295) hdeacp + (0.01) ocdacp + (0.09) tdeacp → acp + (0.01) agly3p_LLA
Glycolaldehyde dehydrogenase	[c] : gcald + h2o + nad → glyclt + (2) h + nadh
Glutamine-fructose-6-phosphate transaminase	[c] : f6p + gln-L → gam6p + glu-L
Glycine hydroxymethyltransferase	[c] : ser-L + thf ↔ gly + h2o + mlthf
Guanylate kinase (GMP:ATP)	[c] : atp + gmp ↔ adp + gdp
Guanylate kinase (GMP:dATP)	[c] : datp + gmp ↔ dadp + gdp
Glycogen phosphorylase	[c] : glycogen + pi → g1p
D-Glucose transport via PEP:Pyr PTS	glc-D[e] + pep[c] → g6p[c] + pyr[c]
Glucose transport via facilitated diffusion	glc-D[e] ↔ glc-D[c]

Table B.2 – continued from previous page

Name	Equation
L-glutamine transport via ABC system	$\text{atp}[c] + \text{gln-L}[e] + \text{h2o}[c] \rightarrow \text{adp}[c] + \text{gln-L}[c] + \text{h}[c] + \text{pi}[c]$
Glutamine synthetase	$[c] : \text{atp} + \text{glu-L} + \text{nh4} \rightarrow \text{adp} + \text{gln-L} + \text{h} + \text{pi}$
Glutamyl-tRNA(Gln):L-glutamine amido-ligase (ADP-forming)	$[c] : \text{atp} + \text{gln-L} + \text{glutrna} + \text{h2o} \leftrightarrow \text{adp} + \text{glntrna} + \text{glu-L} + \text{h} + \text{pi}$
Glutaminyl-tRNA synthetase	$[c] : \text{atp} + \text{glutrnagln} + \text{nh4} \rightarrow \text{amp} + \text{glntrna} + \text{h} + \text{ppi}$
Glucose lipoteichoic acid ligase	$[c] : (0.01) \text{LTA_LLA} + (25) \text{udpg} \rightarrow (0.01) \text{LTAglc_LLA} + (25) \text{h} + (25) \text{udp}$
Glutamate 5-kinase	$[c] : \text{atp} + \text{glu-L} \rightarrow \text{adp} + \text{glu5p}$
L-Glutamine transport via ABC system	$\text{atp}[c] + \text{gln-L}[e] + \text{h2o}[c] \rightarrow \text{adp}[c] + \text{gln-L}[c] + \text{h}[c] + \text{pi}[c]$
Glutamine phosphoribosyldiphosphate amidotransferase	$[c] : \text{gln-L} + \text{h2o} + \text{prpp} \rightarrow \text{glu-L} + \text{ppi} + \text{pram}$
Glutamate racemase	$[c] : \text{glu-D} \leftrightarrow \text{glu-L}$
L-Glutamate transport in/out via proton symporter	$\text{glu-L}[e] + \text{h}[e] \leftrightarrow \text{glu-L}[c] + \text{h}[c]$
Glutamyl-tRNA synthetase	$[c] : \text{atp} + \text{glu-L} + \text{trnaglu} \rightarrow \text{amp} + \text{glutrna} + \text{h} + \text{ppi}$
Glutamyl-tRNAgln synthetase	$[c] : \text{atp} + \text{glu-L} + \text{trnagln} \rightarrow \text{amp} + \text{glutrnagln} + \text{h} + \text{ppi}$
glycine betaine transport via ABC system	$\text{atp}[c] + \text{glyb}[e] + \text{h2o}[c] \rightarrow \text{adp}[c] + \text{glyb}[c] + \text{h}[c] + \text{pi}[c]$
glycerate kinase	$[c] : \text{atp} + \text{glyc-R} \rightarrow 3\text{pg} + \text{adp} + \text{h}$
glycolate transport via proton symport, reversible storage/mobilisation of glycogen	$\text{glyclt}[e] + \text{h}[e] \leftrightarrow \text{glyclt}[c] + \text{h}[c]$ $\text{glycogen}[c] \leftrightarrow \text{glycogen}[e]$
glycerol transport via uniport (facilitated diffusion)	$\text{glyc}[e] \rightarrow \text{glyc}[c]$
glycerol kinase	$[c] : \text{atp} + \text{glyc} \rightarrow \text{adp} + \text{glyc3p} + \text{h}$
glycine transport in/out via proton symport	$\text{gly}[e] + \text{h}[e] \leftrightarrow \text{gly}[c] + \text{h}[c]$
Glycyl-tRNA synthetase	$[c] : \text{atp} + \text{gly} + \text{trnagly} \rightarrow \text{amp} + \text{glytrna} + \text{h} + \text{ppi}$
GMP reductase	$[c] : \text{gmp} + (2) \text{h} + \text{nadph} \rightarrow \text{imp} + \text{nadp} + \text{nh4}$
GMP synthase (glutamine-hydrolysing)	$[c] : \text{atp} + \text{gln-L} + \text{h2o} + \text{xmp} \rightarrow \text{amp} + \text{glu-L} + \text{gmp} + (2) \text{h} + \text{ppi}$
Glycerophosphodiester phosphodiesterase (sn-Glycero-3-phosphocholine)	$[c] : \text{g3pc} + \text{h2o} \rightarrow \text{chol} + \text{glyc3p} + \text{h}$
Glycerophosphodiester phosphodiesterase (Glycerophosphoethanolamine)	$[c] : \text{g3pe} + \text{h2o} \rightarrow \text{etha} + \text{glyc3p} + \text{h}$
Glycerophosphodiester phosphodiesterase (Glycerophosphoserine)	$[c] : \text{g3ps} + \text{h2o} \rightarrow \text{glyc3p} + \text{h} + \text{ser-L}$
Glycerophosphodiester phosphodiesterase (Glycerophosphoglycerol)	$[c] : \text{g3pg} + \text{h2o} \rightarrow \text{glyc} + \text{glyc3p} + \text{h}$
Glycerophosphodiester phosphodiesterase (Glycerophosphoinositol)	$[c] : \text{g3pi} + \text{h2o} \rightarrow \text{glyc3p} + \text{h} + \text{inost}$
geranyltransterase	$[c] : \text{grdp} + \text{ipdp} \rightarrow \text{frdp} + \text{ppi}$
glutathione peroxidase	$[c] : (2) \text{gthrd} + \text{h2o2} \rightarrow \text{gthox} + (2) \text{h2o}$
glutathione-disulfide reductase	$[c] : (2) \text{gthrd} + \text{nadp} \leftrightarrow \text{gthox} + \text{h} + \text{nadph}$
GTP cyclohydrolase I	$[c] : \text{gtp} + \text{h2o} \rightarrow \text{ahdt} + \text{for} + \text{h}$
GTP diphosphokinase	$[c] : \text{atp} + \text{gtp} \rightarrow \text{amp} + \text{gdptp} + \text{h}$
guanine phosphoribosyltransferase	$[c] : \text{gua} + \text{prpp} \rightarrow \text{gmp} + \text{ppi}$
guanine transport in via proton symport	$\text{gua}[e] + \text{h}[e] \rightarrow \text{gua}[c] + \text{h}[c]$
H ₂ O transport via diffusion	$\text{h2o}[e] \leftrightarrow \text{h2o}[c]$
(3R)-3-Hydroxybutanoyl-[acyl-carrier-protein] hydro-lyase	$[c] : 3\text{hbacp} \rightarrow 2\text{beacp} + \text{h2o}$
(3R)-3-Hydroxybutanoyl-[acyl-carrier protein]:NADP+ oxidoreductase	$[c] : \text{aaacp} + \text{h} + \text{nadph} \rightarrow 3\text{hbacp} + \text{nadp}$
carbonate dehydratase (HCO ₃ equilibration reaction)	$[c] : \text{co2} + \text{h2o} \leftrightarrow \text{h} + \text{hco3}$
homocysteine S-methyltransferase	$[c] : \text{amet} + \text{hcys-L} \rightarrow \text{ahcys} + \text{h} + \text{met-L}$
(3R)-3-Hydroxybutanoyl-[acyl-carrier-protein] hydro-lyase	$[c] : 3\text{hddacp} \rightarrow 2\text{tddacp} + \text{h2o}$
(3R)-3-Hydroxydodecanoyl-[acyl-carrier-protein]:NADP+ oxidoreductase	$[c] : 3\text{oxddacp} + \text{h} + \text{nadph} \rightarrow 3\text{hddacp} + \text{nadp}$
(3R)-3-Hydroxybutanoyl-[acyl-carrier-protein] hydro-lyase	$[c] : 3\text{hdeacp} \rightarrow 2\text{tdeacp} + \text{h2o}$
(3R)-3-Hydroxydecanoyl-[acyl-carrier-protein]:NADP+ oxidoreductase	$[c] : 3\text{oxdeacp} + \text{h} + \text{nadph} \rightarrow 3\text{hdeacp} + \text{nadp}$
Hexadecanoyl-[acyl-carrier protein]:malonyl-CoA C-acyltransferase	$[c] : 2\text{thdeacp} + \text{h} + \text{nadh} \rightarrow \text{hdeacp} + \text{nad}$
Hexanoyl-[acyl-carrier protein]:malonyl-CoA C-acyltransferase	$[c] : 2\text{theacp} + \text{h} + \text{nadh} \rightarrow \text{hexacp} + \text{nad}$
hexokinase (D-glucose:ATP)	$[c] : \text{atp} + \text{glc-D} \rightarrow \text{adp} + \text{g6p} + \text{h}$
(3R)-3-Hydroxypalmitoyl-[acyl-carrier-protein] hydro-lyase	$[c] : 3\text{hpaacp} \rightarrow 2\text{thdeacp} + \text{h2o}$
(3R)-3-Hydroxypalmitoyl-[acyl-carrier-protein]:NADP+ oxidoreductase	$[c] : 3\text{oxhdacp} + \text{h} + \text{nadph} \rightarrow 3\text{hpaacp} + \text{nadp}$
(3R)-3-Hydroxybutanoyl-[acyl-carrier-protein] hydro-lyase	$[c] : 3\text{hhacp} \rightarrow 2\text{theacp} + \text{h2o}$
(3R)-3-Hydroxyhexanoyl-[acyl-carrier-protein]:NADP+ oxidoreductase	$[c] : 3\text{oxhacp} + \text{h} + \text{nadph} \rightarrow 3\text{hhacp} + \text{nadp}$
histidine decarboxylase	$[c] : \text{h} + \text{his-L} \rightarrow \text{co2} + \text{hista}$
L-histidine transport in via proton symport	$\text{h}[e] + \text{his-L}[e] \leftrightarrow \text{h}[c] + \text{his-L}[c]$
histidine transaminase	$[c] : \text{akg} + \text{his-L} \leftrightarrow \text{glu-L} + \text{impyr}$
histide/histamine antiporter	$\text{his-L}[c] + \text{hista}[e] \leftrightarrow \text{his-L}[e] + \text{hista}[c]$

Table B.2 – continued from previous page

Name	Equation
Histidyl-tRNA synthetase	$[c] : \text{atp} + \text{his-L} + \text{trnahis} \rightarrow \text{amp} + \text{h} + \text{histrna} + \text{ppi}$
Hydroxymethylglutaryl CoA reductase	$[c] : \text{coa} + \text{mev-R} + (2) \text{nadp} \leftrightarrow (2) \text{h} + \text{hmgcoa} + (2) \text{nadph}$
Hydroxymethylglutaryl CoA synthase	$[c] : \text{coa} + \text{h} + \text{hmgcoa} \leftrightarrow \text{aacoa} + \text{accoa} + \text{h}_2\text{o}$
hydroxymethylpyrimidine kinase (ATP)	$[c] : 4\text{ahmmp} + \text{atp} \rightarrow 4\text{ampm} + \text{adp} + \text{h}$
(3R)-3-Hydroxybutanoyl-[acyl-carrier-protein] hydro-lyase	$[c] : 3\text{hocacp} \rightarrow 2\text{toceacp} + \text{h}_2\text{o}$
(3R)-3-Hydroxyoctanoyl-[acyl-carrier-protein]:NADP+ oxidoreductase	$[c] : 3\text{oxocacp} + \text{h} + \text{nadph} \rightarrow 3\text{hocacp} + \text{nadp}$
(3R)-3-Hydroxyoctadecanoyl-[acyl-carrier-protein] hydro-lyase	$[c] : 3\text{hocdacp} \rightarrow 2\text{tocdacp} + \text{h}_2\text{o}$
(3R)-3-Hydroxyoctadecanoyl-[acyl-carrier-protein]:NADP+ oxidoreductase	$[c] : 3\text{oxocdacp} + \text{h} + \text{nadph} \rightarrow 3\text{hocdacp} + \text{nadp}$
hydroxyphenylpyruvate reductase	$[c] : 34\text{hpp} + \text{h} + \text{nadh} \leftrightarrow 34\text{hplac} + \text{nad}$
hydroxyphenyl lactate transport (H^+ symport)	$34\text{hplac}[c] + \text{h}[c] \leftrightarrow 34\text{hplac}[e] + \text{h}[e]$
2-amino-4-hydroxy-6-hydroxymethylidihydropteridine diphosphokinase	$[c] : 2\text{ahhmp} + \text{atp} \rightarrow 2\text{ahhmd} + \text{amp} + \text{h}$
Acetyl-CoA:L-homoserine O-acetyltransferase	$[c] : \text{accoa} + \text{hom-L} \leftrightarrow \text{achms} + \text{coa}$
homoserine kinase	$[c] : \text{atp} + \text{hom-L} \rightarrow \text{adp} + \text{h} + \text{phom}$
(3R)-3-Hydroxypalmitoyl-[acyl-carrier-protein] hydro-lyase	$[c] : 3\text{htdacp} \rightarrow 2\text{ttdeacp} + \text{h}_2\text{o}$
3R)-3-Hydroxytetradecanoyl-[acyl-carrier-protein]:NADP+ oxidoreductase	$[c] : 3\text{oxtdacp} + \text{h} + \text{nadph} \rightarrow 3\text{htdacp} + \text{nadp}$
hypoxanthine transport in via proton symport	$\text{h}[e] + \text{hxan}[e] \rightarrow \text{h}[c] + \text{hxan}[c]$
hypoxanthine phosphoribosyltransferase (Hypoxanthine)	$[c] : \text{hxan} + \text{prpp} \rightarrow \text{imp} + \text{ppi}$
indolelactate dehydrogenase	$[c] : (2) \text{h} + \text{indpyr} + \text{nadh} \leftrightarrow \text{indlac} + \text{nad}$
L-isoleucine transport in/out via proton symport	$\text{h}[e] + \text{ile-L}[e] \leftrightarrow \text{h}[c] + \text{ile-L}[c]$
isoleucine transaminase	$[c] : \text{akg} + \text{ile-L} \leftrightarrow 3\text{mop} + \text{glu-L}$
Isoleucyl-tRNA synthetase	$[c] : \text{atp} + \text{ile-L} + \text{trnaile} \rightarrow \text{amp} + \text{h} + \text{iletrna} + \text{ppi}$
imidazole lactate transport (H^+ symport)	$\text{h}[c] + \text{imlac}[c] \leftrightarrow \text{h}[e] + \text{imlac}[e]$
imidazole dehydrogenase	$[c] : \text{h} + \text{impyr} + \text{nadh} \leftrightarrow \text{imlac} + \text{nad}$
IMP cyclohydrolase	$[c] : \text{h}_2\text{o} + \text{imp} \leftrightarrow \text{fprica}$
IMP dehydrogenase	$[c] : \text{h}_2\text{o} + \text{imp} + \text{nad} \rightarrow \text{h} + \text{nadh} + \text{xmp}$
indolelactate diffusion	$\text{indlac}[c] \rightarrow \text{indlac}[e]$
inosine transport in via proton symport, reversible	$\text{h}[e] + \text{ins}[e] \leftrightarrow \text{h}[c] + \text{ins}[c]$
isopentenyl-diphosphate D-isomerase	$[c] : \text{ipdp} \leftrightarrow \text{dmpp}$
β -ketoacyl-ACP synthase III	$[c] : \text{accoa} + \text{h} + \text{malacp} \rightarrow \text{aaacp} + \text{co}_2 + \text{coa}$
L-lactate reversible transport via proton symport	$\text{h}[e] + \text{lac-L}[e] \leftrightarrow \text{h}[c] + \text{lac-L}[c]$
D-lactate dehydrogenase	$[c] : \text{lac-D} + \text{nad} \leftrightarrow \text{h} + \text{nadh} + \text{pyr}$
L-lactate dehydrogenase	$[c] : \text{lac-L} + \text{nad} \leftrightarrow \text{h} + \text{nadh} + \text{pyr}$
L-leucine transport in/out via proton symport	$\text{h}[e] + \text{leu-L}[e] \leftrightarrow \text{h}[c] + \text{leu-L}[c]$
leucine transaminase	$[c] : \text{akg} + \text{leu-L} \leftrightarrow 4\text{mop} + \text{glu-L}$
Leucyl-tRNA synthetase	$[c] : \text{atp} + \text{leu-L} + \text{trnaleu} \rightarrow \text{amp} + \text{h} + \text{leutrna} + \text{ppi}$
L-lactate oxidase	$[c] : \text{lac-L} + \text{o}_2 \rightarrow \text{h}_2\text{o}_2 + \text{pyr}$
lysylphosphatidyl-glycerol synthetase	$[c] : \text{lystrna} + (0.01) \text{pg_LLA} \rightarrow (0.01) \text{lyspg_LLA} + \text{trnalys}$
Lipoteichoic acid synthase (<i>L. lactis</i> specific)	$[c] : (0.01) \text{d12dg_LLA} + (0.16) \text{pg_LLA} \rightarrow (0.16) \text{12dgr_LLA} + (0.01) \text{LTA_LLA}$
L-lysine transport in/out via proton symport	$\text{h}[e] + \text{lys-L}[e] \leftrightarrow \text{h}[c] + \text{lys-L}[c]$
Lysyl-tRNA synthetase	$[c] : \text{atp} + \text{lys-L} + \text{trnalys} \rightarrow \text{amp} + \text{h} + \text{lystrna} + \text{ppi}$
Malonyl-CoA:[acyl-carrier-protein] S-malonyltransferase	$[c] : \text{acp} + \text{malcoa} \rightarrow \text{coa} + \text{malacp}$
maltose phosphorylase	$[c] : \text{malt} + \text{pi} \leftrightarrow \text{g1p-B} + \text{glc-D}$
malate symporter	$\text{h}[e] + \text{mal-L}[e] \leftrightarrow \text{h}[c] + \text{mal-L}[c]$
maltose transport via ABC system	$\text{atp}[c] + \text{h}_2\text{o}[c] + \text{malt}[e] \rightarrow \text{adp}[c] + \text{h}[c] + \text{malt}[c] + \text{pi}[c]$
mannose-6-phosphate isomerase	$[c] : \text{man6p} \leftrightarrow \text{f6p}$
D-mannose transport via PEP:Pyruvate PTS	$\text{man}[e] + \text{pep}[c] \rightarrow \text{man6p}[c] + \text{pyr}[c]$
Butyryl-[acyl-carrier protein]:malonyl-[acyl-carrier-protein]-C-acyltransferase (decarboxylating)	$[c] : \text{butacp} + \text{h} + \text{malacp} \rightarrow 3\text{oxhacp} + \text{acp} + \text{co}_2$
Hexanoyl-[acyl-carrier protein]:malonyl-[acyl-carrier-protein] C-acyltransferase	$[c] : \text{h} + \text{hexacp} + \text{malacp} \rightarrow 3\text{oxocacp} + \text{acp} + \text{co}_2$
Octanoyl-[acyl-carrier protein]:malonyl-[acyl-carrier-protein] C-acyltransferase (decarboxylating)	$[c] : \text{h} + \text{malacp} + \text{octacp} \rightarrow 3\text{oxdeacp} + \text{acp} + \text{co}_2$
Decanoyl-[acyl-carrier protein]:malonyl-[acyl-carrier-protein] C-acyltransferase	$[c] : \text{decacp} + \text{h} + \text{malacp} \rightarrow 3\text{oxddacp} + \text{acp} + \text{co}_2$
Dodecanoyl-[acyl-carrier-protein]:malonyl-[acyl-carrier-protein] C-acyltransferase	$[c] : \text{ddeacp} + \text{h} + \text{malacp} \rightarrow 3\text{oxtdacp} + \text{acp} + \text{co}_2$
Tetradecanoyl-[acyl-carrier-protein]:malonyl-[acyl-carrier-protein] C-acyltransferase	$[c] : \text{h} + \text{malacp} + \text{tdeacp} \rightarrow 3\text{oxhdacp} + \text{acp} + \text{co}_2$
Hexadecanoyl-[acyl-carrier-protein]:malonyl-[acyl-carrier-protein] C-acyltransferase	$[c] : \text{h} + \text{hdeacp} + \text{malacp} \rightarrow 3\text{oxocdacp} + \text{acp} + \text{co}_2$
malic enzyme (NAD)	$[c] : \text{mal-L} + \text{nad} \rightarrow \text{co}_2 + \text{nadh} + \text{pyr}$
L-methionine transport via ABC system	$\text{atp}[c] + \text{met-L}[e] + \text{h}_2\text{o}[c] \rightarrow \text{adp}[c] + \text{met-L}[c] + \text{h}[c] + \text{pi}[c]$
O-Acetyl-L-homoserine acetate-lyase (adding methanethiol)	$[c] : \text{achms} + \text{h}_2\text{s} \leftrightarrow \text{ac} + \text{h} + \text{hcys-L}$

Table B.2 – continued from previous page

Name	Equation
methionine adenosyltransferase	$[c] : \text{atp} + \text{h2o} + \text{met-L} \rightarrow \text{amet} + \text{pi} + \text{ppi}$
Methional transport	$\text{methal}[c] \leftrightarrow \text{methal}[e]$
methionine synthase	$[c] : 5\text{mthf} + \text{hcsy-L} \rightarrow \text{h} + \text{met-L} + \text{thf}$
L-methionine transport in/out via proton symport	$\text{met-L}[e] + \text{h}[e] \leftrightarrow \text{met-L}[c] + \text{h}[c]$
methionine transaminase	$[c] : \text{akg} + \text{h} + \text{met-L} \leftrightarrow 4\text{met2obut} + \text{glu-L}$
Methionyl-tRNA synthetase	$[c] : \text{atp} + \text{met-L} + \text{trnamet} \rightarrow \text{amp} + \text{h} + \text{mettrna} + \text{ppi}$
mevalonate kinase	$[c] : \text{atp} + \text{mev-R} \rightarrow 5\text{pmev} + \text{adp} + \text{h}$
myo-inositol 1-phosphatase	$[c] : \text{h2o} + \text{mi1p-D} \rightarrow \text{inost} + \text{pi}$
manganese transport via ABC system	$\text{atp}[c] + \text{h2o}[c] + \text{mn2}[e] \rightarrow \text{adp}[c] + \text{h}[c] + \text{mn2}[c] + \text{pi}[c]$
mannitol transport via PEP:Pyr PTS	$\text{mnl}[e] + \text{pep}[c] \rightarrow \text{mnl1p}[c] + \text{pyr}[c]$
MoaD:cysteine sulfur transferase	$[c] : \text{MCOOH} + \text{atp} + \text{cys-L} + \text{h2o} \rightarrow \text{MCOSH} + \text{amp} + \text{ppi} + \text{ser-L}$
Methylthioadenosine nucleosidase	$[c] : 5\text{mta} + \text{h2o} \rightarrow 5\text{mtr} + \text{ade}$
methenyltetrahydrofolate cyclohydrolase	$[c] : \text{h2o} + \text{methf} \leftrightarrow 10\text{fthf} + \text{h}$
Methylenetetrahydrofolate dehydrogenase (NADP)	$[c] : \text{mlthf} + \text{nadp} \leftrightarrow \text{methf} + \text{nadph}$
Nicotinic acid uptake	$\text{nac}[e] \rightarrow \text{nac}[c]$
NAD kinase	$[c] : \text{atp} + \text{nad} \rightarrow \text{adp} + \text{h} + \text{nadp}$
NAD nucleosidase	$[c] : \text{h2o} + \text{nad} \rightarrow \text{adprib} + \text{h} + \text{ncam}$
NAD synthase (nh4)	$[c] : \text{atp} + \text{dnad} + \text{nh4} \rightarrow \text{amp} + \text{h} + \text{nad} + \text{ppi}$
NAPRTase	$[c] : \text{h} + \text{nac} + \text{prpp} \rightarrow \text{nicrnt} + \text{ppi}$
nucleoside-diphosphate kinase (ATP:GDP)	$[c] : \text{atp} + \text{gdp} \leftrightarrow \text{adp} + \text{gtp}$
nucleoside-diphosphate kinase (ATP:UDP)	$[c] : \text{atp} + \text{udp} \leftrightarrow \text{adp} + \text{utp}$
nucleoside-diphosphate kinase (ATP:CDP)	$[c] : \text{atp} + \text{cdp} \leftrightarrow \text{adp} + \text{ctp}$
nucleoside-diphosphate kinase (ATP:dTDP)	$[c] : \text{atp} + \text{dtdp} \leftrightarrow \text{adp} + \text{dttp}$
nucleoside-diphosphate kinase (ATP:dGDP)	$[c] : \text{atp} + \text{dgdg} \leftrightarrow \text{adp} + \text{dgtg}$
nucleoside-diphosphate kinase (ATP:dUDP)	$[c] : \text{atp} + \text{dudp} \leftrightarrow \text{adp} + \text{dutp}$
nucleoside-diphosphate kinase (ATP:dCDP)	$[c] : \text{atp} + \text{dcdp} \leftrightarrow \text{adp} + \text{dctp}$
nucleoside-diphosphate kinase (ATP:dADP)	$[c] : \text{atp} + \text{dadp} \leftrightarrow \text{adp} + \text{datp}$
nucleoside-diphosphate kinase (ATP:IDP)	$[c] : \text{atp} + \text{idp} \leftrightarrow \text{adp} + \text{itp}$
ammonia transport via diffusion	$\text{nh3}[e] \leftrightarrow \text{nh3}[c]$
nh4 Dissociation	$[c] : \text{nh4} \leftrightarrow \text{h} + \text{nh3}$
nh4 Dissociation extracellular	$[e] : \text{nh4} \leftrightarrow \text{h} + \text{nh3}$
nicotinamidase, reversible	$[c] : \text{h2o} + \text{ncam} \leftrightarrow \text{nac} + \text{nh4}$
nicotinate-nucleotide adenyltransferase	$[c] : \text{atp} + \text{h} + \text{nicrnt} \rightarrow \text{dnad} + \text{ppi}$
nitrite transport out via proton antiport	$\text{h}[e] + \text{no2}[c] \rightarrow \text{h}[c] + \text{no2}[e]$
nitrate transport via ABC system	$\text{atp}[c] + \text{h2o}[c] + \text{no3}[e] \rightarrow \text{adp}[c] + \text{h}[c] + \text{no3}[c] + \text{pi}[c]$
NADH oxidase (H ₂ O ₂ forming)	$[c] : \text{h} + \text{nadh} + \text{o2} \rightarrow \text{h2o2} + \text{nad}$
NADH oxidase (H ₂ O forming)	$[c] : (2) \text{h} + (2) \text{nadh} + \text{o2} \rightarrow (2) \text{h2o} + (2) \text{nad}$
NADH peroxidase	$[c] : \text{h} + \text{h2o2} + \text{nadh} \rightarrow (2) \text{h2o} + \text{nad}$
O ₂ transport in via diffusion	$\text{o2}[e] \leftrightarrow \text{o2}[c]$
ornithine carbamoyltransferase	$[c] : \text{cbp} + \text{orn-L} \leftrightarrow \text{citr-L} + \text{h} + \text{pi}$
Octadecanoyl-[acyl-carrier protein]:malonyl-CoA C-acyltransferase	$[c] : 2\text{toceacp} + \text{h} + \text{nadh} \rightarrow \text{nad} + \text{ocdaccp}$
Octanoyl-[acyl-carrier protein]:malonyl-CoA C-acyltransferase	$[c] : 2\text{toceacp} + \text{h} + \text{nadh} \rightarrow \text{nad} + \text{octacp}$
orotidine-5'-phosphate decarboxylase	$[c] : \text{h} + \text{orot5p} \rightarrow \text{co2} + \text{ump}$
L-ornithine transport in/out via proton symport	$\text{orn-L}[e] + \text{h}[e] \leftrightarrow \text{orn-L}[c] + \text{h}[c]$
Orotic acid transport in/out via proton symporter	$\text{h}[e] + \text{orot}[e] \leftrightarrow \text{h}[c] + \text{orot}[c]$
orotate phosphoribosyltransferase	$[c] : \text{orot5p} + \text{ppi} \leftrightarrow \text{orot} + \text{prpp}$
pyrroline-5-carboxylate reductase	$[c] : 1\text{pyr5c} + (2) \text{h} + \text{nadh} \leftrightarrow \text{nadp} + \text{pro-L}$
para aminobenzoic acid transport	$4\text{abz}[e] \leftrightarrow 4\text{abz}[c]$
phenylacetaldehyde transport	$\text{pacald}[c] \leftrightarrow \text{pacald}[e]$
phosphatidic acid phosphatase	$[c] : \text{h2o} + (0.01) \text{pa_LLA} \rightarrow (0.01) 12\text{dgr_LLA} + \text{pi}$
phospho-N-acetylmuramoyl-pentapeptide-transferase (meso-2,6-diaminopimelate)	$[c] : \text{uAgl} + \text{udcpp} \rightarrow \text{uaAgl} + \text{ump}$
pyruvate dehydrogenase	$[c] : \text{coa} + \text{nad} + \text{pyr} \rightarrow \text{accoa} + \text{co2} + \text{nadh}$
pyridoxin transport via proton symport	$\text{h}[e] + \text{pydxn}[e] \rightarrow \text{h}[c] + \text{pydxn}[c]$
phenylethylalcohol transport	$\text{pea}[c] \leftrightarrow \text{pea}[e]$
phosphofructokinase	$[c] : \text{atp} + \text{f6p} \rightarrow \text{adp} + \text{fdp} + \text{h}$
Formate C-acetyltransferase	$[c] : \text{coa} + \text{pyr} \leftrightarrow \text{accoa} + \text{for}$
phosphoglucosamine mutase	$[c] : \text{gam1p} \leftrightarrow \text{gam6p}$
6-phospho-β-glucosidase	$[c] : 6\text{pgg} + \text{h2o} \rightarrow \text{g6p} + \text{glc-D}$
peptidoglycan glycosyltransferase	$[c] : \text{uaaAgl} \rightarrow \text{PG} + \text{udcpdp}$
glucose-6-phosphate isomerase	$[c] : \text{g6p} \leftrightarrow \text{f6p}$
phosphoglycerate kinase	$[c] : 13\text{dpg} + \text{adp} \leftrightarrow 3\text{pg} + \text{atp}$
phosphoglycolate phosphatase	$[c] : 2\text{pglyc} + \text{h2o} \rightarrow \text{glyclt} + \text{pi}$
phosphoglycerate mutase	$[c] : 3\text{pg} \leftrightarrow 2\text{pg}$
phosphoglucomutase	$[c] : \text{g1p} \leftrightarrow \text{g6p}$
b-phosphoglucomutase	$[c] : \text{g6p-B} \leftrightarrow \text{g1p-B}$

Table B.2 – continued from previous page

Name	Equation
Phosphatidylglycerol phosphate phosphatase (Lactis specific)	$[c] : h2o + (0.01) \text{pgp_LLA} \rightarrow (0.01) \text{pg_LLA} + \text{pi}$
Phosphatidylglycerol synthase (lactis specific)	$[c] : (0.01) \text{cdpdag_LLA} + \text{glyc3p} \leftrightarrow \text{cmp} + \text{h} + (0.01) \text{pgp_LLA}$
Phenol transport	$\text{phenol}[c] \leftrightarrow \text{phenol}[e]$
L-phenylalanine transport in/out via proton symport	$\text{h}[e] + \text{phe-L}[e] \leftrightarrow \text{h}[c] + \text{phe-L}[c]$
Phenylalanyl-tRNA synthetase	$[c] : \text{atp} + \text{phe-L} + \text{trnaphe} \rightarrow \text{amp} + \text{h} + \text{phetrna} + \text{ppi}$
phosphate transport via ABC system	$\text{atp}[c] + \text{h2o}[c] + \text{pi}[e] \rightarrow \text{adp}[c] + \text{h}[c] + (2) \text{pi}[c]$
phosphate transport in/out via proton symporter	$\text{h}[e] + \text{pi}[e] \leftrightarrow \text{h}[c] + \text{pi}[c]$
phosphomannomutase	$[c] : \text{man1p} \leftrightarrow \text{man6p}$
phosphomevalonate kinase	$[c] : 5\text{pmev} + \text{atp} \rightarrow 5\text{dpmev} + \text{adp}$
phosphomethylpyrimidine kinase	$[c] : 4\text{ampm} + \text{atp} \rightarrow 2\text{mahmp} + \text{adp}$
pantothenate kinase	$[c] : \text{atp} + \text{pnto-R} \rightarrow 4\text{ppan} + \text{adp} + \text{h}$
Pantothenate reversible transport via proton symport	$\text{h}[e] + \text{pnto-R}[e] \leftrightarrow \text{h}[c] + \text{pnto-R}[c]$
inorganic diphosphatase	$[c] : \text{h2o} + \text{ppi} \rightarrow \text{h} + (2) \text{pi}$
phosphopantothenoylcysteine decarboxylase	$[c] : 4\text{ppcys} + \text{h} \rightarrow \text{co2} + \text{pan4p}$
phosphopentomutase (deoxyribose)	$[c] : 2\text{dr1p} \leftrightarrow 2\text{dr5p}$
phosphopantothenate-cysteine ligase	$[c] : 4\text{ppan} + \text{ctp} + \text{cys-L} \rightarrow 4\text{ppcys} + \text{cdp} + \text{h} + \text{pi}$
phosphoribosylglycinamide synthetase	$[c] : \text{atp} + \text{gly} + \text{pram} \rightarrow \text{adp} + \text{gar} + \text{h} + \text{pi}$
phosphoribosylaminoimidazole synthetase	$[c] : \text{atp} + \text{fpram} \rightarrow \text{adp} + \text{air} + \text{h} + \text{pi}$
phosphoribosylaminoimidazolesuccinocarboxamide synthase	$[c] : 5\text{aizc} + \text{asp-L} + \text{atp} \leftrightarrow 25\text{aics} + \text{adp} + \text{h} + \text{pi}$
phosphoribosylformylglycinamide synthase	$[c] : \text{atp} + \text{fgam} + \text{gln-L} + \text{h2o} \rightarrow \text{adp} + \text{fpram} + \text{glu-L} + (2) \text{h} + \text{pi}$
L-prolin transport via ABC system	$\text{atp}[c] + \text{pro-L}[e] + \text{h2o}[c] \rightarrow \text{adp}[c] + \text{pro-L}[c] + \text{h}[c] + \text{pi}[c]$
L-proline transport in/out via proton symport	$\text{h}[e] + \text{pro-L}[e] \leftrightarrow \text{h}[c] + \text{pro-L}[c]$
Prolyl-tRNA synthetase	$[c] : \text{atp} + \text{pro-L} + \text{trnapro} \rightarrow \text{amp} + \text{h} + \text{ppi} + \text{protrna}$
protein synthesis_LLA for lactis	$[c] : (0.086) \text{alatrna} + (0.041) \text{argtrna} + (0.059) \text{asntrna} + (0.031) \text{asptrna} + (0.306) \text{atp} + (0.034) \text{cysrna} + (0.064) \text{glntrna} + (0.036) \text{glutrna} + (0.092) \text{glytrna} + (2) \text{gtp} + (2.306) \text{h2o} + (0.015) \text{histrna} + (0.061) \text{iletrna} + (0.087) \text{leutrna} + (0.072) \text{lystrna} + (0.025) \text{mettrna} + (0.038) \text{phetrna} + (0.035) \text{protrna} + (0.051) \text{sertrna} + (0.056) \text{thrrna} + (0.017) \text{trprtrna} + (0.027) \text{tyrtrna} + (0.072) \text{valtrna} \rightarrow (0.306) \text{adp} + (2) \text{gdp} + (2.306) \text{h} + (2.306) \text{pi} + (0.001) \text{prot_LLA} + (0.086) \text{trnaala} + (0.041) \text{trnaarg} + (0.059) \text{trnaasn} + (0.031) \text{trnaasp} + (0.034) \text{trnacys} + (0.064) \text{trnagln} + (0.036) \text{trnaglu} + (0.092) \text{trnagly} + (0.015) \text{trnahis} + (0.061) \text{trnaile} + (0.087) \text{trnaleu} + (0.072) \text{trnaly} + (0.025) \text{trnamet} + (0.038) \text{trnaphe} + (0.035) \text{trnapro} + (0.051) \text{trnaser} + (0.056) \text{trnathr} + (0.017) \text{trnatrp} + (0.027) \text{trnatyr} + (0.072) \text{trnaval}$
phosphoribosylpyrophosphate synthetase	$[c] : \text{atp} + \text{r5p} \leftrightarrow \text{amp} + \text{h} + \text{prpp}$
3-phosphoshikimate 1-carboxyvinyltransferase	$[c] : \text{pep} + \text{skm5p} \leftrightarrow 3\text{psme} + \text{pi}$
pseudouridylylase synthase	$[c] : \text{r5p} + \text{ura} \rightarrow \text{h2o} + \text{psd5p}$
phosphotransacetylase	$[c] : \text{accoa} + \text{pi} \leftrightarrow \text{actp} + \text{coa}$
pantetheine-phosphate adenyltransferase	$[c] : \text{atp} + \text{h} + \text{pan4p} \leftrightarrow \text{dpcoa} + \text{ppi}$
putrescine transport via ABC system	$\text{atp}[c] + \text{h2o}[c] + \text{ptrc}[e] \rightarrow \text{adp}[c] + \text{h}[c] + \text{pi}[c] + \text{ptrc}[c]$
purine-nucleoside phosphorylase (Adenosine)	$[c] : \text{adn} + \text{pi} \leftrightarrow \text{ade} + \text{r1p}$
purine-nucleoside phosphorylase (Deoxyadenosine)	$[c] : \text{dad-2} + \text{pi} \leftrightarrow 2\text{dr1p} + \text{ade}$
purine-nucleoside phosphorylase (Guanosine)	$[c] : \text{gsn} + \text{pi} \leftrightarrow \text{gua} + \text{r1p}$
purine-nucleoside phosphorylase (Deoxyguanosine)	$[c] : \text{dgsn} + \text{pi} \leftrightarrow 2\text{dr1p} + \text{gua}$
purine-nucleoside phosphorylase (Inosine)	$[c] : \text{ins} + \text{pi} \leftrightarrow \text{hxan} + \text{r1p}$
purine-nucleoside phosphorylase (Deoxyinosine)	$[c] : \text{din} + \text{pi} \leftrightarrow 2\text{dr1p} + \text{hxan}$
purine-nucleoside phosphorylase (Xanthosine)	$[c] : \text{pi} + \text{xtsn} \leftrightarrow \text{r1p} + \text{xan}$
pyridoxal kinase (Pyridoxamine)	$[c] : \text{atp} + \text{pydam} \rightarrow \text{adp} + \text{h} + \text{pyam5p}$
pyridoxamine transport	$\text{h}[e] + \text{pydam}[e] \leftrightarrow \text{h}[c] + \text{pydam}[c]$
pyridoxal kinase (Pyridoxal)	$[c] : \text{atp} + \text{pydx} \rightarrow \text{adp} + (2) \text{h} + \text{pydx5p}$
pyruvate kinase	$[c] : \text{adp} + \text{h} + \text{pep} \rightarrow \text{atp} + \text{pyr}$
pyruvate reversible transport via proton symport	$\text{h}[e] + \text{pyr}[e] \leftrightarrow \text{h}[c] + \text{pyr}[c]$
riboflavin kinase	$[c] : \text{atp} + \text{ribflv} \rightarrow \text{adp} + \text{fmn} + \text{h}$
ribokinase	$[c] : \text{atp} + \text{rib-D} \rightarrow \text{adp} + \text{h} + \text{r5p}$
L-ribulose-phosphate 4-epimerase	$[c] : \text{ru5p-L} \leftrightarrow \text{xu5p-D}$
ribosylhomocysteinase	$[c] : \text{h2o} + \text{rhcys} \rightarrow \text{hcys-L} + \text{rib-D}$
riboflavin transport in via proton symport	$\text{h}[e] + \text{ribflv}[e] \rightarrow \text{h}[c] + \text{ribflv}[c]$
ribose transport in via proton symporter	$\text{h}[e] + \text{rib-D}[e] \rightarrow \text{h}[c] + \text{rib-D}[c]$
RNA synthesis, lactis specific	$[c] : (0.66) \text{atp} + (0.2) \text{ctp} + (0.32) \text{gtp} + (0.4) \text{h2o} + (0.22) \text{utp} \rightarrow (0.01) \text{RNA_LLA} + (0.4) \text{adp} + (0.4) \text{h} + (0.4) \text{pi} + \text{ppi}$
ribonucleoside-diphosphate reductase (ADP)	$[c] : \text{adp} + \text{trdrd} \rightarrow \text{dadp} + \text{h2o} + \text{trdox}$
ribonucleoside-diphosphate reductase (GDP)	$[c] : \text{gdp} + \text{trdrd} \rightarrow \text{dgd} + \text{h2o} + \text{trdox}$

Table B.2 – continued from previous page

Name	Equation
ribonucleoside-diphosphate reductase (CDP)	$[c] : \text{cdp} + \text{trdrd} \rightarrow \text{dcdp} + \text{h2o} + \text{trdox}$
ribonucleoside-diphosphate reductase (UDP)	$[c] : \text{trdrd} + \text{udp} \rightarrow \text{dudp} + \text{h2o} + \text{trdox}$
ribonucleoside-triphosphate reductase (ATP)	$[c] : \text{atp} + \text{trdrd} \rightarrow \text{datp} + \text{h2o} + \text{trdox}$
ribonucleoside-triphosphate reductase (GTP)	$[c] : \text{gtp} + \text{trdrd} \rightarrow \text{dgtp} + \text{h2o} + \text{trdox}$
ribonucleoside-triphosphate reductase (CTP)	$[c] : \text{ctp} + \text{trdrd} \rightarrow \text{dctp} + \text{h2o} + \text{trdox}$
ribonucleoside-triphosphate reductase (UTP)	$[c] : \text{trdrd} + \text{utp} \rightarrow \text{dutp} + \text{h2o} + \text{trdox}$
ribulose 5-phosphate 3-epimerase	$[c] : \text{ru5p-D} \leftrightarrow \text{xu5p-D}$
ribose-5-phosphate isomerase	$[c] : \text{r5p} \leftrightarrow \text{ru5p-D}$
sorbitol-6-phosphatase	$[c] : \text{h2o} + \text{sbt6p} \rightarrow \text{pi} + \text{sbt-D}$
D-sorbitol transport via PEP:Pyr PTS	$\text{pep}[c] + \text{sbt-D}[e] \rightarrow \text{pyr}[c] + \text{sbt6p}[c]$
D-sorbitol transport in via proton symport	$\text{h}[e] + \text{sbt-D}[e] \leftrightarrow \text{h}[c] + \text{sbt-D}[c]$
succinyl-diaminopimelate desuccinylase	$[c] : \text{h2o} + \text{sl26da} \rightarrow \text{26dap-LL} + \text{succ}$
serine O-acetyltransferase	$[c] : \text{accoa} + \text{ser-L} \leftrightarrow \text{acser} + \text{coa}$
L-serine deaminase	$[c] : \text{ser-L} \rightarrow \text{nh4} + \text{pyr}$
L-serine transport in/out via proton symport	$\text{h}[e] + \text{ser-L}[e] \leftrightarrow \text{h}[c] + \text{ser-L}[c]$
Seryl-tRNA synthetase	$[c] : \text{atp} + \text{ser-L} + \text{trnaser} \rightarrow \text{amp} + \text{h} + \text{ppi} + \text{sertrna}$
shikimate dehydrogenase	$[c] : \text{3dhsk} + \text{h} + \text{nadph} \leftrightarrow \text{nadp} + \text{skm}$
shikimate kinase	$[c] : \text{atp} + \text{skm} \rightarrow \text{adp} + \text{h} + \text{skm5p}$
O-acetylhomoserine lysase (L-cysteine)	$[c] : \text{achms} + \text{cys-L} \rightarrow \text{ac} + \text{cysth-L} + \text{h}$
sulfate transport in/out via sodium symport	$\text{na1}[e] + \text{so4}[e] \leftrightarrow \text{na1}[c] + \text{so4}[c]$
spermidine transport via ABC system	$\text{atp}[c] + \text{h2o}[c] + \text{spmd}[e] \rightarrow \text{adp}[c] + \text{h}[c] + \text{pi}[c] + \text{spmd}[c]$
succinate-semialdehyde dehydrogenase (NADP)	$[c] : \text{h2o} + \text{nadp} + \text{sucsal} \rightarrow (2) \text{h} + \text{nadph} + \text{succ}$
sucrose 6-phosphate hydrolase	$[c] : \text{h2o} + \text{suc6p} \rightarrow \text{pi} + \text{sucr}$
succinate transporter in/out via proton symport	$\text{h}[e] + \text{succ}[e] \leftrightarrow \text{h}[c] + \text{succ}[c]$
succinate dehydrogenase (menaquinone 7)	$[c] : \text{mqn7} + \text{succ} \leftrightarrow \text{fum} + \text{mq17}$
α -glucoside glucohydrolase	$[c] : \text{h2o} + \text{sucr} \rightarrow \text{fru} + \text{glc-D}$
sucrose transport via PEP:Pyr PTS	$\text{pep}[c] + \text{sucr}[e] \rightarrow \text{pyr}[c] + \text{suc6p}[c]$
transaldolase	$[c] : \text{g3p} + \text{s7p} \leftrightarrow \text{e4p} + \text{f6p}$
Thiocysteine degradation	$[c] : \text{tcys} + (2) \text{h} \rightarrow \text{cys-L} + \text{h2s}$
Tetradecanoyl-[acyl-carrier protein]:malonyl-CoA acyltransferase	C- $[c] : \text{2ttdeacp} + \text{h} + \text{nadh} \rightarrow \text{nad} + \text{tdeacp}$
dTDP-4-dehydrorhamnose 3,5-epimerase	$[c] : \text{dtdpddg} \leftrightarrow \text{dtdpddm}$
dTDP-4-dehydrorhamnose reductase	$[c] : \text{dtdp6dm} + \text{nadp} \leftrightarrow \text{dtdpddm} + \text{h} + \text{nadph}$
dTDPglucose 4,6-dehydratase	$[c] : \text{dtdpglc} \rightarrow \text{dtdpddg} + \text{h2o}$
Tetrahydrofolate:L-glutamate γ -ligase (ADP-forming)	$[c] : \text{atp} + \text{glu-L} + \text{thf} \leftrightarrow \text{adp} + \text{h} + \text{pi} + \text{thfglu}$
thiamine transport via ABC system	$\text{atp}[c] + \text{h2o}[c] + \text{thm}[e] \rightarrow \text{adp}[c] + \text{h}[c] + \text{pi}[c] + \text{thm}[c]$
thymidine transport in via proton symport	$\text{h}[e] + \text{thymd}[e] \rightarrow \text{h}[c] + \text{thymd}[c]$
threonine aldolase	$[c] : \text{thr-L} \leftrightarrow \text{acald} + \text{gly}$
threonine synthase	$[c] : \text{h2o} + \text{phom} \rightarrow \text{pi} + \text{thr-L}$
L-threonine transport in/out via proton symporter	$\text{h}[e] + \text{thr-L}[e] \leftrightarrow \text{h}[c] + \text{thr-L}[c]$
Threonyl-tRNA synthetase	$[c] : \text{atp} + \text{thr-L} + \text{trnathr} \rightarrow \text{amp} + \text{h} + \text{ppi} + \text{thrtrna}$
transketolase	$[c] : \text{r5p} + \text{xu5p-D} \leftrightarrow \text{g3p} + \text{s7p}$
transketolase	$[c] : \text{e4p} + \text{xu5p-D} \leftrightarrow \text{f6p} + \text{g3p}$
thymidine kinase (ATP:thymidine)	$[c] : \text{atp} + \text{thymd} \rightarrow \text{adp} + \text{dtmp} + \text{h}$
thymidine kinase (GTP:Thymidine)	$[c] : \text{gtp} + \text{thymd} \rightarrow \text{dtmp} + \text{gdp} + \text{h}$
thiamine diphosphokinase	$[c] : \text{atp} + \text{thm} \rightarrow \text{amp} + \text{h} + \text{thmpp}$
thymidylate synthase	$[c] : \text{dump} + \text{mlthf} \rightarrow \text{dhf} + \text{dtmp}$
thiamine-phosphate kinase	$[c] : \text{atp} + \text{thmpp} \leftrightarrow \text{adp} + \text{thmp}$
triose-phosphate isomerase	$[c] : \text{dhap} \leftrightarrow \text{g3p}$
thioredoxin reductase (NADPH)	$[c] : \text{h} + \text{nadph} + \text{trdox} \rightarrow \text{nadp} + \text{trdrd}$
trehalose-6-phosphate hydrolase	$[c] : \text{h2o} + \text{tre6p} \rightarrow \text{g6p} + \text{glc-D}$
trehalose transport via PEP:Pyr PTS	$\text{pep}[c] + \text{tre}[e] \rightarrow \text{pyr}[c] + \text{tre6p}[c]$
L-tryptophan transport in/out via proton symport	$\text{h}[e] + \text{trp-L}[e] \leftrightarrow \text{h}[c] + \text{trp-L}[c]$
Tryptophanyl-tRNA synthetase	$[c] : \text{atp} + \text{trnatrp} + \text{trp-L} \rightarrow \text{amp} + \text{h} + \text{ppi} + \text{trptrna}$
L-tyrosine transport in/out via proton symport	$\text{h}[e] + \text{tyr-L}[e] \leftrightarrow \text{h}[c] + \text{tyr-L}[c]$
Tyrosyl-tRNA synthetase	$[c] : \text{atp} + \text{trnatyr} + \text{tyr-L} \rightarrow \text{amp} + \text{h} + \text{ppi} + \text{tyrtrna}$
UDP-N-acetylmuramoyl-L-alanyl-D-glutamyl-meso-2,6-diaminopimelate synthetase	$[c] : \text{26dap-M} + \text{atp} + \text{uamag} \rightarrow \text{adp} + \text{h} + \text{pi} + \text{ugmd}$
UDP-N-acetylmuramoyl-L-alanyl-D-glutamate-lysine thetase (α -glutamate)	syn- $[c] : \text{atp} + \text{lys-L} + \text{uamag} \rightarrow \text{adp} + (2) \text{h} + \text{pi} + \text{uAgl}$
UDP-N-acetylglucosamine 1-carboxyvinyltransferase	$[c] : \text{pep} + \text{uacgam} \rightarrow \text{pi} + \text{uaccg}$
UDP-N-acetylglucosamine diphosphorylase	$[c] : \text{acgam1p} + \text{h} + \text{utp} \rightarrow \text{ppi} + \text{uacgam}$
UDP-N-acetylglucosamine-N-acetylmuramyl-(pentapeptide)pyrophosphoryl-undecaprenol acetylglucosamine transferase	N- $[c] : \text{uaAgl1a} + \text{uacgam} \rightarrow \text{h} + \text{uaaAgl1a} + \text{udp}$
UDP-N-acetylmuramoyl-L-alanyl-D-glutamate synthetase	$[c] : \text{atp} + \text{glu-D} + \text{uama} \rightarrow \text{adp} + \text{h} + \text{pi} + \text{uamag}$
UDP-N-acetylmuramoyl-L-alanine synthetase	$[c] : \text{ala-L} + \text{atp} + \text{uamr} \rightarrow \text{adp} + \text{h} + \text{pi} + \text{uama}$
UDP-N-acetylenolpyruvoylglucosamine reductase	$[c] : \text{h} + \text{nadph} + \text{uaccg} \rightarrow \text{nadp} + \text{uamr}$

Table B.2 – continued from previous page

Name	Equation
undecaprenyl-diphosphatase	[c] : h2o + udcpdp → h + pi + udcpp
Undecaprenyl diphosphate synthase	[c] : frdp + (8) ipdp → (8) ppi + udcpdp
UDPglucose 4-epimerase	[c] : udpg ↔ udpgal
UDP-N-acetylmuramoyl-L-alanyl-D-glutamyl-L-lysyl-D-alanyl-D-alanine synthetase (α-glutamate)	[c] : alaala + atp + uAgl → adp + pi + uAgl _a
UDP-N-acetylmuramoyl-L-alanyl-D-glutamyl-meso-2,6-diaminopimeloyl-D-alanyl-D-lactate synthetase	[c] : alalac + atp + ugmd → adp + h + pi + ugmdalac
UDP-glucosyltransferase (monoacylglycerol)	[c] : (0.01) 12dgr_LLA + udpg → h + (0.01) m12dg_LLA + udp
UDP-glucosyltransferase (diacylglycerol)	[c] : (0.01) m12dg_LLA + udpg → (0.01) d12dg_LLA + h + udp
uracil phosphoribosyltransferase	[c] : prpp + ura → ppi + ump
uracil transport in via proton symport	h[e] + ura[e] → h[c] + ura[c]
uridylyate kinase (UMP)	[c] : atp + ump → adp + udp
uridylyate kinase (dUMP)	[c] : atp + dUMP → adp + dudp
uridine kinase (ATP:Uridine)	[c] : atp + uri → adp + h + ump
uridine kinase (GTP:Uridine)	[c] : gtp + uri → gdp + h + ump
uridine kinase (ITP:Uridine)	[c] : itp + uri → h + idp + ump
L-valine transport in/out via proton symport	h[e] + val-L[e] ↔ h[c] + val-L[c]
valine transaminase	[c] : akgl + val-L ↔ 3mob + glu-L
Valyl-tRNA synthetase	[c] : atp + trnaval + val-L → amp + h + ppi + valtrna
xanthine transport in via proton symport	h[e] + xan[e] → h[c] + xan[c]
xanthine phosphoribosyltransferase	[c] : prpp + xan → ppi + xmp
yUMP synthetase	[c] : r5p + ura ↔ h2o + psd5p

B.3 Constraints

For every experimental condition, boundaries for the exchange reactions were calculated from the measured fluxes v_i^m . The lower and upper bounds are calculated as $v_i^m \pm \varepsilon$ with $\varepsilon = 20\%$. We calculated constraints for both pHs and both dilution rates for the wild-type and the *ldh*-deletion strain. For some species no fluxes were measured. In that case we assumed lower and upper boundaries which were applied for the simulation of all experimental set-ups (see Table B.3). The constraints are given in the following Tables B.3 to B.7.

Table B.3: Assumed constraints on reaction fluxes which were not measured. These boundaries are used for all experimental conditions.

Uptake or production	Lower Bound	Upper Bound
Aminobenzoate	-1	1
Acetoin	0	0
Adenine	-1	0
Asparagine	-1	0
Butanediol	0	0
Biotin	-1	1
Cellobiose	0	0
Citrate	0	0

Table B.3 – continued from previous page

Uptake or production	Lower Bound	Upper Bound
CO ₂	0	1
Cytosine	-1	0
Cystine	-1	0
Glutamine	-1	0
Glycolate	0	1
Guanine	-1	0
Inosine	-1	1
Maltose	0	0
Mannose	0	0
Nicotinate	-1	1
NH ₄	0	1
NO ₂	0	1
NO ₃	0	1
O ₂	0	0
Orotate	-1	1
Phosphate	-1	1
Pantothenate	-1	1
Pyridoxamine	-1	1
Pyridoxine	-1	1
Riboflavin	-1	1
SO ₄	0	1
Spermidine	0	1
Succinate	0	0
Sucrose	0	0
Thiamine	-1	1
Thymidine	-1	0
Trehalose	0	0
Tryptophan	-1	0
Xanthine	-1	0

Table B.4: Constraints calculated from measured reaction fluxes for *S. pyogenes* wild-type strain at pH 6.5 and both dilution rates, $d = 0.05 \text{ h}^{-1}$ and $d = 0.15 \text{ h}^{-1}$.

Uptake or production	$d = 0.05 \text{ h}^{-1}$		$d = 0.15 \text{ h}^{-1}$	
	Lower Bound	Upper Bound	Lower Bound	Upper Bound
ATP maintenance	1.35	1.35	1.35	1.35
Acetate	0.9351	0.9733	0.8021	10
Alanine	-0.0988	0	-0.1817	0
Arginine	-0.0306	0	-0.0526	0

Table B.4 – continued from previous page

Uptake or production	d = 0.05 h ⁻¹		d = 0.15 h ⁻¹	
	Lower Bound	Upper Bound	Lower Bound	Upper Bound
Aspartate	-0.1156	0	-0.2205	-0.2119
Cysteine	-0.0352	0	-0.065	0
Ethanol	0.7865	0.8186	0.6272	10
Formate	1.4459	2	1.0275	10
Glucose	-2.5947	-2.4929	-4.7901	-4.6060
Glutamate	-0.1228	0	-0.2338	0
Glycine	-0.0844	-0.081	-0.161	-0.1546
H ⁺	-1000	1000	-1000	1000
H ₂ O	-1000	1000	-1000	1000
Histidine	-0.0373	0	-0.0693	0
Isoleucine	-0.0611	0	-0.113	0
D-Lactate	0	1	0	1
L-Lactate	2.8571	2.9737	1	6.5743
Leucine	-0.1363	0	-0.2523	0
Lysine	-0.0916	0	-0.1716	0
Methionine	-0.0305	0	-0.059	0
NH ₃	0.0695	0.0723	0.1459	0.1519
Ornithine	0.000104	0.000108	0.000098	0.000102
Phenylalanine	-0.0598	0	-0.1123	0
Proline	-0.2134	0	-0.3979	0
Pyruvate	0.0613	0.0648	0	0
Serine	-0.1360	0	-0.2532	-0.2432
Threonine	-0.0711	-0.0683	-0.1329	0
Tyrosine	-0.0475	0	-0.0961	0
Valine	-0.1033	0	-0.1921	0

Table B.5: Constraints calculated from measured reaction fluxes for *S. pyogenes* wild-type strain at pH 7.5 and both dilution rates, d = 0.05 h⁻¹ and d = 0.15 h⁻¹.

Uptake or production	d = 0.05 h ⁻¹		d = 0.15 h ⁻¹	
	Lower Bound	Upper Bound	Lower Bound	Upper Bound
ATP maintenance	0.8	0.8	0.8	0.8
Acetate	1.812	1.884	1.1789	5
Alanine	-0.4287	0	-0.3798	0
Arginine	-0.1574	0	-0.1073	0
Aspartate	-0.4634	0	-0.4514	0
Cysteine	-0.1813	0	-0.1267	0
Ethanol	0	0	1.6170	1.6830

Table B.5 – continued from previous page

Uptake or production	d = 0.05 h ⁻¹		d = 0.15 h ⁻¹	
	Lower Bound	Upper Bound	Lower Bound	Upper Bound
Formate	1.7094	1.7792	2	3.1656
Glucose	-8	0	-6.75	-4
Glutamate	-0.4917	0	-0.4806	0
Glycine	-0.3492	0	-0.3186	-0.3062
H ⁺	-1000	1000	-1000	1000
H ₂ O	-1000	1000	-1000	1000
Histidine	-0.1725	0	-0.1313	0
Isoleucine	-0.3297	0	-0.2289	0
D-Lactate	0	10	0	10
L-Lactate	10	21.7851	8.2643	8.6017
Leucine	-0.5711	0	-0.5089	0
Lysine	-0.3909	0	-0.3466	0
Methionine	-0.1312	0	-0.1128	0
NH ₃	1.1711	1.2189	0.1816	0.189
Ornithine	0.001028	0.001070	0.000069	0.000071
Phenylalanine	-0.3628	0	-0.2135	0
Proline	-0.7857	0	-0.8001	0
Pyruvate	0.03024	0.3148	0	0
Serine	-0.7025	0	-0.4948	-0.4754
Threonine	-0.2880	0	-0.2628	-0.2524
Tyrosine	-0.1740	0	-0.1700	0
Valine	-0.4180	0	-0.3893	0

Table B.6: Constraints calculated from measured reaction fluxes for *S. pyogenes* *ldh*-deletion strain at pH 6.5 and both dilution rates, d = 0.05 h⁻¹ and d = 0.15 h⁻¹.

Uptake or production	d = 0.05 h ⁻¹		d = 0.15 h ⁻¹	
	Lower Bound	Upper Bound	Lower Bound	Upper Bound
ATP maintenance	1.35	1.35	1.35	1.35
Acetate	1.3789	1.4351	2.156	2.244
Alanine	0	0.1607	0	0.204
Arginine	-0.1151	0	-0.1558	0
Aspartate	-0.0367	0	-0.0565	0
Cysteine	-0.1443	0	-0.2209	0
Ethanol	0	0	0	0
Formate	-0.0422	0	-0.0649	0
Glucose	2.1629	2.2511	4.6045	4.7925
Glutamate	3.2066	3.3374	5.3877	5.6077

Table B.6 – continued from previous page

Uptake or production	d = 0.05 h ⁻¹		d = 0.15 h ⁻¹	
	Lower Bound	Upper Bound	Lower Bound	Upper Bound
Glycine	-3.1136	-2.9915	-8	-4.6023
H ⁺	-0.1544	0	-0.2364	0
H ₂ O	-0.1053	0	-0.1665	0
Histidine	-0.0469	0	-0.071	0
Isoleucine	-0.0771	0	-0.1223	0
D-Lactate	0	5	0	10
L-Lactate	0	0.0893	0	0.1349
Leucine	-0.1693	0	-0.271	0
Lysine	-0.1115	0	-0.1722	0
Methionine	-0.0379	0	-0.0587	0
NH ₃	0.0781	0.0813	0.1594	1
Ornithine	0.0001	0.000104	0.000072	1
Phenylalanine	-0.0745	0	-0.113	0
Proline	-0.263	0	-0.3972	0
Pyruvate	0.4018	0.4182	1.1572	1.2044
Serine	-0.1647	0	-0.2536	0
Threonine	-0.0873	0	-0.1316	0
Tyrosine	-0.0605	0	-0.0968	0
Valine	-0.1288	0	-0.2043	0

Table B.7: Constraints calculated from measured reaction fluxes for *S. pyogenes* *ldh*-deletion strain at pH 7.5 and both dilution rates, d = 0.05 h⁻¹ and d = 0.15 h⁻¹.

Uptake or production	d = 0.05 h ⁻¹		d = 0.15 h ⁻¹	
	Lower Bound	Upper Bound	Lower Bound	Upper Bound
ATP maintenance	0.8	0.8	0.8	0.8
Acetate	3.5186	3.6622	3.8346	3.9912
Alanine	0	0.3648	0	0.3658
Arginine	-0.2505	0	-0.3634	0
Aspartate	-0.0881	0	-0.1038	0
Cysteine	-0.3171	0	-0.4448	0
Ethanol	0	0	0	1
Formate	-0.1013	0	-0.1204	0
Glucose	6.5444	6.8116	7.7364	8.0522
Glutamate	8.773	9.131	9.66	10.0542
Glycine	-7.4725	0	-8.8958	-8
H ⁺	-0.3421	0	-0.4791	0
H ₂ O	-0.2337	0	-0.3291	0

Table B.7 – continued from previous page

Uptake or production	d = 0.05 h ⁻¹		d = 0.15 h ⁻¹	
	Lower Bound	Upper Bound	Lower Bound	Upper Bound
Histidine	-0.093	0	-0.138	0
Isoleucine	-0.18	0	-0.2304	0
D-Lactate	0	1	0	1
L-Lactate	0	0.2754	0	0.1166
Leucine	-0.3913	0	-0.5159	0
Lysine	-0.2549	0	-0.3406	0
Methionine	-0.0831	0	-0.1175	0
NH ₃	0.1984	0.2064	0.0946	0.0984
Ornithine	0.00032	0.000334	0.000055	0.000057
Phenylalanine	-0.1687	0	-0.2329	0
Proline	-0.5738	0	-0.8162	0
Pyruvate	2.2967	2.3905	2.1028	2.1886
Serine	-0.3928	0	-0.4711	0
Threonine	-0.1955	0	-0.2666	0
Tyrosine	-0.1231	0	-0.1907	0
Valine	-0.2908	0	-0.3948	0

B.4 Simulation results

After the definition of the biomass equation as objective and the application of boundaries on the uptake and production fluxes the developed genome-scale model is simulated using FBA. The results for two different dilution rates and two different pH values are displayed in the following tables.

Table B.8: Optimal solution from FBA for *S. pyogenes* wild-type and its *ldh*-deletion at pH 6.5 and two dilution rates (D, h⁻¹) in continuous fermentation on CDM-LAB medium. Values indicate flux through the reaction taking up or secreting the compound per hour.

Uptake or production	M49		M49 Δ <i>ldh</i>	
	D = 0.05	D = 0.15	D = 0.05	D = 0.15
ATP maintenance	1.35	1.35	1.35	1.35
Biomass	0.050626	0.157688	0.065553	0.132988
Acetate	0.9733	5.189755	1.4351	2.156
Acetoin	0	0	0	0

Table B.8 – continued from previous page

Uptake or production	M49		M49 Δldh	
	D = 0.05	D = 0.15	D = 0.05	D = 0.15
Alanine	-0.04092	-0.127457	-0.052986	-0.107493
Arginine	-0.00872	-0.02716	-0.011291	-0.022906
Asparagine	-0.012548	0	-0.267972	-0.829382
Aspartate	-0.006593	-0.2119	0	-0.2209
CO ₂	0.028568	0	0	0
Cystine	-0.00322	-0.010029	-0.004169	-0.008458
Cysteine	0	0	0	0
Ethanol	0.7865	4.767266	2.1629	4.6045
Formate	1.627911	9.773135	3.3374	5.6077
Glucose	-2.5947	-5.5	-3.1136	-8
Glutamine	-0.012049	-0.03753	-0.015602	-0.071695
Glutamate	-0.015244	-0.047482	-0.019739	0
Glycine	-0.081	-0.1546	0	-0.1665
Histidine	-0.00319	-0.009937	-0.004131	-0.00838
Isoleucine	-0.012974	-0.040409	-0.016799	-0.03408
D-Lactate	0.492684	0	2.141865	8.110925
L-Lactate	2.9737	1	0	0
Leucine	-0.018503	-0.057633	-0.023959	-0.048605
Lysine	-0.021403	-0.066666	-0.027714	-0.056224
Methionine	-0.006119	-0.019058	-0.007923	-0.016073
NH ₃	0.0723	0.1459	0.0781	0.18095
Ornithine	0.000108	0.000102	0.000104	1
Phenylalanine	-0.008082	-0.025173	-0.010465	-0.02123
Proline	-0.007444	-0.023186	-0.009639	-0.019554
Pyruvate	0.0613	0	0.4182	1.1572
Serine	0	-0.2532	-0.059649	-0.180812
Threonine	-0.0683	-0.11648	-0.077728	-0.1316
Tryptophan	-0.003616	-0.011262	-0.004682	-0.009498
Tyrosine	-0.005742	-0.017886	-0.007436	-0.015084
Valine	-0.015313	-0.047696	-0.019828	-0.040225
Xanthine	0	0	0	0

Table B.8 – continued from previous page

Uptake or production	M49		M49 Δldh	
	D = 0.05	D = 0.15	D = 0.05	D = 0.15
D-LDH	-0.392684	0	-2.141865	-8.110925
L-LDH	-1000	-1000	0	0
Aminobenzoate	-0.000001	-0.000002	-0.000001	-0.000001
Adenine	-0.005641	-0.01757	-0.007304	-0.014818
Butanediol	0	0	0	0
Biotin	0	0	0	0
Cellobiose	0	0	0	0
Citrate	0	0	0	0
Cytosine	0	0	-0.009931	-0.023297
Glycolate	0.000001	0.000002	0.000001	0.000001
Guanine	-0.006005	-0.018703	-0.007775	-0.015774
H ⁺	5.953719	15.742469	7.518837	17.735504
H ₂ O	-0.423779	-3.328439	-0.614428	0.346263
Inosine	0	0	0	0
Maltose	0	0	0	0
Mannose	0	0	0	0
Nicotinate	-0.000101	-0.000315	-0.000131	-0.000266
NH ₄	0.16958	0	0	0
NO ₂	0	0	0	0
NO ₃	0	0	0	0
O ₂	0	0	0	0
Orotate	-0.00767	0.12839	0.243187	1
Phosphate	-0.034903	-0.108714	-0.045194	-0.091685
Pantothenate	-0.00001	-0.000032	-0.000013	-0.000027
Pyridoxamine	0	0	0	0
Pyridoxine	0	0	0	0
Riboflavin	0	0	0	0
SO ₄	0	0	0	0
Spermidine	0	0	0	0
Succinate	0	0	0	0
Sucrose	0	0	0	0

Table B.8 – continued from previous page

Uptake or production	M49		M49 Δldh	
	D = 0.05	D = 0.15	D = 0.05	D = 0.15
Thiamine	-0.000001	-0.000002	-0.000001	-0.000001
Thymidine	-0.001199	-0.003734	-0.001552	0
Trehalose	0	0	0	0

Table B.9: Optimal solution from FBA for *S. pyogenes* wild-type and its *ldh*-deletion at pH 7.5 and two dilution rates (D, h⁻¹) in continuous fermentation on CDM-LAB medium. Values indicate flux through the reaction taking up or secreting the compound per hour.

Uptake or production	M49		M49 Δldh	
	D = 0.05	D = 0.15	D = 0.05	D = 0.15
ATP maintenance	0.8	0.8	0.8	0.8
Biomass	0.144266	0.150519	0.163726	0.172089
Acetate	1.812	2.402287	3.5186	3.9912
Acetoin	0	0	0	0
Alanine	-0.116608	-0.121662	-0.132337	-0.139097
Arginine	-0.024848	-0.025925	-0.0282	-0.029641
Asparagine	-0.035758	-0.037307	-0.678136	-0.567619
Aspartate	-0.019134	-0.379254	-0.059297	-0.408041
CO ₂	0	0	0	1
Cystine	-0.009175	-0.009573	-0.010413	-0.010945
Cysteine	0	0	0	0
Ethanol	0	1.617	6.5444	8.0522
Formate	1.7094	3.1656	9.131	10.0542
Glucose	-8	-6.75	-6.781085	-8
Glutamine	-0.034335	0	-0.038967	-0.040957
Glutamate	-0.064652	-0.081146	-0.049299	-0.051818
Glycine	-0.3492	-0.3062	-0.210246	-0.3291
Histidine	-0.009091	-0.009485	-0.010317	-0.010844
Isoleucine	-0.03697	-0.038572	-0.041956	-0.0441
D-Lactate	3.9312	1.850163	1	1
L-Lactate	10	8.2643	0	0
Leucine	-0.052727	-0.055013	-0.05984	-0.062896

Table B.9 – continued from previous page

Uptake or production	M49		M49 Δldh	
	D = 0.05	D = 0.15	D = 0.05	D = 0.15
Lysine	-0.060992	-0.063635	-0.069219	-0.072754
Methionine	-0.017436	-0.018192	-0.019788	-0.020798
NH ₃	1.2189	0.189	0.1984	0.0946
Ornithine	0.00107	0.000071	0.000334	0.000057
Phenylalanine	-0.02303	-0.024028	-0.026137	-0.027472
Proline	0	-0.022132	-0.024073	-0.025303
Pyruvate	0.03024	0	2.3905	2.1886
Serine	-0.7025	-0.4754	0	0
Threonine	-0.026718	-0.2524	-0.1955	-0.053909
Tryptophan	-0.010303	-0.01075	-0.011693	-0.01229
Tyrosine	-0.016364	-0.017073	-0.018571	-0.019519
Valine	-0.043636	-0.045528	-0.049522	-0.052052
Xanthine	0	0	0	0
D-LDH	-3.9312	-1.850163	-1	-1
L-LDH	-1000	-1000	0	0
Aminobenzoate	-0.000001	-0.000002	-0.000002	-0.000002
Adenine	-0.016074	-0.016771	-0.018242	-0.019174
Butanediol	0	0	0	0
Biotin	0	0	0	0
Cellobiose	0	0	0	0
Citrate	0	0	0	0
Cytosine	-0.025272	-0.022804	-0.024804	-0.030146
Glycolate	0.000001	0.000002	0.000002	0.000002
Guanine	-0.437389	-0.017853	-0.019419	-0.29158
H ⁺	17.183959	15.202423	16.514181	17.587141
H ₂ O	0.996741	0.078548	-1.129835	-0.151876
Inosine	0.420278	0	0	0.271169
Maltose	0	0	0	0
Mannose	0	0	0	0
Nicotinate	-0.000289	-0.000301	-0.000327	-0.000344
NH ₄	0.133625	0.293816	0	0

Table B.9 – continued from previous page

Uptake or production	M49		M49 Δldh	
	D = 0.05	D = 0.15	D = 0.05	D = 0.15
NO ₂	0	0	0	0
NO ₃	0	0	0	0
O ₂	0	0	0	0
Orotate	0.000346	0.359652	0.67553	0.910595
Phosphate	-0.940016	-0.103771	-0.112876	-0.660979
Pantothenate	-0.000029	-0.00003	-0.000033	-0.000034
Pyridoxamine	0	0	0	0
Pyridoxine	0	0	0	0
Riboflavin	0	0	0	0
SO ₄	0	0	0	0
Spermidine	0	0	0	0
Succinate	0	0	0	0
Sucrose	0	0	0	0
Thiamine	-0.000001	-0.000002	-0.000002	-0.000002
Thymidine	0	-0.003564	-0.003877	0
Trehalose	0	0	0	0

